A polarimetry study of starburst galaxies

Paul Alton

A Polarimetry Study of Starburst Galaxies

Paul Alton B.Sc.

A thesis submitted to the University of Durham
for the degree of Doctor of Philosophy.

Department of Physics
February 1996

The copyright of this thesis rests with the author.
No quotation from it should be published without
his prior written consent and information derived
from it should be acknowledged.

Abstract

Optical imaging polarimetry has been carried out for a number of starburst galaxies under various morphological classifications. In several cases, kpc-scale reflection nebulae are detected which arise from dust grains scattering starburst radiation towards the observer. In general, the scattering medium is displaced up to several kpc from the current star-forming environment and in one case, the dust distribution extends above and below the galactic disk in a manner reminiscent of M82. It is now well established that galactic-scale outflows (superwinds) are prevalent in starburst galaxies and it is tempting to attribute the anomalous dust distributions detected in this thesis with these powerful processes. Furthermore, there is increasing evidence that tidal encounters initiate starburst activity and in some cases a dynamic event of this kind may also be responsible for the observed distribution of scattering material.

Mie scattering models were constructed for two of the objects observed in this work. An optically-thin approximation was used which, for many plausible distributions of the dust along the line-of-sight, can be shown to be roughly valid. Although the estimates derived from this technique have a range of values, in all cases the dust component detected in scattered light appears to be at least an order of magnitude more massive than the amount of FIR-emitting dust derived from IRAS data. This is not too surprising – the material detected via polarimetry is probably too cold for IRAS which is sensitive to dust warmer than about 30-50 K.

Contents

Declaration

Most of the data presented in this thesis were recorded by the author during observing trips to the Anglo-Australian Telescope and the South African Observatory in January 1993 and November 1993 respectively. The observational data for NGC 1705, NGC 3077 and the February 1993 data for NGC 3125 were collected by other members of the Durham Polarimetry Group but, for all the objects in this work, the reduction, analysis and final interpretation of the data have been carried out by the author alone. Results for NGC 3077 had already been published in Scarrott *et al.* (1990a) but a fresh analysis was made by the author. Some of the results presented in this thesis have already been published in Alton *et al.* (1994).

None of the material contained within this thesis has previously been submitted for a degree at Durham University or any other university.

The data in this thesis were taken on telescope allocations made to Dr.S.M.Scarrott, Dr.R.D.Wolstencroft and Mr.P.Alton and their permission must be obtained by anyone wishing to publish or use the results beyond this thesis.

Chapter 1

Starburst Galaxies

1.1 Introduction

Starburst galaxies are galaxies experiencing an intense burst of star formation within a large proportion of their interstellar medium (ISM). The burst is short-lived compared with a Hubble time, and in fact cannot usually be sustained for more than $\sim 10^8$ years without all the gas in the ISM being turned into new stars (Leitherer 1993; Rieke *et al.* 1985). Although a preponderance of starburst galaxies, particularly starbursting spirals, have recent star formation concentrated in their nuclei or central regions, this is not always the case. Many late type spirals, for example, which may qualify as starburst galaxies according to the above definition, are characterized by prolific star formation in the disk and spiral arms (e.g. Ryder *et al.* 1995; Pildis *et al.* 1994). Equally, some blue irregular galaxies possess a fairly uniform distribution of young stars throughout their ISM with perhaps bright HII regions located some distance from the gravitational centre of the galaxy (Gallagher and Hunter 1987).

It is clear from the above examples that starburst galaxies constitute a fairly heterogeneous collection of galaxies. Indeed the starburst phenomenon has often been diagnosed in galaxies that were initially investigated under some other pretext. Arp (1966), for example, identified galaxies with disturbed optical morphologies; Zwicky (1964) searched for systems[1] with prominent optical emission lines; and the Markarian sample was selected on the basis of strong ultraviolet continuua (Mazzarella and Balzano 1986). Many of the galaxies featured in these surveys are now known to be starbursting (although other phenomena, such as AGN activity[2] are also evident).

The Infrared Astronomical Satellite (hereafter IRAS) identified a new class of starburst galaxy that emits most of its energy at wavelengths beyond a few microns. Such galaxies

[1] Unless otherwise stated, the word 'system' is used synonymously with the word 'galaxy' throughout this thesis.

[2] Usage of the term 'AGN' within this thesis is restricted to nuclear activity powered by a black hole. 'Active galaxies', on the other hand, encompass galaxies harbouring an AGN and/or a starburst.

have become known as far-infrared galaxies (FIRGs). Star formation in FIRGs is often quite inconspicuous at optical wavelengths due to large amounts of obscuring dust which absorb more energetic photons from the starburst and re-emit the energy at longer wavelengths ($1 - 1000\mu$m). For much of this spectral range, in particular $> 20\mu$m, the sky is opaque necessitating the use of satellite missions. The launch of IRAS in 1983, however, allowed the Universe to be explored in the far-infrared (FIR)[3]. One of the main results from the IRAS survey was the recognition that starburst galaxies are more commonplace than optical studies had originally indicated (Soifer *et al.* 1987).

Much of the subsequent work carried out on starburst galaxies has concentrated on FIRGs although, as mentioned above, the starburst phenomenon is found, and is indeed prevalent in galaxies under several other classifications. Recent analysis of data from the International Ultraviolet Explorer (IUE) has identified a sample of less obscured starburst galaxies (Kinney *et al.* 1993) and it will be of interest to learn of any morphological or evolutionary connection between these systems and FIRGs (Storchi-Bergmann *et al.* 1995). In view of the wealth of data that has been procured for FIRGs, these galaxies are discussed in some detail in the next section. One should note, however, that many of the phenomena associated with FIRGs are just as relevant to other types of starburst galaxy. In particular, the existence of prodigious quantities of gas at the centre of FIRGs and the presence of starburst-driven outflows in these same systems, may be a common feature of most starburst types. A comprehensive description of all galactic systems that show at least some evidence for prolific star formation, is beyond the scope of this thesis. FIRGs, dwarf emission line objects and small blue irregulars, which together constitute a large proportion of starburst galaxies in the local Universe, are discussed in some detail either here or in later sections (they are relevant to the data presented in this thesis). It is hoped that unifying properties will become apparent in the course of these discussions.

My review is set out in the following way: First, I discuss the energy source within FIRGs and its manifestation at different wavelengths. I then address the issue of how star formation is fuelled in these powerful systems. By virtue of its proximity, the nearby FIRG M82 has a wealth of observational data to its name and this galaxy is given some special attention in the discussion. Finally, I turn my attention to a topic which has captivated the minds of many workers in the field – starburst-driven superwinds.

1.2 Far-Infrared Galaxies

Far-infrared galaxies (or FIRGs) is the term generally given to galaxies with far infrared luminosities of $10^{10} - 10^{12} L_{\odot}$. A class of galaxies with higher luminosities than this, so-called *ultraluminous* infrared galaxies, has been discovered by IRAS but the nature of the dust-

[3]strictly speaking IRAS is only capable of measuring the FIR flux between 40μm and 120μm. In general, however, this constitutes a fair approximation to emission over a far broader wavelength range ($1 - 500\mu$m). See Lonsdale *et al.* (1985) for details.

heating source in these extreme systems is unclear and could include an AGN (Lonsdale 1993). The nature of ultraluminous infrared galaxies is discussed briefly in §1.2.1. As points of reference, the FIR luminosity of our own galaxy is estimated to be $\sim 1.5 \times 10^{10} L_{\odot}$ (Cox *et al.* 1986) whilst the most well-studied FIRG, M82, has a FIR luminosity of $2 \times 10^{10} L_{\odot}$ (§9.6). M82, incidentally, is less massive than most spirals (Thronson *et al.* 1991; Davies *et al.* 1989).

Although the FIR luminosity delineating the boundary between normal galaxies and FIRGs is not well defined, FIRGs can usually be recognised by their high FIR-to-blue luminosity ratio (10-100 compared with < 1 for normal galaxies; Soifer *et al.* 1987). This suggests that, within FIRGs, a far larger proportion of the ISM is heated by young stars compared with say normal spirals. Although IRAS generally lacks the spatial resolution to trace out the distribution of the FIR-emitting region, the FIR spectrum is consistent with a cool (30-80 K) blackbody (§9.6). Observations in the mid-infrared confirm that the emission is extended, consistent with dust heated by young stars (Telesco *et al.* 1993). To reproduce the typical FIR luminosity of FIRGs, Soifer *et al.* (1987) concluded that $4 \times 10^{6} M_{\odot}$ of dust is required at a blackbody temperature of 35 K. Thus, if dust and gas occur in the same mass ratio as that found in The Galaxy, the gas associated with the FIR-emitting region is $\sim 10^{9} M_{\odot}$. This is comparable to the total gas mass found in the ISM of a spiral galaxy.

Direct evidence for young stars in FIRGs, purely on the basis of stellar emission lines, is quite sparse. Armus *et al.* (1989), for example, carried out long-slit spectroscopy of nearly 50 FIRGs and found broadened emission, attributable to Wolf-Rayet (WR) stars, in only a very small proportion of their sample. WR stars are the post main-sequence product of very massive stars which live for only a few $\times 10^{6}$ years (§6.3). Their detection usually indicates the presence of a *very* young stellar population (10^{6-7} years old). WR stars have been discovered in an increasing number of starburst galaxies (see Conti 1991 for a review) although detections in FIRGs are perhaps somewhat infrequent (probably due to the presence of dust). The primary manifestation of young stars in FIRGs, at least at optical wavelengths, comes *indirectly* from bright Hα emission (Young *et al.* 1988). Gas at the centre of the starburst is ionized by luminous stars existing within an almost continuous collection of energetic HII regions (Telesco 1988). The strength of the recombination radiation suggests that the starburst contains very young (age $\sim 10^{7}$ years) massive O stars (Armus *et al.* 1989).

Observations outside the optical waveband confirm the picture of young stars providing the engine in FIRGs (see, in addition, §1.3 for recent HST images of the super starclusters in M82). Observations at longer wavelengths, such as the mid-infrared, can probe the 'veil' of dust sufficiently well to show that young stars occupy the central few hundred parsecs of the starburst galaxy (e.g. Telesco *et al.* 1993). A lot can also be learned from the radio continuum.

Condon *et al.* (1982) selected radio-bright galaxies for sub-arcsec to arcsec imaging with the VLA. A comparison with the complete list of IRAS galaxies (Soifer *et al.* 1989) shows that most of these radio-bright galaxies are in fact FIRGs. On average, radio continuum emission from FIRGs is brighter than that detected in normal spirals by about a factor of 10 (Condon *et al.* 1982). Emission is concentrated in the central few hundred parsecs of the galaxy i.e. cospatial with the starburst. Edge-on galaxies in the sample of Condon *et al.* (1982) manifest double or triple emission peaks that may correspond to a ring of young stars, perhaps a few hundred parsecs in diameter, surrounding the gravitational centre of the galaxy. Similar structures are sometimes seen in the molecular gas at the centre of FIRGs (see below) which might indicate that dense gas, and the star formation that it fuels, are concentrated at particular radii within the galaxy. The distribution of the radio continuum, in conjunction with its steep spectral slope (where available), suggests that an extended non-thermal source is responsible for the emission. The general consensus is that supernova remnants (SNR) generate the radio emission by accelerating electrons in the magnetic field of the disk. The radio flux is well correlated with FIR emission suggesting a common or related origin (Condon *et al.* 1991). Star formation provides a natural explanation for these phenomena – the same hot massive stars that heat the FIR-emitting dust eventually explode as supernovae which then give rise to the radio emission. Recent high resolution VLA imaging of nearby Sersic-Pastoriza galaxies (starburst galaxies characterized by conspicuous star forming 'hot-spots' in their nuclear region) confirm that compact ($\sim 10^{0-1}$ pc), spectrally steep features punctuate the radio emission in starburst galaxies and that these features can be associated with bright (and therefore very young) SNR (Saikia *et al.* 1994; Collison *et al.* 1994).

There is increasing evidence that high FIR emission in FIRGs is related to tidal perturbation (Lonsdale 1993 and references therein) and that the highest FIR luminosities are found in galaxies undergoing the strongest gravitational interactions, such as mergers (Leech *et al.* 1994). Numerical simulations by Mihos and Hernquist (1994) and Noguchi (1991) suggest that galactic collisions provide the conditions for large amounts of gas to collect at the centre of the merging system. This material may subsequently form new stars. In contrast to the stellar components of the interacting galaxies, the collision of gas clouds is inelastic and sufficient energy can be dissipated through shocks that gas collapses towards the gravitational centre. At the same time, angular momentum is given up to the disk stars. Interestingly, Hernquist (1989) has shown that the collision of a small satellite with a more massive gas-rich companion is sufficient to cause the large-scale inflow of gas towards the centre of the larger body. The timescale for complete gas inflow is surprisingly short (Hernquist estimates $\leq 10^8$ years for 35% of the gas in a large spiral to enter a nuclear region of 400pc). The disk of the more massive body is distorted but not destroyed whereas the satellite is completely cannibalised. Large concentrations of dense gas have been observed at the centre of starburst galaxies and are believed to fuel the prolific star formation in these galaxies. This is discussed below.

It should be emphasized that some FIRGs, admittedly those with lower FIR lumi-

nosities, appear to be fairly isolated galaxies and show less evidence for tidal distortion. Telesco *et al.* (1993) used the mid-infra red to show that star formation in many FIRGs is often cospatial with or, at least very close to, dense (molecular) gas that has collected in circumnuclear rings situated 1 kpc or less from the centre of the system. Although, many galaxies in their sample show only weak signs of gravitational interaction, the authors note a preponderance of bars. They suggest that the interplay of the orbital rotation of the bar with the frequency of the stellar orbits leads to the concentration of gas between particular radii. These radii are known as Lindblad resonances and in the sample of Telesco *et al.* the correspondence between star formation and these resonance points is very convincing. It appears that the presence of a bar might be of great importance in the transportation of gas to the centre of the galaxy where it is available for star formation. Many galaxies that have undergone weaker tidal interactions (i.e. non-mergers) appear to be barred and it seems likely that the bar arises as a result of gravitational instability (Barnes and Hernquist 1991; Hernquist 1989). It should be noted, however, that some barred spirals (which may or may not be starbursting), appear to be completely isolated. The nearby FIRG NGC 253 might be an example of an isolated barred spiral. How bars become established in isolated systems is not yet known.

The observational evidence for large concentrations of atomic and molecular gas at the centre of starburst galaxies is quite stunning. Mirabel and Sanders (1988) surveyed a large sample of FIRGs in the emission line and continuum at 21cm. They detected large amounts of neutral hydrogen ($\sim 10^{9-10}M_{\odot}$) in absorption against the nuclear continuum source. In addition, many of the absorption features were broadened suggesting non-circular motions of several hundred kms^{-1}. It should be noted that the large gas masses detected in this survey are equivalent to the gaseous inventory of a large spiral (the Milky Way, for example has about $\sim 10^{10}M_{\odot}$ in atomic form; Sanders *et al.* 1984). For $10^{9-10}M_{\odot}$ to collect at the centre of a large spiral within the dynamic timescale of a tidal collision ($\sim 10^{8}$ years) implies infall velocities in excess of 50 kms^{-1} (Mirabel 1992). Intriguingly, within the sample of Mirabel and Sanders (1988) there *is* a systematic offset between the HI systemic velocity and the optical redshift. This is of order 90 kms^{-1} and could well be interpreted as evidence for infall. The issue is, however, somewhat less clear-cut because, as we shall see shortly, emission-line gas is also known to be expanding out of the centre of many FIRGs and this could be partly responsible for the observed difference in velocity.

FIRGs are now known to contain as much **molecular** gas as they do atomic gas (Sanders *et al.* 1991; Mirabel *et al.* 1990). For comparison, the Milky Way has about 40% in molecular form (Sanders *et al.* 1984). The strong association between molecular gas within our own galaxy and sites of recent star formation help us understand why FIRGs are so rich in molecular gas. Molecular gas is most abundant in regions of enhanced gas density which, by the same token, are congenial to the creation of new stars. Perhaps the most striking feature about the molecular gas in FIRGs is that the bulk of H_2 is concentrated in the inner kpc, where it is available for star formation (Scoville *et al.* 1991).

There are certain caveats associated with the estimation of molecular gas in external galaxies. In particular, the brightness of the J=1 $\rightarrow$ 0 CO rotation line, which is used to determine the molecular hydrogen abundance, may well vary according to the physical environment of the gas. The uncertainty introduced by the conditions of the gas is still a matter of controversy although most workers in the field seem to feel that it should not be too great (Mirabel 1992; although see Gledhill (1987) and Aalto *et al.* 1995 for alternative viewpoints). The detection of HCN in several FIRGs confirms that a large proportion of the molecular gas in FIRGs resides in an extreme environment (Solomon *et al.* 1992). HCN emission tends to characterize molecular gas in a very high density phase ($\geq 10^4 \mathrm{cm}^{-3}$ as opposed to $\sim 10^{2-3} \mathrm{cm}^{-3}$ for CO emission). FIRGs contain at least ten times more of this high density gas compared with our own galaxy.

Presently, I wish to turn my attention to M82 which, by virtue of its proximity, lends itself to a closer inspection of the starburst interior. Before doing so, however, I address briefly the issue of *ultraluminous* infrared galaxies and how they relate to starburst activity.

1.2.1 Ultraluminous Infrared Galaxies

Within the literature a distinction is usually made between FIRGs and the more energetic far-infrared phenomena discovered by IRAS. Galaxies with FIR luminosities $> 10^{12} \mathrm{L}_{\odot}$ are generally thought of as ultraluminous infrared galaxies (Lonsdale 1993). In some cases these objects have been positively identified with high redshift objects such as quasars (Hines *et al.* 1995) but for a large fraction there is still some controversy about whether they are powered by recent star formation, an AGN or by both (Lonsdale 1993). If star formation is indeed the primary energy source within these ultraluminous sources then the rate at which stars are being formed is astonishingly large ($\sim 100 \mathrm{M}_{\odot} \mathrm{yr}^{-1}$). A starburst of this magnitude might appear to deplete its gas reserves on timescales that are unlikely to be observed but the discovery of very large amounts of (dense) gas at the centre of ultraluminous infrared galaxies means that we cannot preclude the possibility of a pure starburst 'engine' (Mirabel 1992). Indeed, many authors prefer this interpretation because ultraluminous far-infrared galaxies behave as more energetic versions of starburst-powered FIRGs (Armus *et al.* 1989).

It should be pointed out that evidence for AGNs amongst FIRGs is not particularly common although composite systems (starburst+seyfert), falling under the FIRG classification, *do* occur (e.g. NGC 1068; Lester *et al.* 1987; Telesco *et al.* 1984). It appears that even amongst known 'composites', the properties of the galaxy in question tend to be dominated by young stars. For example, Telesco *et al.* (1993), who imaged a sample of FIRGs in the mid-IR, found that emission was cospatial with recent star formation even amongst those galaxies known to harbour a Seyfert 2 nucleus. Similarly, Baum *et al.* (1993) concluded that the radio continuum emission detected in their sample of 13 Seyfert 2's arises from circumnuclear star formation rather than a compact source. In connection with this point, it should be noted that emission-line diagnostics often fail to provide an unambigu-

ous distinction between different types of activity because high velocity gas can be detected in both Seyfert 2's and starburst galaxies (Armus *et al.* 1989). The corollary to recognizing that star formation may dominate the properties observed in composite systems, is that highly obscured, radio-quiet Seyfert 2's could remain undetected in some FIRGs.

1.3 The Nearby Starburst in M82

It has frequently been termed 'the archetypal starburst galaxy' and with such a wealth of observational data to its name, M82 deserves some special discussion. I wish to emphasize from the outset, however, that in giving this galaxy individual attention I am not implying that it provides the metaphorical blue-prints for far-infrared galaxies or starburst galaxies as a whole. Whilst many of the phenomena associated with M82 have subsequently been discovered in more distant starburst galaxies, astronomers will have to wait until details for a more complete sample are in place before they know how typical, or indeed how archetypal, this nearby (3.25 Mpc; Sandage and Tammann 1975) FIRG really is.

Since its early identification as a highly disturbed galaxy experiencing some kind of 'explosion' (Burbidge *et al.* 1964 and references therein), M82 (or NGC 3034) has been studied in considerable detail at various wavelengths. To elucidate the description that follows I have included in figure 1.1 the compilation of data presented by Telesco (1988). Most of the observations compiled in this figure are either annotated or described in the caption.

At $\geq 10\mu$m, M82 is characterized by a 'ridge' of emission which extends along the disk and occupies the central 500 pc of the galaxy. This feature can be associated with a starburst region which radiates 3×10^{10} $L_{\odot}$ longward of 3μm (84% of its bolometric luminosity) and is generated by young hot stars heating the surrounding dust (Telesco 1988). The starburst was probably initiated by a close encounter with M81, which lies only 36 kpc away on the plane of the sky (Cottrell 1977). A closer inspection of the central 10μm emission reveals a clumpy structure resolved into two dominant peaks separated by $15 - 20''$ (a few hundred parsecs). These two maxima, which constitute the most intense recent star formation in the galaxy, straddle, rather asymmetrically, the brightest 2μm source detected in the galaxy. The 2μm peak occupies the kinematic, and hence gravitational, centre of M82. The western 10μm lobe has been resolved into two local maxima by some authors (e.g. Achtermann and Lacy 1995 at 12.8μm). One of these maxima appears to be a particularly active region of the starburst. It is bright in the radio continuum and is visible as a second 2μm peak in the galaxy.

Large concentrations of atomic and molecular gas appear to surround the starburst in M82 in what could be interpreted as a gas ring or torus (Loiseau *et al.* 1990). It is possible that this neutral material may rotate around the centre of the galaxy although according

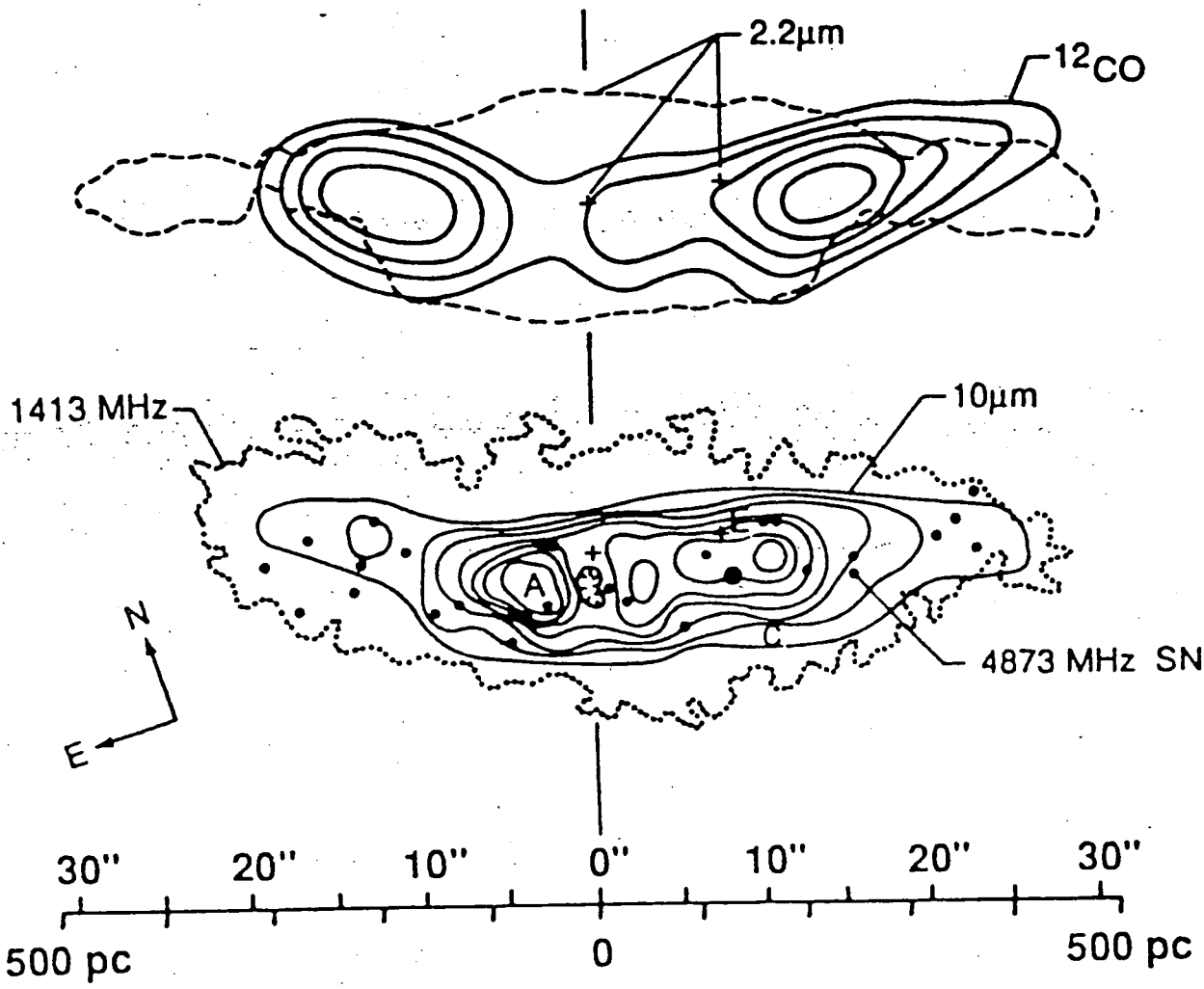

Figure 1.1: The starburst in M82. A compilation of observations taken from Telesco (1988). Data are given for the the near-IR, mid-IR, radio continuum and CO rotation line. 'A' and 'E' are regions of the starburst which are partly visible from the ground. In general, however, the young stellar population is obscured at optical wavelengths by large amounts of dust. The horizontal axis shows the distance in parsecs from the gravitational centre of the galaxy.

to Lo *et al.* (1987) the kinematic data are more complex. At the limb-brightened edges of the ring, small faint spurs of neutral gas extend away from the starburst along the minor axis. This may be associated with inflowing or outflowing material. The region enclosed by the gas torus is pervaded by ionized gas and, judging from the strength of the Brγ line, this hot phase has a volume filling factor of nearly unity (Seaquist *et al.* 1985). Hughes *et al.* (1994) carried out 450μm imaging of the cool dust at the centre of M82 using an improved resolution of 15″. Intriguingly, they identified an emission structure similar to the gas torus mentioned above. They also note the presence of faint spurs extending away from the disk. This dusty torus resides between the ring of molecular gas and the ionized gas of the starburst.

Within the interior of the putative gas torus, super starclusters have been seen directly by ground-based optical telescopes. The centre of M82 is heavily reddened by dust lanes running perpendicular to the disk but, where the obscuring material is somewhat thinner, bright clumpy star forming regions become apparent (O'Connell and Mangano 1978). These less obscured features show structure on the scale of a few arcseconds. O'Connell *et al.* 1995) used the planetary camera on board HST to resolve the star forming regions into a multitude of super starclusters (over 100). Each of these objects is typically only 0″.2 (3pc) in size but has an average luminosity in excess of the brightest star forming region in the Local Group (30-Dor in the LMC). Objects of a similar size have been discovered in HST images of other starburst galaxies (§8.1) and have been identified with young globular clusters (Conti and Vacca 1994; O'Connell *et al.* 1994). The majority are, however, intrinsically brighter than those at the centre of M82 (by about an order of magnitude).

Evidence that the superclusters in M82 contain very massive (and hence very young) stars comes from FIR fine structure lines emitted by the ionized gas. The strength of the doubly ionized oxygen line (52μm) can be compared with emission in the Brα line to derive a temperature for the stars exciting the ISM. Using this technique, Duffy *et al.* (1987) conclude that the starburst in M82 is dominated by stars with an average temperature of 35,000 K. This corresponds to an O8.5 spectral type. The flux at 52μm can be reproduced by 5×10^5 of these early type stars - an abundance sufficient to account for most of the bolometric luminosity in M82. Presumably there is some uncertainty in this analysis due to inexact knowledge of the extinction affecting the centre of the galaxy.

Bregman *et al.* (1995) used the high resolution imager onboard ROSAT to study M82. In addition to point sources close to the nucleus (probably attributable to x-ray binaries or young supernovae), they detected diffuse emission from hot ionized gas situated both inside the starburst region, as we would expect, and most astonishingly **along the minor axis**. Emission along the minor axis is bipolar and extends up to 5-6 kpc from the disk. A similar result had previously been found by Watson *et al.* (1984) using EINSTEIN. Images of M82 in the Hα line are characterized by a similar morphology although the emission-line gas is not detected so far from the disk (up to 2 kpc). These unusual observations can be explained if one assumes that hot gas is escaping from the starburst in a bipolar outflow.

Similar phenomena have been detected in several other starburst galaxies in the last few years, including systems not classified as FIRGs (§6.7). The outflow of hot gas has been termed **the superwind** and it is now described in some detail because of its relevance to observations made in this thesis.

1.4 The Superwind

The theoretical framework describing the effect of individual supernovae or a collection of supernovae exploding in the gaseous disk of a galaxy has already been in place for a number of years. It has, for example, been used to explain HI 'holes' and 'shells' in our own galaxy (Heiles 1990) and forms an integral feedback effect in some models of galaxy evolution (White and Frenk 1991). Chevalier and Clegg (1985) were perhaps the first to examine analytically the connection between high star formation rates in starburst galaxies and the onset of a galactic-scale wind through the collective effect of supernovae (SNe).

In essence, a galactic-scale wind or superwind will occur when the kinetic energy of SNe, plus the winds from their massive star progenitors, is efficiently thermalized rather than lost to radiation. This can occur, for example, via shocks during the collision of ejecta (Heckman *et al.* 1990; Leitherer *et al.* 1993). Under these energy-conserving conditions a bubble of hot ($\leq 10^8 K$) ionized gas is created in the injection (starburst) region which is overpressurised with repect to the ambient (non-starburst) ISM. The bubble of hot gas expands in a direction along the steepest pressure gradient, usually the minor axis, where it pushes against the ambient gas of the disk and halo. As the ambient gas is swept up by the hot gas of the superwind, a thin shell of denser, ambient gas situated at the interface of the two media, is shocked. At a few times the scale height of the disk, the presence of a tenuous superwind fluid beneath the denser medium of halo gas becomes unstable (a 'Rayleigh-Taylor instability') and the shell of swept-up material fragments so that the superwind fluid can escape into the intergalactic medium. The shell of shocked ambient gas is expected to be a bright source of optical emission lines and soft x-rays. The hot superwind fluid, on the other hand, is expected to emit most of its radiation as hard x-rays ($>$ 1keV) as it undergoes internal shocks.

The first indications that superwinds are operating in starburst galaxies came from studies of M82 (§1.3). This galaxy exhibits a remarkable filamentary bipolar nebula along its minor axis which is visible in both optical emission lines as well as soft x-rays (McCarthy *et al.* 1987 and Watson *et al.* 1984 respectively). Since that time, observations have extended to many other galaxies which show evidence for high star formation rates, in particular to far-infrared galaxies (FIRGs). Armus *et al.* (1990) obtained Hα emission-line images of 40 FIRGs and the majority showed evidence for diffuse emission-line gas extending several to tens of kpc beyond the starforming regions. Loops and filaments characterize the ionized gas in a manner that corresponds strikingly well to the thin shells

of shocked gas predicted by the superwind model (Suchov *et al.* 1994). Amongst the edge-on disk systems that were observed, there was a preference for outflow along the minor axis. This axis offers least resistance to hot gas attempting to escape from the starburst.

An important spectroscopic study carried out by Heckman *et al.* (1990) confirmed that the emission-line nebulae described above are expanding away from the starburst. Optical spectra were obtained for 13 FIRGs by placing a long narrow slit along the regions of diffuse Hα emission. Most of the spectral profiles were double-peaked indicating expansion velocities of typically 200-600 kms^{-1} (or up to 1000 kms^{-1} for very energetic FIRGs). The doppler-shifted emission-line radiation appears to arise from shocked gas expanding along the edges of a bipolar bubble or bi-cone. The shocked gas is too dense ($\sim 10^2$cm^{-3}) to belong to the superwind fluid itself, but exists rather as a thin shell expanding with the superwind. These observations are consistent with hot gas expanding into denser ambient medium which it then entrains through the action of low velocity shocks.

The outflow in M82 has been modelled in considerable detail through studies of spectroscopic data (see McKeith *et al.* 1995 and references therein; Axon and Taylor 1978). A position-velocity diagram, taken from the recent spectral study by McKeith *et al.* (1995), is shown in figure 1.2. Open circles denote the peak velocity of various emission lines (e.g. Hα) relative to the systemic velocity. To obtain these data a spectral slit, $1.5'' \times 4'$, was placed along the minor axis of M82 (P.A.=150°). Solid circles, in the same plot, show velocity measurements of the stellar CaII absorption triplet. They were obtained in the same manner as the emission-line velocities and may be relevant to the issue of scattered light in the halo of M82 (§2.2.1). The velocities in figure 1.2 imply that an outflow is taking place along the minor axis (almost perpendicular to the line of sight). Inflexion points in figure 1.2, at about 300pc above and below the galactic plane (dotted lines), suggest that the outflow has an 'hourglass' shape. McKeith *et al.* claim that for $\mid z \mid \leq$ 300pc, energy injection from the starburst causes the superwind to accelerate. For $\mid z \mid >$ 300pc the outflow tends to a constant velocity and can therefore be described as free. Figure 1.3 is schematic diagram of this interpretation (also taken from McKeith *et al.*). The Roman numerals in this figure cross-correlate with those in figure 1.2. The small central ellipse corresponds to the main CO concentration in M82 (figure 1.1) and approximately delineates the starburst region. Apparent velocities of the emission-line gas are annotated in kms^{-1}.

In addition to optical emission lines, galactic-scale outflows can be expected to produce soft x-rays from shocked ambient gas ($<$ 1 keV) and possibly a hard x-ray component (several keV) from internal shocks in the hot superwind fluid itself. X-rays have indeed been detected by EINSTEIN and ROSAT, although most information comes from a small number of nearby starburst galaxies such as M82 and NGC 253 (Watson *et al.* 1984 and Pietsch 1993 respectively). More detailed information is beginning to appear for a larger sample of galaxies (Fabbiano *et al.* 1990; Armus *et al.* 1995) and should continue to do so in the near future. Although interpretation of the x-ray data is not yet settled (probably because ROSAT's high resolution imager provides very little spectral information), it

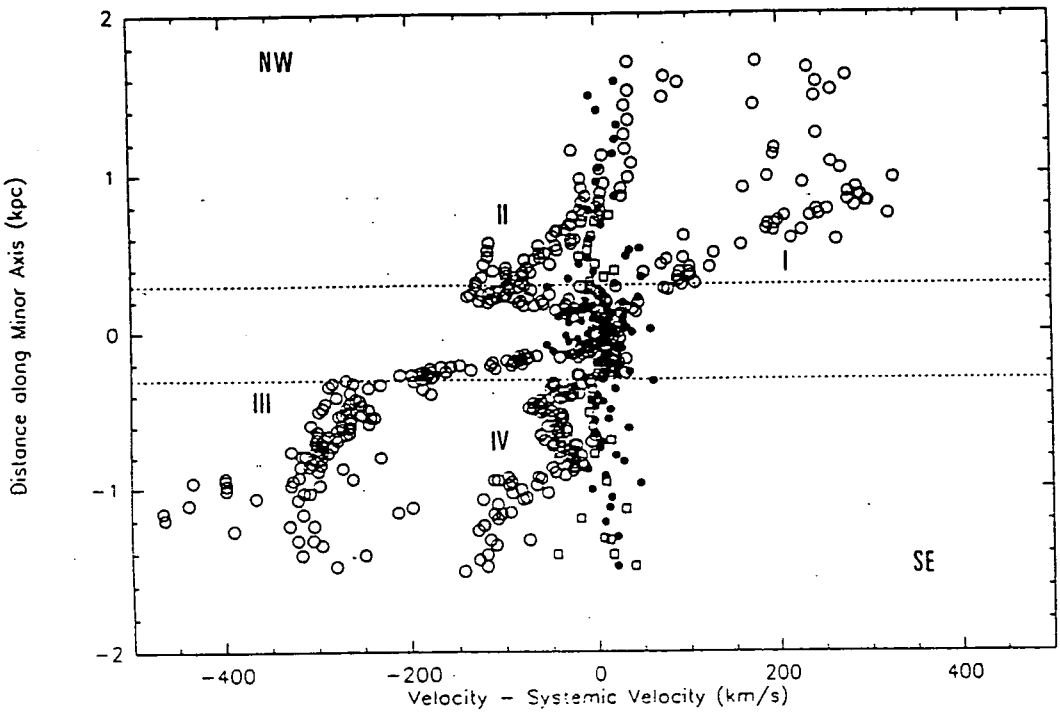

Figure 1.2: A position-velocity diagram for the emission lines detected along the minor axis of M82 (taken from McKeith *et al.* 1995). Open circles denote measurements for Hα, Hγ, N[II], S[II] and S[III]. Solid circles correspond to velocities obtained from the CaII absorption triplet. See text for further details.

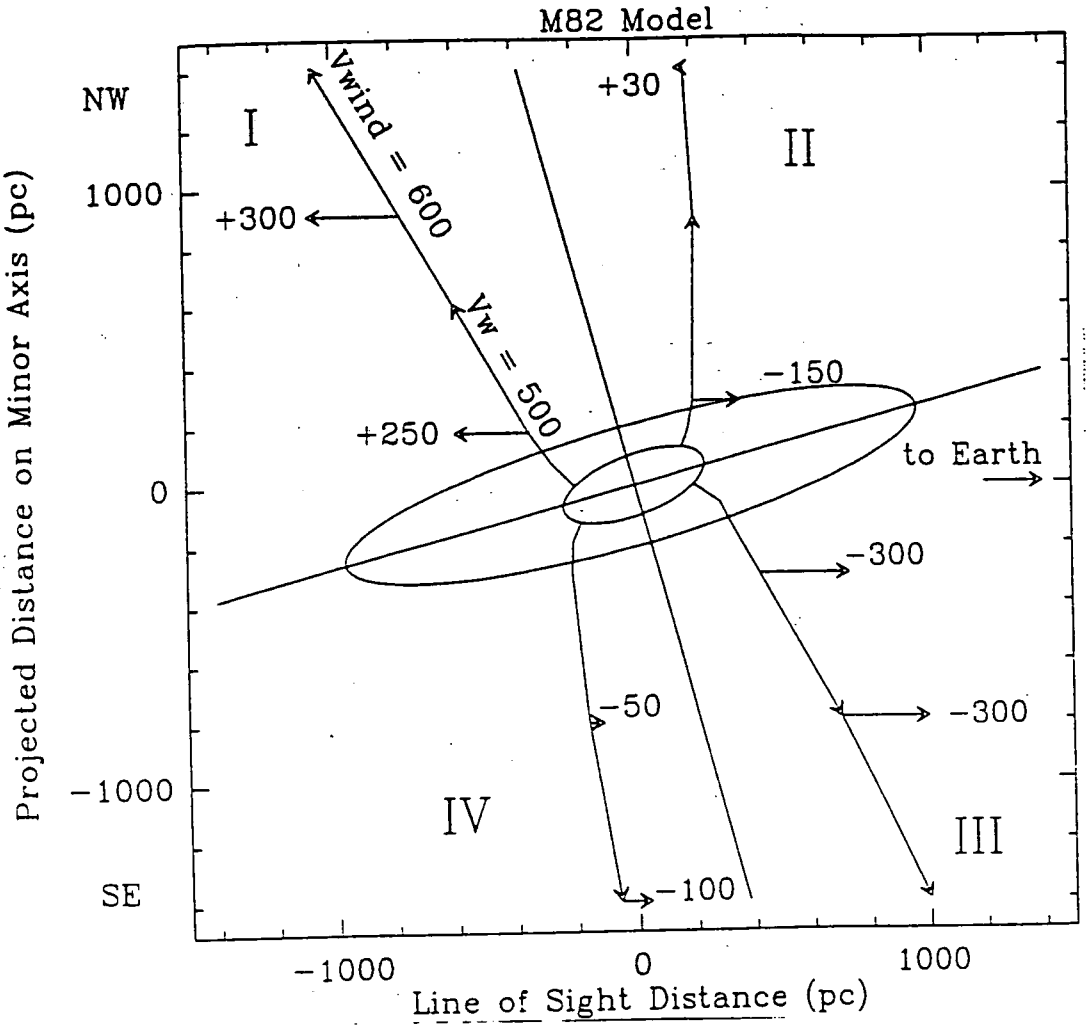

Figure 1.3: A schematic interpretation of the emission-line velocities plotted in figure 1.2 (taken from McKeith *et al.* 1995). The Roman numerals cross-correlate with those in figure 1.2. The velocity of the outflow, both radially and along the line-of-sight, is annotated in kms^{-1}.

appears that a soft component of x-rays does indeed originate from a filamentary nebula resembling that seen in emission lines. In NGC 253 this structure extends up to 10 kpc from the the disk (Pietsch 1993). In harder bands (> 1keV), emission appears to originate mostly from point sources, such as x-ray binaries, and from very hot ($\sim 10^8$ K) diffuse gas in the starburst region itself.

1.5 Summary

It is instructive to summarize our present understanding of FIRGs on the basis of observational data described in the preceding sections. A region at the centre of the disk, several 100 parsecs in length, harbours many young luminous stars contained in densely-populated, compact superclusters. These young stars, in particular the more massive O stars, ionize most of the surrounding ISM but are often difficult to detect at optical wavelengths. This is due to dust which absorbs their energetic emission and reradiates the energy in the FIR. In the mid-IR and radio continuum the distribution of star forming regions at the centre of the galaxy becomes easier to detect. Large quantities of atomic and molecular gas surround the central starburst, sometimes in a ring-like structure. This material has probably collected at the centre of the system under the influence of a gravitational instability and from it new stars are being born. Stars more massive than 8 $M_\odot$ are fairly short-lived and soon end their lives as supernovae. Exploding supernovae, as well as the stellar winds from massive stars, drive hot ionized gas out of the starburst along the minor axis of the galaxy. This phenomenon that has become known as a superwind and its presence can be inferred from x-ray emission and extended emission-line radiation. The latter is caused by the superwind impinging on ambient gas in the disk and halo.

Many of the phenomena summarized above have been detected in galaxies that are not classified as FIRGs but which are, nonetheless, experiencing intense star formation. As mentioned at the beginning of the discussion, the extent to which this is true may begin to become apparent in the course of this thesis.

Chapter 2

Polarization Studies of Starburst Galaxies

2.1 Introduction

There have been very few polarization studies of starburst galaxies. This applies as much to observations in the radio and near-IR as it does to optical polarimetry. A small number of nearby galaxies have been examined using either optical (Ward-Thompson 1987; Scarrott *et al.* 1987; Scarrott *et al.* 1990a) or radio polarimetry (Ruzmaikin *et al.* 1990; Beck *et al.* 1990) but most of the observed objects have been quiescent[1] spirals. In general, the fruits of such investigations have been maps of the magnetic field in the observed system. At radio wavelengths, polarized emission arises from electrons gyrating around the magnetic field in the disk (synchrotron radiation) whereas polarized optical radiation results from interstellar dust grains aligned in the same field (§2.3.3). In a very recent development, some radio astronomers have turned their attention to the superwind region of some starburst galaxies (Reuter *et al.* 1995; Carilli *et al.* 1992). In some cases, radio emission originates from relativistic electrons that have left the starburst in the outflow and now gyrate around a poloidal magnetic field (field lines directed radially outwards). This unusual magnetic field is most probably generated by the superwind itself (Hummel and Dettmar 1990) and its configuration is deduced from the polarization of the radio emission.

Optical polarization studies of starburst galaxies have, until very recently, been restricted almost exclusively to M82. The polarization properties of this nearby galaxy have been known for some time now although it is probably fair to say that the polarization data throw up as many questions as they answer. M82 has been the inspiration for an ongoing project undertaken by the Durham Optical Polarimetry Group. The intention has been to gather polarimetric data for a larger sample of starburst galaxies. The author's contribution to the study is described by this thesis. In this chapter, I summarize the primary aims and observational techniques of the project. At the time of writing the publications

[1] non-starburst/non-AGN

resulting from the study are: Scarrott *et al.* (1991a) for M82; Scarrott *et al.* (1993) for NGC 1808; and Alton *et al.* (1994) for NGC 3125. Results published for M82 and NGC 1808, which predate most of the work in this thesis, are discussed below. Observations for NGC 3125 are presented as part of this work in §7.3.

2.2 Previous Studies

2.2.1 M82

Polarization studies of M82 have been carried out in both the optical continuum and in the Hα emission line. Both sets of observations tell us something different about this unusual galaxy.

M82 has been the subject of several polarization studies in the optical continuum (Schmidt *et al.* 1976; Bingham *et al.* 1976; Chesterman and Pallister 1980). This edge-on (i$\simeq$ 80°) galaxy has a halo of polarized light extending for a kiloparsec or so above and below the plane of the disk. The polarization pattern is fairly smooth and is generally associated with scattering from copious dust clouds surrounding the galaxy. One can infer from the direction of polarization that the dust is illuminated by stars both in the disk and in the star-forming regions of the nuclear region. The red photometric colours of M82, and the dark lanes that cross the disk, are consistent with prodigious quantities of dust outside the disk (Sandage 1961).

The possibility that the polarized optical continuum arises from high energy synchrotron emission has been discounted on the grounds that polarized emission lines are also observed in the halo. This suggests that scattering provides the polarizing mechanism. Dust grains must almost certainly provide the scattering surface because electrons cannot reproduce the scattered light without producing far more recombination radiation than is actually observed (Solinger 1969; see also §9.2). Polarization levels in the optical continuum are typically 10-15% but they may reach up to 30% in regions further away from the disk. Also of note, is the fact that the polarization levels in red light are somewhat lower than those measured in the blue. The reason for this is not yet clear although some suggestions are given in the concluding chapter of this work (§10.2.2).

Whilst the general consensus appears to be that the scattered optical continuum originates mostly from the disk of M82 (Solinger and Markert 1975), the case for reflected emission-line radiation is less clear. As noted in §1.3, emission-line images of M82 are characterized by a kpc-scale bipolar nebula which is composed of filaments and loops of shocked gas - the fingerprint of a galactic outflow or superwind. It was Bland and Tully (1988) who suggested that the spectroscopic profile of the emission line region actually consisted of two components. One component is satisfactorily accounted for by hot gas expanding along the sides of a cone. Superimposed on this is a broad component (FWHM

$\sim$ 300kms^{-1}) which lies close to the systemic velocity of the galaxy. It is not created *in situ* but must be scattered from somewhere in the disk, probably the star forming nucleus which is known to be a bright source of emission-line radiation. Intriguingly, the broad component is still visible in spectra taken outside the superwind region although it appears to become more faint there.

Scarrott *et al.* (1991a) have confirmed, with an Hα polarization map of M82, that there is indeed a scattered emission-line component in the halo and that it is cospatial with the region of outflow. The authors claim that the scattered light originates from a compact region of the starburst, probably the active region to the west of the gravitational centre, which forms a secondary maximum at 2μm (§1.3). Polarization levels are approximately 10-30% suggesting that a significant proportion of the emission-line radiation is scattered rather than created *in situ*. Since filamentary structure is not evident in the scattered continuum, Scarrott *et al.* argue that the scattered component of the emission-line nebula results from variable illumination rather than dust inhomogeneities in the halo. They propose that high velocity dust clouds eclipse the starburst as they move through the nuclear region leading to variable illumination of the scattering material.

McKeith *et al.* (1995) also claim to have measured a scattered component in the emission-line region of M82. Returning to figure 1.2 of the last chapter, one notes that, in distinct contrast to the emission-line profile, the CaII absorption triplet (denoted by solid circles) remains at the systemic velocity all the way along the minor axis. The authors attribute this absorption feature to late-type stars in the disk. The light they emit is scattered by dust residing in the halo. One puzzling aspect to the scattered component is its observed velocity. It can be shown quite easily that, for dust moving radially away from the starburst (perhaps entrained in the outflow), the nuclear light that it scatters will be redshifted when it reaches the observer at earth (Sanders and Balamore 1971). This is because the speed with which the dust moves away from the centre will always exceed the speed with which the dust approaches the observer. Since the scattered components detected by Bland and Tully (1988) and by McKeith *et al.* (1995) are neither significantly redshifted nor blueshifted it would appear that the dust is **not** moving radially. It must have a significant velocity component parallel to the plane of the disk or in fact be stationary. If the dust is not moving (or is moving very slowly) one has to ask how it came to be at least one kiloparsec outside the disk. Clearly spectro-polarimetry is required to clarify the situation.

2.2.2 NGC 1808

The barred Sersic-Pastoriza (§1.2) spiral galaxy NGC 1808 was observed by the Durham Imaging Polarimetry Group as part of a continuing polarimetric study of M82-like objects i.e. FIRGs with known outflows (Scarrott *et al.* 1993). The outflow in NGC 1808 has been described in some detail by Phillips (1993). The optical polarization pattern of this star-

burst galaxy is characterized by a spiral pattern in the disk and most intriguingly, a huge reflection nebula cospatial with the inner kpc of the outflow region. The spiral pattern in the disk arises from grains aligned in the magnetic field and a similar effect has been observed in several nearby spiral galaxies (§2.3.3). The detection of scattered light along the minor axis is quite unusual and can really only be compared with the phenomenon in M82. Polarization levels in the scattering region of NGC 1808 are lower than those measured in M82 ($\sim$ 3% c.f. $\sim 10 - 15\%$) but this may, at least in part, be due to the difference in inclination angle between the two galaxies ($\simeq 80°$ against $\simeq 57°$). Higher inclination angles will lead to a greater dilution of scattered light with unpolarized stellar light from the halo and disk.

The outflow region in NGC 1808 is already known to be dusty from the colour maps produced by Phillips (1993). His B-R image shows sheets and filaments of dust leaving the starburst region and occupying the minor axis of the galaxy. Some of the filaments extend up to 3 kpc from the plane of the disk. The dust giving rise to the polarized scattered light appears to be cospatial with the lower part of these dust filaments. It is illuminated by the nucleus and star forming hot-spots in the central few hundred parsecs of the galaxy (Scarrott *et al.* 1993). I shall return to the nature of the dust filaments in NGC 1808 when discussing the observations carried out in this thesis (§10.2).

2.3 Present Study

The primary aim of this project is to discover how the polarization properties of starburst galaxies relate to the unusual phenomena that otherwise characterize these systems (e.g. high star formation rates, the superwind etc.). One issue that might also be addressed is the frequency with which galactic-scale reflection nebulae, like those observed in M82 and NGC 1808, occur amongst affiliated systems. I begin by discussing the techniques used to image starburst galaxies in polarized light. I then present a short resumé of the mechanisms capable of producing polarized light in galaxies. The galaxies observed for this thesis are all starburst galaxies. Three of them are FIRGs (§1.2), a fourth is a dwarf irregular but might be considered as a FIRG on the basis of its high FIR-to-blue luminosity. The remaining two galaxies are low mass emission-line objects called blue compact dwarf galaxies.

2.3.1 Observational Technique

Light is a transverse wave which possesses an electric field oscillating at 90° to the direction of propagation (see, for example, Hecht 1987). For natural or unpolarized light the oscillations of the electric field, over any appreciable length of time, will be random in the plane of vibration. In contrast, the electric field of linearly polarized light exhibits a preference for oscillation in one particular direction. This preference is expressed by the degree of linear polarization (P) and is conventionally measured as a percentage. Thus:

$$P = \frac{100}{I} \times (Q^2 + U^2)^{\frac{1}{2}} \tag{2.1}$$

where I is the total intensity of the light and Q and U are the Stokes Parameters defined thus:

$$Q = I_0 - I_{90} \qquad U = I_{45} - I_{135} \tag{2.2}$$

Here, I_θ refers to the intensity of light vibrating with position angle θ in the plane of vibration. The direction of polarization, ϕ, can be calculated from:

$$\tan 2\phi = \frac{U}{Q} \tag{2.3}$$

and is defined in the same reference frame as θ. One other relevant quantity is the polarized intensity (PI) which is the fractional polarization ($\equiv \frac{P}{100}$) multiplied by the total light intensity:

$$PI = \frac{P}{100} \times I = (Q^2 + U^2)^{\frac{1}{2}} \tag{2.4}$$

The total intensity, I, is given by $(I_0 + I_{90})$ or, equivalently, $(I_{45} + I_{135})$.

The Durham Optical Polarimeter measures the polarization of astronomical objects by measuring I_θ. This is carried out using a Wollaston prism and a half-wave plate (see figure 2.1). The Wollaston prism splits the light entering the telescope into two beams. The electric field of the two beams are mutually perpendicular - they correspond to I_0 and I_{90} (or I_{45} and I_{135}) - and they diverge by about one degree when leaving the prism. This dual beam is focused onto a blue-coated CCD chip. To avoid the overlapping of images on the chip, a mask is present before the polarization optics. This blocks out alternate strips of the telescope image (see figure 2.2). The position angle, θ, is controlled by a retardance device known as a superachromatic half-wave plate (Draper 1987). This rotates the polarization of the light before it is incident on the prism. In this way the light intensity at all four angles (0°, 90°, 45° and 135°) can be measured. A more complete description of the optics in the Durham Optical Polarimeter is found in Scarrott *et al.* (1983).

In general, the intensities I_θ, defined above, are measured twice. The position angles of the dual beam are exchanged between exposures to account for any (small) difference between the optical paths of the left and right ray. Since, for any given exposure, two orthogonal states (either I_0 and I_{90} or I_{45} and I_{135}) are recorded, a total of four exposures is required. The mask blocks half of the image incident at the telescope focus. Therefore the telescope has to be moved (usually twice) to image the whole of the target. The mosaic of exposures (4×3) allows the level and direction of polarization, across the whole of the object, to be ascertained. An intensity image is also obtained as a natural 'by-product' of the measurement process. It is important to remember that dual-beam polarimetry can easily correct for variations in the transparency of the night sky whereas the calibration of

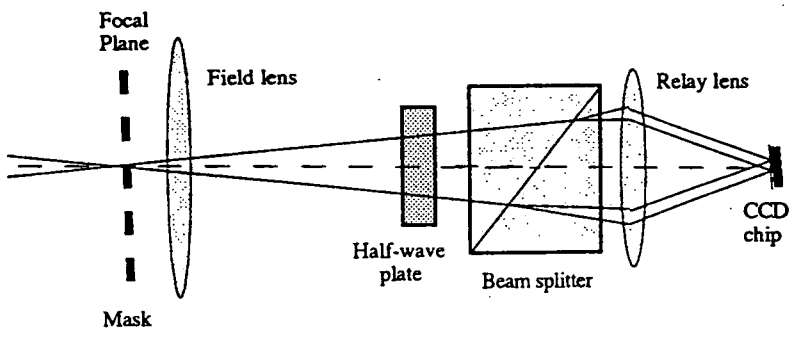

Figure 2.1: The optics of the Durham Imaging Polarimeter (taken from Scarrott 1991). Light from the telescope enters the instrument from the left and is split by a Wollaston prism ('Beam splitter'). The dual beam is focussed onto a blue-coated CCD chip. The polarization angles of the dual beam are controlled by a retardance device known as a half-wave plate.

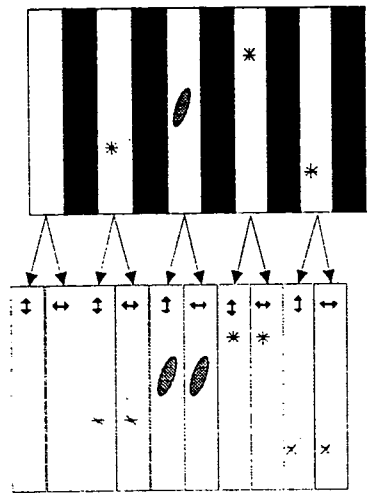

Figure 2.2: The light entering and leaving the polarimeter optics (taken from Scarrott 1991). The figure shows how a mask present at the entrance aperture of the polarimeter (upper image) blocks out alternate strips of the telescope image. The light that is allowed into the instrument is split by the optics of figure 2.1 into two beams which are juxtaposed onto the CCD (bottom image).

single beam polarimetry requires the observation of polarized standards.

The reduction of raw data from the Durham optical polarimeter has been described in detail elsewhere (Draper 1987; Warren-Smith 1979). Therefore I summarize it only briefly here. Object frames from the CCD are flatfielded using flatfield frames obtained during the same observing schedule. The left and right hand beams of all the flat-fielded object frames are then aligned using fiducial stars present in the images. The sky signal is subtracted from the aligned images and then the frames are calibrated to eliminate differences between the two polarimeter channels and variations in the sky transparency. From these calibrated images one obtains the level and direction of polarization across the whole field of view. A suite of computer programs, developed by various (ex-)members of the Durham Optical Polarimetry Group, is available to carry out the reduction procedure outlined above.

2.3.2 Errors in the Measurement

The calculation of errors in two channel polarimetry is complicated. In addition to the usual uncertainties afflicting observational CCD astronomy - photon noise, detector read-out noise, uncertainties in sky subtraction and flatfielding - other considerations have to be made concerning errors which affect both channels of the instrument. The advantage of two channel polarimetry, over direct or single beam polarimetry, is that errors common to both beams may often cancel or exert only minor influence on the final measurement. Even errors affecting the two channels differentially may eventually cancel out because the polarization state detected in each of the beams is exchanged during the measurement process (§2.3.1). The reduction software allows a more complicated error determination to be carried out and this procedure makes *some* allowance for error cancellation. It is thought, however, that even this may fail, at times, to extract the true errors. Despite this rather frustrating aspect to the measurement technique, it seems likely that the true errors cannot lie too far from their calculated value. Sensible signal-to-noise cuts on the data eliminate disordered (non-physical) polarization vector patterns from the sky and object regions. I use the more sophisticated error model, which allows for error cancellation, for the polarization measurements presented in this thesis.

Using the error model discussed above, I compare two sets of observations carried out for one of objects in this thesis (NGC 3125; §7). To this end I define the ratio, r, as:

$$r = \frac{P_1 - P_2}{(dP_1{}^2 + dP_2{}^2)^{\frac{1}{2}}} \tag{2.5}$$

where P_1 and P_2 are the polarization values derived from two independent observing schedules. dP_1 and dP_2 are the respective errors in these measurements. P_1 and P_2 are measured for the same positions on the object. In figure 2.3, I plot r for parts of the object which appear significantly polarized. The light intensity at each measurement position is used to plot the points in the horizontal direction. It would appear, on the basis of figure 2.3, that

the calculated errors, dP_1 and dP_2, give a fair representation of the uncertainty in the measured values. This may be inferred from the fact that most of the points in figure 2.3 lie well inside the region $-1 < r < +1$. If anything, there might be a tendency for the cited errors to slightly overestimate the true errors. One draws a similar conclusion when comparing the polarization angles recorded by independent data sets along with their respective errors.

More generally, independent polarization measurements provide a valuable check on the self-consistency of the data. This is particularly helpful in guarding against systematic errors that may lie outside the error analysis outlined above. For example, it is sometimes possible that the large scale structure of the flatfield is inadequately modelled (although this tends to effect areas towards the edge of the CCD and not the object itself). Caution must also be exercised with respect to the normalization of frames taken at different telecope positions (§2.3.1). The calibration relies on overlapping regions of adjacent frames. If for some reason the amount of overlap is small or, if overlap occurs in regions of the object subject to steep brightness gradients, then the calibration can be significantly impaired. Another irregularity which on occasions is troublesome is the presence of extraneous scattered light entering the instrument. This can occur if the moon is bright or a bright star is close to the field of view. In principle, extraneous scattered light can be removed as part of the sky. Unforseen, systematic errors, similar to those mentioned above, are best identified by careful examination of the images and checks on the self-consistency of the data.

Having expounded on the potential sources of error associated with the measurement technique, I should emphasize that polarizations of only 1-2% can usually be satisfactorily measured by the Durham Optical Polarimeter. This conclusion is based on previous polarimetric studies of galaxies (Ward-Thompson 1987; Scarrott *et al.* 1990a). The ability of the polarimeter to detect such small polarizations is important because, the level of polarization in many galaxies is expected to be fairly low (perhaps only a few percent).

2.3.3 Polarizing Mechanisms Observed in Astronomy

There are three main astrophysical mechanisms that can produce polarized light: (a) scattering from small dust grains and electrons; (b) synchrotron emission from charged particles moving relativistically in a magnetic field; and (c) preferential extinction by dust grains aligned in a magnetic field. These are discussed in turn below.

(a) When light impinges on dust grains that are of the same size, or smaller, than its own wavelength, the scattered beam is likely to be highly polarized (typically $\geq$ 30%). The electric field of the scattered radiation, which conventionally determines the direction of polarization, will generally be polarized at 90° to the scattering plane (i.e. the plane containing the incident and scattered beams) (van der Hulst 1957; Bohren and Huffman 1983). Maximum levels of polarization tend to occur at scattering angles that are close to 90°. The reflection nebulae surrounding young stars (e.g. the Orion Nebula M42) are good examples of light that is mostly reflected by dust surrounding a luminous source. There

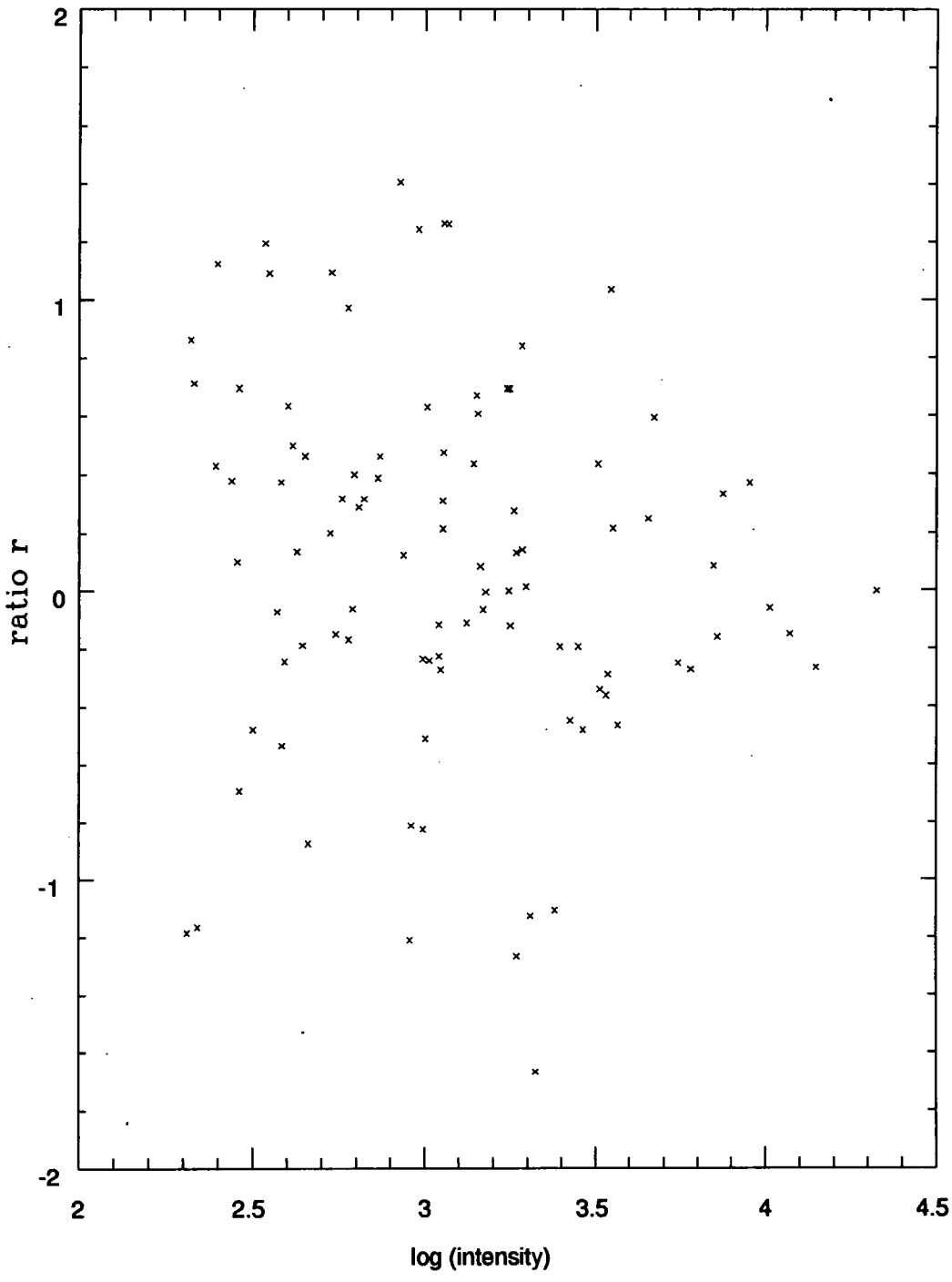

Figure 2.3: A comparison of the polarization recorded by the Durham Polarimeter using independent sets of data. See text for details.

have been several polarization studies of reflection nebulae (e.g. Scarrott *et al.* 1990b; Scarrott 1988).

Scatterers that are very small compared with the wavelength of the incident light (small dust grains and molecules), can induce very high polarizations in the scattered light - up to 100% in fact. This interaction is known as Rayleigh scattering (Hecht 1987). A familiar example of this phenomenon is provided by the blue light that can be seen in a cloudless sky. This is sunlight which has been scattered by molecules in the atmosphere. It is blue because shorter wavelength radiation is scattered more strongly by Rayleigh scatterers than longer wavelength radiation. Scattering by dust grains is discussed in more detail in §9.

(b) At least part of the dust in the ISM takes the form of elongated paramagnetic grains. Under suitable conditions, these dust particles are likely to align themselves with the interstellar (or local) magnetic field in which they reside. The torque which brings about this alignment, is provided by the interaction of the grain's dipole moment with the magnetic field in which it rotates. In the original analysis of this phenomenon Davis and Greenstein (1951) assumed that the rotation or spin of the grain was provided by the collision of gas atoms with the grain. In this case, a necessary condition for alignment is that the grain temperature is much less than the gas temperature so that thermal fluctuations of the dipole do not dominate over the magnetic oscillations that provide the torque. At the same time collisions should not be so frequent that the grains are randomized rather than aligned. The first of these conditions has, in effect, been circumvented by a modification to the spin mechanism. Purcell (1979) suggested that suprathermal spinning may be taking place. In this scenario, hydrogen atoms form molecules on the catalytic surface of grains. The binding energy released by the reaction allows the newly-formed molecule to be ejected causing the host grain to spin up. Grains are known to form coats in dense regions of the ISM and it is within this environment that grains are most likely to be aligned in this way (see Gledhill 1987 for an introduction to the subject).

Given the right conditions then, dust grains can be expected to align themselves with an external magnetic field so that their minor axis is parallel to the field lines. Light possessing an electric field perpendicular to the magnetic field is preferentially absorbed so that a polarization parallel to the magnetic field, is induced into the light that escapes. This process is known as dichroic extinction. The magnetic field of our own galaxy has been mapped out by noting how stellar light is polarized by absorption in the intervening ISM (Matthewson and Ford 1970; Axon and Ellis 1976). Similarly, Ward-Thompson (1987), more recently, traced out the spiral magnetic field in some nearby galaxies by measuring the polarized light escaping from their disks.

The level of polarization induced by aligned grains is generally about 2-3% in the optical waveband. Systematic variations with wavelength have also been observed for aligned grains in our own galaxy and this behaviour is described by an empirical relation

known as the Serkowski Law (Serkowski *et al.* 1975):

$$\frac{P_\lambda}{P_{max}} = \exp\left\{-K \ln^2\left(\frac{\lambda_{max}}{\lambda}\right)\right\} \tag{2.6}$$

where P_λ is the level of polarization at wavelength λ. P_{max} is the peak level of polarization and this occurs at $\lambda = \lambda_{max}$. When P_λ/P_{max} is plotted against λ_{max}/λ (figure 2.4), the spectral dependance of polarization shows an asymmetric peak about P_{max} and the width of the peak is determined by the parameter K. In the original analysis by Serkowski, K was given the constant value of 1.15 (which is also used in figure 2.4), but later refinements of equation 2.6 have allowed this parameter to vary somewhat (Wilking *et al.* 1982). Observationally determined values of λ_{max} tend to be $\simeq 0.55\mu$m but the peak wavelength may shift (typically $\pm 0.2\mu$m) according to the environment of the grains (Wilking *et al.* 1982).

(c) The third polarizing mechanism which is of relevance to astronomical observations is that associated with some high energy phenomena. Supernova remnants (e.g. the Crab Nebula; Hecht and Zajac 1974) and the jets found in some active galaxies (e.g. 3C273; Scarrott and Rolph 1989) can show quite high polarizations ($> 10\%$). In this case, the mechanism responsible is synchrotron radiation emitted by relativistic, charged particles gyrating around a magnetic field (either intrinsic to the object or pervading the ISM). The electric field of the emitted radiation is parallel to the direction of acceleration i.e. perpendicular to direction of the magnetic field.

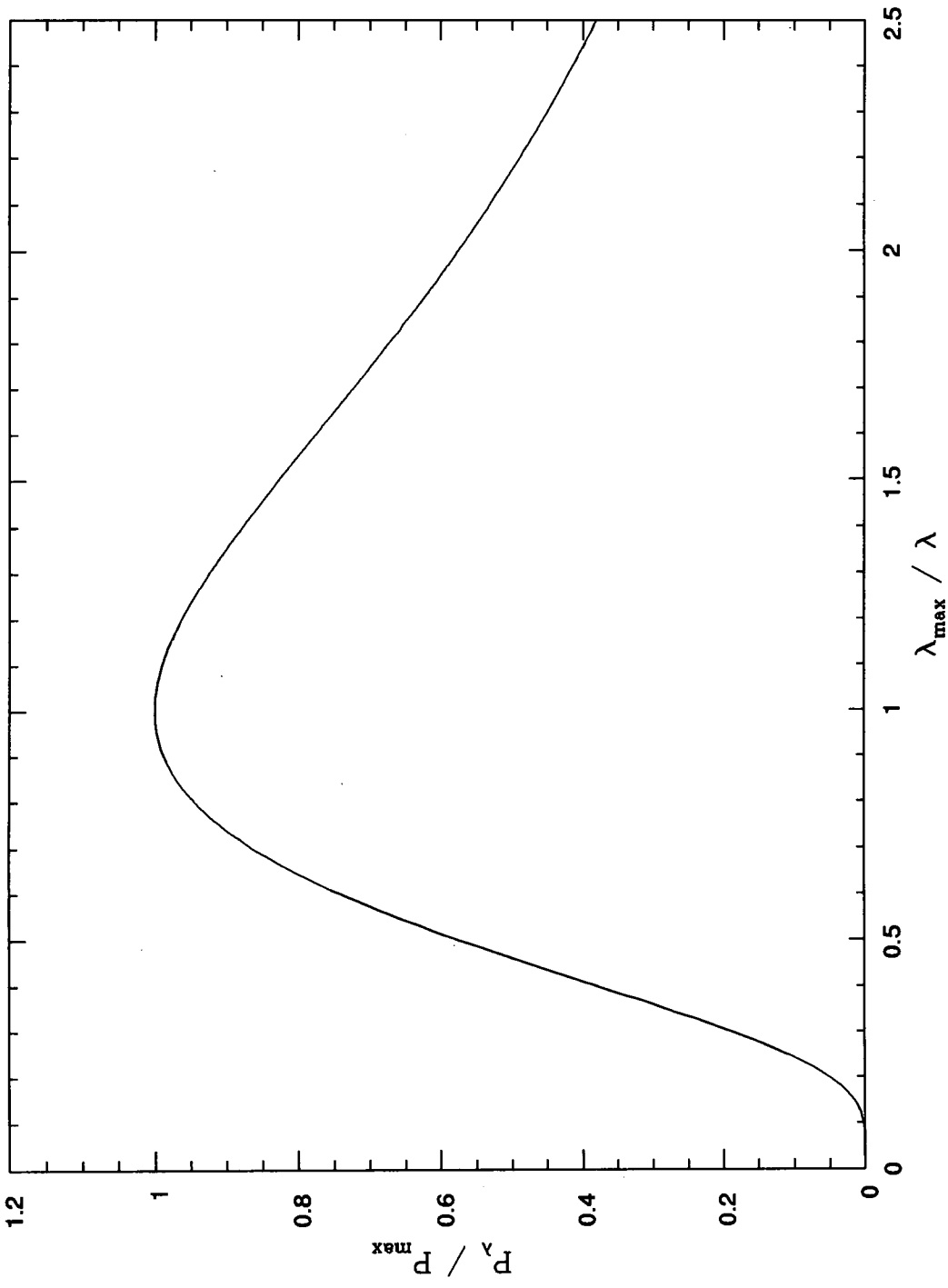

Figure 2.4: The Serkowski Law for aligned interstellar dust grains. See text for details.

Chapter 3

NGC 660

3.1 Introduction

NGC 660 is an almost edge-on (i=70°) barred spiral with a far-infrared luminosity of $2 \times 10^{10} L_{\odot}$ (van Driel *et al.* 1995). It has a FIR-to-blue luminosity of 4.7 suggestive of a low power FIRG (§1.2). Armus *et al.* (1990) identified the nucleus of NGC 660 with a LINER (low ionization nuclear emission region) spectrum. LINERs have optical emission-line ratios intermediate between the photo-ionization models used to described some AGN and the superwind model used to describe starburst galaxies (Heckman 1987; Heckman 1986). Most of the observational data indicate that NGC 660 is undergoing a starburst. NGC 660 constitutes one of three galaxies observed with the Durham Imaging Polarimeter as part of a project to study the polarization properties of far-infrared galaxies. The other two galaxies, NGC 1667 and NGC 1614, are both discussed in the next chapter.

Figures 3.1 and 3.2 show optical continuum images of NGC 660. The V-band image in figure 3.1 was obtained in connection with new observations presented in this chapter. It has a scale of approximately 4′ by 6.5′. Figure 3.2 shows an R-band image of NGC 660 kindly made available by L. Armus from The Palomar Observatory, Caltech. It has an approximate scale of 2.5′ by 2.5′. The images in figure 3.1 and 3.2 are orientated with north at the top and east to the left. A distance of 13 Mpc is adopted for NGC 660 (H_o=75 $kms^{-1}Mpc^{-1}$; van Driel *et al.* 1995). One arcminute corresponds to 3.8 kpc at this distance.

NGC 660 looks perhaps most spectacular when imaged in the Hα emission line. Figure 3.3 is an Hα image also generously provided by L. Armus. It has the same image scale and orientation as figure 3.2. Luminous recombination emission in the nucleus and central disk indicates the presence of recent and prolific star formation. Two fainter curvi-linear structures extend 0.5′ (2 kpc) from the nuclear region in a north-westerly direction. Armus *et al.* (1990) tentatively identify these features with the incomplete or broken sides of an emission-line bubble. In the past, weak emission-line features detected outside the galactic disk have usually indicated the presence of a superwind expanding away from the starburst

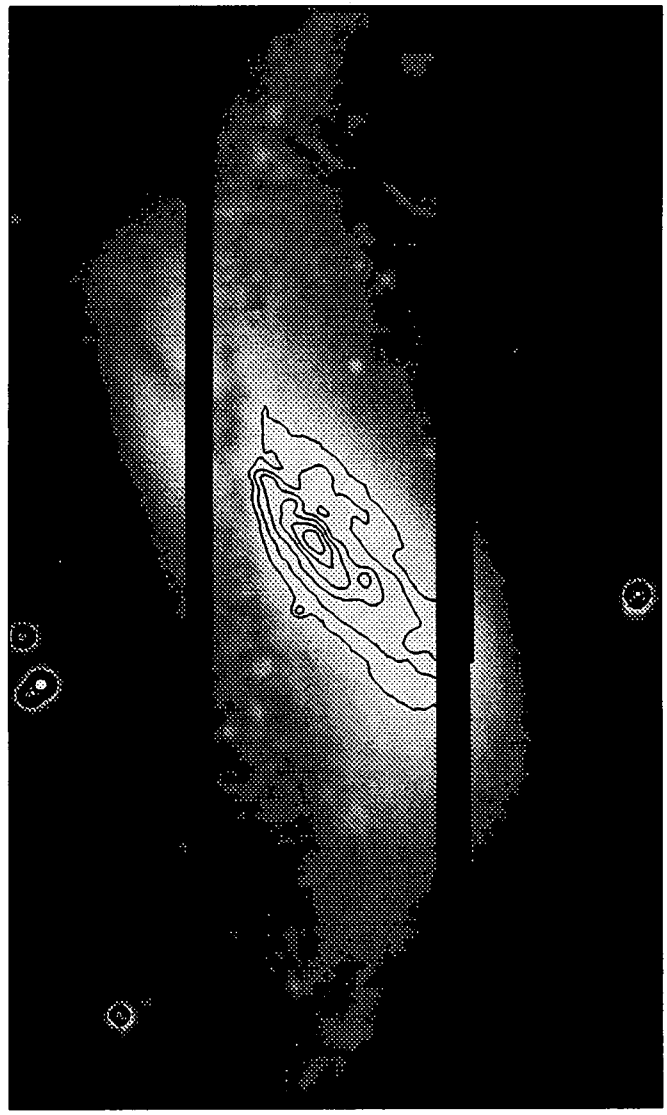

Figure 3.1: A V-band image of NGC 660

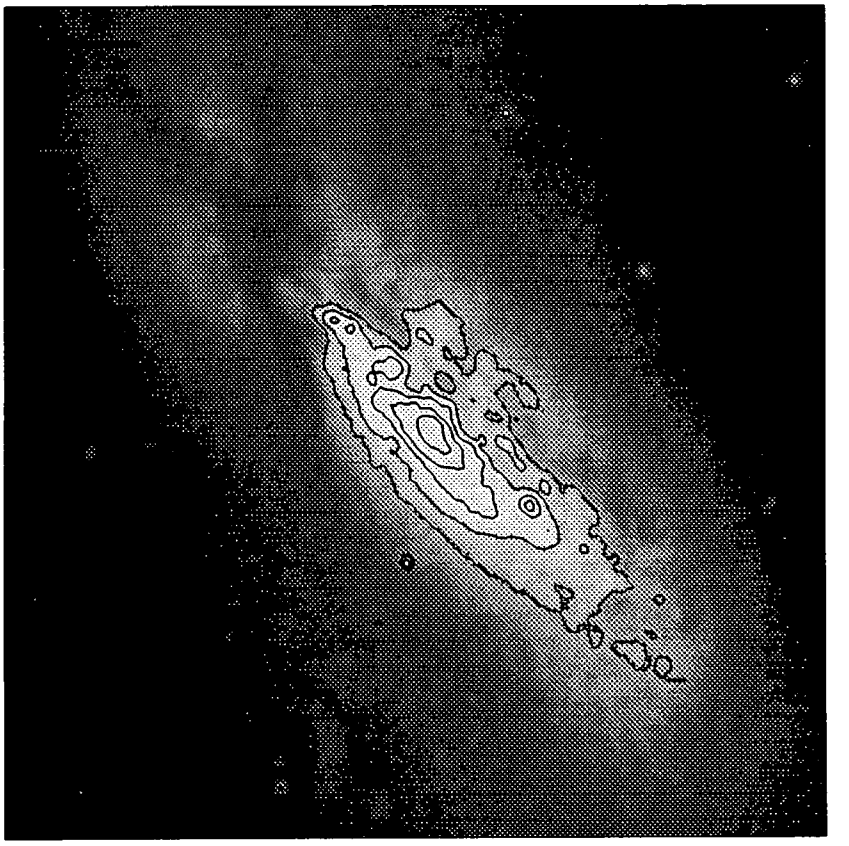

Figure 3.2: An R-band image of NGC 660

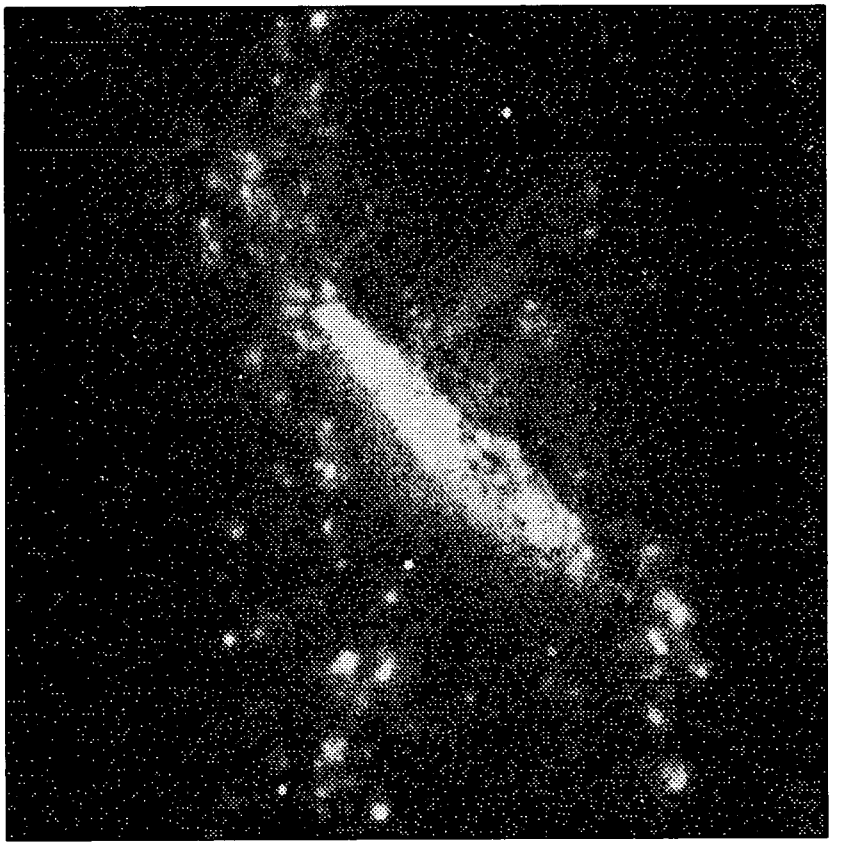

Figure 3.3: A continuum-subtracted Hα (+NII) image of NGC 660

(§1.4). Intriguingly, the first spectrum of NGC 660, taken by Benvenuti *et al.* (1976), shows a steepening Hα velocity gradient as the spectrograph slit is aligned closer to the minor axis. The authors are puzzled by this, but an outflow perpendicular to the disk could almost certainly explain this anomalous behaviour.

Figure 3.3 is also characterized by a collection of HII knots which runs north-south 'grazing' the eastern edge of the disk. The new stars are part of an unusual ring encircling the disk. This impressive feature, described as a 'polar ring' by most authors (despite its inclination), has drawn much attention to the galaxy (e.g. Arnaboldi and Galletta 1993). It has a radius of 12 kpc and is inclined by $45° - 55°$ to the plane of the disk (figure 3.1). Polar rings are rare phenomena believed to form during a close encounter (or merger) of two galaxies (Schweizer *et al.* 1983). In general, the smaller of the colliding systems will be catastrophically disrupted and part of the ruptured material forms rings or shells. The ring in NGC 660 is something of an enigma because its angle of inclination with respect to the disk is not considered stable. Differential rotation along the structure should cause its dissipation on timescales $< 10^9$ years (Combes *et al.* 1992). The colour of the 'polar' ring is blue (V-I$\simeq$1; van Driel *et al.* 1995) suggesting that stars have been forming out of the accreted material. Van Driel *et al.* (1995), however, estimate an overall age of several gigayears for the ring's stellar population by using stellar synthesis models. This is something of a surprise because, as already noted above, copious Hα radiation is detected from some parts of the ring. Furthermore, several gigayears is longer than the predicted stability timescale. I suggest a possible solution to this paradox in §3.3.3.

NGC 660 radiates brightly in the radio continuum. Its morphology has been mapped out with sub-arcsecond resolution by Condon *et al.* (1982) who found that most of the emission was concentrated in a bi-lobal structure centred on the nucleus. This structure is very reminiscent of the gas tori seen at the centre of some starburst galaxies and may indicate enhanced star formation on the inner surface of gas encircling the central starburst (§1.2). The radio spectral index of NGC 660 is fairly steep indicative of synchrotron radiation from young supernova remnants. The radio lobes are separated by about 250 pc.

NGC 660 is gas rich. It contains $5.4 \times 10^9 M_\odot$ of neutral hydrogen and a comparable amount of molecular gas ($3.4 \times 10^9 M_\odot$; van Driel *et al.* 1995). Remarkably, 75% of the HI is found in the 'polar ring' mentioned above. The ring also contains a large molecular component ($\simeq 10^9 M_\odot$). The large gas content of the polar ring suggests that the galaxy which collided with NGC 660 was comparable in mass.

Half of the H_2 detected in the disk of NGC 660 resides in a region less than 1.3 kpc from the nucleus (Combes *et al.* 1992). This high concentration of 'nuclear gas' is a common feature of starburst galaxies (§1.2). Much of the HI component is seen *in absorption* against the continuum radio emission from the nucleus. Although the galaxy is slightly inclined, the disk is warped to such an extent that the true nucleus is obscured by a dust lane (figure 3.2). Neutral gas in the inner few hundred parsecs of NGC 660 is characterized by

strong velocity gradients and possibly non-circular flow (Baan *et al.* 1992). This may be due to the presence of a bar which is detected by van Driel *et al.* (1995) in the near-IR.

3.2 Observational Details

NGC 660 was observed at the f/15 Cassegrain focus of the 1-meter SAAO telescope during November 1993. The Durham imaging CCD polarimeter was used in conjunction with a V filter (550±130nm). In all, 12 CCD frames were obtained each lasting 600 seconds. Exposures were centred primarily on the disk of the galaxy, to ensure adequate signal levels in those regions. As a result, there was not complete coverage of the object which would have been desirable. For those parts of the object that *were* observed there was significant overlap between frames taken at different telescope positions. This allowed the data to be checked for self-consistency.

Two images of NGC 660 were kindly made available by Lee Armus from Palomar Observatory, Caltech. One is taken in continuum-free Hα + [NII] emission (hereafter referenced simply as Hα) and the other is an R-band image (broad-band Mould R filter). Both images have already been presented elsewhere (Armus *et al.* 1990). Registration between the V-band image, which is derived from the polarimetric observations, and the R-band image was possible using fiducial stars. The error in this alignment process is estimated to be less than 1″. The Hα and R-band image were already aligned with each other.

Astrometric calibration was carried out by means of the HST guide star catalogue and the relevant POSS (Palomar Sky Survey) plate. Since none of the stars in the polarimeter's field of view were bright enough for inclusion in the HST catalogue, the POSS plate was calibrated and then the positions of stars common to both the POSS plate and the field of view were determined. Using this procedure, the 1950 equatorial coordinates of the NGC 660 nucleus, as determined from the V-band image, is estimated to be: 01° 40′ 21.72″; +13h 23m 37s (±1″). In galactic coordinates this corresponds to the position: l=141.6°, b=−47.3°.

3.3 Results

3.3.1 Continuum Images

Figures 3.1– 3.3 show images of NGC 660 in V, R and Hα respectively. In all cases north is at the top and east to the left. The scales are 4′ by 6.5′ for the V image and 2.5′ by 2.5′ for the R and Hα images. Contours, separated by roughly half a magnitude, are overlayed onto the brightest regions of the continuum images. The V-band image is incomplete because polarimetric observations were not obtained for all parts of the object (the intensity image is produced by combining images taken in different polarization states). There is also a spurious 'wave-like' feature in figure 3.1 at $\simeq$ 2′ above the disk. This is due to foreign

particles lying in the optical path of the instrument. The emission-line image in figure 3.3 has already been described in §3.1.

The polar ring, discussed in §3.1, is best appreciated by inspecting figure 3.1. It runs north-south crossing the disk at about 50″ north-east of the nucleus. The diameter appears to be about 6.5′ or 25 kpc. The disk of NGC 660 is most clear in the R-band image of figure 3.2. Although the morphology is somewhat 'warped', the prominence of a dust lane north-west of the nucleus suggests that this is the near side.

Attempts were made to generate a colour map using aligned images in the V and R bands. The results are not felt to be of sufficient quality for inclusion here (difficulties due to differences in the point spread function between the V and R band may have not have been completely resolved). The V-I colour image of van Driel *et al.* (1995) shows the polar ring to be blue relative to the nucleus. This can be explained by the presence of young stars in the ring (see, for example, the Hα image of figure 3.3) and significant obscuration of the starburst. Starburst nuclei are usually heavily reddened due to enhanced gas (dust) densities at the gravitational centre. NGC 660 also has a dust lane occluding part of the inner disk.

3.3.2 Polarimetry Maps

Figure 3.4 shows a polarization map of NGC 660 superimposed onto a V-band greyscale image of the galaxy. For this, and all figures that follow, the coordinate system is in arcseconds and is centred at the nuclear position determined from the V-band (§3.2). One arcsecond corresponds to 63 pc at the distance adopted for NGC 660 (§3.1). Vectors denote significant polarization measurements made in $11'' \times 11''$ bins (although, integration bins $\pm(40 - 60)''$ of the nucleus may, in fact, only have an effective size of about half that due to incomplete object coverage). Following convention, the length of the vector represents the linear percentage polarization and its orientation indicates the direction of the electric field. The bins are spaced at intervals of 6″. Errors in the percentage polarization and the direction of polarization are of the order of 0.5-1% and 15° respectively (but may increase for fainter parts of the object). The data in figure 3.4 show that large parts of NGC 660 are polarized up to the level of about 3-4%. Various patterns are evident across different regions of the galaxy. These are now described in turn.

The south-west part of NGC 660 exhibits a semi-circular vector pattern which extends significantly above and below the plane of the disk. It is centred on the brightest part of the galaxy in a fashion that can almost certainly be attributed to scattering of starburst radiation. (Recall from §2.3.3 that the polarization induced by scattering is perpendicular to an imaginary line on the plane of the sky which connects the source of incident radiation with the scattering medium). The scattering must arise from dust grains residing outside the disk of the galaxy. There are various reasons why electrons are unlikely to constitute

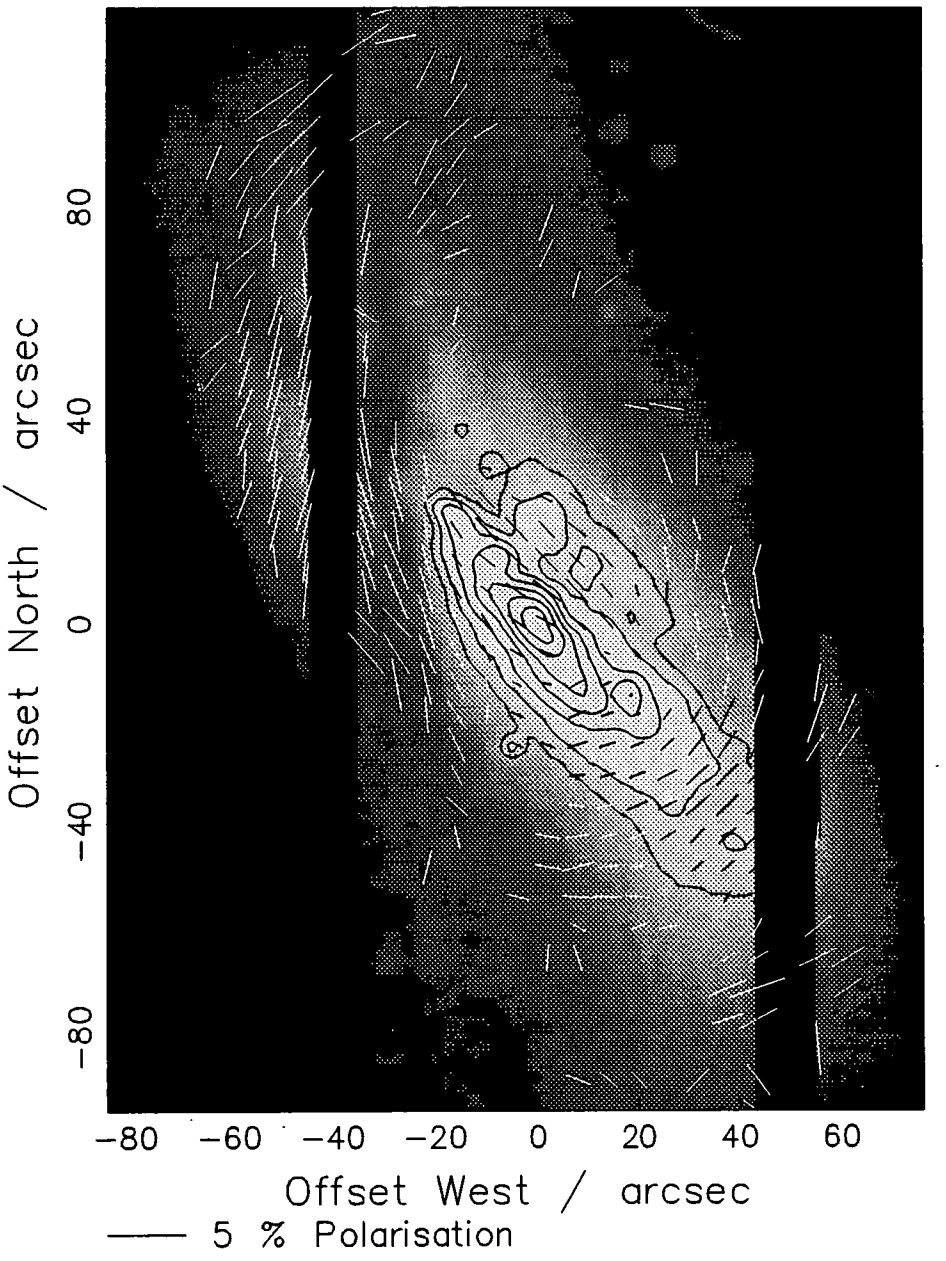

Figure 3.4: A V-band polarization map of NGC 660.

the scattering medium. These are elaborated in §9.2 where electron scattering is analysed in quantitative detail and dismissed for all galaxies observed in this thesis.

Figure 3.5 shows the disk of NGC 660 in Hα emission and R-band continuum. The vectors of figure 3.4 have been superimposed. The dust lane running northeast-southwest, on the nearside of the disk, can be followed almost to the back of the galaxy and this helps to define the plane of the main disk in this rather warped, morphologically complex system. Bearing this in mind, one notes that significant polarization is detected at a projected distance of several kiloparsecs above and below the plane of the disk. In fact, judging from the Hα emission in the same figure, dust scattering is detected up to 40″ or 2.5 kpc away from the star-forming disk!

Although significant amounts of scattering material appear to reside in the halo of NGC 660, there is some evidence that scattering is also taking place fairly close to the disk. This conclusion is based upon sampling the polarimetry data at a higher resolution to that used for figure 3.4. A bright HII region about 25″ south-west of the nucleus is surrounded by a centro-symmetric polarization pattern suggesting that it is the primary source of illumination over that small $(6-7'')$ region. It is difficult to see how this effect could be produced if *all* the dust in the south-west part of the galaxy were greatly displaced from the star forming disk.

In addition to what amounts to a giant reflection nebula in the south-west half of the galaxy, scattered light is also detected in an extended ($\simeq$ 2 kpc) region north-west of the nucleus (figure 3.5). The same region has already been discussed in connection with the emission-line filaments detected by Armus *et al.* (1990) and it is possible that a superwind expands out of the central disk along the minor axis (§3.1). It is difficult to judge, purely on the basis of the polarization vectors in figure 3.5, whether scattering material north-west of the nucleus is simply part of the reflection nebula seen in the south-west half of the disk. It is possible that the two regions are spatially independent despite overlapping in the plane of the sky.

Superwinds in starburst galaxies tend to be characterized by bipolar outflow (§1.4). In this context, it seems somewhat unusual that the emission-line filaments of figure 3.3 appear to be restricted to the north side of the disk even though the south side is probably closer to the observer. It may be of interest to examine the nearside of NGC 660 with a view to finding a counterpart to the scattering region detected on the north side of the disk. To this end, figure 3.6 shows a high resolution polarization map of the inner disk. In this plot, vectors denote significant polarization measurements made in $6'' \times 6''$ bins. The bins are separated by 3.5″. A greyscale image shows the V-band continuum and contours, separated by nearly half a magnitude, have been overlayed onto the very brightest part of the galaxy. In addition, two crosses mark the location of the double-peaked continuum radio source found by Condon *et al.* (1982) (§3.1). Within the figure, one can make out the polar ring skirting the edge of the disk about 20″ east of the nucleus.

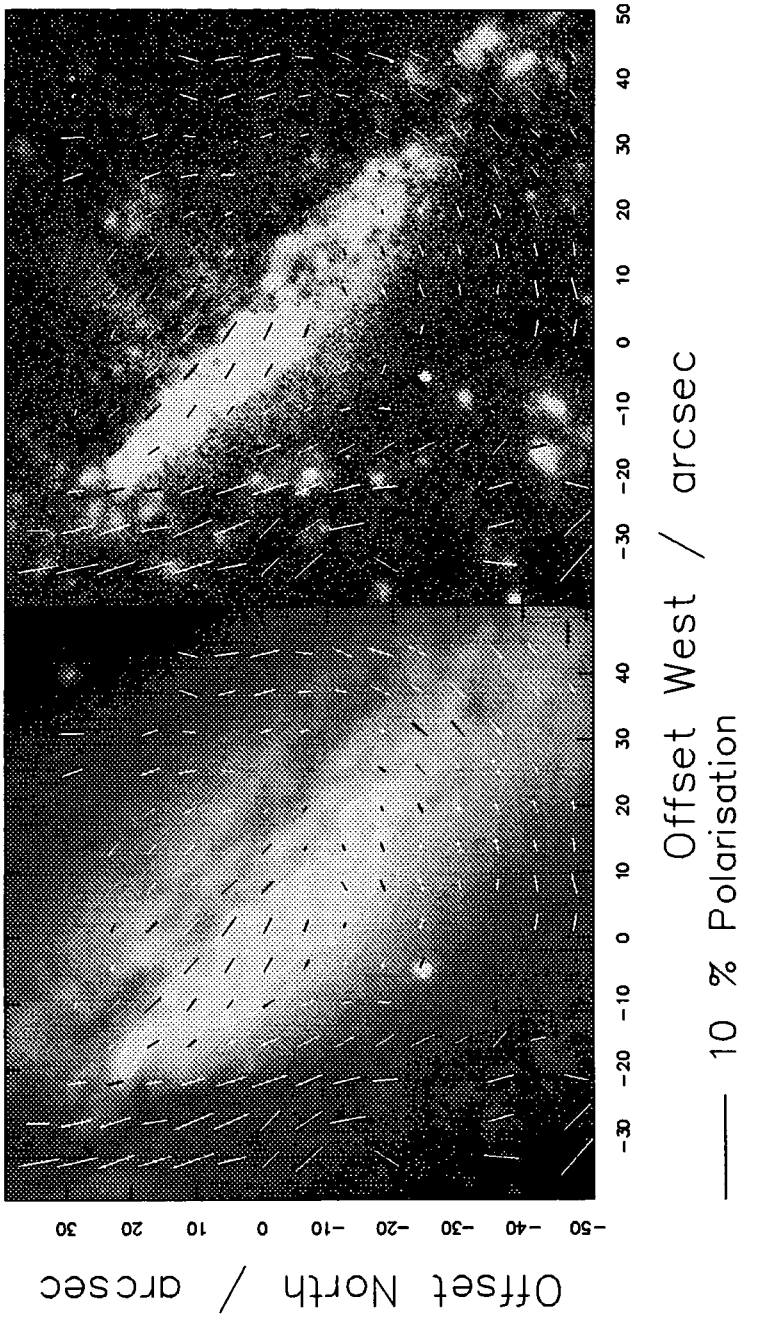

Figure 3.5: Polarization vectors overlayed onto the R-band image of NGC 660 (bottom) and the corresponding Hα image (top). The polar ring encircling the galaxy runs north-south crossing the disk 30″ east of the nucleus.

The polarizing mechanisms operating in the disk and nucleus of NGC 660 are somewhat ambiguous. Polarized light from the dark dust lane running the length of the disk, is likely to be associated with dichroic extinction from aligned dust grains. The polarization angle is faithful to the direction of the dust lane rather than exhibiting a centro-symmetric pattern about the bright nucleus (which would indicate scattering). Similar features have been detected in several nearby galaxies observed in polarized light (Ward-Thompson 1987; Scarrott *et al.* 1990a) and the general consensus is that the effect is caused by dust grains in the ISM aligning themselves with the spiral magnetic field pervading the disk (§2.3.3). The true nucleus of NGC 660 is probably obscured, at least in part, by the aforementioned dust lane. Indeed, one can see from figure 3.6 that the peak radio continuum emission, which in most starburst galaxies either surrounds or is cospatial with the nucleus, is displaced by several arcseconds from the optical peak in NGC 660 (the registration between the radio and optical data is better than 2″). The polarization pattern associated with aligned grains in the dust lane might, therefore, extend eastwards up to the location of the radio maxima. $5-10''$ further south-east, scattering may become important again because the vector pattern is once more centro-symmetrically orientated about the nucleus which suggests illumination of dust by the starburst.

It would appear on the basis of figure 3.6 that there is some reason to believe that scattering along the minor axis of NGC 660 is bipolar even if the extended emission-line filaments of figure 3.3 are not. One should bear in mind, however, that the disk of NGC 660 is eclipsed by both the polar ring in the east and the dust lane to the north-west. Both of these regions are polarized (the polarization of the polar ring is discussed below) and under such circumstances it is difficult to be absolutely certain about the origin of polarized light in the central disk. It may be possible to clarify the situation using multi-wavelength polarimetry. Regions polarized by the presence of aligned grains are expected to show a wavelength dependance similar to that given by Serkowski (1975; §2.3.3). There are, however, at least two main difficulties which may confound attempts to fit multi-wavelength data with a Serkowski-type polarization law. Firstly, if polarization measurements are restricted to the optical waveband they have to be of a high signal-to-noise. This is because the variation in this part of the spectrum is generally expected to be quite small (several tenths of 1%). Secondly, the aligned grains are expected to be foreground of any light sources. If this is not true, or if the dust and stars are mixed in any way, this will modify the observed wavelength behaviour. Clearly inferences made from multi-wavelength data can rapidly become quite complicated. There are very few examples of Serkowski-type fits being successfully applied to external galaxies (e.g. Hough *et al.* 1987; Scarrott *et al.* 1990a).

Dust scattering within a galactic environment will also show a frequency-dependent polarization behaviour but this may not be easy to predict because the **observed** polarization does not just depend on the scattering mechanism itself. Since scattered light is significantly diluted by unpolarized stellar emission from the disk, the measured polarization relies heavily on the colour of the galaxy. The colour of spiral galaxies can show

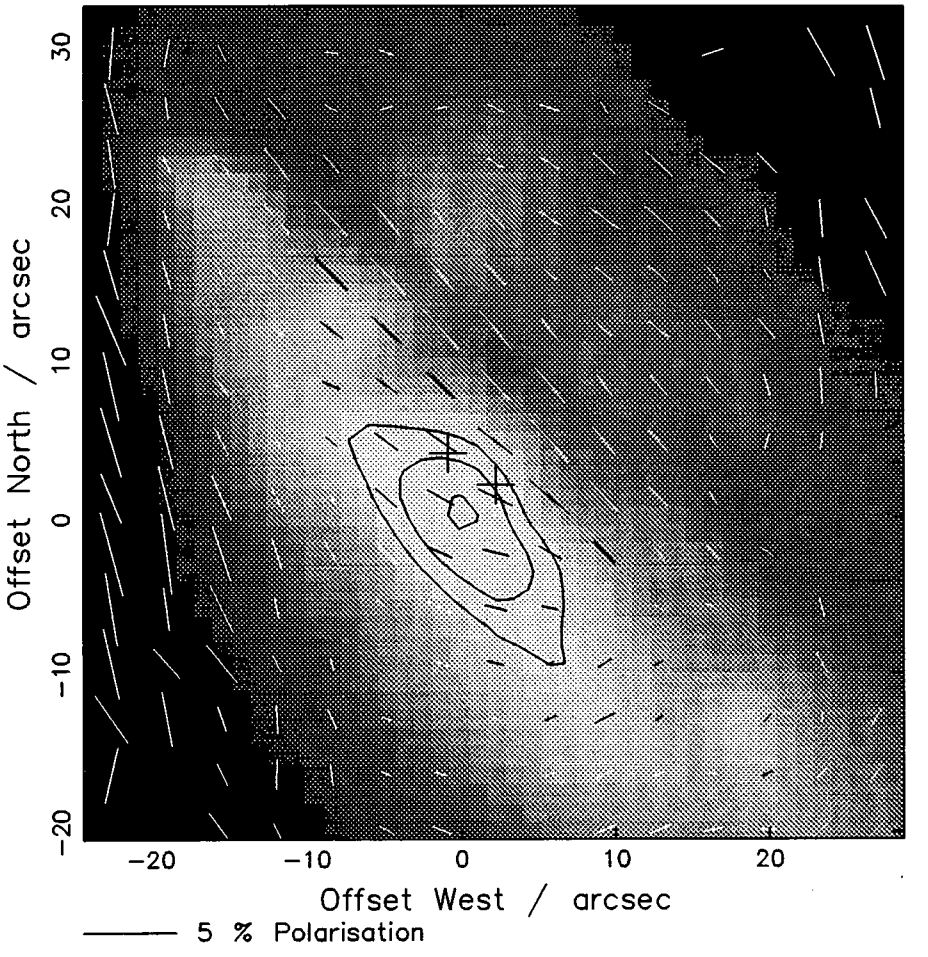

Figure 3.6: Polarization of the inner disk region. Two crosses mark the location of the double-peaked radio continuum source discovered by Condon *et al.* (1982).

considerable variation both internally and between individual systems (de Jong and van der Kruit 1994).

3.3.3 The Polar Ring

The polar ring in NGC 660 is of great astrophysical interest not least because NGC 660 may be the only known case of a gas-rich, disk galaxy that possesses such a morphologically unusual structure (van Driel *et al.* 1995). Authors have drawn attention to the vast amounts of gas detected in the ring of NGC 660 and how it has led to star formation outside of the disk (§3.1). Incidentally, evidence for recent star formation in the polar rings of other galaxies is not lacking (Marston and Appleton 1995). I would like to emphasize that the ring in NGC 660 is also *dust* rich - it partially obscures the disk of NGC 660 at 30″ east of the nucleus and it is also a source of polarized light (figures 3.4 and 3.5).

It is tempting to attribute the polarization of the polar ring to dichroic extinction by aligned grains. The extinction in the ring is similar to that of a galactic dust lane and the polarization angle is aligned with the direction of the ring rather than centro-symmetric about the bright inner disk. This is particularly evident in the far north-east part of figure 3.5 where scattering does not seem to be able to account for direction of the vector pattern. It is worth noting, however, that the level of polarization is somewhat higher than the dust lane in the disk ($\sim 4\%$ as opposed to $\sim 2\%$).

The region to the east of the polar ring also appears to be polarized (see top left of figure 3.4 for example) but measurements are close to the level of the noise. If the measurements are reliable, it is not obvious what causes the polarization in this region because the vectors do not appear to be associated with a dark dust lane. Clearly more data are required with full coverage of the polar ring and outer disk.

I will assume, for the sake of what follows, that where the polar ring crosses the disk of NGC 660, polarized light arises purely from preferential extinction by aligned grains. Now, dust grains aligned in the magnetic field of our own galaxy produce polarization and extinction which are related in the following way (Whittet 1992):

$$\frac{P_V}{E_{B-V}} \leq 9.0\ \%\, mag^{-1} \tag{3.1}$$

where P_V is the percentage polarization in the middle of the visual waveband (0.55μm) and E_{B-V} is the selective extinction. The above relation, which is empirically determined, expresses the maximum efficiency with which dust grains, aligned in the Galactic magnetic field, can polarize light reaching the observer. Using the average extinction curve for grains in the Galactic ISM, E_{B-V} can be expressed as $A_V/3$ and the relation 3.1 becomes:

$$P_V \leq 3A_V\ \% \tag{3.2}$$

where A_V is the visual extinction.

It was of interest to establish whether a relation similar to (3.2) existed for the polar ring in NGC 660. The extinction caused by the polar ring was derived in the following way. The inclination of the disk was deduced from the Hα image of figure 3.3 (P.A.=45° which agrees with the value given by van Driel *et al.* 1995). The galaxy was then reflected 180° about the minor axis so that the polar ring in the original image was covered by an unobscured region on the diametrically opposite side of the disk. Contours superimposed on both the original and reflected images seemed to suggest the fit was, for the most part, quite good. A bright HII region in the reflected image did, however, have to be masked out. The unreflected image was divided by the reflected image so that the extinction could be derived for 8″ diameter apertures along the polar ring. The error in this measurement was taken from the rms scatter in each aperture (these errors were larger than those anticipated from an imperfect alignment between the original and reflected images). Polarization measurements were made over the same regions of the polar ring and the extinction and polarization were plotted in figure 3.7.

One can see, from figure 3.7, that there is a tendency for more reddened parts of the polar ring to have higher levels of polarization. However, the correlation is very tentative due to the magnitude of the polarization errors. Most of the scatter in the plot can, in fact, be accounted for by large errors in the polarization measurement, but other sources of error, stemming from the method itself, are conceivable. For example, the polar ring is known to contain stars (§3.1) and I have neglected this intrinsic luminosity in the calculation of extinction. In addition, I assumed that the part of the galaxy reflected onto the polar ring, was totally unobscured. We already know, however, from the polarization maps described above, that dust clouds surround the south-west (i.e. reflected) part of the disk. (Note that regions affected by the dust lane in the disk were not used in the analysis).

The dotted line in figure 3.7 denotes the upper limit given by relation 3.2. One can see that, for the most part, the polarization measurements lie either close to or below the line. If one assumes that any correlation in figure 3.7 must go through the origin then a magnetic field not too dissimilar to that pervading the disk of our own Galaxy could reproduce the data points.

A mass estimate for the dust and gas contained in the polar ring can be calculated if one assumes that the extinction values derived for figure 3.7 are roughly correct. I take 20″ (0.95 kpc) and 25 kpc as the width and diameter of the ring respectively and use an average extinction of $A_V = 1$ mag for the ring. With the proviso that the dust grains in NGC 660 are similar to those found in the ISM of our own galaxy (see §9.3 why this might be true), I use the correlation found by Bohlin *et al.* (1978) which connects Galactic reddening with mean gas column density. In this way, I derive masses of $2 \times 10^9 M_\odot$ and $1 \times 10^7 M_\odot$ for the gas and dust respectively. Van Driel *et al.* (1995) measure the gas content of the polar ring directly and calculate a value of $5 \times 10^9 M_\odot$. Interestingly, the dust residing in the polar

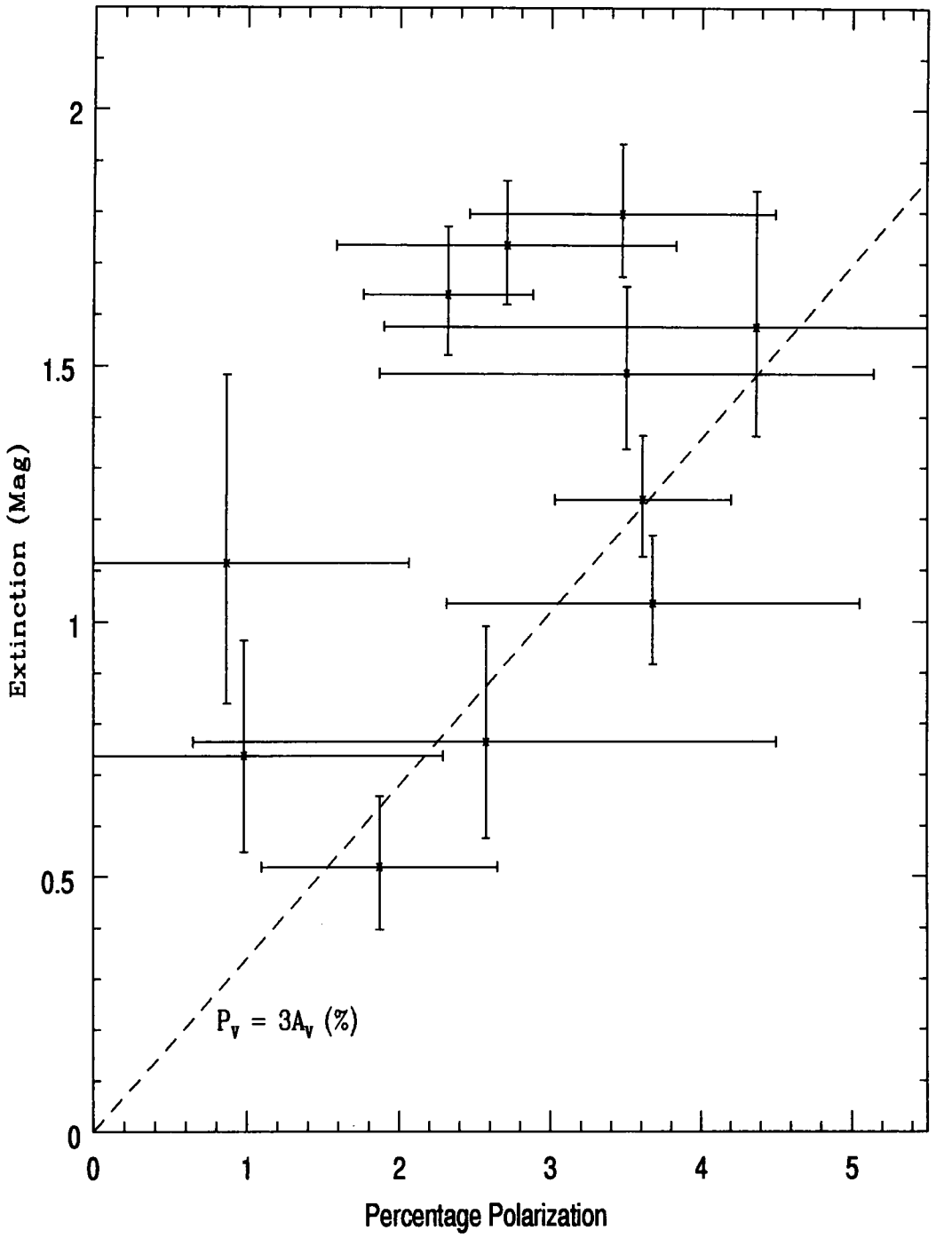

Figure 3.7: Extinction against polarization for the polar ring. The dashed line forms an empirical boundary discovered for similar measurements carried out for dust in The Galaxy.

ring of NGC 660 may provide a solution to its paradoxical longevity (§3.1). Reddening from the dust will tend to 'artificially age' the stellar population of the ring leading to an overestimation of the ring's lifetime.

3.4 Discussion

NGC 660 has all the symptoms of a galaxy that has experienced a violent collision and is now undergoing an intense starburst. It is characterized by: (a) an unusual morphology; (b) enhanced star formation both inside and outside the disk; and (c) the presence of dust and gas outside the disk. It is likely that the galactic collision which preceded the present activity was an on-axis encounter (Marston and Appleton 1995). Furthermore, the large quantities of gas found in the polar ring also suggest that the 'intruder' was similar in mass to NGC 660. NIR images of NGC 660 (van Driel *et al.* 1995) give no indication that the disk contains multiple nuclei. Therefore, it seems likely that the galaxy which collided with NGC 660 was either destroyed completely or escaped as a heavily ruptured system into the inter-galactic medium.

One can inspect the region of the sky surrounding NGC 660 to look for collision candidates. The POSS plates show two galaxies that could have conceivably interacted with NGC 660 in the last 10^8 years (this assumes a velocity dispersion of a few hundred kms^{-1}). One of these galaxies, UGC 01200, is an SO or dwarf elliptical galaxy and lies $30'$ to the south. The second (UGC 01195), is an irregular looking galaxy situated $22'$ north-east of NGC 660. Both galaxies have similar redshifts to NGC 660 (Willick *et al.* 1990) but neither appear as massive. The knotted structure of UCG 01195, which is quite possibly a result of recent star formation, makes this galaxy the more favorable collision candidate. Unfortunately, however, its HI mass is significantly less than the amount of gas detected in the polar ring of NGC 660 (Huchtmeier and Richter 1989; van Driel *et al.* 1995). Neither of two galaxies closest to NGC 660 are convincing collision candidates.

Although the history of NGC 660 remains something of an enigma, it is not implausible that much of the dust currently seen in scattered light originated from the galaxy that collided with NGC 660. Alternatively, or indeed in conjuction with this, an outflow along the minor axis may have expelled dust from the disk into the halo. The scattered light detected along the minor axis of the galaxy makes this second scenario very appealing. Once in the halo the dust grains may escape from the galaxy or, in lieu of sufficient kinetic energy, fall back towards the disk. The presence of dust outside the stellar disk and along the minor axis is very reminscient of M82. In contrast to M82, however, the levels of polarization in the scattering regions of NGC 660 are quite low ($\sim 3\%$ as opposed to $\sim 15-30\%$ for M82). The difference in polarization levels can probably be accounted for by the distribution of stars within the disk. Although both galaxies are viewed nearly edge-on, the disk of NGC 660 is warped to such an extent that any scattering light is diluted by a significant amounts of unpolarized starlight from disk stars. (It is also conceivable that, in the aftermath of a

violent galactic collision, stars remain dispersed in the halo environment of NGC 660.)

One curious aspect to the putative outflow in NGC 660, is that the emission-line filaments along the minor axis do not appear to emanate directly from the nucleus (figure 3.5). This is true even if the central radio emission is taken as the location of the true nucleus (§3.3.2). The situation is not dissimilar to the *dust* filaments in NGC 1808 which probably trace an energetic outflow in that galaxy (§2.2.2). The filaments in NGC 1808 originate from star forming, hot-spot regions close to (< 1 kpc), but not actually at, the nucleus of the galaxy. They are seen in absorption against the disk - evidence for emission-line filaments in the same region is less obvious (Phillips 1993).

3.5 Summary and Future Observations

The unusual starburst galaxy NGC 660 is very dusty. Remarkably, a significant proportion of the dust resides outside the main star forming disk in both the halo and a highly-inclined 'polar ring'. The dust grains in the halo scatter optical radiation from the starburst whilst aligned grains in the polar ring manifest themselves through dichroic extinction. It is possible that a violent galactic collision dispersed dust into its present location but scattering detected along the minor axis suggests that material might also escape from the disk in association with a superwind. Emission-line filaments in the same region point strongly towards the presence of a galactic outflow in NGC 660 although long slit spectroscopy is required to provide more substantial proof.

New things have been learned about the 'polar ring' in NGC 660. Not only is it dusty but it contains a magnetic field which may not be unlike the one found in the disk of The Galaxy. Multi-wavelength imaging polarimetry is required to separate, with greater confidence, regions of scattering and regions of dichroism within the inner disk of NGC 660. Unambiguous results may, however, be difficult to obtain. Polarization measurements in the Hα emission line would enable a closer comparison with M82 (which NGC 660 resembles in many ways). In scattered emission-line radiation, M82 is characterized by a bipolar nebula orientated along the minor axis (§2.2.1). A closer study of the neutral gas in the NGC 660 system and its various kinematic components, might enlighten us to the tidal event which initiated the exciting phenomena we see today.

Chapter 4

NGC 1614 and NGC 1667

4.1 Introduction

NGC 1614 and NGC 1667 are both morphologically disturbed, face-on spiral galaxies which are somewhat more distant than most of the systems studied in this work (64 Mpc and 60 Mpc respectively; $H_o = 75$ kms^{-1}Mpc^{-1} and redshifts from Armus *et al.* 1990). They are both powerful emitters in the far-infrared ($2 \times 10^{11} L_\odot$ and $4 \times 10^{10} L_\odot$ respectively) and, on the basis of their high FIR-to-blue ratio (Soifer *et al.* 1987), can be classified as FIRGs (§1.2). I now proceed to describe briefly the salient features of each object before presenting new observations.

Figure 4.1 shows a contoured V-band image of NGC 1614 which is derived from observations presented in this chapter. North is at the top and east to the left. The size of the image is $50'' \times 70''$ (15.5×22 kpc). Contours separated by approximately half a magnitude are overlayed onto the brightest regions. Although figure 4.1 does not contain complete coverage of the fainter regions of the galaxy, the unusual morphology of NGC 1614 is still apparent. A spiral-like structure exists in the inner disk which is otherwise dominated by a bright, point-like nucleus. A large 'spiral arm' sweeps eastwards across the disk to a maximum distance of 10 kpc from the nucleus. To the south-west one can see part of a linear 'tail', which, in the more extensive R-band image of Armus *et al.* (1990), extends up to 20 kpc from the centre. The galaxy is bright in the Hα emission line indicating recent enhanced star formation (Armus *et al.* 1990). Copious emission-line radiation originates from the nucleus and inner disk but a knotted emission-line structure also exists part way along the linear 'tail' in the south-west.

Further evidence that an intense starburst is occuring in NGC 1614 comes from the spectral data obtained by Armus *et al.* (1989). They carried out long-slit optical spectroscopy of a large sample of FIRGs with a view to understanding the energy sources in this class of galaxy. NGC 1614 has emission-line ratios similar to those derived for HII regions. Out of the 28 galaxies in the survey that had their Balmer line fluxes dereddened,

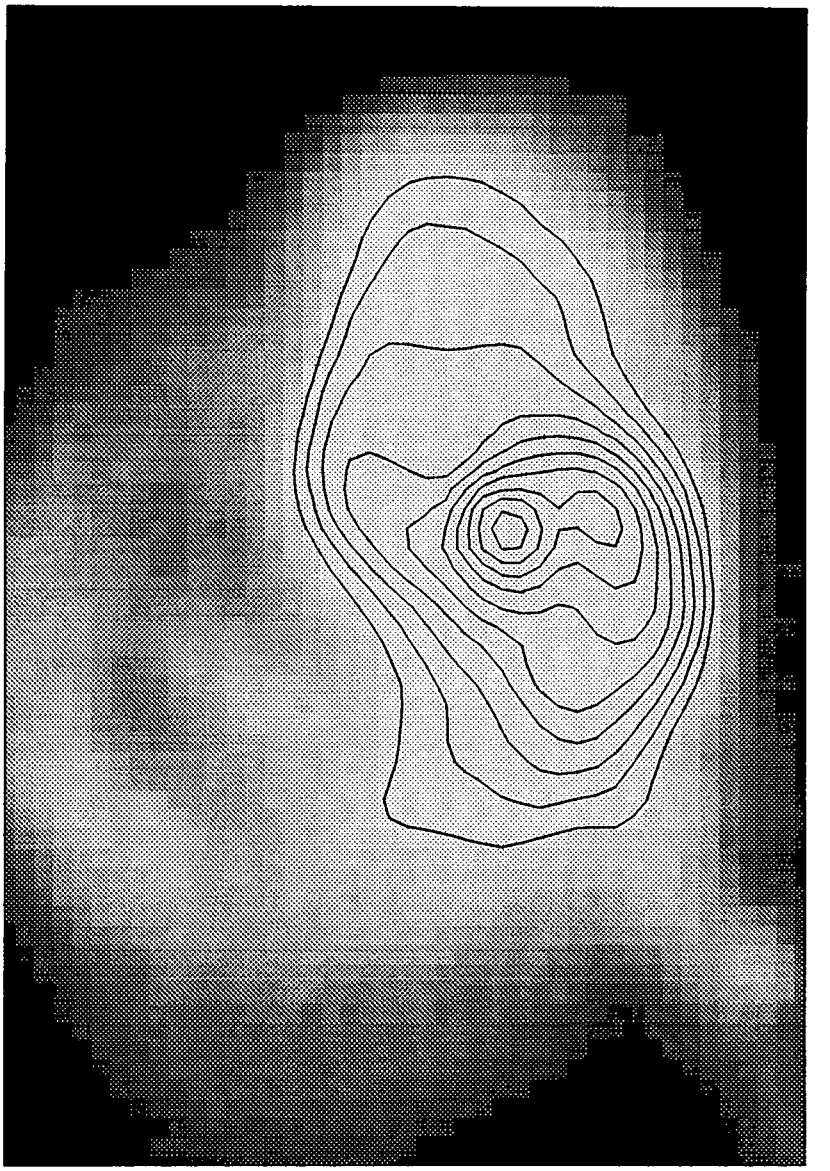

Figure 4.1: V-band Image of NGC 1614

NGC 1614 proved to be one of the most luminous in the Hα emission line. Further manifestations of recent and intense star formation are found in the radio continuum map of Condon *et al.* (1982) and the mid-infrared image of Wright *et al.* (1988). Both are consistent with an extended energy source – almost certainly young stars. In common with many other FIRGs, NGC 1614 is rich in molecular gas (Sanders 1991; Casoli *et al.* 1991). Enhanced gas densities are required to fuel prolific star formation.

The morphology of NGC 1614 is very suggestive of a merger and indeed the galaxy has been classified as such in the literature (e.g. Casoli *et al.* 1991). A closer inspection of figure 4.1 reveals, what appears to be, a second nuclear component in the central region. This lies about 6″ (1.8 kpc) west of the true nucleus. It is **not** apparent in the Hα image of Armus *et al.* (1990) which suggests that it is not an emission-line region. According to the photometry of Mazzarella and Boroson (1993) the feature is red (B-R=2.0 mag). It is therefore quite conceivably the remnant of a merged nucleus. If this is the case, a merger event may have activated the current star formation. NGC 1614, by virtue of its ultraviolet excess, has been classified as a Markarian galaxy (Mrk 617; Mazzarella *et al.* 1991). It also appears in the Arp catalogue of morphologically disturbed galaxies (Arp 186; Arp 1966).

The starburst in NGC 1667, judging by its FIR luminosity, is less energetic than that in NGC 1614. NGC 1667 has appeared in several surveys as a 'low-level Seyfert 2' (e.g. Ho *et al.* 1993; Thuan 1984). The optical emission-line luminosity is approximately two orders of magnitude lower than that found in most Seyfert 2s and the 'narrow line region' (FWHM OIII $\lambda\lambda$5007 $\simeq$ 300kms^{-1}) may be explained equally well by a starburst superwind (§1.4). The argument for Seyfert 2 activity is, however, strengthened by the IUE-detection of high ionization lines in the far ultraviolet (Thuan 1984). Even if the centre of NGC 1667 *does* harbour an AGN, there is convincing evidence for enhanced star formation both close to the nucleus and in large HII regions populating the disk. From the same IUE data mentioned above, Thuan (1984) finds that a significant fraction of ultraviolet emission is extended ($\sim 10 - 20''$) whilst the Hα image of Armus *et al.* (1990) confirms the presence of extended star formation. Sanders *et al.* (1991) discovered a large concentration of molecular gas at the centre of NGC 1667, which is reminscient of many other FIRGs (§1.2).

Figure 4.2 shows a V-band image of the NGC 1667 system which is derived from the polarimetry observations discussed below. North is at the top and east to the left. The image scale is 40″ × 120″ (15 kpc by 46 kpc) which is sufficient to see most of the disk in NGC 1667 as well as a small elliptically-shaped companion located 1 arcmin (23 kpc) to the south. A faint 'bridge of nebulosity' connects the smaller galaxy with the disk indicating that the two galaxies are physically coupled. Contours, separated by nearly half a magnitude, outline the bright nuclei in both systems and the star forming regions in the disk of NGC 1667.[1] It seems likely that the tidal interaction between NGC 1667 and its small neighbor may have initiated the current bout of star formation taking place in the

[1]Henceforth, I shall refer to the larger galaxy in figure 4.2 as 'NGC 1667'.

larger galaxy (§1.2). Incidentally, the small companion does not appear in the Hα image of Armus *et al.* (1990) although it is optically brighter than much of the star forming disk in NGC 1667. This might suggest that star formation is restricted to the larger galaxy.

4.2 Observational Details

Both NGC 1614 and NGC 1667 were observed at the f/15 Cassegrain focus of the 1-meter SAAO telescope during November 1993. The Durham imaging CCD polarimeter was used in conjunction with a broad V-filter (550±130nm). In all, 16 exposures were made for NGC 1614 and 8 for NGC 1667. The exposure time for each frame was 600 seconds. The data were reduced in the standard manner described in §2.3.1.

4.3 Results

4.3.1 NGC 1667

Figure 4.3 shows the polarization detected in NGC 1667. The data have been sampled using $6'' \times 6''$ bins spaced at intervals of $3.5''$. Contours, separated by 0.4 mag, are overlayed onto the brightest regions of the galaxy and offsets from the nucleus (which is well defined) are given in arcseconds. One can see that polarization levels of 1-2% are recorded and that the vector pattern possesses a spiral structure. Typical errors in the level and angle of polarization are 0.3% and 15° respectively.

The visual impression of a spiral polarization pattern in NGC 1667 is strengthened by figure 4.4. Here, concentric circles about the nucleus have been overlayed onto the polarization pattern of figure 4.3. If light from the bright nuclear starburst were being scattered into our line of sight we would expect the vectors in figure 4.4 to be centro-symmetric about the center of the galaxy. This is clearly not the case. In fact, the vector pattern traces out the spiral magnetic field of the galaxy. Dust grains aligned in this magnetic field preferentially absorb background light possessing an electric field parallel to the field direction. The radiation that escapes to the observer is therefore polarized (§2.3.3).

One curious aspect to the vector patterns displayed in figure 4.4, is that the polarization of NGC 1667 is not restricted to the dark lanes of the galaxy. Recalling the discussion of §3.3.3, one can anticipate a correlation between the polarizing effect of magnetically aligned grains and the (preferential) extinction they cause. To confirm my visual impression, I carried out aperture polarimetry both inside and outside the dark lanes of NGC 1667. Figure 4.5 shows the position and results of measurements made for this analysis. All aperture bins had a diameter of $3.5''$ and were mutually independent. The 11 measurements carried out in the darker regions of the galaxy have been labelled with a 'd' and the 16 measurements taken in the brighter regions are labelled with a 'b'. The aperture used

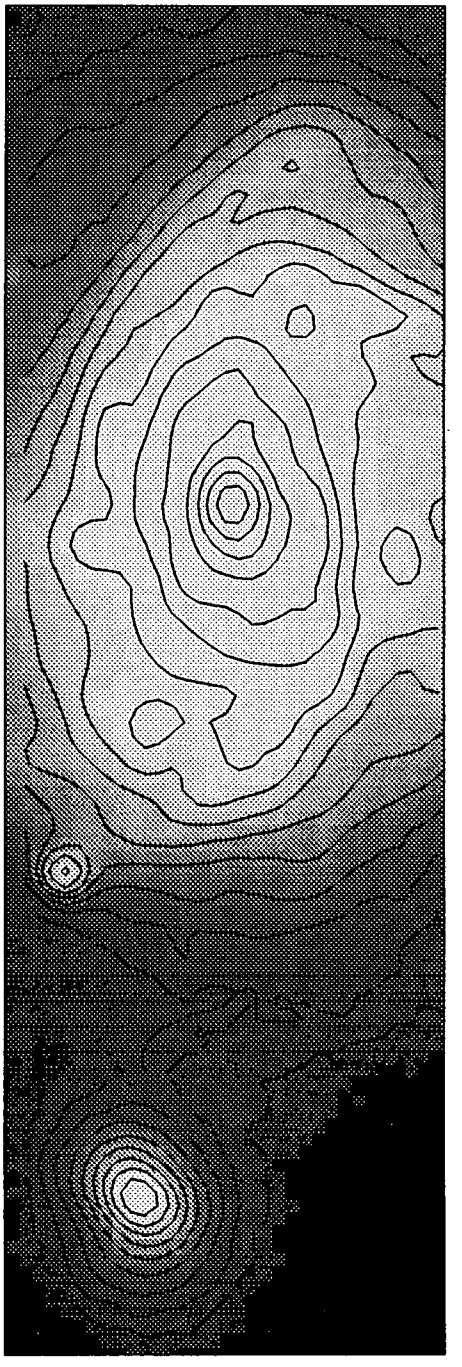

Figure 4.2: A V-band image of NGC 1667

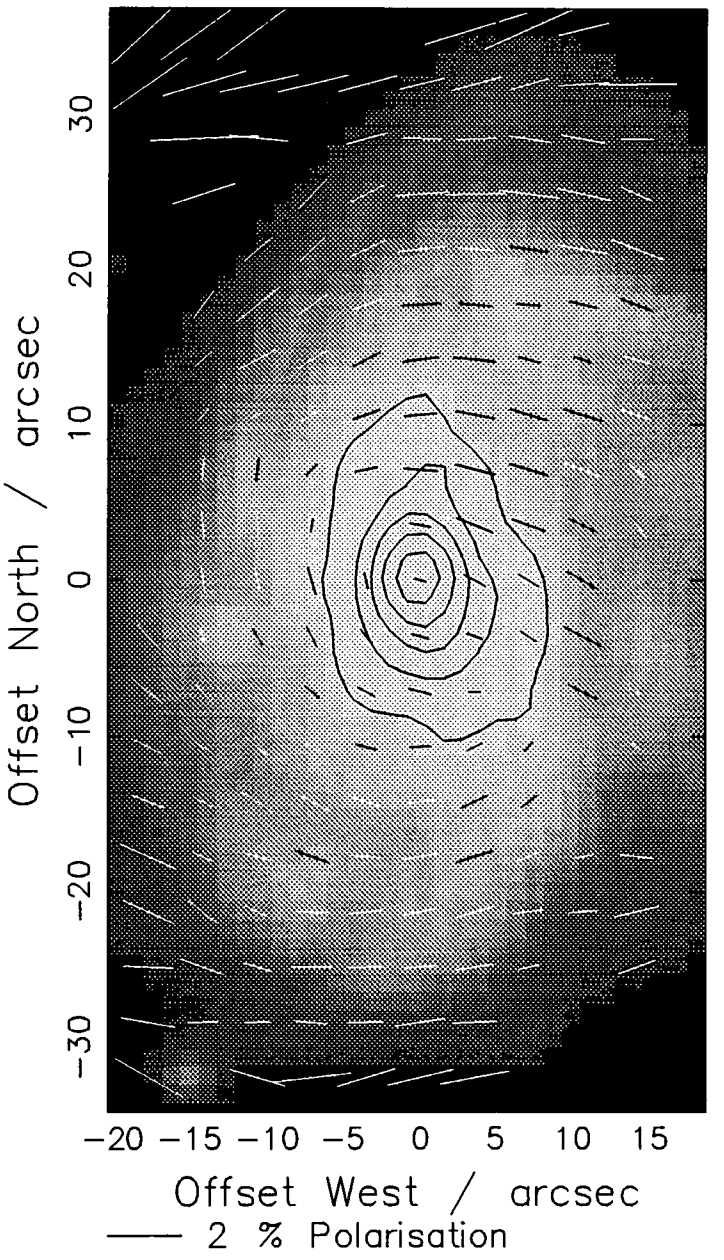

Figure 4.3: A polarization map of NGC 1667

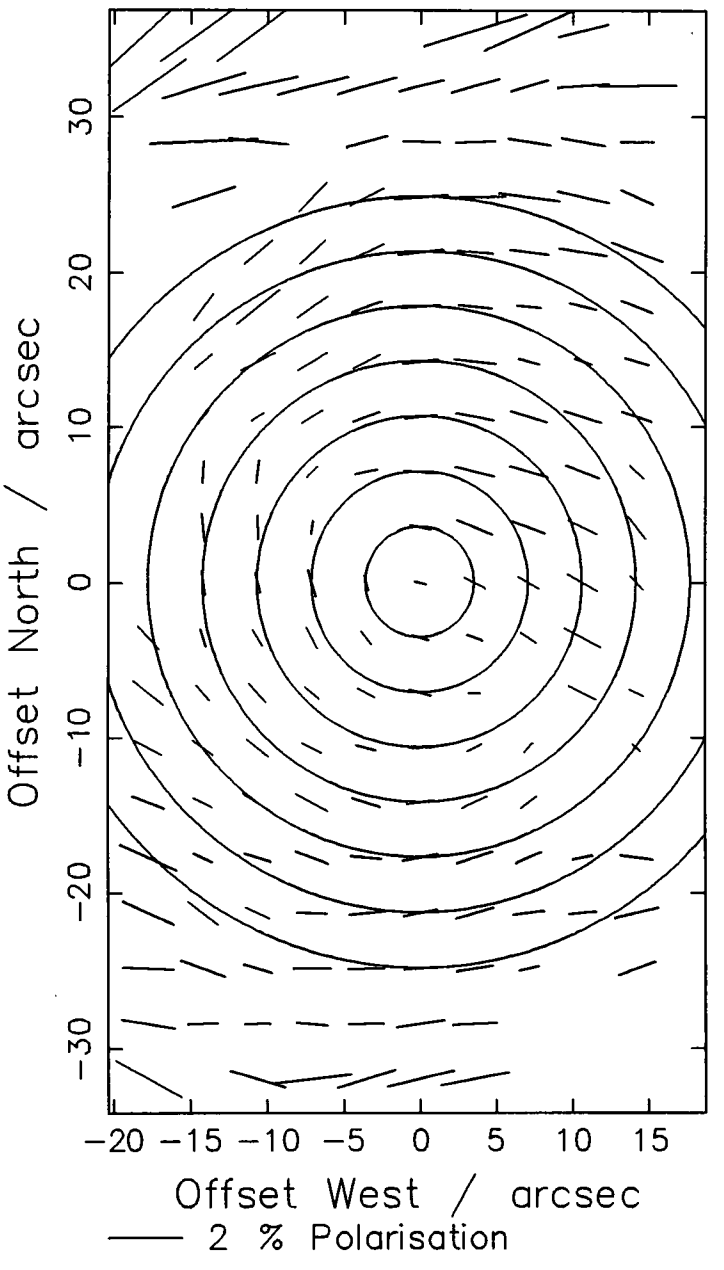

Figure 4.4: A spiral pattern in NGC 1667. Concentric circles have been overlayed onto a polarization map of NGC 1667 so as to highlight the spirality of the vector pattern.

for the measurements was small enough to marginally resolve the spiral arm structure. The weighted mean polarization, and its corresponding error, are 1.07 ± 0.11 % and 0.82 ± 0.08 % for the dark lanes and bright lanes respectively. This suggests that the two regions have quite similar polarization properties. The implications of this result will be discussed in full below.

4.3.2 NGC 1614

Due to intense, non-uniform, recent star formation, the surface of NGC 1614 is subject to extremely steep isophote gradients (figure 4.1). As a consequence of this, it was difficult to obtain reliable polarization measurements over some parts of the object (changes in the 'seeing' disk during observations or small errors in the alignment of image frames can lead to spurious measurements over steep brightness gradients or close to point sources). The quality of the data is such that the author feels that there is little value in their presentation. In regions of the galaxy characterized by a less steep brightness gradient, a spiral pattern similar to that in NGC 1667 was evident.

4.4 Discussion

Both NGC 1667 and NGC 1614 are FIR-powerful, starburst galaxies which may be subject to the kind of galactic-scale outflows found amongst others members of their class (§1.4). We recall, from chapter 3, that polarization observations of a similar system, NGC 660, provided evidence for scattering material residing in extensive regions outside the main star-forming disk. In a tentative manner, I associated these dust grains with a possible outflow along the minor axis and/or the tidal forces of a recent galactic collision. The polarization properties of NGC 1667 and NGC 1614 are characterized solely by dichroic extinction from aligned grains in the disk. There is no evidence for scattering outside the disk even though both galaxies have almost certainly been subject to recent tidal events and may now be experiencing galactic-scale outflows. Why do galaxies with such similar global characteristics show distinct differences in their polarization properties?

It seems quite likely that orientation effects can explain the diversity of observations for starburst galaxies. It is almost certainly no coincidence that those starburst galaxies boasting a polarized halo (NGC 660, M82, NGC 1808) are also highly inclined with respect to the observer's line-of-sight. Light scattered in the halos of these galaxies is less diluted by unpolarized stellar light from the disk. The polarization levels recorded in NGC 660 and NGC 1808 are sufficiently low ($\sim 2 - 4\%$) that any scattered component would probably become undetectable if these galaxies were viewed nearly face-on. (Polarization by dichroism, on the other hand, is far less affected by viewing angle because the polarizing mechanism relies on preferential extinction of disk light). The face-on orientation of NGC

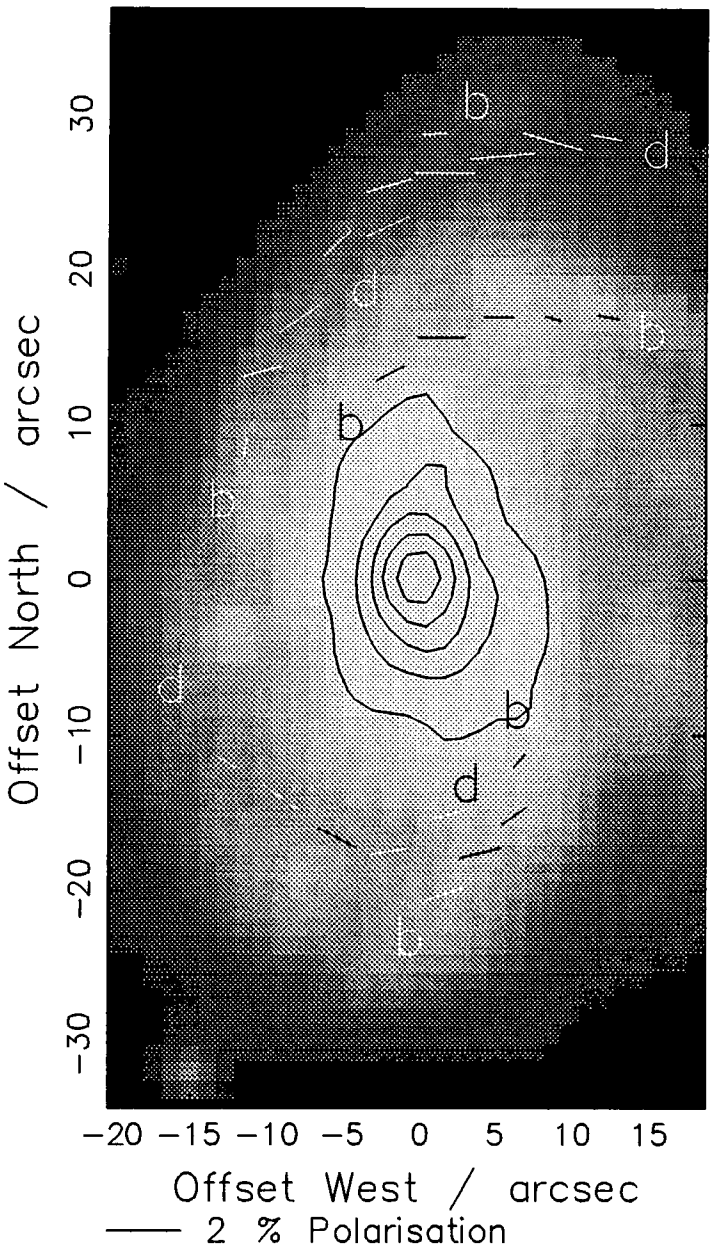

Figure 4.5: Aperture polarimetry of the spiral lanes in NGC 1667. See text for details.

1667 and NGC 1614 may explain why we do not detect polarized halos in these galaxies.

It should be noted that the spiral polarization patterns detected in NGC 1667 and NGC 1614 are similar to those discovered in other (near) face-on spiral galaxies (e.g. NGC 1068; Scarrott *et al.* 1991b). Intriguingly, the level of polarization recorded in all cases is $\sim 1-2\%$. Since this is controlled by the magnetic field strength and the properties of the interstellar grains (Spitzer 1978; Johnson 1982), this would seem to suggest that the ISM in these galaxies is quite similar.

In §4.3.1, I came to the conclusion that the polarization levels in the bright arms of NGC 1667 did not vary significantly from those recorded in the inter-arm regions of the galaxy. These observations may be important for theories of spiral structure in disk galaxies. A favoured model is the spiral density wave hypothesis which predicts that spiral structure is created by gaseous material in the disk flowing through regions of compression (Roberts and Hausman 1984). As the gas, dust and magnetic field of the ISM are compressed dust lanes are formed within the disk. In the wake of the density wave new stars are formed leading to the creation of bright spiral arms. If this model is applied to NGC 1667 we might interpret the dark regions, labelled 'd' in figure 4.5, as compression regions and the bright regions, labelled 'b', as the trailing edge of the density wave. (Indeed, the clumpy nature of the bright spiral arms strongly suggests that new stars exist within these regions).

The polarization levels within NGC 1667 might be difficult to accommodate within the framework of the density wave hypothesis. Inside the compression regions one might expect enhanced polarization levels due to: (a) increased dust density and (b) an increase in magnetic field flux (alignment efficiency is increased for stronger magnetic fields - Spitzer 1978). Observationally, there is little distinction between the level of polarization recorded in the bright spiral arms and those characterizing inter-arm regions (§4.3.1). This is consistent with the macroscopic properties of the ISM (magnetic field strength, dust and gas densities) remaining fairly constant across the disk rather than undergoing an increase within compression regions. If a density wave exists within NGC 1667 either the magnitude of the compression is too small to be detected through increased polarization levels or, alternatively, the scale-length of the compression region is less than the resolution of the observations (3″ or 1 kpc).

4.5 Summary

The two face-on, FIR-bright, starburst galaxies, NGC 1667 and NGC 1614, exhibit a spiral polarization pattern in their galactic disks. This is attributable to dust grains aligned in a spiral magnetic field. A closer inspection of NGC 1667 shows that the level of polarization varies only slightly between the bright, star-forming arms of the galaxy and the darker inter-arm regions. This suggests that, within the resolution of the observations (~ 1 kpc), all parts of the disk are subject to similar dust (gas) densities and magnetic forces.

There is **no** evidence within NGC 1667 and NGC 1614 for the type of galactic-scale scattering seen in the starburst galaxies NGC 660 (§3) and M82 (§2.2.1), This is perhaps attributable to orientation effects rather than physical differences in the dust properties of various FIRGs (although the latter cannot be ruled out by the present observations). If we wish to detect the more unusual dust properties of starburst galaxies, future observations with the Durham Imaging Polarimeter should concentrate on systems that have large inclination angles with respect to the observer's line of sight. This will allow the minor (superwind) axis to become visible.

Chapter 5

NGC 3077

5.1 Introduction

NGC 3077 is a bright dwarf galaxy situated in the nearby M81 group. It has a mostly elliptical appearance but has been classified as an irregular by Sandage (1961). Although the FIR luminosity of NGC 3077 ($2.4 \times 10^8 L_\odot$; §9.6), is less than that of the far-infrared galaxies discussed in preceding chapters, its FIR-to-blue luminosity ratio is quite high ($\simeq 2$; Thronson *et al.* 1991). Furthermore, this low mass system possesses many other properties that can be associated with prolific star formation. These are now discussed before polarization measurements for the galaxy are presented.

The centre of NGC 3077 is very blue and ultraviolet spectra obtained for the galaxy are characterized by stars which are only a few $\times 10^7$ years old (Benacchio and Galletta 1981). Most of these hot, young stars appear to reside in a number of luminous clusters (or superclusters) which are situated close to the physical centre of the galaxy. There are also some smaller starforming regions scattered throughout the main body of the galaxy (Barbieri *et al.* 1974). Thronson *et al.* (1991) note that, at the centre of NGC 3077, the star formation rate per unit surface area is some two orders of magnitude greater than the average rate for 'normal' spirals.

An Hα image produced by Thronson *et al.* (1991) indicates that a large bubble of ionized gas occupies the central 40″ (600pc) of NGC 3077. The gas has almost certainly been ionized by young stars in the superclusters and is now attempting to escape from the centre of the galaxy. Barbieri *et al.* (1974) showed that, at fainter light levels, NGC 3077 has an 'explosive appearance' in ionised gas. This diffuse emission-line gas is characterized by kpc-scale filaments and shells which are very reminiscent of the emission-line 'nebulae' detected in other starburst galaxies (§1.4). Although there is no spectroscopic evidence for an outflow in NGC 3077, the detection of diffuse emission-line filaments in other starburst galaxies has usually meant that galactic-scale winds *are* present. The filaments in NGC 3077 are radially oriented but show no preferred axis. Emission-line shells and filaments

have been seen in other low mass starburst galaxies (Marlowe *et al.* 1995) and they are discussed in some detail in §6.7.

Another unusual property of NGC 3077 is the appearance of, what appears to be, 'patches' of dust against the body of the galaxy. These features are best seen in figure 5.1 which is an optical image of the galaxy derived from polarimetric observations described in §5.2. The size of the image is $1.5' \times 1.5'$. This corresponds to 1.4 kpc × 1.4 kpc at the distance generally adopted for the M81 group (3.25 Mpc; Sandage and Tammann 1975). Figure 5.1 is orientated with north at the top and east to the left. Contours, separated by 0.3 mag, are overlayed onto the brightest parts of the galaxy. The dust patches mentioned above are discussed in more detail in §5.4.

NGC 3077 is a lesser-studied member of the tightly-bound M81 group. In some ways, it has been 'upstaged' by its more familiar neighbor, M82 (§1.3), which lies little more than 56 kpc to the north. Figure 5.2 shows the position of NGC 3077 relative to the rest of the group. It is a CCD image taken from the Digitized Sky Survey.[1]

Thus far, most of the interest in NGC 3077 has surrounded a bridge of neutral gas which connects NGC 3077 with the disk of M81 (van der Hulst 1979; Appleton *et al.* 1981; Yun *et al.* 1994). A similar bridge exists between M82 and M81 suggesting that tidal interactions within the trio are responsible for the starbursts now evident in M82 and NGC 3077. Both M82 and NGC 3077 are gas-rich. NGC 3077 has roughly 1/3 of its total mass in neutral gas (Thronson *et al.* 1991). It is possible that M81 has supplied gas to both its smaller neighbours during recent galactic interactions (Appelton *et al.* 1981).

Large amounts of gas have been detected at the centre of NGC 3077. Becker *et al.* (1989) used the CO (J=1-0) transition to map out the galaxy in molecular gas. They detected a molecular complex of $10^7 M_\odot$ enclosing the inner 300 pc of the system. At least one tenth of the gas in NGC 3077 exists within molecules (van der Hulst 1979). Price and Gullixson (1989) detected a dense cloud of gas and dust a few arcseconds south of the superclusters in the nuclear region. Clouds of similar mass ($\sim 10^5 M_\odot$) and size are found in our own galaxy and they are known to act as 'nurseries' for new stars.

Observations outside the optical waveband confirm that the centre of NGC 3077 is the site of unusually powerful star formation. A compact radio source has been detected by several authors (van der Kruit 1971; van der Hulst 1979; Hummel *et al.* 1987). Hummel *et al.*, using the VLA, claim to have resolved the emission into an extended ($7 - 8''$) component and a $0.7'' \times 0.4''$ core. The radio spectral index is indicative of synchrotron radiation emitted by young supernova remnants (van der Hulst 1979).

[1]The Digitized Sky Survey was produced at the Space Telescope Science Institute under U.S. Government grant NAG W-2166. The images on these discs are based on photographic data obtained using the Oschin Schmidt Telescope on Palomar Mountain and the UK Schmidt Telescope.

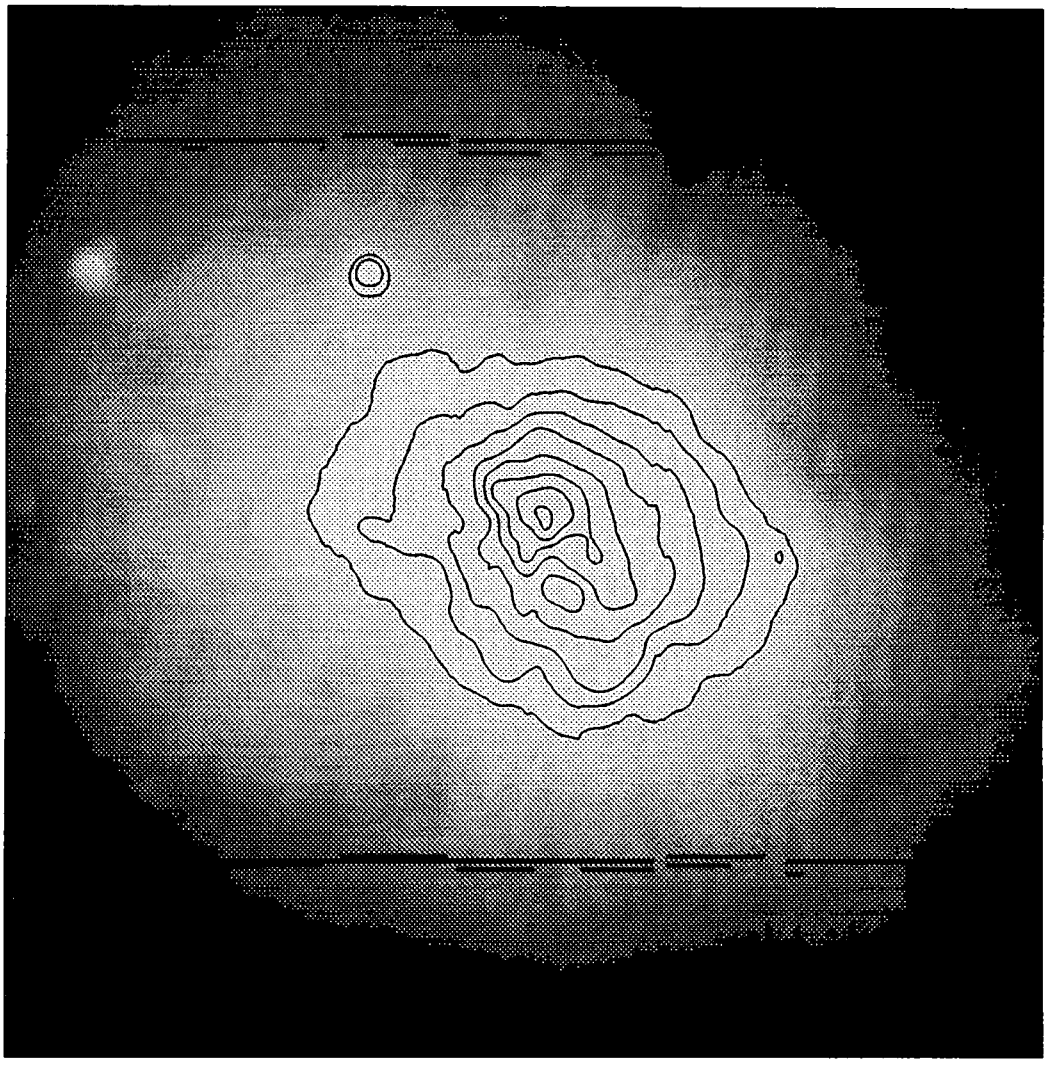

Figure 5.1: An optical continuum image of NGC 3077. The image was obtained using the Durham Optical Polarimeter without a filter. The rows of invalid pixels $\simeq \frac{1}{2}''$ above and below the centre of the galaxy are 'dead' regions of the CCD which had to be masked out.

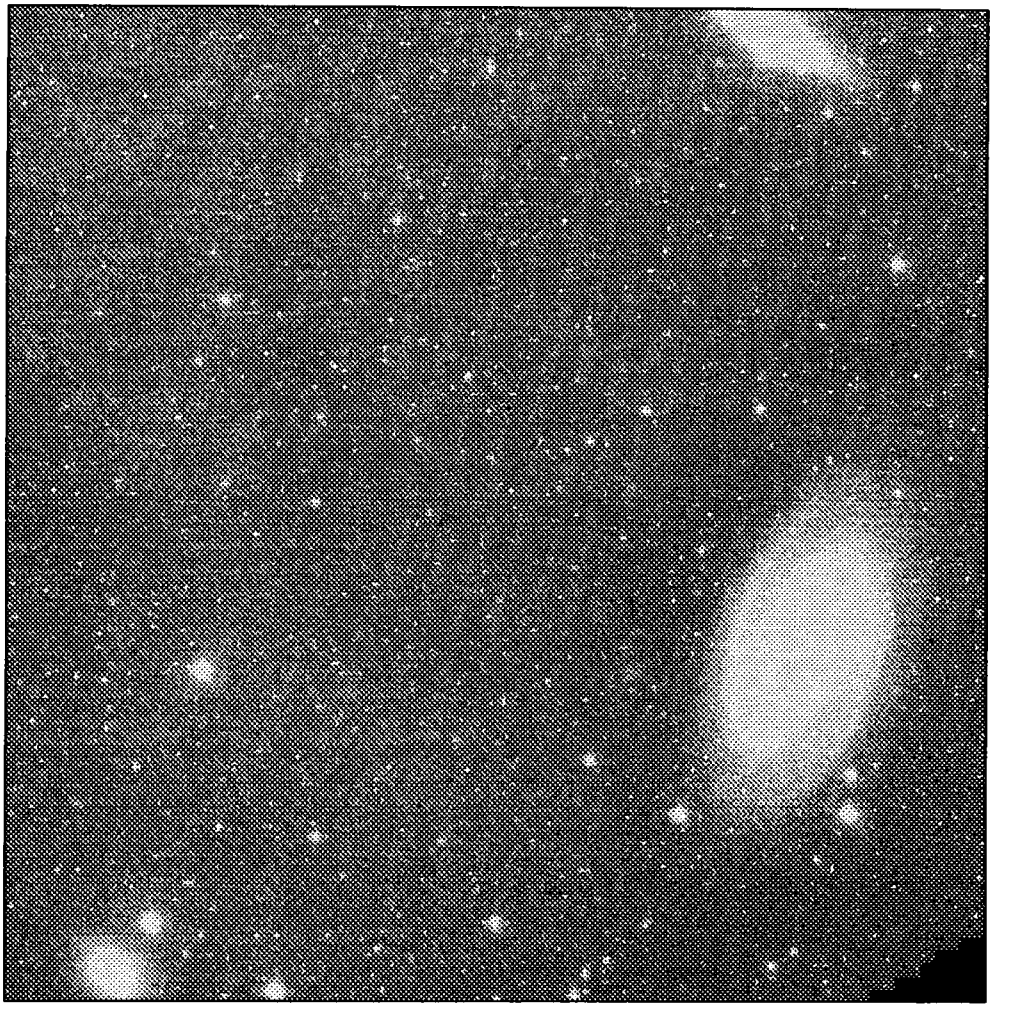

Figure 5.2: The position of NGC 3077 within the M81 group. This image was obtained from the Digitized Sky Survey and is taken in the B waveband. The field of view is $1° \times 1°$ which corresponds to 56 kpc by 56 kpc at the distance of NGC 3077. North is at the top and east to the left. M81 is the large spiral on the right, M82 is to the north and NGC 3077 is the small galaxy at the bottom left.

Recently, NGC 3077 has also been detected by the ROSAT PSPC (Bi *et al.* 1994). X-ray emission is believed to arise from a compact source (deconvolved size $\simeq 5''$) possessing an unabsorbed luminosity of $2.1(\pm 1.1) \times 10^{38}$ erg sec^{-1}. Its location is within a few arcseconds of the optical centre of the galaxy. The authors suggest that x-rays emanate from a hot bremsstrahlung gas (kT= 0.65 ± 0.51 keV) ionized by young stars. Unfortunately, since the PSPC provides little spatial and spectral information, it is difficult to rule out other sources of x-ray emission in NGC 3077 (e.g. x-ray binaries and inverse Compton scattering).

Many of the observations described above are re-discussed in the context of polarization measurements carried out with the Durham Optical Polarimeter. It is these observations which I now wish to present.

5.2 Polarimetric Observations

NGC 3077 was observed with the Durham Imaging Polarimeter at the f/15 Cassegrain focus of the 2.5m Isaac Newton Telescope (INT). Twelve 300s exposures and four 100s exposures were made in January 1987 without using a filter.[2] The CCD used at that time had an unfiltered response that peaked around 700nm and a FWHM of roughly 350nm (Draper 1987). Shorter exposures were made in order to guarantee information for the brightest regions of the object (where saturation of the CCD chip was most likely).

To some extent, the data for NGC 3077 had already been analysed by a former member of the Durham Polarimetry Group, C.D. Rolph (Scarrott *et al.* 1990a). The interpretation made at that time was that grains aligned in a galactic magnetic field were responsible for the polarization of the object. Over the last few years the Durham Polarimetry Group has gained a far greater insight into the phenemona that characterize starburst galaxies (§2.2) and a re-investigation into the polarimetric properties of this galaxy was deemed worthwhile. The author began the study with a reduction of the flatfielded CCD frames left by Rolph.

NGC 3077 is at a distance of 3.25 Mpc (Sandage and Tammann 1975) which gives a scale of 15.5 pc per arcsec.

5.2.1 Data Reduction

It should be mentioned from the outset that the reduction procedure was beset by certain difficulties with the data. Bleeding from bright stars was present in the frames and after this was masked out the number of fiducial stars available for the alignment of image frames was greatly reduced. The instrumental set-up *currently* in use by the Durham Polarimetry Group allows the grid mask to be removed so that reference images can be obtained during

[2]These observations pre-date the author's involvement in the Durham Polarimetry Group.

observations but in 1987 this was not possible (the polarimeter in use at that time being manual).

During the reduction process, it became apparent that some extraneous scattered light was also present in the frames. In all probability, this originated from an eighth magnitude star situated a few arcminutes to the north-west of the polarimeter's field of view (FOV). The scattered light was successfully subtracted, as part of the sky, but since the object filled most of the FOV a small amount of object signal was also removed. It can be shown (Appendix A) that the subtraction of unpolarized object signal does not affect the polarized intensity nor the direction of polarization that is recorded. It *does*, however, lead to a slight increase in the recorded level of polarization. The size of this effect, which decreases quickly in the brighter parts of the object, is discussed below. It should be pointed out that the unfortunate removal of object signal would have been untenable if the object signal at the edges of the chip had been *polarized.* This, however, was **not** the case. Polarized light from the object was only incident on the central area of the CCD whereas only outer regions of the detector were used in the sky subtraction.

Figure 5.3 shows the polarization data after subtraction of the extraneous light. The magnitude and direction of **polarized intensity** are plotted as vectors in the reference frame of the CCD. The data are sampled with independent 7×7 pixel bins and then superimposed onto a greyscale image of the galaxy. The greyscale image is derived from combining all the image frames of the galaxy. The galaxy has not yet been rotated to its correct orientation on the sky nor have signal-to-noise cuts been applied to the polarimetric measurements. The purpose of figure 5.3 is to show that the scattered (polarized) extraneous light, that once contaminated large parts of the right hand side and bottom part of the CCD, has been successfully removed and that the polarized light that remains is associated with the centre of the galaxy itself. The low levels of polarized light measured on the far left of the chip are due to poor flatfielding close to the edges of the chip.

The removal of extraneous scattered light, which was carried out above, has for the most part only a small effect on the polarization recorded at the centre of the object. Nevertheless, as a precautionary measure against any errors in the subtraction process, I neglected from any further analysis those polarized intensities in figure 5.3 where the recorded values were less than or equal to the extraneous polarized intensity that had already been removed as part of the sky. As mentioned above, the unavoidable loss of object signal during the subtraction of extraneous light, also leads to a small systematic increase in the recorded polarization on the object. For those parts of the galaxy which remain after the cut on polarized intensity is made, the maximum fractional increase in the recorded polarization is $\frac{4}{3}$. For the brighter parts of the galaxy the systematic increase is much less than this value.

In view of the dearth of fiducial stars available for image frame alignment, it was important to test that the image frames had been aligned with sufficient accuracy to make

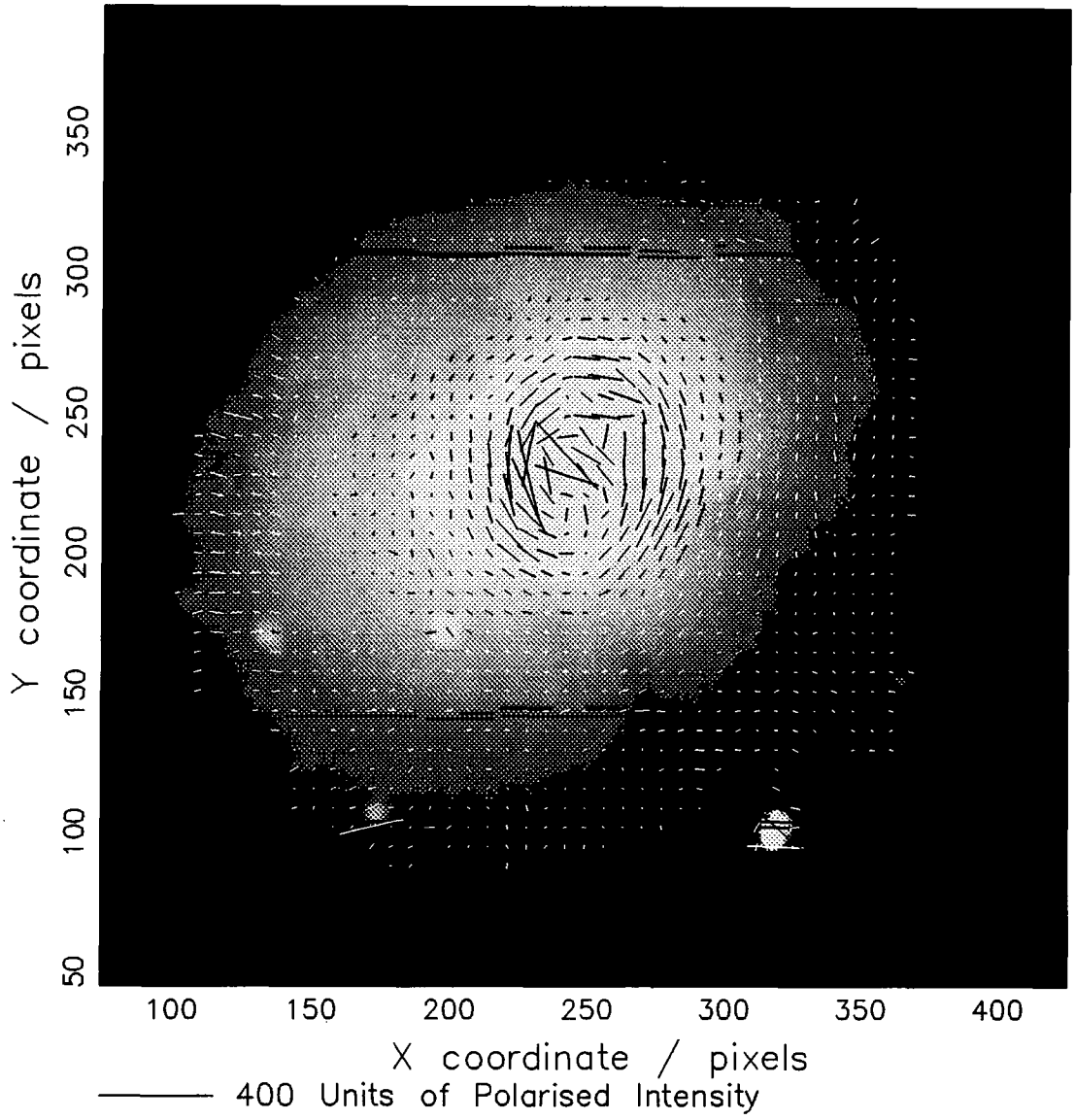

Figure 5.3: Polarized intensity recorded across the CCD. This is after removal of some extraneous scattered light formerly affecting the bottom right part of the detector.

reliable polarization measurements. To this end, image frames were arbitrairily shifted with respect to each other by an amount corresponding to the estimated error in the alignment transformation. After the displacement, new polarization vectors were generated and any differences in the vector pattern were noted. This procedure confirmed that part of the data, which had been aligned using only two fiducial stellar positions, was probably subject to a systematic error caused by inadequate alignment. The vector pattern showed large ($> 45°$) angle changes over very short scale-lengths (a few arcseconds). This is unlikely to be a physical property of the galaxy and the author feels obliged to omit this part of the data from further analysis.

5.2.2 Results and Checks on the Data

Figures 5.4 and 5.5 show the inner $1'$ (900 pc) of NGC 3077 in percentage polarization and polarized intensity respectively. All vectors are independent of one another and the data are sampled with $1.3'' \times 1.3''$ bins. The plotted vectors are significant measurements which are not omitted for any of the reasons given in the previous section. (Vectors approximately $3 \rightarrow 10''$ west of the origin, for example, are omitted because image frames for this region could not be aligned with sufficient accuracy to provide reliable measurements). The galaxy has been rotated to its correct orientation on the plane of the sky and offsets, in arcseconds, are given relative to the peak in polarized intensity measured at the centre of the galaxy (the galaxy does not appear to have a well-defined nucleus at optical wavelengths). A brief description of figures 5.4 and 5.5 now follows before some checks on the data are carried out.

NGC 3077 appears to be polarized over a large part of its interior ($\simeq 1$ kpc). Polarization levels are typically 1-2% and the vector pattern, for the most part, is centro-symmetric about the brightest part of the galaxy (i.e. the central starburst). The main exception to this, is a small peak in polarized light actually at the centre of the galaxy. Within this region the direction of polarization appears to be independent of the centro-symmetric pattern evident in the main body of the galaxy. To the east of the starburst region, the polarization vectors seem to be arranged in filament-like structures.

About $20''$ west of the central starburst there appears to be something of a minor discontinuity in the polarization pattern (figure 5.4). This probably arises from imperfect normalization between image frames taken at different telescope positions (§2.3.1). Imperfect normalization generally occurs when the overlap between adjacent frames is small (the method relies on comparing the signal levels in different image frames for the same location on the object). In this case, however, normalization might have been impaired by the subtraction of extraneous light carried out in §5.2.1. (The removal of unwanted light was basically successful but the subtraction may have been incomplete or imperfect over some parts of the detector). If this is the case, the error for most of the vectors in figure 5.4 should not be too great. The normalization was carried out using the brightest part of galaxy where the removal of extraneous light has only minor influence on the

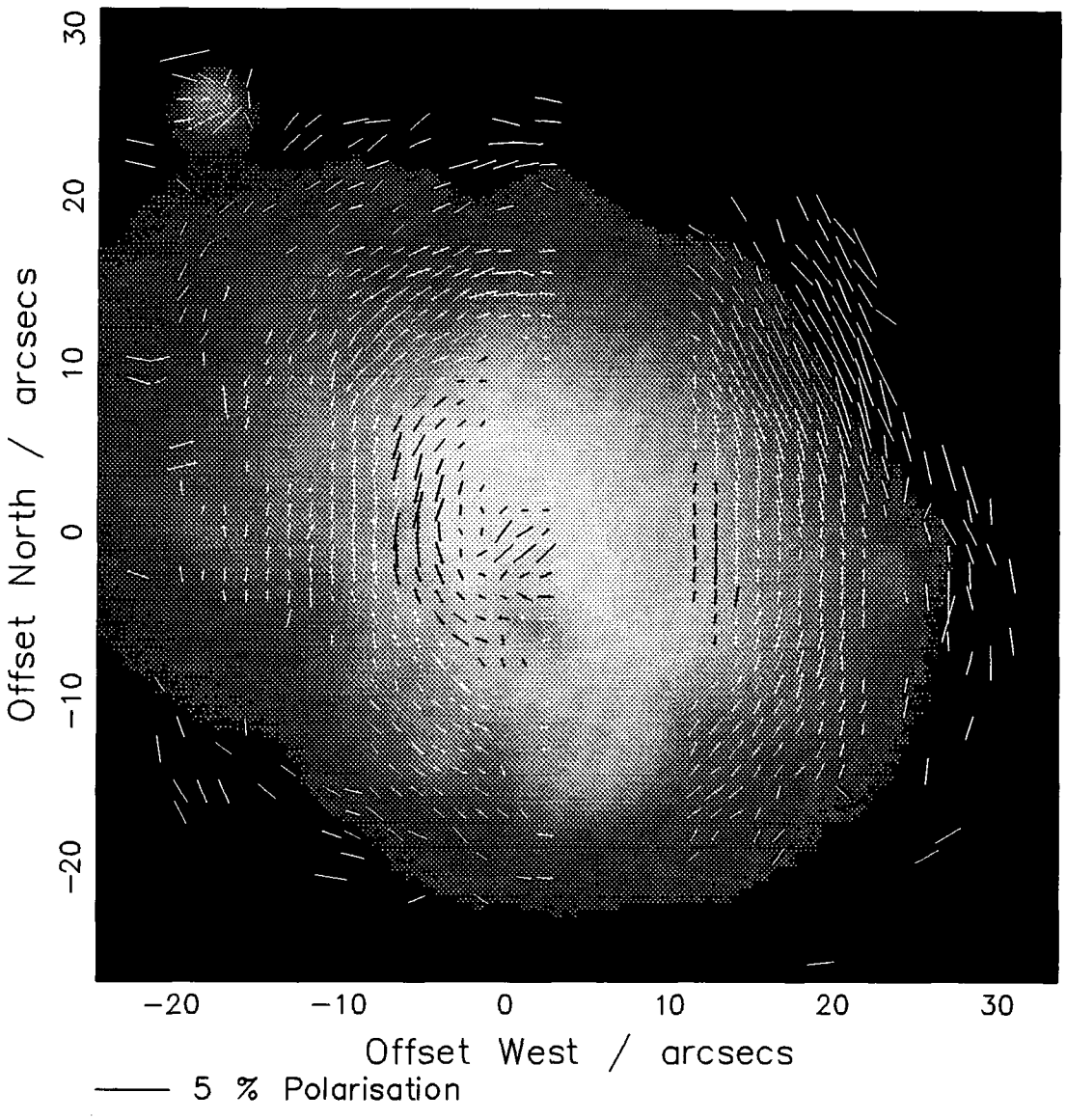

Figure 5.4: A polarization map of NGC 3077

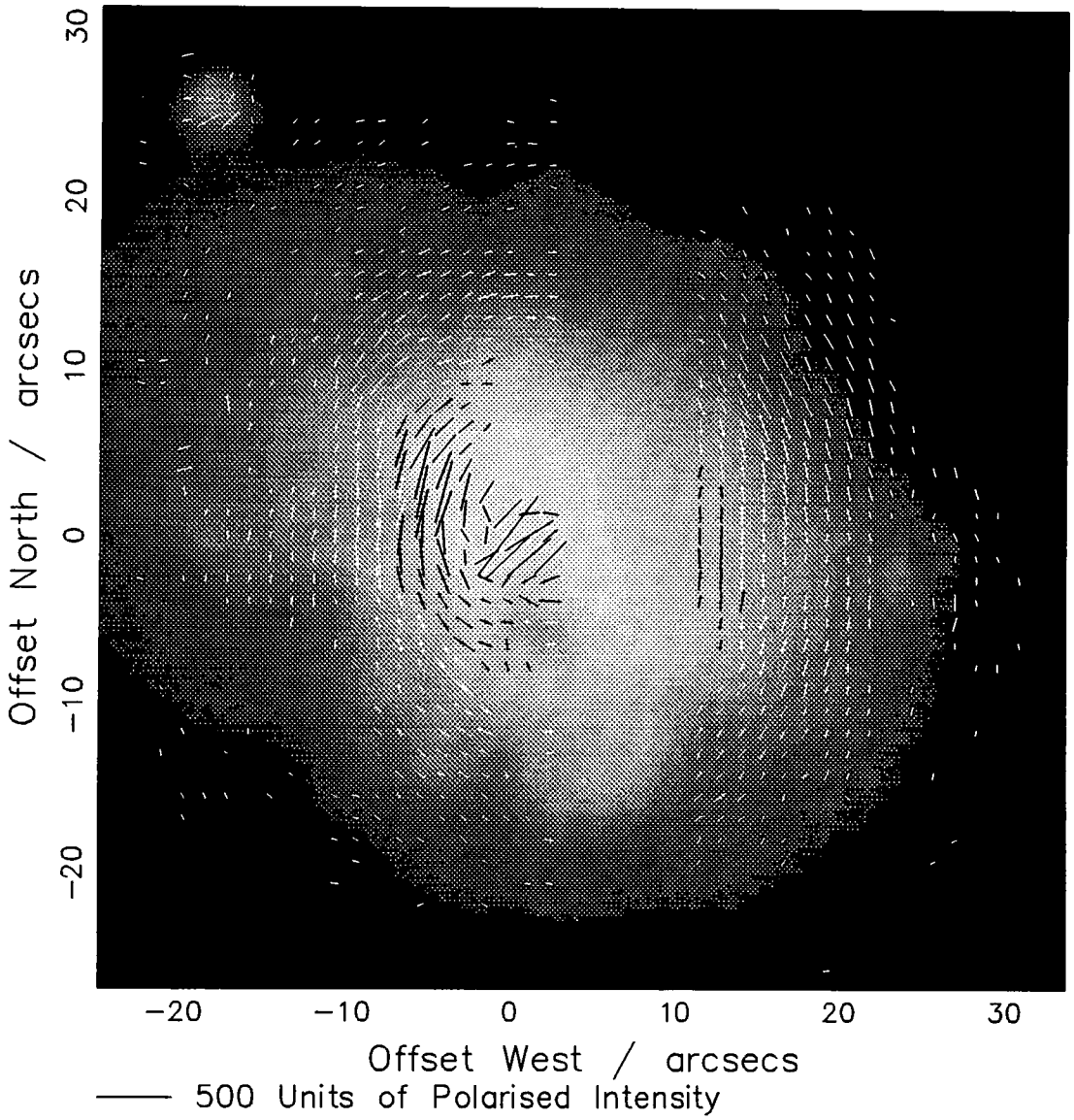

Figure 5.5: The polarized intensity detected from NGC 3077

recorded intensity and polarized intensity. The areas of the galaxy worst affected should be those $20 - 30''$ from the central starburst where the polarized intensity from the object approaches the polarized intensity subtracted as part of the extraneous component. The true extent to which the peripheral regions of figures 5.4 and 5.5 are polarized, awaits an improved data set which is free from extraneous scattered light.

The set of short exposures made for the brightest part of NGC 3077 (§5.2) allowed a check to be made on the polarization recorded in the inner region. Figures 5.6 and 5.7 show polarimetry measurements for the region in question. Figure 5.6 is derived from the longer (300 second) exposures whilst figure 5.7 is produced from the shorter (100 second) exposures. It is important to emphasize that, apart from being divided by the same flat field, the shorter and longer exposures have been handled separately. Figures 5.6 and 5.7 constitute, therefore, two approximately independent sets of measurements. In both figures, vectors denote polarization measurements made from independent $1.3'' \times 1.3''$ bins and a greyscale image records the polarized intensity. Logarithmic contours from the optical image of figure 5.1 are also superposed onto the figures. The very brightest part of the galaxy in this filter is marked with a cross.

Despite significant differences in signal-to-noise, similar polarization features are evident in both figures 5.6 and 5.7. Both sets of exposures manifest filamentary-like structures to the east of the starburst. These are discernible in polarized intensity as well as linear polarization. A compact source of polarized light, just south of the optical maximum, also appears in both figures.

The peak in polarized light at the centre of NGC 3077 is most unusual. It is slightly displaced from the optical maximum and possesses a direction of polarization which is quite different from the large scale polarization pattern observed against the main body of the galaxy. I have tabulated in table 5.1 the properties of this feature using data in figures 5.6 and 5.7. To be certain that the feature is not the artifact of a poor flat field, I also took the original 300 second CCD image frames, divided by a unity flat field and remeasured the properties of the compact polarized source. These results are also shown in table 5.1. For each of the above (three) cases, I give the level of polarization and its corresponding direction for the central polarized source. Its displacement from the optical maximum is also stated. This information is determined using two different aperture sizes ($2.5''$ and $3.8''$).

Table 5.1 shows that a peak in polarized light is consistently detected at $\simeq 1''$ south of the optical maximum in NGC 3077. Its linear polarization is about 2% although a measurement to an accuracy of better than 0.5% is probably not possible with the data presently available. (Incidentally, the errors cited in table 5.1 are 'normal errors' due to photon noise etc. - the removal of extraneous light detailed in §5.2.1 has negligible effect on the polarization recorded at the centre of the object). The idea that the central polarized feature is a result of poor flatfielding or some other flaw in the data is clearly not tenable.

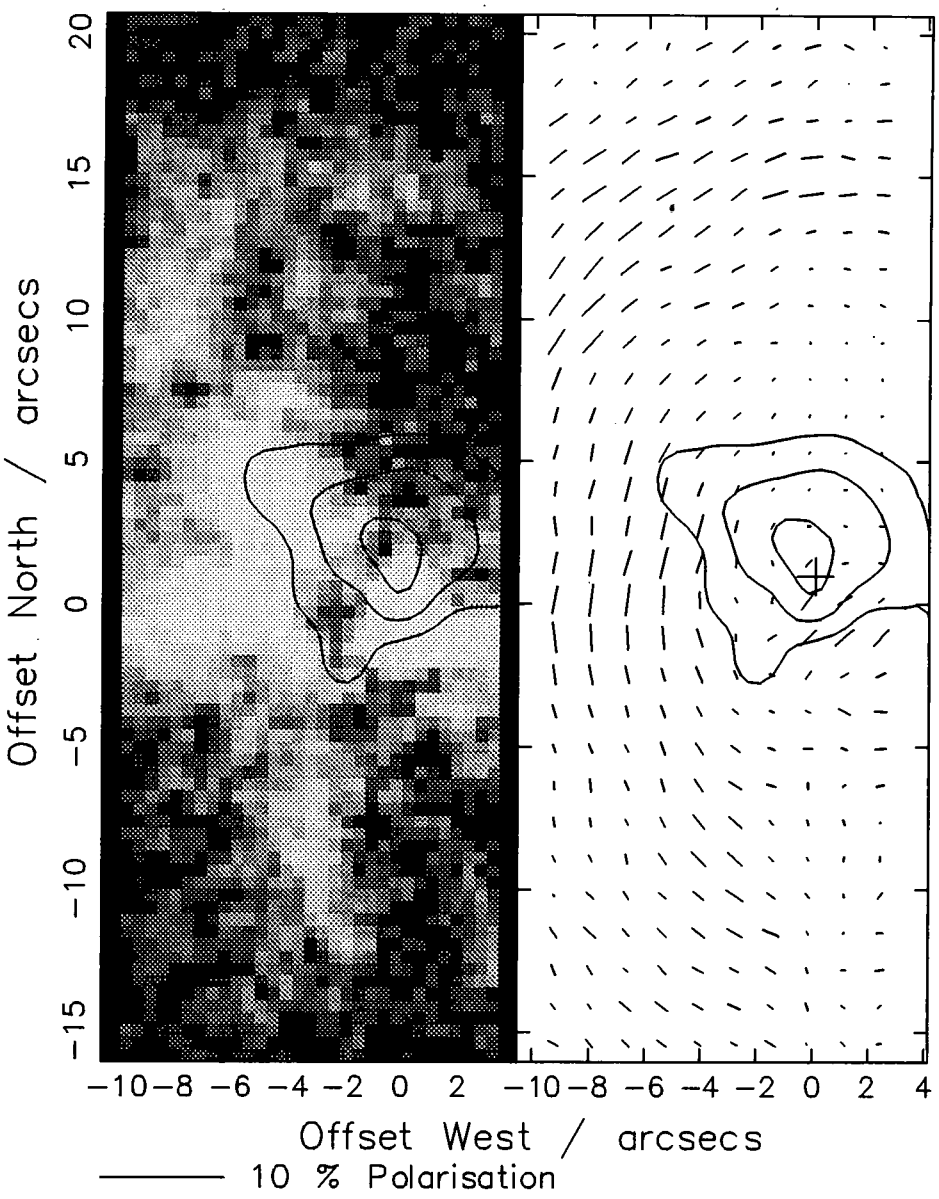

Figure 5.6: Polarimetry measurements for the centre of NGC 3077 derived from a set of 300 second exposures. Lighter shades of the greyscale image represent higher levels of polarized intensity. Contours denote the central starburst. See text for further details.

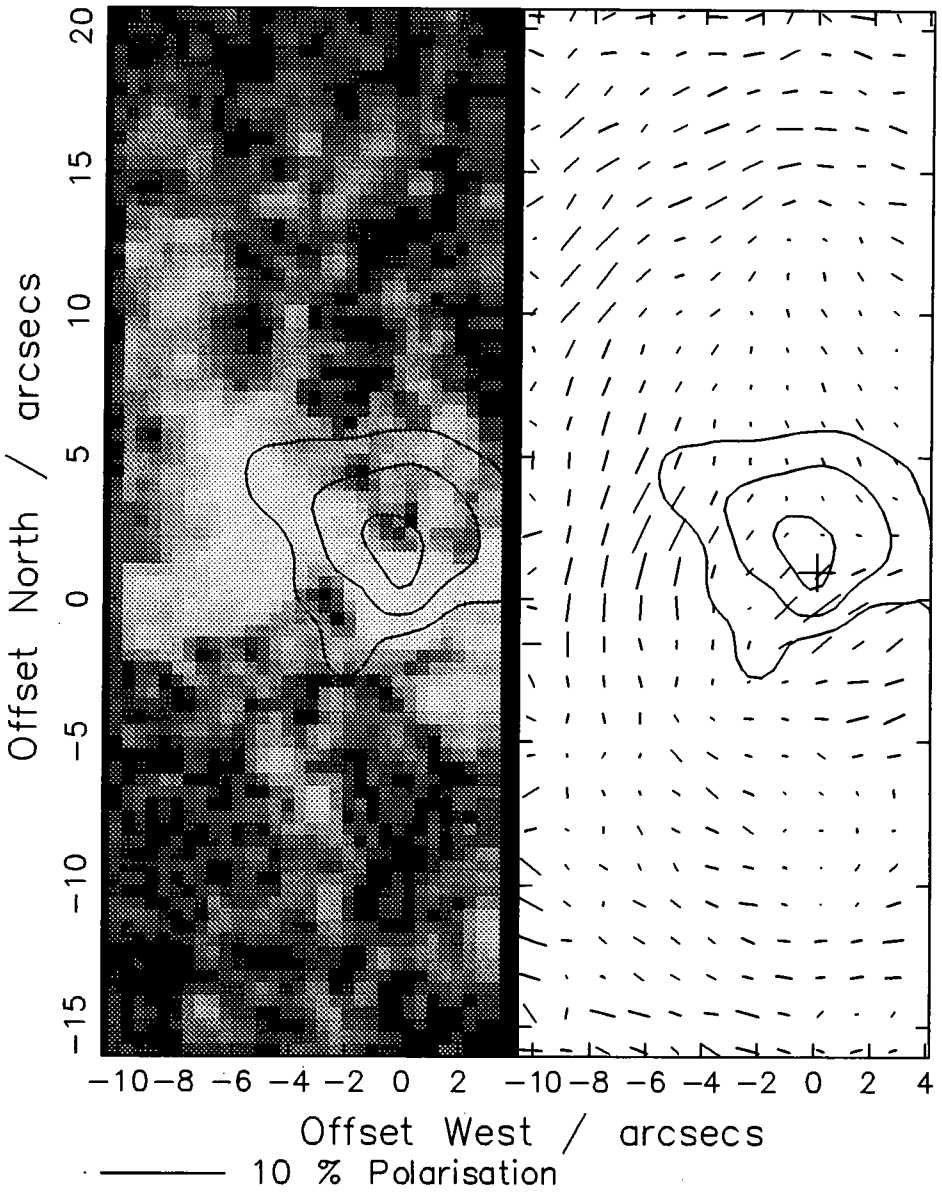

Figure 5.7: Polarimetry measurements for the centre of NGC 3077 derived from a set of 100 second exposures. Lighter shades of the greyscale image represent higher levels of polarized intensity. Contours denote the central starburst. See text for further details.

I, therefore, adopt it as a real property of the galaxy. Although the peak in polarized intensity appears to extend in a westerly direction in figures 5.6 and 5.7 the brightest part of the feature is quite compact. In fact, its FWHM is close to the size of the effective seeing disk ($\simeq 2''$). One may infer from this that the true size of the feature may be extremely compact ($\leq$ 30 pc). Hereafter, reference to the "central polarized feature" implies this compact intense source of polarized light at the centre of NGC 3077.

5.3 Astrometry and Comparison with Other Observations

Dr Ray Wolstencroft kindly provided a chart of the sky near NGC 3077. It was produced from the Digitized Sky Survey (DSS). Three stellar positions from the chart were identified as potential astrometric calibrators for the polarimetry images. Unfortunately, of these three stars, only one was well defined in the image frames. As a consequence of this, I sought alternative means of calibrating the images.

Of all the authors in the literature, Barbieri *et al.* (1974) have carried out the most accurate astrometry for NGC 3077. They used several SAO stars to determine the position of bright starforming regions both at the 'nucleus' and throughout the body of the galaxy (they quote an accuracy of $0.5''$). In the absence of sufficient stars to make my own astrometric calibration, I used their cited positions for three compact, well-defined features located $\geq 0.5'$ from the centre of the galaxy (knots 'a', 'm' and '1' in Barbieri *et al.*). With this information, and one useable stellar position from the DSS chart, I calibrated the polarimetry images to an estimated accuracy of $1 - 2''$. The calibration was in good agreement with previous calibrations of the CCD at the base of the Isaac Newton Telescope.

Figure 5.8 shows a greyscale intensity image of the brightest part of NGC 3077. Contours, separated by 0.3 mag, are superimposed onto the greyscale image and the positions of various detections have been overlayed using the astrometric calibration described above. These detections are derived from observations of NGC 3077 in several wavebands and have been discussed in §5.1. Table 5.2 gives a summary of the data as well as a key to the markers plotted in figure 5.8. The central polarized feature, identified in the previous section, was used as the origin of figure 5.8. The reasons for this were as follows: (a) the optical maximum is not particularly well defined and its position may well be wavelength-dependent (Price and Gullixson 1989; Thronson *et al.* 1991); (b) the location of the central polarized feature appears to be constant within the polarimetry data (§5.2.2). For reference, the origin of figure 5.8 is RA=9h 59 19.7 and DEC=+68 58 32.3 (1950).

The size of the markers in figure 5.8 generally represents the positional uncertainties cited by their respective authors. Exceptions to this are as follows: (a) the size of the circle denoting the central polarized feature corresponds to its FWHM; (b) the *width* of

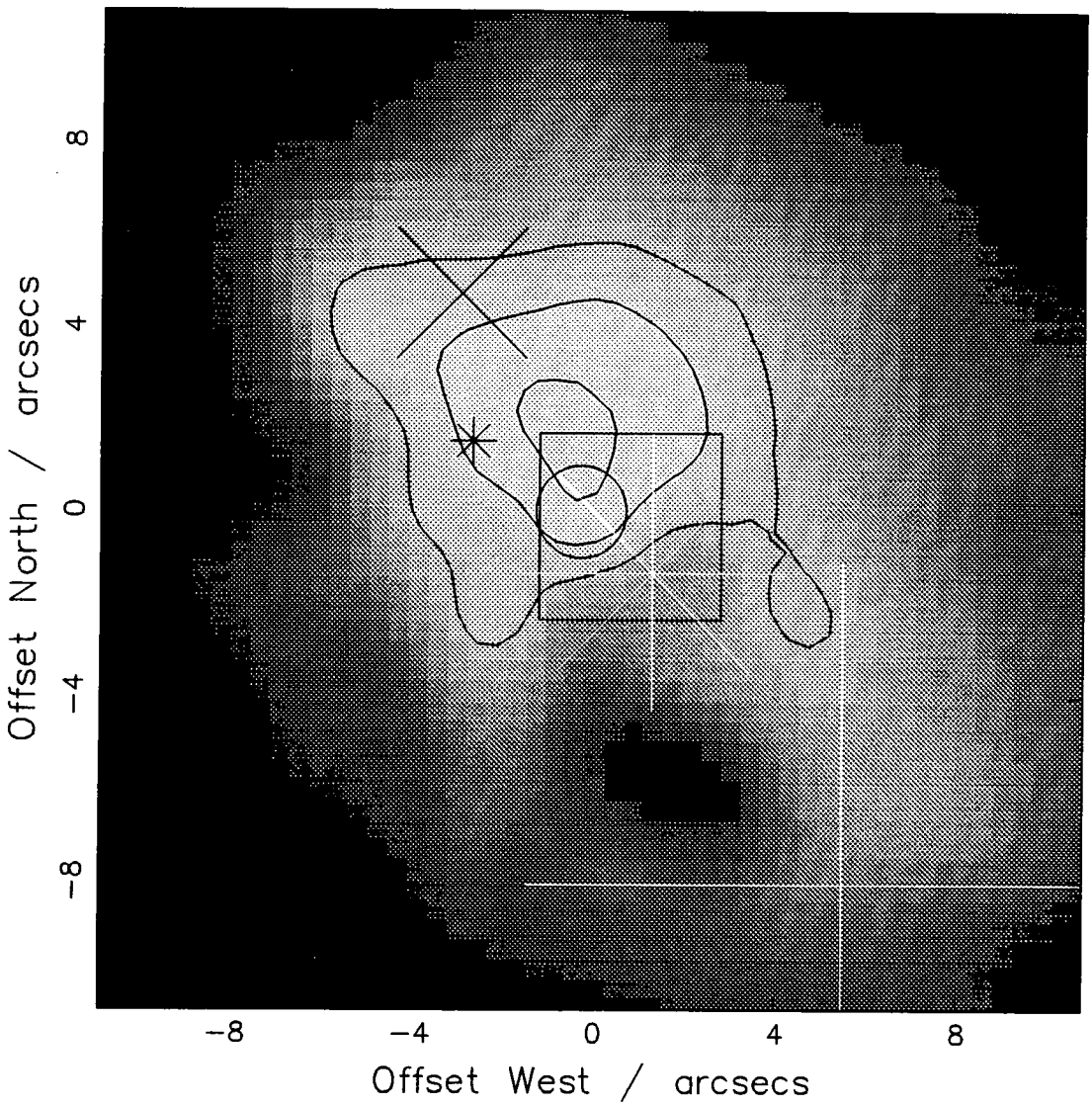

Figure 5.8: Comparison of observations carried out for NGC 3077. A key to the plotted markers is given in table 5.2.

the radio marker should be larger by nearly a factor of three (only symmetrical markers could be drawn using the adopted plotting package). The radio position given by van der Kruit (1971) is plotted in preference to that given by Hummel *et al.* (1987) because the latter do not give their positional accuracy. Incidentally, the dense gas cloud detected by Price and Gullixson (1989), and also discussed in §5.1, manifests itself in figure 5.8 as an absorption feature 6″ south of the origin.

A few comments are in order about the positions shown in figure 5.8. The position given by Price and Gullixson (1989) for the 2.2μm centroid is somewhat dubious. The authors made their astrometric calibration using a single star (SAO 015066) which was offset, by several degrees, from the galaxy itself. Furthermore, the fiducial position cited by the authors does not agree with that in the SAO catalogue[3]. Price and Gullixson (1989) have imaged NGC 3077 in various optical filters but it is difficult to know, in view of a potential error, to what extent the position of their images can be inter-compared.

The second comment relevant to figure 5.8 concerns the displacement between the Hα centre and the brightest part of the greyscale image. The optical appearance at the centre of NGC 3077 is clearly dominated by continuum emission from the starburst (figure 5.1). Furthermore, emission-line radiation can almost certainly be expected from hot gas residing within the same regions. It is, therefore, somewhat surprising that the emission-line and continuum maxima are not cospatial within figure 5.8. Although the centre of NGC 3077 may be subject to significant obscuration in places (e.g. the dust cloud 6″ south of the polarized source), the effective 'filter' used for the greyscale image is close to the wavelength of the Hα line (658nm) (see §5.2). This suggests that extinction is **not** responsible for the separation between the Hα peak and optical maximum. Now, as mentioned above, Price and Gullixson (1989) have imaged NGC 3077 in various optical filters and the peak emission in their images *does* show some positional variation according to wavelength. It appears, however, that only light blueward of 700nm (U,B and V) is displaced to the west of the Hα centre. This may not be at variance with figure 5.8 if the centre of NGC 3077 is particularly blue and mostly blue light has been incident on the polarimeter detector (the effective FWHM of the detector is 350 nm). One should note, however, that the absolute, and perhaps relative positions, cited by Price and Gullixson (1989) may be unreliable (see preceding paragraph).

Clearly, a more accurate astrometry is required for the detections plotted in figure 5.8. Regardless of present uncertainties in the positional data, the central 10″ of NGC 3077 is evidently a very active region. The nature of this activity is discussed in the next section.

[3]Smithsonian Astrophyiscal Observatory Star Catalog Vol.1 (1966)

Table 5.1: The central polarized source in NGC 3077

Data Frames	Aperture (arcsecs)	Polarization %	P.A. (degrees)	Displacement (arcsecs)
300 secs.	2.5	1.7 ±0.3	-57±5	0.9
	3.8	1.3 ±0.3	-58±7	0.9
100 secs.	2.5	2.5 ±0.8	-49±9	0.8
	3.8	1.8 ±0.8	-50±12	0.8
300 secs.	2.5	2.5 ±0.4	-57±5	0.9
unity flat field	3.8	1.6 ±0.4	-58±7	0.9

Table 5.2: Multi-wavelength detections at the centre of NGC 3077

Marker	Detection	Authors	Position (1950)		Uncertainty (″)	
			R.A.	DEC.	R.A.	DEC.
diagonal cross	2.2μm centre	1	9 59 20.20	+68 58 37.0	2	2
small star	Hα centre	2	9 59 20.15	+68 58 33.8	0.5	0.5
square	20cm radio	3	9 59 19.50	+68 58 32.0	5.6	2.1
large star	CO centre	4	9 59 19.4	+68 58 31	3	3
large cross	x-ray (ROSAT)	5	9 59 18.60	+68 58 24.3	7	7
circle	polarized source	6	9 59 19.7	+68 58 32.3	2	2

1: Price and Gullixson (1989)
2: Barbieri *et al.* (1974)
3: van der Kruit (1971)
4: Becker *et al.* (1989)
5: Bi *et al.* (1994)
6: this work

5.4 Discussion

The large-scale ($\sim$ 1 kpc) polarization of NGC 3077 almost certainly arises from **dust scattering**. This conclusion is based on the following considerations.

It seems unlikely that grains aligned in a magnetic field are responsible for the polarization pattern seen in figure 5.4. The vector pattern is centro-symmetric about the starburst, which is suggestive of scattering, and is also partly characterized by a filamentary-like structure. There is **no** indication of the kind of smooth spiral or elliptical polarization structure which, in disk galaxies for example, traces out the galactic magnetic field (§4.3.1). Moreover, polarized light is only detected from the centre of NGC 3077 (figure 5.3) whereas a galactic-scale magnetic field can be expected to permeate most of the ISM. Other observations that argue against the presence of aligned grains are as follows: (a) the older stellar population has a luminosity profile more akin to an elliptical galaxy rather than a disk galaxy (Price and Gullixson 1989). Aligned grains tend to occur within the disks of spiral galaxies; (b) there is no evidence for sizeable rotation (Demoulin 1969). This may be necessary for the generation of a magnetic field (Donner and Brandenburg 1990); (c) aligned grains are expected to produce significant levels of extinction ($A_R \simeq 0.5$ mag for polarization levels of 2-3%; §3.3.3). There is no evidence for dust lanes or any other galactic-scale absorption regions.

Since ionized gas in NGC 3077 is found over a similar sized region to the polarization pattern in figure 5.5 (§5.1) one may be tempted to postulate that electron scattering is responsible for the polarized light detected from this galaxy. This hypothesis, however, is quantitatively ruled out in §9.2 where electron scattering is dismissed for all the galaxies observed in this thesis.

One concludes that scattering from diffuse dust is the likely cause of the large-scale polarization pattern observed in NGC 3077. Indeed, scattering simulations carried out in §9.5.6 satisfactorily reproduce the observations and even deliver information about the amount of dust that might be present. For many plausible model parameters, a dust mass of a $1 \times 10^5 M_\odot$ sparsely distributed over the inner square kiloparsec of NGC 3077 provides a satisfactory solution (there is, however, a degree of uncertainty attached to this calculation; §9.5.6). In effect, a giant reflection nebula occupies the central kiloparsec of NGC 3077 ! The dust is illuminated by the starburst at the centre of the galaxy. Since illumination from the central starburst takes place in a radial direction, dust to the east of the starburst must be arranged in filament-like structures to account for polarized light detected in this part of the galaxy. It is apparent from figures 5.6 and 5.7 that these structures are morphologically tied to the starburst suggesting that the present scattering material might have originated from the starburst itself. Indeed, the distribution of scatterers to the east of the starburst is very reminiscent, morphologically speaking, of the emission-line shells and filaments left by the superwind in some starburst galaxies (§3.1 and §6.7). They are also not too dissimilar, in shape, to the dust filaments emanating from the starburst in

NGC 1808 (§2.2.2). This resemblance may not simply be a coincidence. The dust detected in polarized light may have been expelled and 'snow-ploughed' in a similar fashion to the ambient dust and gas in superwind galaxies (§1.4).

In the past, gas ingestion has been invoked to explain some of the features observed in NGC 3077. Thronson *et al.* (1991), imaging in several optical filters, claim to detect small rings and shells against the main body of the galaxy. They attribute these inhomogeneities to gas infall, probably from the bridge of neutral material that connects NGC 3077 to M81 (§5.1). Likewise, Barbieri *et al.* (1974) note the presence of small 'dust patches' in their images which, in principle, could be part of the same process (they are also apparent in figure 5.1). It should be pointed out, however, that most of these absorption features tend to be some distance from the 'nucleus' (typically $\geq 20''$). There is no spatial correlation between the polarization of NGC 3077 and this purported infalling material. It seems likely that the observed scattering is associated with gas outflow rather than gas infall.

Attention is now drawn to the compact polarized source detected close to the central starburst (figures 5.6 and 5.7). The level of polarization ($\simeq 2\%$) is similar to that found in other parts of the galaxy but, if scattering constitutes the relevant polarizing mechanism, it is difficult to see why the central feature is morphologically and directionally independent of the giant reflection nebula identified above. The level of polarization at the central feature is also typical of grains aligned in a magnetic field (e.g. NGC 1667; §4). Whilst it has already been concluded earlier in the text, that a galactic-scale magnetic field in NGC 3077 is unlikely, this should not preclude the existence of a magnetic field local to the central starburst. Clearly this is all very speculative until a more indepth study of the central region is carried out. In particular, polarization measurements are required for the whole of the central region (which, unfortunately, was not possible with the current set of data). Spectro-polarimetry may also help to determine the nature of the central polarized source. In lieu of more detailed polarimetric information I turn my attention to detections in other wavebands.

It is evident from figure 5.8 that the central $10''$ (150pc) of NGC 3077 is a very 'active' region. There is ample evidence for recent and intense star formation - namely blue colours, ultraviolet emission, copious Hα and x-ray emission etc. (§5.1). The detection of dense gas and dust clouds in the same region suggests that star formation may still be proceeding. The compact nature of the polarized source ($\leq$ 30 pc) indicates that the centre of NGC 3077 is potentially the site of more exotic phenomena. Intriguingly, the radio source detected at the centre of NGC 3077 has an energetic, compact ($\leq$ 10 pc) core (Hummel *et al.* 1987). It also coincides, within positional errors, with the polarized source (figure 5.8). The luminosity and small size of the radio core are remarkably similar to the radio sources recently discovered in Sersic-Pastoriza galaxies (Saika *et al.* 1994). Sersic-Pastoriza galaxies are starburst systems characterized by a small number of bright star forming features lying $\sim$ 1kpc from the nucleus. Within the galaxies they observed, Saika *et al.* (1994) found one or more compact radio sources cospatial with the star forming regions. The authors

attribute these unusual features to young supernova remnants (although the luminosity of their detections is typically 1-2 dex higher than the SNR detected in our own galaxy or nearby M82). By virtue of its proximity to a similar radio feature in NGC 3077, one could speculate that the central polarization feature is associated with a luminous supernova or collection of supernovae in the starburst.

It should be pointed out there is **no** evidence for an unresolved energy source in NGC 3077. The x-ray and radio data obtained for this low mass galaxy (§5.1) do **not** indicate the presence of a Seyfert nucleus. Moreover, a preliminary spectroscopic study carried out by Demoulin (1969) did not find the kind of broadened emission associated with the NLR of an AGN. At first sight, a lack of broadened emission might also appear to rule out the existence of an outflow in NGC 3077 (which was hinted at in §5.2). We note from §6.7, however, that superwinds in low mass starburst systems tend to be characterized by quite low emission-line velocities ($\simeq$ 50 kms^{-1}). Velocities of this order would not have been detected in the spectroscopic study made by Demoulin (1969). This, incidentally, emphasizes the need for a higher resolution spectral study of this somewhat overlooked galaxy.

5.5 Summary and Future Observations

The central kiloparsec of the nearby, low mass starburst galaxy NGC 3077 is characterized by a giant reflection nebula. Diffuse dust within this galaxy scatters optical radiation from the central starburst giving rise to detectable levels of polarization ($\simeq 1-2\%$). In places, the scattering material appears to be distributed in filamentary-like structures which are probably physically connected to the starburst itself. One possibility is that dust has been expelled in an outflow from the centre. Concrete evidence for a superwind in NGC 3077 can, however, only be provided by high resolution spectra.

A compact ($\leq$ 30 pc) source of polarized optical radiation is also detected in NGC 3077. This lies at the most active part of the central starburst. The nature of this feature cannot be ascertained from the current polarimetric data - spectro-polarimetry may be required. High resolution, astrometrically-precise observations outside the optical waveband would also be helpful. For example, a tentative connection was made between the polarized source and a compact radio source at the same location. Radio features of this size and luminosity have recently been detected in other starburst galaxies and are believed to be associated with young supernova remnants (Saika *et al.* 1994).

Improved polarimetric data are required to ascertain the true extent of the reflection nebula found in NGC 3077. The current observations were impaired by the presence of extraneous light in the image frames and this meant that reliable polarization measurements could only be obtained for the central arcminute of the galaxy. Due to its proximity, NGC 3077 should be imaged with a smaller telescope (2-meter or less). Alternatively, an exten-

sive 'mosaic' of exposures could be obtained at different positions of the telescope. This would allow the sky to be sampled correctly and may provide more fiducial stellar positions. (The latter are necessary for the alignment of exposures taken with the polarimeter. They also enable high precision astrometry to be carried out).

Chapter 6

Blue Compact Dwarf Galaxies

6.1 Introduction

Blue compact dwarf galaxies (hereafter BCDGs) are low mass galaxies that are dominated, visually, by very recent or on-going star formation in a compact region of their ISM. The young stars are usually concentrated in a small number of emission-line knots which lie up to a few hundred parsecs from the geometric centre of the system. The host galaxy tends to be a few kiloparsecs in size, although, as we shall see, there is some diversity in the optical morphology of the class.

BCDGs first caught the attention of observers because they are characterized by strong emission lines which resemble those emitted by Galactic HII regions (Searle and Sargent 1972). For that reason, BCDGs are also sometimes classified as HII galaxies. In the past, the term *blue compact galaxies* (or BCGs) has often been used synonymously with BCDGs. Strictly speaking, however, BCDGs form a sub-set of BCGs, as the latter can sometimes include larger emission-line objects such as starbursting spirals (Keel 1988). Although BCDGs probably constitute the majority of galaxies that have been termed blue compact galaxies, the present discussion, as well as the polarimetric data analysed in this thesis, only refer to the former low mass systems. Henceforth I use the term BCDG to avoid any confusion that may arise.

In the following sections I review the salient features of BCDGs emphasizing the evidence for recent star formation and the manifestation of galactic outflow. Some discussion is given to the ISM of BCDGs because this may be relevant to the polarization properties of this class. At the close I make some brief comments about how BCDGs compare with other starburst galaxies such as far-infrared galaxies (FIRGs; §1.2). As a prelude to these topics, however, it may be appropriate to clarify the classification of BCDGs with respect to other low mass galaxies.

6.2 Classification of Dwarf Galaxies

The classification of dwarf galaxies appears to be a more complex (and perhaps slightly more ambiguous) problem than that associated with larger galaxies such as spirals and ellipticals. It is probably fair to say that the reason behind this is that less is generally known about the former due to their smaller size and fainter luminosity. A sensible division of dwarf types can usually be made on gas content and evidence for recent star formation (Gallagher and Hunter 1987 and references therein). Collectively, irregular dwarf galaxies and BCDGs form the family of **gas rich** dwarfs which show evidence for young stars (ages $\sim 10^8$ yrs or less). This contrasts with the group of **gas poor** dwarfs which includes dwarf ellipticals and dwarf spheroidals. Gas poor dwarfs tend to show little evidence for ongoing or recent star formation. A distinction can be made between BCDGs and dwarf irregulars in that the former have recent star formation concentrated in a few compact regions at the centre of the galaxy. Dwarf irregulars, on the other hand, are characterized by a more uniform distribution of young stars across their ISM. The LMC and SMC serve as examples of the latter. A possible evolutionary link between gas-rich and gas-poor systems is discussed in §6.7 where the issue of gas loss via energetic outflow is addressed.

6.3 Recent Star Formation - the Starburst

In contrast to the young stellar clusters in most FIRGs (§1.2), the starburst in BCDGs is relatively unobscured at optical wavelengths. BCDGs are characterized by intense optical emission lines which have been the subject of several spectroscopic studies (e.g. Campbell *et al.* 1986). The emission line widths and line ratios are consistent with the presence of a hot (10,000-20,000 K) gas ionized by massive, luminous O stars. The number of O stars must be large. Emission in the Hβ line is typically 10 times more intense than that detected from the large HII region 30 Doradus in the LMC !

The photometric colours of the emission-line region indicate **very recent** star formation. Thuan (1983) used optical colours in conjunction with the stellar models of Struck-Marcell and Tinsley (1978) to infer ages of $\sim 10^7$ years or less for the starburst in many BCDGs. Marlowe *et al.* (1995) came to a similar conclusion comparing UBV colours with the colour-age relationship determined for nearby star clusters in the Magallanic Clouds. The International Ultraviolet Explorer (IUE) has successfully detected ultraviolet emission lines from the young stellar population in some cases (Kinney *et al.* 1993). Once again the spectra are consistent with the presence of very massive (and therefore young) stars.

The spectra detected from some BCDGs have aroused considerably interest amongst some observers because they are a source of broadened HeII ($\lambda\lambda$4686) emission (Vacca and Conti 1992; Kunth and Sargent 1981). This spectral feature can be associated with the energetic winds that characterize **Wolf-Rayet** (WR) stars. WR stars are the post main-sequence descendants of the most massive O stars (initial masses $\geq$ 35 $M_\odot$). They lose

the majority of their hydrogen envelope in a fast ($\sim$ 2500-3000 kms^{-1}) dense wind which exposes the fusion products of the hydrogen-burning core (see Conti 1991 for a review). Probably the most impressive aspect of the WR spectral features detected in some BCDGs is the implied ratio of WR to O stars. Under conditions of continuous star formation this ratio is expected to be quite low (Vacca and Conti 1992). This reflects the short duration of the WR phase ($\sim 10^5$ years) compared with the main sequence lifetime of the O star progenitor (roughly ten times longer). The relatively large number of WR stars detected in some BCDGs suggests that star creation ceased only 10^6 years ago. The possibility of observing young stellar clusters in such a short-lived phase indicates that star formation must be occurring in very short (10^{6-7} yr) bursts.

The picture that is emerging for BCDGs is that they undergo short episodic bursts of star formation and that these episodes may occur without the stimulus of galactic collisions. As we shall see in §6.4, the metallicity of BCDGs is generally believed to be quite low and yet current star formation is evidently extremely intense. This constrains star formation to proceed in short intense bursts. Most BCDGs are characterized by several star forming, emission-line knots (or hot-spots) which are separated by tens to hundreds of parsecs (e.g figure 7.1 which is discussed in chapter 7). Kunth *et al.* (1988) used B-I photometry to examine the hot-spots in two BCDGs. From the observed colours they inferred different ages for the various features. This is consistent with non-continuous star formation proceeding in localized compact bursts.

Gerola *et al.* (1980) have simulated the starbursting behaviour of dwarf galaxies by predicting the star formation rate as a function of time for galaxies of differing mass. They assume that star formation propagates stochastically through the ISM via the injection of mass and energy from massive stars and supernovae. They found that low mass systems, by virtue of their small ISM, can effectively 'burn themselves out'. Thus, whilst larger galaxies can sustain star formation over at least some part of their ISM, star formation in dwarf galaxies fluctuates between high and low states of excitation. Within this context, BCDGs may represent a high excitation state of gas-rich dwarf galaxies.

6.4 The ISM of BCDGs

Observations of BCDGs seem to indicate that their ISM is quite young. Spectra of their emission-line regions suggest that star formation is taking place in a metal-poor environment (abundances 0.05-0.5 solar; Campbell *et al.* 1986). In one extreme case, the observed fraction of heavy elements is consistent with only one other previous burst of star formation (see IZw18; Kunth and Sargent 1986) There are a few caveats to the conclusion that BCDGs are metal-poor systems. Firstly, there is mounting evidence that galactic-scale winds operate in many BCDGs. These have sufficient energy to remove gas and newly-synthesized metals from the starburst region (§6.7) and may, therefore, be an essential

ingredient in any models of chemical evolution (Marconi *et al.* 1994). In addition, some of the most metal-poor BCDGs may also be subject to **gas inflow** from the intergalactic medium. It is this topic which I wish to discuss next.

It is now well established that BCDGs are gas-rich, having gas fractions (ratio of gas mass to mass in stars) of order 0.1-0.5 (Thuan and Martin 1981). In some cases it appears that the galaxy in question is still condensing out of the intergalactic medium. Viallefond and Thuan (1983) carried out radio interferometry for a small number of BCDGs with very low metallicity. They found that in neutral hydrogen these galaxies consist of a dense core surrounded by a halo of gas clouds which extend far beyond the current star forming regions (several kpc as opposed to $\sim$ 100 pc). The current star formation appears to be associated with the HI core rather than the halo clouds. One possibility is that the peripheral gas clouds constitute material that is currently being accrued from the intergalactic medium.

Although rich in atomic gas, BCDGs appear to be poor in molecules (Arnault *et al.* 1988; Israel *et al.* 1995). This is somewhat surprising because molecular gas is a tracer of dense gas and it is within regions of enhanced gas density that new stars are born. (By way of contrast, FIRGs, which are discussed in §1.2, have typically half of their gas in molecular form). It is possible that the low metallicity of BCDGs no longer allows the CO molecule to be a good tracer of molecular hydrogen. Alternatively the conditions of the gas may quite different to those prevailing in the giant molecular clouds that make up the bulk of H_2 in our own galaxy (§1.2).

6.5 Previous Star Formation

The impression of BCDGs that has been given so far, is that of young, metal poor objects that may still be condensing out of the intergalactic medium. In many cases, this description is wholly appropriate. For a sizeable fraction of BCDGs, however, there is evidence for a background population of older stars. The older stellar population is quite often dim at optical wavelengths so that the appearance of the galaxy is still dominated by the bright star forming regions near the centre of the galaxy. Figures 7.1 and 8.1 show optical continuum images of two BCDGs which fit this description.

Evidence for a background stellar population in at least some BCDGs may be inferred from colour maps and possibly from NIR measurements. Kunth *et al.* (1988) traced the B-I luminosity profile in a small number of BCDGs and found that the stellar population becomes redder at larger radii. This is consistent with an increasing contribution from older stars outside the starburst region (ages $\sim 10^9$ yrs). Thuan (1983) carried out JHK photometry of 36 blue compact dwarf galaxies and claims to have detected the presence of red giants. Unfortunately, NIR colours alone are poor discriminators between red giants

and red **supergiants** (which are much younger). CO indices are required in order to distinguish between low mass and high mass stars (Campbell and Terlevich 1984).

Whilst direct evidence for older stars has not been particularly forthcoming, some observations imply the presence of 'missing mass' in BCDGs. If, for example, the neutral gas clouds detected in some BCDGs by Viallefond and Thuan (§6.4) are to be virialized, $10^{8-9}M_{\odot}$ must exists either within an older stellar population or in a halo of dark matter (Thuan 1983). If older stars are to account for the 'missing mass' their distribution must be far more extensive than the current star forming regions. The low luminosity halo which surrounds the emission-line regions in many BCDGs is consistent with this requirement.

6.6 Dust in BCDGs

The dust content of blue compact dwarf galaxies may be of direct relevance to some of the observations made in this thesis. The reason for this is that the optical polarization of galaxies results predominantly from the interaction light with dust grains (§2.3.3). The low metallicity generally measured in BCDGs immediately suggests that these systems are likely to be dust poor (Issa *et al.* 1990). Indeed, the intense optical and ultraviolet line emission detected from many of these galaxies (§6.3) is a testament to the absence of obscuring material.

The Balmer decrements measured for BCDGs tend to confirm that the starburst is relatively unobscured (typically $A_v < 1$ mag; Terlevich *et al.* 1991). Such measurements can, however, sometimes be greatly misleading. Aitken *et al.* (1982), for example, detected a large silicate feature in their mid-infrared spectra of the BCDG NGC 5253. From this they estimated a visual extinction of more than 8 magnitudes, although the Balmer decrement was consistent with little or no extinction. The two findings are reconcilable if the dust is distributed between the stars of the emission-line region. The Balmer decrement, in this case, gives a lower limit to the amount of extinction taking place.

In the past, the low IRAS fluxes detected from some BCDGs have been explained within the context of a low dust content. Gondhalekar *et al.* (1986), for example, used the IRAS fluxes to calculate a dust mass of $10^4M_{\odot}$ for one BCDG. Using the same technique they placed an upper limit of $10^2M_{\odot}$ on the dust mass detected in two others. There are at least two caveats to this analysis which should be noted. The first is that IRAS is only sensitive to warm ($\sim$ 50 K) dust. Dust distributed outside the star forming environment is likely to be too cool to be detected. The second point concerns the lack of correlation between IRAS fluxes and the metallicity of BCDGs (Kunth and Sevre 1985). Kunth and Sevre find that amongst a large number of BCDGs, the strongest correlation is that between Hβ luminosity and FIR luminosity (higher Hβ emission is accompanied by a higher FIR luminosity). The most obvious interpretation of this trend is that IRAS emission is

not determined primarily by dust mass but rather by the intensity of star formation. The rôle of dust is to convert optical and ultraviolet radiation into longer wavelength radiation which escapes from the galaxy. A more indepth discussion of this point is given in §8.3.

To summarize what is known about the dust properties of blue compact dwarf galaxies; there are sufficient reasons to believe that BCDGs might be dust poor but the issue has not yet been settled beyond all doubt.

6.7 Evidence for Outflow

In recent years, the possibility that galactic-scale winds might exist within BCDGs has caught the imagination of several workers in the field. Interest has been heightened by the increasing number of starburst-driven outflows discovered in larger galaxies such as FIRGs (§1.4). Until very recently, most indications that low mass systems might also be subject to outflow came fortuitously through emission-line photographs of morphologically peculiar galaxies. Graham (1981), for example, took a 3.5 hour exposure of NGC 5253 in the OIII ($\lambda\lambda$5007) emission line. The image was characterized by kpc-scale radial structures which gave the galaxy an 'M82-like' appearance in ionized gas. The pioneering work of Hodge should be acknowledged. He procured deep photographic exposures of several dwarf starburst galaxies in the Hα emission line (Hodge 1974; Hodge 1966). Although the extended filamentary structures seen in these photographs aroused considerable interest, their meaning was not fully understood at the time.

De Vaucouleurs *et al.* (1974) probably provided the first kinematic evidence that **outflow** might be associated with the extended emission-line features seen in some dwarf galaxies. They obtained high-resolution Fabry-Perot interferograms of nearby NGC 1569 (strictly speaking a dwarf irregular rather than a BCDG). Rather than finding a velocity field consistent with rotation, the emission-line gas appeared to be expanding away from the centre of the galaxy. They proposed a model in which hot gas escaped inside a cone-like structure aligned along the minor axis. The velocity of the Hα filaments within M82 had already been measured by that time (Lynds and Sandage 1963; §1.3).

Some of the strongest evidence that large scale outflows might be widespread amongst blue compact dwarf galaxies, has come from a very recent study carried out by Marlowe *et al.* (1995). They procured Fabry-Perot Hα images and high resolution (0.5-0.7Å) long slit echelle spectra for 13 amorphous star forming dwarfs. Amongst them were many galaxies that have been classified as BCDGs. Over half the sample show convincing evidence for emission-line bubbles and filaments which are created by starburst-driven winds. Larger versions of these phenomena have already been observed in more massive starburst systems (§1.4). They are generally thought to arise from the collective effect of stellar winds and supernovae expelling hot gas from the starburst. The diffuse emission-line nebulae in the sample of Marlowe *et al.* are typically several kiloparsecs in size and extend from the

starburst in a radial direction. They also exhibit a proclivity for the minor axis where hot gas from the starburst can escape more easily from the ISM. Figure 6.1 shows one example of the Hα nebulae that Marlowe *et al.* have detected. The galaxy in question is the BCDG NGC 3125 which is the subject of chapter 7. Figure 7.1 shows an optical continuum image of the same galaxy and one notes a stark contrast between the emission-line morphology and the stellar distribution. Bubbles of hot gas are escaping along the minor axis of this galaxy in a bipolar outflow.

Marlowe *et al.* (1995) obtained echelle spectra for their sample of star-forming dwarfs by placing a long narrow slit along the minor axis of the galaxy. 'Doppler ellipses' were evident in many of their spectra. As the slit is traversed the Hα emission-line profile splits into a double peak and then narrows again at larger galactic radii. The kinematic interpretation of this behaviour is that emission is taking place along the surface of a bubble-like cavity which is expanding away from the starburst. The cavity contains a hot, low density gas which is being expelled by the starburst. Emission-line radiation emanates from the ambient gas of the ISM which is shocked as the cavity expands. Emission-line bubbles in BCDGs expand at velocities of 40-60 kms^{-1}. This is significantly less than the emission-line velocities measured in FIRGs (several hundred kms^{-1}; §1.4) but the star formation rates are also corresponding lower ($\sim 0.05-0.5$ M$_\odot$yr^{-1} against 10-100 M$_\odot$yr^{-1} for FIRGs; Marlowe *et al.* 1995 and Heckman *et al.* 1990 respectively). The dynamic timescale of superbubbles detected in BCDGs is a few $\times 10^7$ yr which is comparable to the age of the stellar clusters found in the central regions.

An interesting issue connected with galactic-scale winds in dwarf galaxies is whether the ISM is catastrophically disrupted by the outflow. De Young and Heckman (1994) have investigated this problem in detail. They find that less massive systems ($\sim 10^7$ M$_\odot$) with low ellipticities are more likely to experience 'blow-away' rather than 'blow-out'. In the latter scenario, the emission-line gas fragments via Rayleigh-Taylor instabilities and the hot gas of the superbubble is able to escape into the intergalactic medium. If 'blow-out' occurs, a large proportion of the ambient gas in the ISM is expelled at the same time. This effectively ruptures the galaxy. Whether BCDGs are susceptible to this more 'cataclysmic' scenario still remains somewhat unresolved. More information is required concerning the gravitational field in BCDGs and the density of their ISM.

If dwarf galaxies do indeed expel a large proportion of their ISM during a period of intense star formation, this may represent a crucial phase in the evolution of dwarf galaxies. One possibility is that gas free dwarf ellipticals may eventually evolve out of gas rich progenitors (Deckel and Silk 1986). Even if the impact of superwinds and superbubbles is less dramatic, it should be recognized that starburst-driven winds offer a means of expelling newly-synthesized metals from the centre of the galaxy. This could in part explain the low metallicities measured in the emission-line region (§6.4).

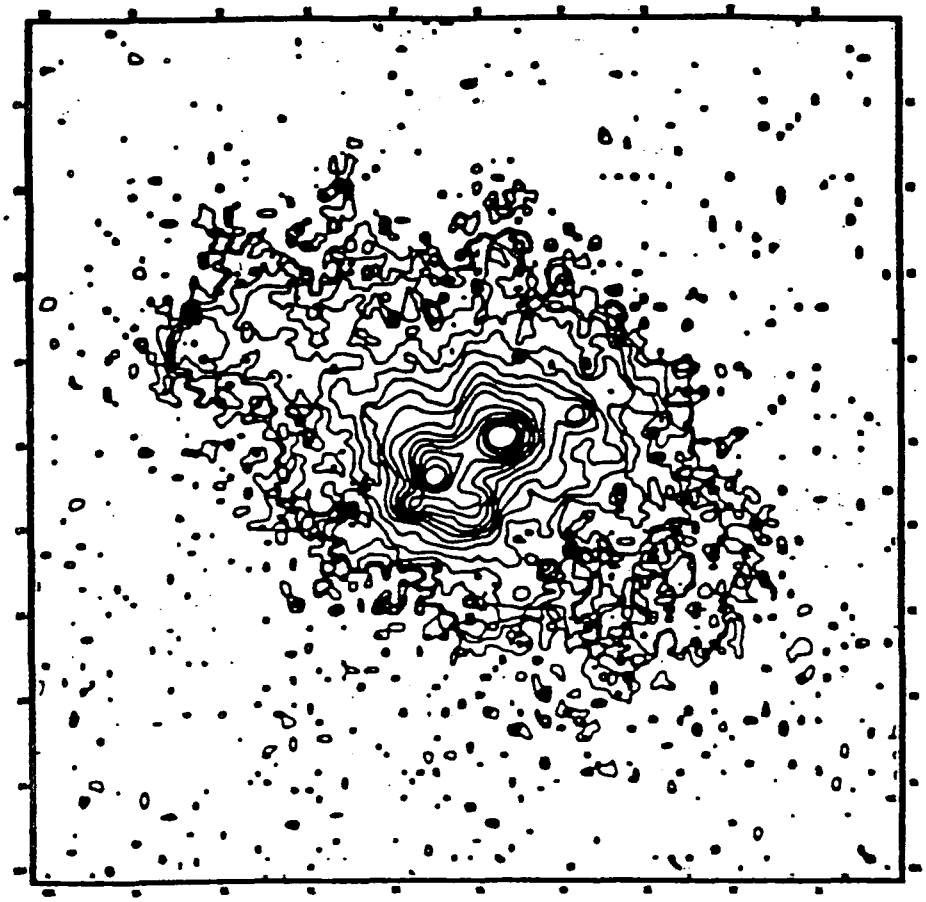

Figure 6.1: A continuum-subtracted Hα (+NII) emission-line contour image of the BCDG NGC 3125 (taken from Marlowe *et al.* 1995). The faintest contour has a surface brightness of 5.8×10^{-17} erg cm^{-2} s^{-1} arcsec^{-2}. Subsequent contours denote an increase of 0.5 mag in surface brightness. The image has a size of $1.8' \times 1.8'$.

6.8 A Comparison of BCDGs with FIRGs

The fact that powerful outflows are found in both BCDGs and FIRGs suggests that similar processes operate in both types of galaxy. At optical wavelengths, the starbursts in FIRGs and BCDGs have quite different appearances. The centre of FIRGs is generally heavily obscured by dust which reprocesses optical and ultraviolet radiation into longer wavelength radiation. BCDGs, on the other hand, have usually been detected on the basis of their strong optical line emission. The star formation rate in BCDGs is less than that characterizing the centre of FIRGs (§6.7) but this is not surprising when one considers that the latter tend to be large disk galaxies containing far greater amounts of gas. It is tempting, nevertheless, to ask ourselves how strongly BCDGs and FIRGs would resemble each other in the absence of obscuring material.

Certainly both BCDGs and FIRGs are powered by young hot stars which exert similar influences on the ISM of their hosts (radiation heating, galactic outflows etc.). Although the young stars in FIRGs are seldom seen directly, the hot gas which they ionize can usually be detected (Hα, Brγ, FIR fine structure etc.). Outside the optical waveband there is significant unification. For example, in both types of galaxy radio luminosity and blue luminosity are strongly correlated (Klein *et al.* 1984) (BCDGs may, however, have a flatter radio spectrum than FIRGs indicative of a larger thermal component). The correlation can be understood if blue emission is dominated by young hot stars. These same stars ionize the gas in the ISM (leading to radio free-free emission) and later explode as supernovae (which are a strong source of radio synchrotron radiation).

A major difference between star formation in BCDGs and that occurring in FIRGs is that propagation in the former may, as already pointed out (§6.3), be more stochastic. FIRGs, by virtue of their larger size and the amount of gas they contain, are capable of sustaining star formation over a far longer length of time. BCDGs, on the other hand, appear to undergo short (10^{6-7} yrs) recurrent bursts of intense star formation.

Chapter 7

NGC 3125

7.1 Introduction

Figure 7.1 shows an inverse greyscale image of the BCDG NGC 3125. It is derived from the V-band polarimetry observations which are described below. North is at the top and east is to the left. The area of the plot is about $1' \times 1'$ which corresponds to 3.3 kpc by 3.3 kpc at the distance of NGC 3125 (11.6 Mpc; §7.2). Within the figure, the brightest part of the galaxy is highlighted by logarithmic contours separated by 0.25 mag. This region contains the current starburst. Two prominent knots separated by $\simeq 10''$ (0.6 kpc) are apparent and these can be associated with the young superclusters known to dominate the optical appearance of BCDGs (§6.3). The bright object to the south-west of the starburst is a foreground star. Outside the hot-spot region, NGC 3125 possesses an elliptical-like morphology which can probably be associated with a secondary, *older* population of stars (§6.5). The north-west knot, which is also the brightest knot in figure 7.1, lies approximately at the centre of the secondary population. Figure 7.1 may give the impression that a galactic merger is in progress, but the similarity is only superficial. It will become apparent from observational data summarized below that the knots in NGC 3125 are very young star clusters and **not** the nuclei of merging galaxies.

For several years, NGC 3125 (or Tololo 3) was simply one of a large number of high excitation emission-line galaxies that had been detected in early objective prism surveys (Smith *et al.* 1976). In 1981, Kunth and Sargent carried out a more indepth spectroscopic study of a small number of low luminosity emission-line galaxies and confirmed that NGC 3125 contained a large number of Wolf-Rayet stars (§6.3). This implied that the galaxy had undergone an intense burst of star formation which had ceased only 4-6 million years ago. More recently, long-slit spectra by Vacca and Conti (1992) confirmed that several hundred Wolf-Rayet stars are present in the two contoured knots of figure 7.1.

Campbell and Terlevich (1984) obtained NIR colours for the centre of NGC 3125. They found that NIR emission from the north-west knot of figure 7.1 was dominated by a hot

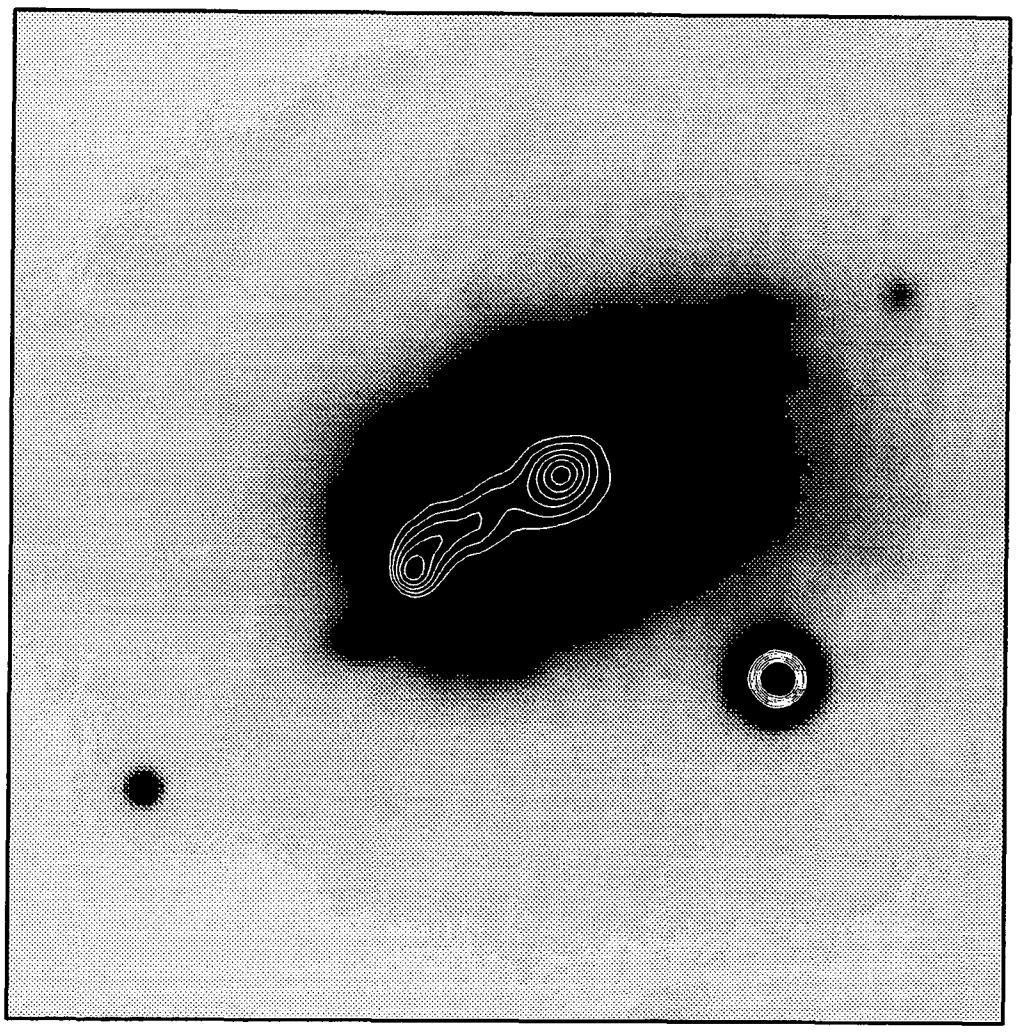

Figure 7.1: An inverse greyscale image of NGC 3125 taken in the V-band.

gas ionized by young stars. They also detected the presence of cool evolved stars, probably red supergiants, several arcseconds to the south-east. The authors took the location of the post main-sequence stars to be that of the south-east optical knot. From observations carried out below, it will become clear that the location and identity of the "south-east knot" depend critically on the wavelength that is detected. It will become evident that a third knot, which is not very prominent in optical images of the galaxy, exists between the two bright knots of figure 7.1. This is the NIR source which Campbell and Terlevich discovered. The nature and location of the various knots in NGC 3125 are rediscussed in §7.4.3.

Kunth *et al.* (1988) examined the B-I colours of NGC 3125. They found that the colours outside the current star forming regions were consistent with the presence of K giants. This result confirms the existence of an older stellar population (age $> 10^9$ yrs) outside the contoured region of figure 7.1. Kunth *et al.* claim that the luminosity profile of this background population is similar to that of a dynamically relaxed system such as a dwarf elliptical. This is refuted by van den Broeck *et al.* (1991), who describe the R-band profile as characteristic of a dwarf disk galaxy.

The starburst region of NGC 3125 is a conspicuous source of Hα radiation and it is also bright in the radio continuum (van Driel *et al.* 1991; van den Broeck *et al.* 1991). This is normal for regions of recent star formation (§1.2). Interestingly, the measurements of van den Broeck *et al.* (1991) detect something of a **diffuse** Hα component outside the hot-spot region. The true extent of this diffuse emission-line gas was not revealed until sensitive Hα measurements were carried out by Marlowe *et al.* (1995). A full description of the observations of Marlowe *et al.* has already been given in §6.7. NGC 3125 was one of 7 dwarf starburst galaxies which the authors associated with energetic outflows from the starburst region. Their Hα Fabry-Perot images and echelle spectra indicate that the outflow in NGC 3125 is taking place along the **minor** axis of the galaxy. Faint Hα emission extends out to a radius of about 40″ (2.8 kpc) from the starburst or hot-spot region. This emission-line nebula is bipolar and extends only in a north-easterly and south-westerly direction. Figure 6.1 shows the Hα image obtained by Marlowe *et al.* .

Long-slit spectra obtained for the south-west half of the Hα nebula in figure 6.1 manifest a 'Doppler ellipse'. This can be attributed to a kpc-scale bubble of hot gas which is expanding at roughly 50 kms^{-1} away from the starburst. The dynamic timescale for the outflow is 3×10^7 years. There is **no** evidence for outflow along the major axis.

NGC 3125 has been detected by the IPC instrument on-board the x-ray satellite EINSTEIN.[1] The x-ray emission appears to be extended along the minor axis of the galaxy but the poor resolution of the instrument makes it difficult to exclude the possibility of contamination by a bright foreground star. A small number of BCDGs have been observed

[1]The Einstein Observatory, Catalog of IPC X-Ray Sources, Smithsonian Astrophysical Observatory

using instruments on board ROSAT but as at the time of writing there were no published results.

To summarize what is known about NGC 3125: NGC 3125 is a BCDG that has undergone its most recent burst of star formation only a few million years ago. There is evidence for an older stellar population which extends far beyond the current emission-line regions. Hot gas is escaping from the starburst in a bipolar outflow along the minor axis.

7.2 Observational Details

NGC 3125 was observed at the f/15 Cassegrain focus of the 3.9m Anglo Australian Telescope (AAT). The galaxy was included in separate observing schedules that took place in January 1993 and February 1993. On both occasions, the Durham Imaging Polarimeter was used in conjunction with a broad-band V filter (550nm±130nm) and twelve 600 second exposures were made. The data were reduced in the standard manner described in §2.3.1. The results from the two observing schedules were consistent with each other and the frames were combined to increase the level of signal.

Wolstencroft and Sekiguchi kindly provided some near-infrared (NIR) exposures of NGC 3125. These were taken with IRCAM during service time on UKIRT. To obtain J(1.25μm), H(1.62μm) and K(2.20μm) images of the galaxy the following procedure was adopted. The dark current was subtracted from both sky and object frames and then the sky was removed from the object frames. Finally, the sky-subtracted object frames were flat-fielded. Flatfields were created by combining all the sky images at any given wavelength. The NIR images were not photometrically calibrated.

NGC 3125 is at a distance of 11.6 Mpc (Kunth and Sargent 1981; $H_o = 75 kms^{-1}Mpc^{-1}$), which gives a scale of 56.2 pc per arcsec.

7.3 Results

Figure 7.2 shows the polarization measured across NGC 3125. The polarimetry data have been integrated over independent $4.3'' \times 4.3''$ bins and significant vectors overlayed onto a greyscale intensity image. North is at the top and east is to the left. The origin is positioned at the foreground star south-west of the hot-spot region. This provides a common reference point for observations carried out in different wavebands. It can be seen that polarized regions lie along the major axis and in the south-east and north-west quadrants of the galaxy. Significant polarization is detected up to $23''$ (1.3 kpc) from the north-west knot (which is roughly at the geometric centre of the galaxy). The north-east and south-west quadrants do **not** show any significant polarization. The overall pattern is roughly circular about the hot-spot region suggesting a giant bipolar reflection nebula has been

detected. The dust is illuminated by the brightest regions of the galaxy. The observed levels of polarization are fairly low (typically ≤ 3 %) which is not surprising as the scattered light is seen against a background of unpolarized starlight.

There are small levels of polarization (<1%) within the hot-spot region itself (the contoured part of figure 7.2). Not all of this may be due to scattering. This idea is strengthened by the finite polarization measured at the north-west knot (0.7 ± 0.2% at P. A. $=-123\pm7°$). The north-west knot appears to be almost at the centre of the bipolar polarization pattern and therefore is not expected to be polarized by scattering. A strong possibility is that the starburst region is partly polarized by dust grains aligned in a magnetic field. This magnetic field may be intrinsic to the object or caused by the intervening ISM of the Milky Way. Axon and Ellis (1976) have observed the polarization induced by dust grains residing in the magnetic field of the Milky Way. For the part of the sky occupied by NGC 3125 (l=265°, b=+21°), the interstellar polarization is expected to be at most a few tenths of one percent. Aperture polarimetry of field stars within the image frames obtained for NGC 3125 fails to detect an interstellar polarization from the Milky Way. In all probability the polarization of the starburst is due to the presence of a magnetic field within the central 10″ of the object.

Figure 7.3 shows the inner 40″ of NGC 3125. The polarization vectors of figure 7.2 have been rotated by 90° in order to locate the light source(s) illuminating the bipolar reflection nebula described above. Vectors actually cospatial with the hot-spot region have been excluded because not all of them may be completely due to scattering (see above). Logarithmic isophotes represent the peak NIR emission detected in the H-band image of NGC 3125. The isophotes are separated by 0.06 mag. Although the H-band image has been chosen to represent the NIR emission, the same salient features are reproduced in the other NIR images (J and K). Registration between the optical and NIR images was achieved by using the foreground star in figure 7.3 and assuming that the peak NIR emission was cospatial with the brightest optical feature (the north-west knot). This gave an image scale for the NIR images which was in good agreement with the 'standard' value adopted for IRCAM.

Figure 7.3 shows that the NIR morphology of NGC 3125 consists of two compact features, or knots, but that the fainter NIR knot does **not** correspond to the south-east knot of the optical image. Indeed the fainter NIR feature appears to lie roughly cospatial with a weak optical feature located at the western end of a tail-like extension to the south-east knot. (This weak optical feature is most conspicuous in the contours of figure 7.2). Van Driel *et al.* (1991) have mapped out the central regions of NGC 3125 at 6cm. In addition to maxima at the two optical knots they too detect something of a weak feature at the location of the fainter NIR knot.

The direction of the rotated vectors in figure 7.3 suggests that the light scattered by the bipolar reflection nebula originates predominantly from the north-west optical knot.

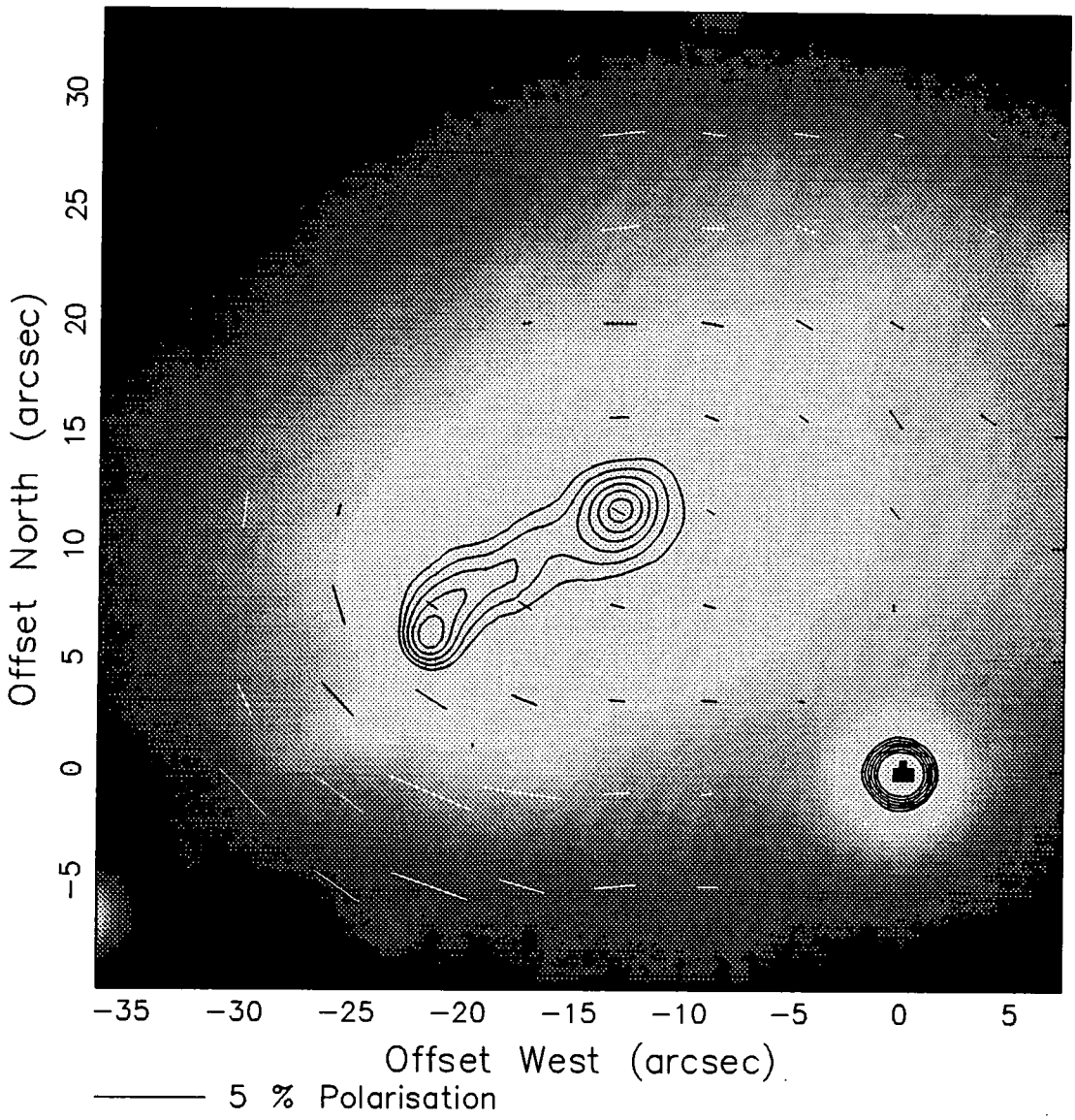

Figure 7.2: A polarization map of NGC 3125 in a V filter.

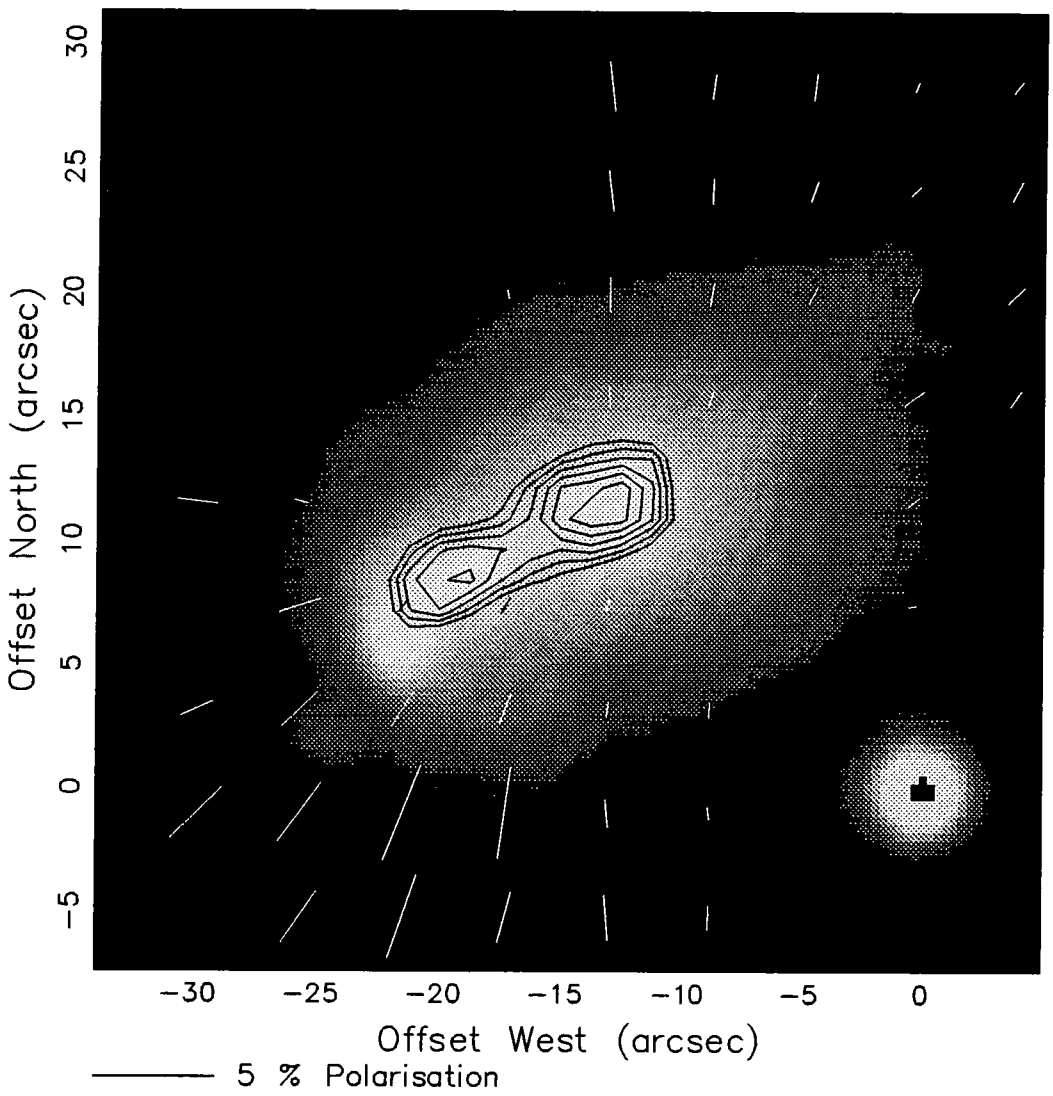

Figure 7.3: The source of illumination in NGC 3125. The vectors of figure 7.2 have been rotated by 90° in order to identify the origin of light scattered towards the observer. The contours overlayed onto the optical image denote peak NIR (1.6μm) emission within the galaxy.

There is *some* deviation from a perfectly centro-symmetric pattern suggesting that regions further east are making a minor contribution to the illumination. There is no evidence that the south-east knot is illuminating the nebula which is surprising because it is nearly as optically bright as the north-west knot. It is highly probable that the south-east knot is at a different physical depth in the galaxy to both the north-west knot and the scattering medium.

7.4 Discussion

The central 2 kpc of NGC 3125 is dominated by a giant bipolar reflection nebula. Scattering takes place from dust which is illuminated primarily by the north-west knot. It is unlikely that the polarization of NGC 3125 (outside the starburst region) arises from grains aligned in a magnetic field. The polarization pattern of figure 7.2 does not exhibit the typical spiral or elliptical morphology which usually characterizes such phenomena. In addition, there are not the levels of extinction that usually accompany the polarizing effect of aligned grains ($A_V \sim 1$ mag for 3% polarization; §3.3.3). Electrons are unlikely to provide the scattering medium in NGC 3125. Recombination radiation is detected primarily from the starburst region and the minor axis (figure 6.1). (Electron scattering is dimissed for all galaxies observed in this thesis by a quantitive analysis carried out in §9.2).

One concludes that scattering by dust grains is responsible for the polarized light detected in NGC 3125. The scattering material appears to be distributed along the major axis of the galaxy. It is unlikely that the bipolarity of the polarization pattern results from anisotropic illumination by the starburst. The star forming knots do not appear to be subject to the kind of patchy obscuration that might provide partial illumination of a more uniform dust cloud. The dust grains responsible for the scattered light must also be sparsely distributed within the ISM of NGC 3125 for there are no prominent absorption features associated with the reflection nebula.

It is somewhat surprising to find appreciable quantities of dust in a blue compact dwarf galaxy such as NGC 3125. Most observations of BCDGs indicate that their metallicity is quite low - typically 20-50% solar (Campbell *et al.* 1986; §6.4). NGC 3125 is a fairly typical case having a metallicity of 40% solar (Kunth and Sargent 1981). Lower metallicities are generally accompanied by smaller amounts of dust and indeed the IRAS fluxes of BCDGs are typically quite low (Gondhalekar *et al.* 1986). One notable caveat to the conclusion that BCDGs are poor in metals and dust, is that the outflows detected in this class may expel material from the emission-line region so that it is longer detected (§6.7). The FIR luminosity of NGC 3125 is much higher than most members of its class ($\simeq 10^9 L_\odot$; §9.6). Whilst this luminosity is still 1-2 orders of magnitude weaker than that detected from larger starburst galaxies, such as FIRGs, it is something of a surprise for such a low mass system. The question of whether NGC 3125 is unusual within its class is reserved until §8.3. At that stage all the observations carried out for BCDGs in this thesis will have been presented.

Two important issues which can be addressed at this point are the amount of dust detected in NGC 3125 and its probable origin. I shall take these issues in that order since knowledge of the former may well be crucial to sensible discussion of the latter.

Alton *et al.* (1995) used a simple scattering model to estimate the amount of dust detected in NGC 3125. It is described only briefly here because a more sophisticated analysis is carried out in chapter 9. Dust responsible for the bipolar reflection nebula in figure 7.2, was assumed to lie in the plane of the sky. It is illuminated by optical radiation from the north-west knot. The reflection nebula is taken to be optically thin so that photons travel from the north-west knot, scatter once and then leave the galaxy. Scattering within the reflection nebula is (naïvely) assumed to be isotropic. Now, by approximating the scattering and size properties of the dust grains, it is possible to estimate the amount of dust required to reproduce the observed polarized intensity. The grain properties were approximated by data based on the ISM of our own galaxy. Thus an albedo of 0.65 was used which is typical of graphite and silicate dust mixtures (Mathis *et al.* 1977). 0.15μm was taken as a typical size for the grains that dominate the scattering of visual radiation (Hildebrand 1983). The polarization of light after scattering from the dust grains was assumed to be $\sim$ 30%. This is typical for 90° scattering from an assembly of ISM-like grains (Warren-smith 1979). Using the above grain properties, in conjunction with a simple isotropic scattering model, Alton *et al.* derived a mass of $\sim 4 \times 10^5$ $M_\odot$ for the dust illuminated by the starburst.

A more rigorous derivation of the dust mass in NGC 3125 is carried out in §9.5.6 based on Mie theory. For many plausible distributions of the dust within the galaxy, the more sophisticated analysis indicates a dust mass of $\sim 4.5 \times 10^5$ $M_\odot$ (within a factor of 4). The dust mass derived from IRAS fluxes is an order of magnitude less than the amount of scattering material (§9.6). This is not too surprising. The dust detected in polarized light is expected to be much cooler than the dust component to which IRAS is sensitive (§9.6).

An important consideration at this point is the amount of dust that can normally be expected to reside within a small galaxy such as NGC 3125. One can use the gas mass in NGC 3125 in conjunction with a theoretical dust-to-gas ratio in order to estimate this quantity. Unfortunately, only upper limits are available for the amount of atomic and molecular gas in NGC 3125. Using data from Reif *et al.* (1982) and from Israel *et al.* (1995) these quantities are 3.0×10^8 $M_\odot$ and 6.5×10^6 $M_\odot$ respectively (assuming a distance of 11.6 Mpc to NGC 3125). Issa *et al.* (1990) have examined the relationship between metallicity and the dust-to-gas ratio in some nearby galaxies. They find an approximately linear correlation between these two quantities. Thus for a metallicity of 40% solar (appropriate to NGC 3125) one can expect a dust-to-gas ratio of roughly half that in our own galaxy, i.e. $\sim \frac{1}{300}$ (Whittet 1992). This leads to an upper limit of $\sim 10^6$ $M_\odot$ for the dust that one might expect to find in NGC 3125. This is about a factor of 2 greater than the amount of dust detected in polarized light.

I now wish to discuss the probable sources of dust in NGC 3125. The three strongest possibilities appear to be: (a) the older stellar population described by Kunth *et al* (1988) as K giants. These older stars (ages $\sim 10^9$ yrs) are traced by elliptical isophotes in the continuum image of figure 7.1 (see also the R-band image of van den Broek *et al.* 1991); (b) the transfer of gas and dust via a galactic collision; and (c) the recent star formation at the centre of the galaxy i.e. the starburst. These three possibilities are discussed in turn below.

7.4.1 Dust from Older Stars

It appears that some BCDGs possess a secondary population of older stars whilst others seem to be very young (almost primeval) objects which are undergoing star formation for the first time (§6.5). NGC 3125 almost certainly belongs to this 'older' group. The young stars of the current starburst (ages $\sim 10^{6-7}$ yrs) coexist with a far more extensive population of older stars (ages $\sim 10^9$ yrs).

It is a commonly held view that most elliptical galaxies underwent an epoch of star formation many gigayears in the past (Tinsley 1978). The ISM in these galaxies is relatively free of gas and dust in comparison to say spiral galaxies (Knapp 1990). Therefore a popular idea is that material in the ISM has been expelled into the halo and intergalactic medium during an energetic epoch of star formation. The situation for dwarf galaxies and how they evolve is less clear. It is possible that BCDGs are dwarf galaxies that have not yet lost their ISM but are still in the process of doing so (§6.7). Indeed, many BCDGs appear to be gas-rich (§6.4). If this is the case, NGC 3125 may still retain a significant fraction of the metals and dust that have been synthesized by its K giant population. If the dust that manifests itself in polarized light **is** attributable to mass loss from an older stellar population, the distribution of scattering material must be considered somewhat surprising. Dust is concentrated along the major axis whereas the distribution of older stars approximates that of an elliptical galaxy (§7.1). These contrasting observations may still be consistent with each other if one assumes that the dust that was originally along the minor axis has been cleared by the outflow in that part of the galaxy. There is *no* evidence for outflow along the major axis and here the dust remains where it was first formed.

7.4.2 Dust from Tidal Collisions

If one refuses to believe that older stars are the source of scattering material in NGC 3125, the two other probable sources of dust are the current starburst or another galaxy. Both intense star formation and galactic collisions are likely to be energetic enough to disperse dust and gas over large parts of the ISM. The current starburst is the cause of powerful outflows observed along the minor axis whilst gravitational forces may allow dust and gas to be transfered between colliding systems. In the past, both mechanisms have been invoked to explain the location and behaviour of gas and dust in starburst galaxies (§10.2).

It has already been remarked upon in §6.3, that the majority of BCDGs appear to be fairly isolated and that current star formation does **not** appear to be stimulated by galactic collisions. One can check that this describes the situation for NGC 3125. Using the POSS plate appropriate to the relevant part of the sky, one notes that NGC 3125 is fairly isolated. At a similar redshift the nearest galaxy is a disturbed spiral, NGC 3137, which lies about one degree away (200 kpc). NGC 3137 is believed to be interacting with its small companion (see AM 1006-284 in Arp and Madore 1989). The significant separation between NGC 3125 and NGC 3137 strongly suggests that a tidal encounter is unlikely to be the cause of the present (or recent) star formation. Assuming a peculiar velocity of 100 kms^{-1} the time since any possible collision is at least 2 gigayears whereas the young stars in NGC 3125 are only 10^{6-7} years old.

Outside the starburst region the optical appearance of NGC 3125 tends towards a fairly regular elliptical structure (figure 7.1). It does not exhibit the kind of distortions or peculiarities which typify mergers or tidally disturbed galaxies. One concludes that NGC 3125 is unlikely to have undergone a galactic collision during its recent past. Therefore, an external source for the scattering material in NGC 3125 seems unlikely.

7.4.3 Dust from the Starburst

The rôle of the starburst in recycling and redistributing gas and dust could be quite complicated. (It is an issue which I hope to address in this thesis). Within large starburst galaxies, such as FIRGs, there is convincing evidence that gas (and presumably dust with it) falls towards the gravitational centre where it is available for star formation (§1.2). Within some BCDGs preliminary observations by Viallefond and Thuan (1983) seem to suggest that gas clouds may accrete onto the region of star formation (§6.4). In this case, the gas may well be primordial in origin and as such cannot be expected to contain dust. For both BCDGs and FIRGs at least part of the gas that reaches the starburst will be converted into stars and eventually some of *that* will be returned to the ISM via stellar winds and supernovae. Leitherer and Heckman (1995) have constructed theoretical models for starburst galaxies and their results suggest that between 10-30% of the gas that is processed into new stars is returned to the ISM in the superwind.

Whilst the starburst may have a dramatic influence on the movement of gas and dust within the host galaxy, a more controversial issue is whether new stars can themselves synthesize large amounts of dust. Within the more familiar environment of our own galaxy, the main sources of dust are believed to be mass-losing stars that have already left the main-sequence (Gehrz 1989). In a starburst of age $\sim 10^7$ years, only stars that are massive enough to end their lives as supernovae are expected to have completed their main-sequence evolution. The least massive stars which explode as supernovae ($8M_{\odot}$) take about 30 million years to complete their main-sequence evolution (Leitherer and Heckman 1995).

Although supernovae (SNe) themselves inject metal-rich material into the ISM there is sparse evidence that dust grains actually condense out of their ejecta. Indeed, SNe might actually be predominantly sites of grain *destruction* rather grain formation (Dwek 1989).

Making some naïve assumptions, it may be possible to predict the amount of dust that a young collection of stars will eventually return to the ISM (initially through stellar winds and possibly SNe – at later times via mass-losing red giants). Marlowe *et al.* (1995) used the observed bolometric luminosity to estimate a mass of 1.6×10^7 $M_\odot$ for the young stellar population in NGC 3125. They assumed that the stars were formed in a burst of star formation occurring 10^7 years ago. This is consistent with the overall photometric colour of the starburst region. Ten percent of the mass converted into stars will eventually be returned to the ISM in stellar winds and SNe (Leitherer and Heckman 1995). Most of this material is returned within a few $\times 10^7$ years if the burst is short ($\sim 10^6$ years). I shall assume, perhaps wrongly, that **all** the material returned to the ISM has a gas-to-dust ratio of 100 (Gehrz 1989). In metal-poor environments, SNe tend to make the dominant contribution to the mass loss process (Leitherer and Heckman 1995) and therefore this assumption may be seriously undermined if supernovae destroy dust rather than create it (see above). However, with these naïve assumptions, I derive an eventual dust output of 2×10^4 $M_\odot$ from the present starburst. This result suggests that NGC 3125 must undergo some 20 bursts of star formation (resembling the one presently observed) before mass loss from new stars and SNe can account for the dust detected in scattered light. At the same time, at least several tenths of the gas in NGC 3125 experience star formation.

Within the observational data, there appears to be *some* evidence that NGC 3125 has undergone more than one burst of star formation in the recent past. NIR emission in the south-easterly part of the starburst is cospatial with a faint optical knot which is also detected as a weak radio feature (§7.3). The feature appears to be redder, and therefore somewhat older, than the two optical knots which dominate the V-band. Campbell and Terlevich (1984) describe the NIR colour of the 'south-east knot' as typical of red supergiants. It follows, in the context of figure 7.3, that the south-east knot of Campbell and Terlevich corresponds to this redder feature rather than the south-east optical knot (they give no positions for their observations). Supergiants are expected to appear when the starburst is about 3-8 million years old. Until then, the NIR colour of the star forming region is expected to be dominated by continuum and line emission from ionized gas (Campbell and Terlevich 1984). The presence of numerous Wolf-Rayet stars in the two bright optical knots suggests a slightly younger stellar population exists within these features ($\simeq$ 5 million years old) compared with the south-east NIR feature.

Even if recent star formation is **not** the source of scattering material detected in NGC 3125, it is still possible that an outflow, similar to the one currently affecting the minor axis of the galaxy, has transported dust to its present location. The outflow timescale is $\sim 10^7$ years using a typical expansion velocity of 50 kms^{-1} (Marlowe *et al.* 1995) and a radius of 1.3 kpc for the reflection nebula (§7.3). This is comparable to the age of the

south-east NIR feature. The distribution of scattering material is somewhat unusual if the **present** outflow is responsible for the transport of dust. Outflow is currently taking place along the *minor* axis whereas polarized light is detected from the *major* axis. If the dust *did* originate from the central regions, it appears to have been expelled **before** the present outflow perhaps in a previous burst of star formation. The effect of the current outflow has probably been to clear the minor axis of dust.

7.5 Summary

Optical polarimetric imaging of the blue compact dwarf galaxy NGC 3125 has revealed the presence of a galactic-scale bipolar reflection nebula. The nebula is illuminated chiefly by a bright emission-line knot in the central starburst. The dust responsible for the scattered light is concentrated along the major axis. The author uses a simple scattering model to estimate a mass of 4×10^5 $M_\odot$ for this dust component. Three potential sources were investigated for the scattering material. These were: (i) mass loss from an older stellar population which is known to exist within the galaxy (ages $\sim 10^9$ yrs); (ii) the transfer of material during a tidal encounter; and (iii) dust manufacture during recent episodes of enhanced star formation. All of these scenarios have their problems but, judging by the isolation of NGC 3125, (ii) seems especially unlikely. If the dust originated from either recent star formation or from older mass-losing stars then gas and dust is retained in part of the ISM. By way of contrast, elliptical galaxies are believed to have lost the gas and dust in their ISM through the action of intense star formation and energetic outflows. Intriguingly, there **is** an outflow in NGC 3125. Hot gas from the starburst is known to be escaping along the minor axis NGC 3125. The effect of this outflow appears to have been the clearance of dust and gas from the minor axis.

Images of NGC 3125 taken at different wavelengths (optical, radio and NIR) indicate that NGC 3125 may have experienced multiple bursts of star formation. This is not unusual for a BCDG.

Chapter 8

NGC 1705

8.1 Introduction

NGC 1705, like NGC 3125 discussed in the previous chapter, is a blue compact dwarf galaxy (BCDG) with a secondary population of older stars. Figure 8.1 shows a V-band image of the galaxy which is derived from polarimetry observations described below. The brightest regions are represented by an inverse greyscale image, whilst logarithmic contours are overlayed over all parts of the galaxy. The contours are separated by half a magnitude. North is at the top and east to the left. The plot covers an area of roughly $100'' \times 100''$, which is about 2.4 kpc by 2.4 kpc at the distance adopted for NGC 1705 (5 Mpc; §8.2).

In essence, NGC 1705 consists of an amorphous, high surface brightness region (hereafter 'HSB region') nested in an otherwise fairly elliptically-shaped galaxy. The HSB region is the site of current (or very recent) star formation i.e. the starburst. It is dominated by a very compact hot-spot feature, which is point-like in figure 8.1. There is a more diffuse knotted structure in the fainter parts of the HSB region but it is not very conspicuous because of the brightness of the central hot-spot. The bright object at the top right of figure 8.1 is a foreground star. NGC 1705 has a similar size to NGC 3125. The radius at a surface brightness of 25 B-magnitudes per square arcsecond (r_{25}) is 1.7 kpc and 2.3 kpc for NGC 1705 and NGC 3125 respectively (Marlowe *et al.* 1995).

The bright hot-spot in NGC 1705 has been described as the 'nucleus' by several authors, probably due to its small size and spherical shape. Although fairly central to the HSB region, it is in fact offset from the main body of the galaxy. It is also quite young and can be associated with a hot, dense starcluster containing massive O stars. The cluster has aroused considerable interest amongst observers because of its intense optical brightness and small size (M_B=-13.9 mag and $< 0.8''$ respectively) (Melnick *et al.* 1985; Meurer *et al.* 1992). This is about the same size as young rich stellar clusters in the local group but the feature in NGC 1705 is at least an order of magnitude more luminous. O'Connell *et al.* (1995), using the pre-Costar HST planetary camera, claim to have marginally resolved

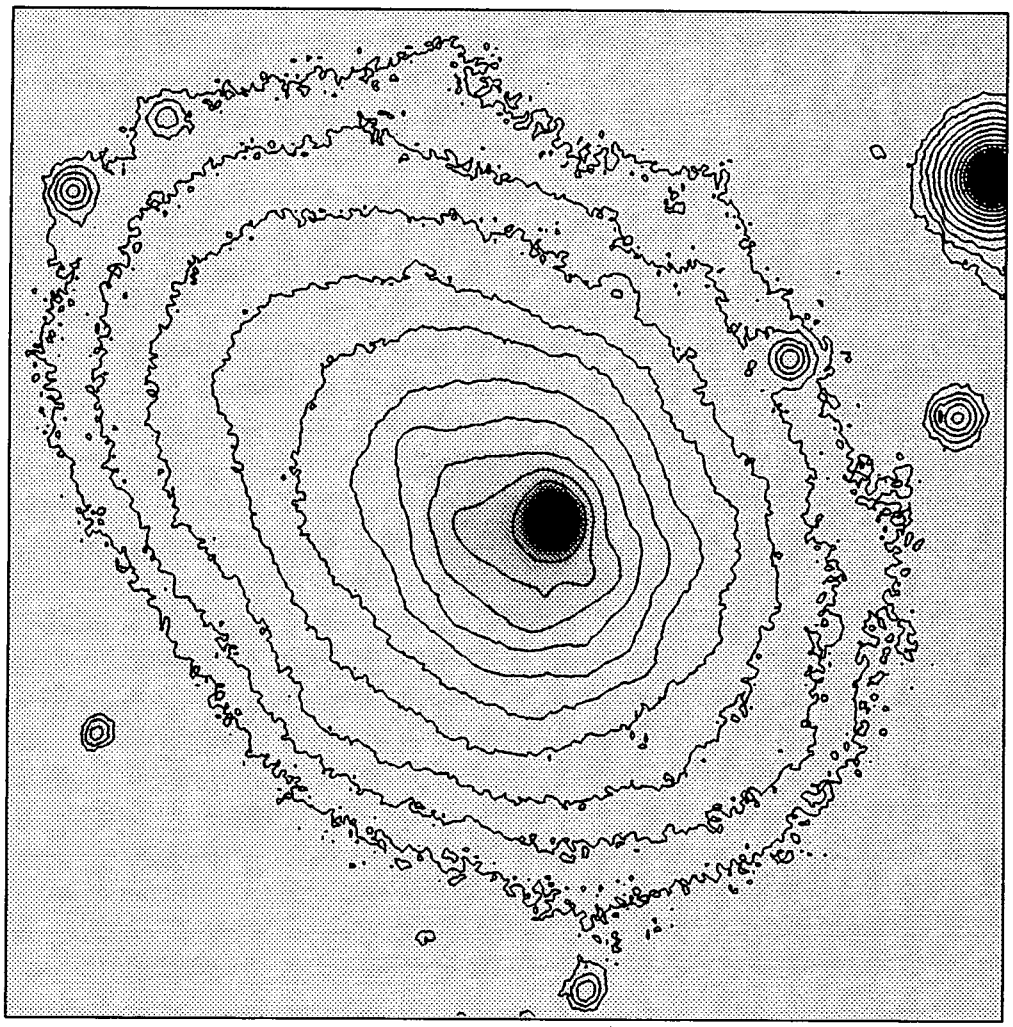

Figure 8.1: A V-band contour image of NGC 1705. The starburst is represented by an inverse greyscale.

the cluster (FWHM = 0.13″ or 3pc). The compact size and powerful luminosity of the central hot-spot are consistent with the properties predicted for young globular clusters. Similar features have been seen in M82 (§1.3) and in the BCDG He2-10 (Conti and Vacca 1994). In the latter two cases, compact star forming regions which have been detected from the ground are resolved into several smaller ($\leq$ 10pc) units by HST.

Lamb *et al.* (1985) find no evidence for Wolf-Rayet stars or P-Cygni profiles in the IUE spectrum of NGC 1705. This suggests that the central hot-spot is at least 5 million years old. NIR colours of the same region are consistent with the presence of evolved stars, probably red supergiants (Meurer *et al.* 1992). Narrow aperture optical photometry of the central hot-spot indicates that a burst of star formation took place $\sim 10^7$ years ago (Meurer *et al.* 1992; Marlowe *et al.* 1995). Interestingly, Meurer *et al.* (1992) claim to find more recent (but sporadic) star formation in the fainter parts of the HSB region.

Meurer *et al.* (1992) have carried out a very informative study of NGC 1705 providing a wealth of observational data for the object. Their continuum images confirm that NGC 1705 has an exponential radial surface brightness similar to that of an elliptical galaxy. The central 20″ (460pc) contains a surface brightness excess which is blue. Optical colours becomes redder at larger radii suggesting the presence of a secondary population of older stars.

Images of NGC 1705 in the Hα emission line, exhibit a bipolar structure centred on the bright hot-spot (Meurer *et al.* 1992; Marlowe *et al.* 1995). The emission-line nebula is characterized by fragmented arcs which lie several kpc from the starburst. Ionization is taking place predominantly along the minor axis suggesting that the starburst is expelling material in this direction. Meurer *et al.* (1992) use their spectral data to model the outflow in NGC 1705. An ellipsoidal shell expanding at $\sim 44 \mathrm{kms}^{-1}$ provides a simple but satisfactory fit to the kinematic data. The dynamic time for the outflow is 11 million years which is close to the predicted age of the central hot-spot. The neutral gas in NGC 1705 exhibits a broadened profile at 21cm (Meurer *et al.* 1992). This indicates that the outflow may be pushing or dragging ambient gas radially outwards.

NGC 1705 possesses most of the properties that epitomize blue compact dwarf galaxies. The Balmer decrement indicates low foreground reddening (E_{B-V}=0.25 mag; Terlevich *et al.* 1991) whilst the oxygen abundance is only 45% solar (Marlowe *et al.* 1995). The galaxy contains $8.7 \times 10^7 M_\odot$ of atomic gas (Meurer *et al.* 1992). This is typical of the amount of gas found in BCDGs (Thuan and Martin 1981).

8.2 Observational Details

NGC 1705 was observed at the f/15 Cassegrain focus of the 3.9m Anglo Australian Telescope (AAT) during January 1994. The Durham Imaging Polarimeter was used in conjuc-

tion with a broad V filter (550 ± 130nm). Twelve 600 second exposure were taken which gave complete coverage of the galaxy. In addition, four 100 seconds frames were obtained for the brightest regions. This ensured that unsaturated frames were available for all parts of the galaxy. The seeing conditions were about 2″. The data were reduced in the standard manner described in §2.3.1.

NGC 1705 is at a distance of 5 Mpc (H_o=75 $kms^{-1}Mpc^{-1}$; Meurer *et al.* 1992). This leads to a scale of 24 pc per arcsecond.

8.3 Results and Discussion

Figure 8.2 shows NGC 1705 over an area slightly smaller than figure 8.1. North is at the top and east to the left. The scale is plotted in arcseconds relative to the central hot-spot. The HSB region is overlayed with contours separated by half a magnitude. In addition, two concentric circles are visible which are discussed in connection with the analysis. The polarimetry data have been integrated over independent 3″ × 3″ bins and significant polarizations have been plotted as vectors in figure 8.2.

It is apparent that NGC 1705 shows very little polarization. The only significant detection is perhaps a small region $\simeq$ 15″ south-west of the central hot-spot. In contrast to the BCDG NGC 3125, which was discussed in the previous chapter, there is no indication that NGC 1705 contains large amounts of scattering material. For comparison, the bipolar reflection nebula detected in the former galaxy extends up to 1.3 kpc from the starburst. This corresponds to nearly 1′ at the distance of NGC 1705.

A question one can sensibly ask is whether a reflection nebula exists in NGC 1705 but the current measurements lack the sensitivity necessary to detect it. NGC 1705 and NGC 3125 have comparable apparent brightnesses (m_B=12.59 and m_B=13.2 respectively; Marlowe *et al.* 1995), therefore, for the same length of exposure, similar signals should have been recorded from both galaxies. One notes, however, that NGC 3125 appeared in two observing schedules whilst NGC 1705 was observed only once (§7.2 and §8.2 respectively). In an attempt to eliminate signal level as a significant parameter, I calculated the polarized light one might expect to detect in NGC 1705 assuming that the dust column density was the same as that in NGC 3125. To do this I used the simple scattering model in §7.4 but reversed the calculation for NGC 1705. Dust was assumed to be present throughout the whole ISM in NGC 1705 with the same average column density as that detected in NGC 3125. Illumination of the dust was assumed to come from the central hot-spot. This is analogous to the brightest knot in NGC 3125 irradiating dust in that galaxy. With this information one can predict the polarized intensity produced by scattering in NGC 1705. The comparison with NGC 3125 is a valid one if the nature of scatterers in both galaxies is similar (which is probably true; §9.3) and the geometry with respect to the source of illumination is the same (which may not be the case).

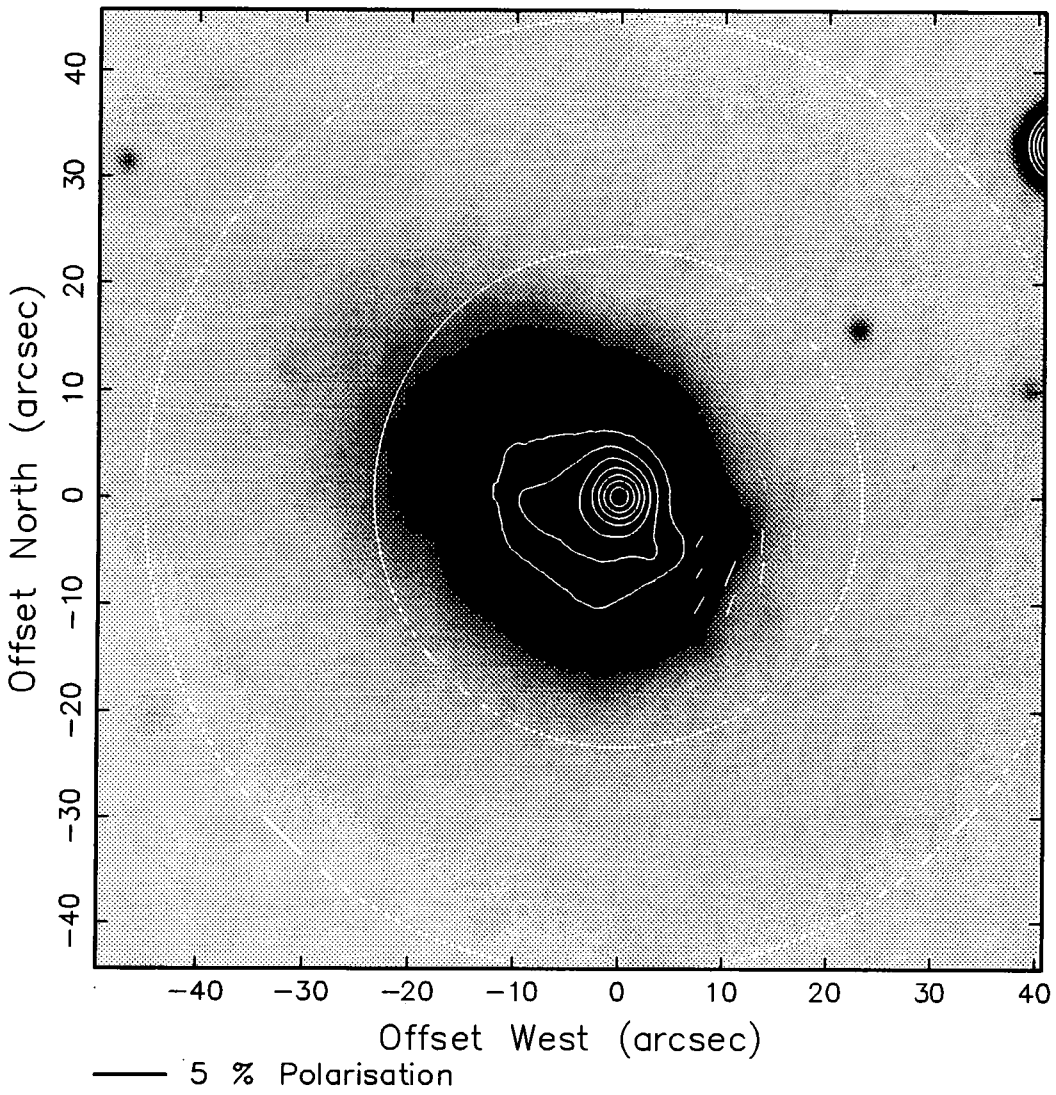

Figure 8.2: An inverse greyscale image of NGC 1705 showing significantly polarized regions of the galaxy. Contours have been overlayed onto the starburst. The two concentric circles relate to a point in the text where NGC 1705 is compared with NGC 3125.

In figure 8.3, I compare the predicted polarized intensities in NGC 1705 (using the above calculation) with their observed values. The observed values were obtained by integrating the polarimetry data over independent $3'' \times 3''$ bins. For most of the galaxy no significant polarization is measured therefore I take the 1σ errors in polarized intensity as the upper limit to the detected polarized intensity. In figure 8.3, these values are plotted against the appropriate distance from the starburst (the central hot-spot). The maximum polarized intensity is given in counts per pixel but for what follows the units are not particularly important. Note also that the segregation of the plotted points into two levels is due to some parts of the galaxy receiving longer exposure than others. This arises naturally from the fact that the object's polarization is determined from a mosaic of image frames. Contiguous frames have significant overlap leading to an effective doubling, in places, of the recorded signal (§2.3.1). Two lines have been drawn into figure 8.3 which denote the predicted level of polarized intensity given that NGC 1705 contains the same average column density of scattering material as NGC 3125. More than one line is present because there is a degree of uncertainty attached to the calculation of predicted values. In particular, the size (and therefore brightness) of the starburst region which can be expected to illuminate any scattering material is not well defined. (Recall in NGC 3125 illumination came primarily from the north-west knot although other parts of the starburst region were nearly as bright). The dashed line gives a conservative value for the predicted polarized intensity. The solid line can be understood as a best estimate.

The 'interesting' regions in figure 8.3 are those where the dashed and solid lines rise above the maximum observed values (radius $< 23''$ and radius $< 45''$ respectively). Within these regions significant polarization is predicted within NGC 1705. The outer limits of these regions are denoted by circles in figure 8.2. Clearly, NGC 1705 does not contain the same level of scattering material as NGC 3125 (even if one uses the conservative values for the predicted polarized intensity). For comparison, polarized light in NGC 3125 was detected up to 1.3 kpc from the starburst. This corresponds to $54''$ at the distance of NGC 1705. One concludes that the contrasting appearance of the two galaxies in polarized light is probably not attributable to differences in signal-to-noise. It stems from real differences in their respective dust properties.

It is somewhat surprising to find two galaxies with otherwise similar global properties having such contrasting dust properties. For NGC 3125, I estimated that $4 \times 10^5 M_\odot$ of dust had been detected in polarized light (§7.4). The scattering material in NGC 1705 amounts to $2 \times 10^3 M_\odot$ if the patch of polarization $15''$ south-west of the starburst is real (which is likely). This is 2 orders of magnitude less.

In all other properties NGC 1705 and NGC 3125 are very alike. In table 8.1, I list some of the parameters that may be relevant to a comparison. Both galaxies can be classified as BCDGs with a secondary population of older stars. There is evidence for recent ($\sim 10^{6-7}$ yrs) star formation in both systems but both are moderately metal poor galax-

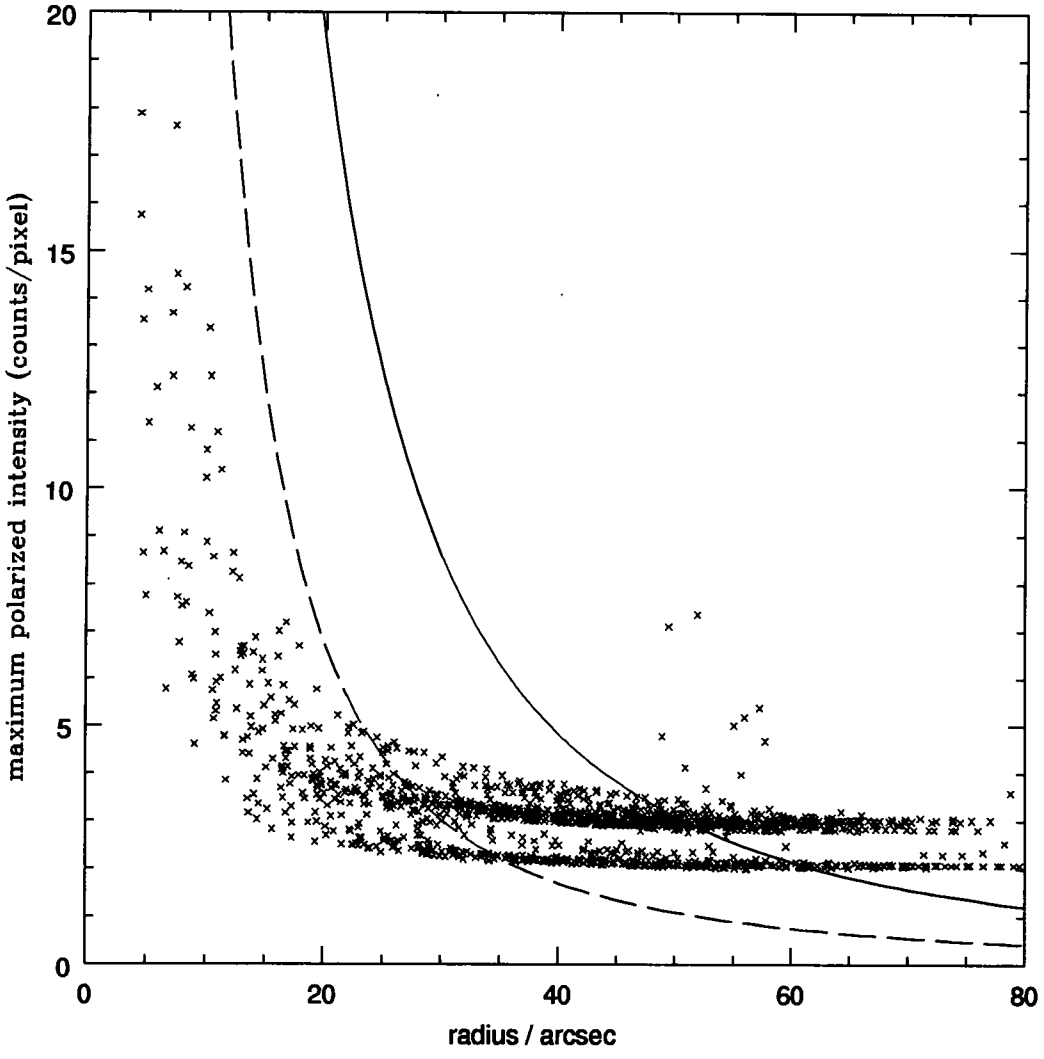

Figure 8.3: The polarized intensity detected from NGC 1705. The two lines denote the predicted values given that NGC 1705 contains the same column density of scattering material as NGC 3125. See text for details.

ies. Neither galaxy shows any evidence for a recent tidal interaction with a neighboring galaxy. The closest galaxy to NGC 1705 is at least 30′ (44 kpc) away. Thus any possible interaction must have occured at least $\sim 10^8$ years ago (assuming a velocity dispersion of ~ 100 kms^{-1}). As already noted in §7.4.2, NGC 3125 is unlikely to have undergone a tidal encounter within the last two gigayears.

NGC 3125 emits at least an order of magnitude more FIR radiation than NGC 1705 ($1 \times 10^9 L_\odot$ against $4 \times 10^7 L_\odot$ for NGC 1705; §9.6). In the past, FIR luminosity has been taken as a measure of how 'dusty' a galaxy is (e.g. Gondhalekar *et al.* 1984). A more careful analysis of the data, however, reveals that such naïve interpretations may be flawed. Figure 8.4 is adapted from Kunth and Sevre (1985). It shows the IRAS data collated for a large sample of galaxies. The infrared-to-blue luminosity ratio is plotted against the ratio of IRAS fluxes at 100μm and 60μm. Dots refer to a sample of 'normal galaxies' investigated by de Jong *et al.* (1984) (mostly spirals that have not been selected by any IRAS or FIR criteria). The crosses relate to a number of BCDGs investigated by Kunth and Sevre (1985). Now, the energy emitted both at blue wavelengths and in the IR, originates either directly or indirectly from young stars (de Jong *et al.* 1984). The infrared-to-blue luminosity ratio can therefore be taken as a measure of **infrared excess**. The 100μm-to-60μm colour, on the other hand, is related to the temperature of the dust. The top scale of figure 8.4 shows the temperature calculated by Kunth and Sevre (1985) assuming that dust emissivity is proportional to frequency.

A reasonable interpretation of figure 8.4 is that infrared excess is correlated with warmer dust temperatures. Warmer dust temperatures, meanwhile, result from stronger ultraviolet irradiation by young stars. The implication of this trend is that more luminous FIR emission reflects higher star formation rates. The rôle of dust is to convert optical and ultraviolet radiation into longer wavelength radiation which escapes from the galaxy. In figure 8.4, the positions of NGC 3125 and NGC 1705 have been marked with a large circle and a large cross respectively. Data for these galaxies are taken from Meurer *et al.* (1992) for NGC 1705 and Kunth and Sevre (1985) for NGC 3125. The blue magnitude given by Kunth and Sevre (1985) for NGC 3125 is slightly larger than that appearing in the Third Reference Catalog of Bright Galaxies (de Vaucouleurs *et al.* 1991). Therefore an arrow is drawn into figure 8.4 to indicate the effect of using the lower value. Both NGC 3125 and NGC 1705 fit the trend in figure 8.4 although the latter is somewhat towards the edge of the scatter. NGC 1705 may be somewhat 'estranged' from the other data because its blue luminosity was taken from a different source. Meurer *et al.* (1992) may have carried out their photometry using a larger aperture. NGC 3125 occupies a position towards the top right of figure 8.4 which suggests that star formation is intense. There is, however, a lot of scatter in the plotted data, suggesting that other factors, such as dust content, may play a significant rôle. Indeed, for any particular IRAS 60μm/100μm colour, the IR excess may vary by up to one order of magnitude.

Given that FIR luminosity correlates with the rate of star formation, it is difficult to

Table 8.1: General Properties of NGC 1705 and NGC 3125

Parameter	NGC 1705	NGC 3125	Units	Reference
R.A.	$4^h53^m6^s$	$10^h4^m18^s$	1950	Meurer *et al.* (1992); astrometry - this work
Dec.	$-53°26'26''$	$-29°40'30''$	coord.	
distance	5	11.6	Mpc	Meurer *et al.* (1992); Kunth and Sargent (1981)
r_{25}	1.7	2.3	kpc	Marlowe *et al.* (1995)
m_B	12.6	13.2	mag.	de Vaucouleurs *et al.* (1991)
metallicity	45%	35%	solar	Marlowe *et al.* (1995)
HI mass	9×10^7	$< 3 \times 10^8$	$M_\odot$	Meurer *et al.* (1992); Reif *et al.* 1982
FIR luminosity	4×10^7	1×10^9	$L_\odot$	§9.6

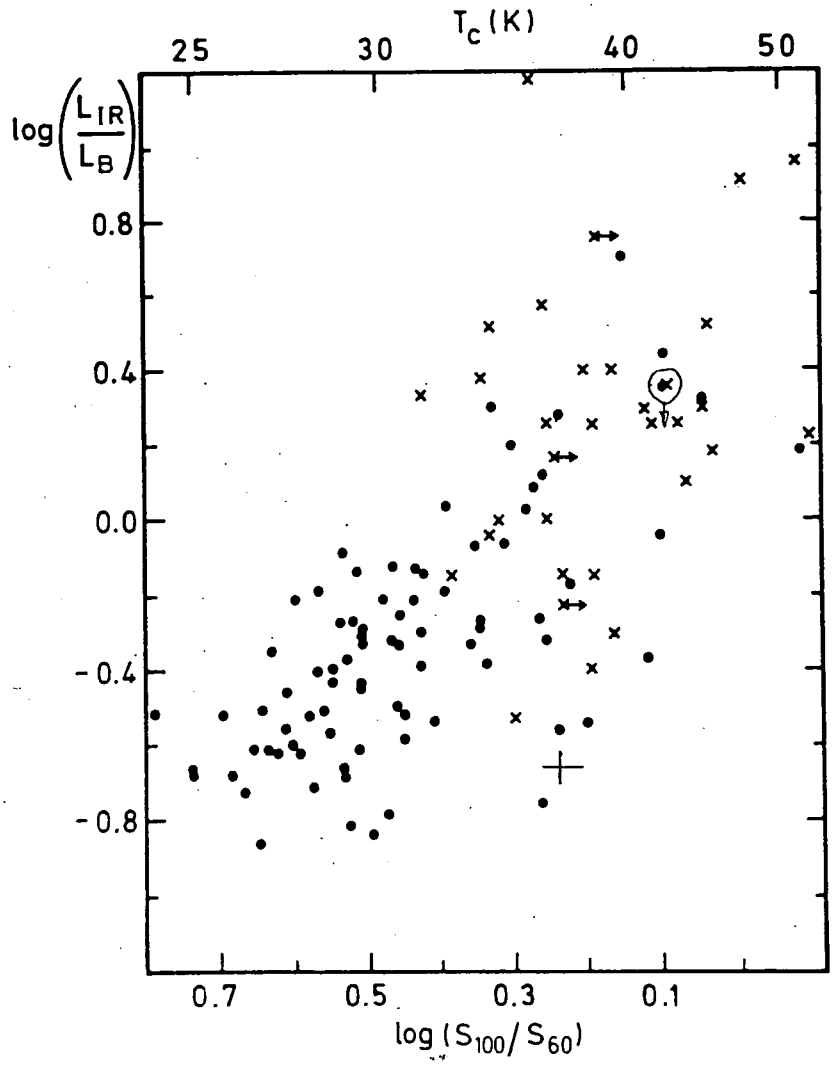

Figure 8.4: Infrared excess versus IRAS temperature for a sample of 'normal' galaxies (large dots) and BCDGs (diagonal crosses). This figure is taken from Kunth and Sevre (1985) (See text for details).

say that NGC 3125 is more dusty than NGC 1705 on the basis of IRAS fluxes alone. In fact, it begs the question of whether IRAS is at all a good indicator of how dusty a galaxy is.

It has been made clear from discourses both in this chapter and in the preceding chapter that galactic-scale outflows operate in NGC 1705 and NGC 3125. Is it possible that *this* phenonemon is the cause of differences in their dust properties ? One possibility resulting from the discussion in §7.4 was that NGC 3125 had lost dust and gas from its minor axis in a recent (or ongoing) outflow. In other parts of the galaxy dust was still evident. One could entertain the possibility that NGC 1705 has expelled much of its ISM during a recent bout of star formation and this explains the present lack of scattering material. The plausibility of intense star formation leading to 'blow away' rather than 'blow out' has already been underlined in §6.7. To recapitulate briefly, significant loss of ambient gas from the ISM (the 'blow-away' scenario) is most likely to occur if: (a) the starburst is extremely energetic; (b) the host galaxy has a low mass; (c) the host galaxy possesses a low ellipticity and; (d) if the ambient ISM has a low gas density.

The Hα images of Marlowe *et al.* (1995) do **not** seem to support the hypothesis that NGC 1705 has experienced 'blow away' whereas NGC 3125 has not. Within NGC 1705, circumferential shells of ionized gas seem to indicate that the superwind is still expanding and has not yet escaped the galaxy. NGC 3125, on the other hand, is characterized by *radial* emission line filaments which may indicate that the superwind has already breached the ISM and now flows freely into the intergalactic environment. Thus if any galaxy has experienced mass loss (to whatever extent) it is likely to be NGC 3125 and **not** NGC 1705.

I now wish to summarize what has been learned from the above discussion.

8.4 Summary

Optical imaging polarimetry has been carried out for the the blue compact dwarf galaxy NGC 1705. In contrast to the BCDG NGC 3125 (chapter 7), large amounts of scattering material are **not** detected in the ISM of NGC 1705. This distinction probably results from real differences in the dust properties of the two galaxies. It does **not** stem from a difference in signal-to-noise. The contrast in behaviour is somewhat striking because NGC 1705 and NGC 3125 appear to be very similar in all other properties (e.g. mass, metallicity, star formation). NGC 3125 is more luminous in the FIR than NGC 1705 but this may reflect a higher rate of star formation rather than the presence of larger quantities of dust.

Outflows are present in both NGC 1705 and NGC 3125. It is not immediately obvious, however, how this can account for their contrasting polarization properties. On the basis of Hα images taken for the two galaxies (Marlowe *et al.* 1995), it does **not** appear that NGC 1705 has suffered significantly more mass loss from its ISM compared with NGC 3125.

Polarimetry observations for a larger sample of BCDGs are required. This will establish whether the giant reflection nebula detected in NGC 3125 is exceptional or not.

Chapter 9

Dust Scattering Models

9.1 Introduction

In the preceding chapters of this work starburst galaxies of various morphological type have been investigated using optical polarimetry. One of the most stunning results from this study has been the detection, in about half of these systems, of kpc-scale reflection nebulae. I propose that dust grains, sparsely distributed throughout selective regions of the host galaxy, reflect some of the copious optical radiation leaving the starburst. The primary purpose of this chapter is to simulate the observations so that: (a) dust scattering can be shown to be viable and (b) the amount of dust present can be estimated. In order to do this, it is necessary to characterize the nature of the scatterers and incorporate them into a geometric model.

This chapter is organised in the following way. First, I show quantitatively that electron scattering is not consistent with the observational data. I then discuss the parameterization of dust within the Milky Way. I propose that ISM-type Milky Way grains probably dominate the optical extinction in starburst galaxies and construct scattering models to include these grains. The dust masses calculated from these models are compared with the FIR-emitting dust detected by IRAS.

9.2 Electron Scattering

The interaction of optical radiation with free electrons is described by Thomson scattering (e.g. Lang 1980). If a cloud of N_e electrons is situated a distance r from a light source, then the intensity of the scattered light (in ergs per second) is given by:

$$I_s = \frac{N_e \sigma_T}{4\pi r^2} I_o \tag{9.1}$$

where σ_T is the Thomson scattering cross-section (6.7×10^{-25} cm^2) and I_o is the intensity of the light source (in ergs per sec). Note also that equation 9.1 assumes that scattering

from free electrons is isotropic (which is true within a factor of 2; Lang 1980). Now, to test the feasibility of electron scattering within starburst galaxies I assume that I_s is 100% polarized (which is only strictly true for scattering taking place in the plane of the sky). The polarimetry data presented in this thesis provide: (a) values for the polarized intensity of the scattered radiation (in counts at the CCD) and (b) the brightness of the illuminating source (also in counts at the CCD). Since both (a) and (b) are measured in the same units it follows from equation 9.1 that:

$$PI = \frac{N_e \sigma_T}{4\pi r^2} B \tag{9.2}$$

where PI is the polarized intensity of the scattered light and B is the brightness of the illuminating source. Equation 9.2 can be solved for N_e. If, in addition, one assumes electrons are distributed along the line-of-sight with the same scale-length as their separation from the illuminating source (i.e. r), N_e can be used to determine the electron number density, n_e.

For NGC 3125, I used the observed values of PI, r and B to estimate an electron density of $n_e \sim 70$ cm^{-3} (the determination of B is described more precisely in §9.5.2 in connection with dust scattering). This density is very high even if the ISM of NGC 3077 is both gas rich and fully ionised. Moreover it is difficult to see how a hot gas of this density is both contained by the ISM or ionized in the first place. If the electrons constitute the plasma expelled by a superwind (§1.4) then the electron density is expected to be much lower (10^{-3}cm^{-3}; T. Heckman private communication). Persisting, nevertheless, with the electron scattering hypothesis, I predict the free-free radiation (Bremsstrahlung) emitted by the electron cloud. Lang (1980) gives the volume emissivity of a plasma at frequency ν as:

$$\epsilon_\nu \simeq 6.8 \times 10^{-38}\, g(\nu,T)\, {n_e}^2\, T^{-0.5}\, exp(\frac{-h\nu}{kT}) \tag{9.3}$$

where ϵ_ν is measured in units of erg sec^{-1} cm^{-3} Hz^{-1}. g is the Gaunt factor, T the temperature of the plasma and n_e is the electron density. I use $T = 10^5$ K (characteristic of ambient gas shocked by a superwind; Heckman *et al.* 1990) and the electron density derived above ($n_e \sim 70$cm^{-3}). Substituting these values into equation 9.3, I estimate the emission at 6cm and compare this with the results of van Driel *et al.* (1991). These authors have mapped out NGC 3125 at 6cm using a low resolution beam of 150 sq. arcsec. **They did not detect radio emission from the scattering regions shown in figure 7.2.** If electrons constitute the scattering medium in NGC 3125 I predict a flux of $\sim$ 450mJy over the beam-size of van Driel *et al.* . This corresponds to a signal-to-noise of 1300. Using equation (1-223) given by Lang (1980) one can confirm that the emission at 6cm will **not** be self-absorbing.

For NGC 3077, the feasibility of electron scattering can be investigated in the same manner as above. In this case, electron densities of $\sim 10^2$cm^{-3} are required, which seem

implausibly high. The resulting radio continuum lies at least 400 times above the level detected by Hummel *et al.* (1987). Significant emission is only detected in the central few arcseconds of the galaxy.

Apart from an absence of radio emission from the scattering regions in NGC 3125 and NGC 3077, the distribution of recombination radiation is incompatible with electron scattering. For NGC 3125, significant Hα emission is only detected along the minor axis. This is the site of a galactic-scale outflow (§7.1). For NGC 3077, one notes that Hα emission is detected over a similar sized region to the scattering regions (§5.1). There is, however, little spatial correspondence between the recombination radiation and polarized regions of the galaxy. One concludes that electrons are unlikely to provide the scattering medium in either NGC 3125 or NGC 3077. Similar arguments can also be applied to NGC 660 which shows evidence for scattering outside the galactic disk (§3.3.2). Although Hα emission *is* detected along the minor axis of this galaxy, radio images of the galaxy suggest that most of the ionized gas is concentrated in the star forming regions of the disk (Condon *et al.* 1982).

Within external galaxies, the strongest case for electron scattering appears to be the narrow emission-line region of Seyfert nuclei (Goodrich and Miller 1994). These environments are characterized by dense electron clouds lying within a few hundred parsecs of a very intense optical source.

9.3 The Nature of Galactic Dust

Having eliminated electrons as the scattering medium in the starburst galaxies observed in this thesis, let us now turn our attention to the nature of dust in galaxies and how *this* is likely to interact with optical radiation.

The characterization of average dust grains within our own galaxy follows primarily from the depletion of elements from the gas phase and the observed Galactic reddening law. Any plausible grain model must be able to reproduce the average interstellar extinction curve over a reasonable frequency range and, in doing so, not exceed the observed elemental depletions. There is a relatively small number of elements or combination of elements that can fulfil both of these conditions (Greenberg 1978) but the solution is not unique. The most favorable models comprise chiefly of carbon (graphite and amorphous carbon) and astronomical silicate ([Fe,Mg] SiO_3, $[Fe,Mg]_2$ SiO_4). There is both spectral and polarimetric evidence that silicates constitute a sizeable proportion of grain material in the Galaxy (Whittet 1992). Carbon, on the other hand, is believed to be an essential ingredient for extinction in the near-IR (Draine and Lee 1984). It is also detected in the mass-loss from some stars (Jura 1986). Carbon and silicate material are all expected to be heavily depleted from the gas phase of the ISM (Jenkins 1989).

Figure 9.1 shows the average normalized reddening curve for the Galaxy. λ^{-1} is the wavenumber and $E(\lambda_1 - \lambda_2)$ is the change in extinction between $\lambda = \lambda_1$ and $\lambda = \lambda_2$. The curve is characterized by increasing extinction at higher radiation frequencies and a broad feature at 2175Å. It is important to note that figure 9.1 describes the general ISM of the Galaxy and **not** extinction within specific environments (e.g. dense molecular clouds or planetary nebulae). Dust grains can show significant variation outside the diffuse ISM.

At optical wavelengths, extinction (the combined effect of both scattering and absorption) is produced by 'classical grains' which have a size of $\sim 0.1\mu$m (Whittet 1992). It should be noted, however, that grains of various composition and size are required if one is to explain all the observational data associated with interstellar dust (see Mathis 1990 for a review). In particular, extinction in the far ultraviolet (FUV), the feature at 2175Å and certain solid state spectral features (so-called Unidentified Interstellar Bands) can almost certainly be ascribed to a mixture of smaller particles ($\leq 0.01\mu$m).

It is within the small particle regime that galaxies seem to show most diversity. Both the Magellanic Clouds, for example, possess a much steeper FUV extinction curve than the Milky Way (Prévot *et al.* 1984; Fitzpatrick 1986; Fitzpatrick 1989). In addition, the 2175Å absorption feature, which is generally attributed to small graphite-like particles, appears to be absent or very much weaker than the same feature in figure 9.1. In a recent study, Kinney *et al.* (1993) collated and compared IUE spectra for bright emission-line galaxies (many of which are starburst galaxies). They concluded that figure 9.1 is not always a good representation of extinction in the far-ultraviolet. Some caution must be exercised, however, when inferring extragalactic reddening laws from IUE data. The IUE aperture captures ultraviolet light from various physical depths along the line-of-sight as well as any component scattered *into* the line-of-sight (Calzetti *et al.* 1994). Both of these effects will tend to undermine the determination of the true reddening law. To measure the reddening law accurately the detected light source must always lie directly behind the grain material.

In summary, it is fair to say that the extinction law outside the Milky Way is not particularly well determined but the first indications are that far-UV extinction can show significant variation between different galaxies.

The nature of very small dust grains in **starburst** galaxies may be even more complicated than that outlined above. Several authors have reported the depletion of small grains at close proximity to the central starburst (Telesco *et al.* 1989; Telesco *et al.* 1993; but see also Roche *et al.* 1991). Small ($\leq 0.01\mu$m) grains, by virtue of their low thermal capacities, can make significant contributions to emission in the mid-IR ($\sim 10\mu$m) (Désert *et al.* 1990). It is therefore possible to infer their presence (or absence) by their influence on the mid-IR colours of a galaxy. The depletion of small grains is likely to arise from the intense UV fields and shock processes associated with starburst and Seyfert nuclei (Seab 1988).

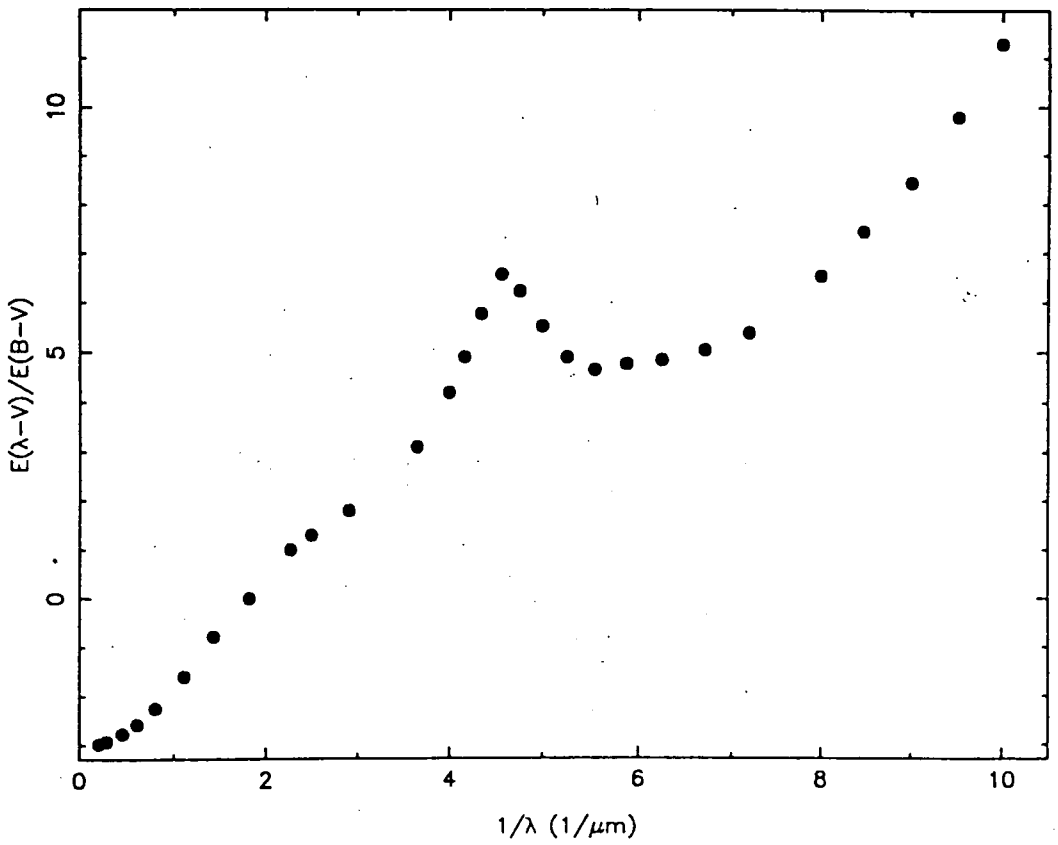

Figure 9.1: The reddening law for the diffuse ISM of the Galaxy

Despite noticeable variations within the small particle regime, optical extinction in external galaxies may be quite similar to that in our own Galaxy. At the present time only the LMC and SMC have been studied in any detail. Most results seem to indicate that the diffuse ISM is subject to an optical/NIR reddening law very similar to that in figure 9.1 (Morgan and Nandy 1982; Fitzpatrick 1989; Bouchet *et al.* 1985). Within the accuracy of the optical scattering models presented in this chapter, ISM-type Galactic grains provide a more than adequate approximation to dust in external galaxies. The parameterization of dust grains in the Milky Way is now discussed.

Mathis *et al.* (1977) have proposed a model for Galactic interstellar grains which is widely used and even predicts certain important observational data. A mixture of uncoated silicate and graphite grains with a power law size distribution given by:

$$n(a) \propto a^{-3.5} \tag{9.4}$$

provide a good fit to the Galactic extinction law over the wavelength interval $0.12 - 1\mu$m (here, a is the particle size and $n(a)$ is the number of particles per unit a that have a size a). This model also predicts, in a pleasing manner; (a) the observed wavelength-dependance of dust albedo and (b) the anticipated opacity of dust in the FIR. (Mathis 1988; Draine and Lee 1984). In the above grain model (hereafter MRN), 65% of the optical extinction is provided by graphite and the remainder arises from silicate grains. The upper and lower size limits of the MRN are, respectively, $a_{min} = 0.005\mu$m and $a_{max} = 0.25\mu$m for graphite and $a_{min} = 0.025\mu$m and $a_{max} = 0.25\mu$m for silicate.

Greenberg (1978) proposed an alternative grain model for interstellar extinction:

$$n(a) \propto \exp\left\{-5\left(\frac{a - a_c}{a_i}\right)^3\right\} \tag{9.5}$$

Once again a and $n(a)$ are the grain size and number density respectively. a_c is a core size and a_i is a cut-off parameter beyond which the number of grains with size a falls rapidly. A mixture of graphite ($a_c = 0$, $a_i = 0.1\mu$m) and silicate ($a_c = 0$, $a_i = 0.25\mu$m) grains can reproduce the NIR and optical Galactic extinction law and still remain within abundance constraints. Greenberg and Chlewicki (1987) proposed a variation of equation 9.5 which consists of a silicate core ($a_c = 0.05\mu$m) and an organic (complex carbon) mantle of thickness $(a - a_c)$. The cut-off size (a_i) is 0.2μm. There is no observational evidence for grain mantles in the **diffuse** interstellar medium but ices *are* known to condense onto grain surfaces in dense molecular clouds (Eiroa and Hodapp 1989 and references therein). Greenberg and workers assume that various photo-chemical reactions can transform the ice coat into an organic surface which remains durable in the harsher climes of the diffuse interstellar medium. Some authors doubt whether mantles can really exist outside molecular clouds (Mathis 1988).

In a relatively recent development, Mathis and Whiffen (1989) recognised that grains

released from the atmosphere of cool stars are unlikely to be separate spheres of well-ordered carbon and silicate. Indeed, the detection of dichroic extinction both within The Galaxy and in the disk of nearby external galaxies (§2.3.3) verifies that grains are elongated and probably quite irregular (see also the discussion of captured interplanetary grains - Brownlee 1987). Mathis and Whiffen propose a composite model in which small graphitic, carbonaceous and silicate particles co-exist within a larger aggregate. The composite grains are assumed to be poorly packed (up to 80% vacuum by volume). Fitting the extinction curve of figure 9.1, Mathis and Whiffen derive a power law similar to equation 9.4 ($n(a) \propto a^{-3.7}$). The lower and upper size limits are given by 0.03μm and 0.9μm respectively.

Other models have been proposed for interstellar dust – notably hydrogenated amorphous carbon grains by Duley and Williams (1988) and biological grains by Hoyle and Wickramasinghe. The latter is unable to explain several aspects of the observational data (Mathis 1990 and references therein) and is not widely discussed in the literature. I am unable to find specific parameters for the model of Duley and Williams. For the purposes of the following sections I adopt the three primary models discussed above (MRN, the Greenberg distribution and the composite model of Mathis and Whiffen). There is sufficient variation within this subset to provide an understanding of how different types of grain scatter optical radiation.

9.4 Mie Scattering

The interaction of electromagnetic radiation with small spherical particles was first treated by Mie (1908) and independently by Debye (1909). It has subsequently become known as Mie theory. The essence of the problem lies in solving Maxwell's electromagnetic equations subject to appropriate boundary conditions. A mathematical treatment is not given here but lucid accounts exist elsewhere (van de Hulst 1957; Bohren and Huffman 1983).

Two essential parameters in the derivation and use of Mie formulae are the dimensionless size parameter, X, and the refractive index of the scattering medium, m. The size parameter is defined thus:

$$X = \frac{2\pi a}{\lambda} \tag{9.6}$$

where a is the radius of the sphere and λ is the wavelength of the incident radiation. The refractive index is complex and defined thus:

$$m = n(\lambda) - ik(\lambda) \tag{9.7}$$

where n and k are, respectively, the real and imaginary parts of the sphere's refractive index. Both n and k are wavelength-dependent. For dielectric (non-absorptive) materials, such as silicates or ice, k is very small. Metals, on the other hand, absorb a large

proportion of the incident radiation and the imaginary part of their refractive index is high.

Given appropriate values for X and m, Mie formulae give two complex amplitude functions $S_1(\theta)$ and $S_2(\theta)$ (notation is based on that of Wickramasinghe 1973). These determine: (a) the fraction of light incident on the spheres which is scattered through an angle θ and; (b) the polarization of the scattered radiation.

Some other quantities of interest are the efficiency factors and the albedo (all of which are wavelength dependent). The scattering efficiency, Q_{scat}, is the ratio of a particle's scattering cross-section (C_{scat}) relative to its geometric cross-section, i.e.:

$$Q_{scat} = \frac{C_{scat}}{\pi a^2} \tag{9.8}$$

Similar relations can be written for the absorption efficiency (Q_{abs}) and for the extinction efficiency (Q_{ext}):

$$Q_{abs} = \frac{C_{abs}}{\pi a^2} \qquad Q_{ext} = \frac{C_{ext}}{\pi a^2} \tag{9.9}$$

where C_{abs} and C_{ext} are the absorption cross-section and extinction cross-section respectively. Note that extinction is the sum scattering and absorption. The albedo of a particle is given by Q_{scat}/Q_{ext} and approaches unity for dielectric scatterers.

A lot can be learned about the scattering behaviour of different sized particles from the plots in figure 9.2. I assume here that unpolarized light, of wavelength 0.55μm, is incident with unit intensity on graphite and silicate spherical particles. I calculate the intensity of light per steradian (denoted I) which is scattered through an angle θ from its direction of incidence. Values of I are derived using Mie formulae (the computation of which is discussed in §9.5.1). In each case, scattering is calculated for individual spheres of graphite and silicate with sizes 0.01μm, 0.1μm or 0.3μm. I is plotted, in all cases, logarithmically. The polarization of the scattered light, P, is also evaluated and the product of P and I gives the polarized intensity of the scattered light. This is denoted by PI in figure 9.2 and is also plotted in the logarithm.

For particles with dimensions much smaller than the incident radiation Mie scattering approaches the Rayleigh regime. Rayleigh scattering describes the interaction of optical light with molecules and the very smallest particulates. In the Rayleigh regime the scattered intensity is symmetric about scattering angles of 90°. The degree of polarization for $\theta = 90°$ is 100%. It is evident from figure 9.2 that particles of size $\sim 0.01\mu$m closely mimic Rayleigh particles when optical radiation is incident. As particle size increases several things begin to happen; (a) scattering becomes more forward-throwing i.e. a larger proportion of the scattered beam is deflected by smaller scattering angles; (b) the overall polarization of the scattered light tends to become smaller and begins to oscillate with respect to θ; and (c) polarization levels can become negative for larger particles. Negative

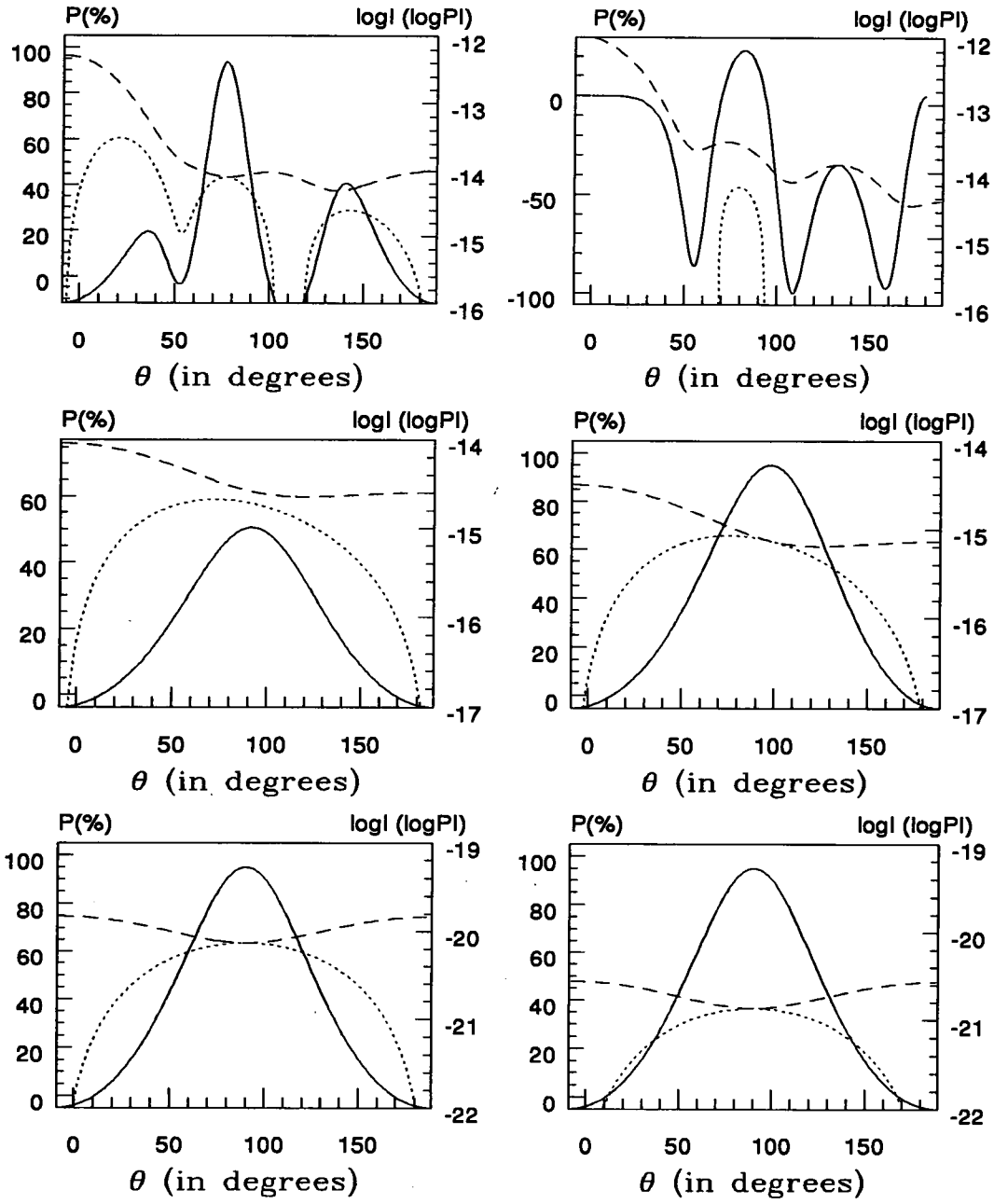

Figure 9.2: The scattering behaviour of homogeneous spherical particles. Graphs on the left refer to graphite spheres of size 0.3μm, 0.1μm and 0.01μm (top to bottom). Those on the right correspond to silicate spheres of size 0.3μm, 0.1μm and 0.01μm (top to bottom). In all cases, the solid line denotes the percentage linear polarization (P), the dashed line denotes the scattered intensity (I) and the dotted line corresponds to the polarized intensity (PI). θ is the angle through which the incident beam has been scattered.

polarizations correspond to the electric vector of the scattered radiation being parallel to the plane containing the incident and scattered beam. In most astrophysical situations the observed polarization is positive. This means that the polarization of the scattered beam forms a tangential vector to an imaginary line connecting the scatterer to the source of incident radiation. The absence of negative polarizations in the galaxies studied in this work, indicates that particles no bigger than a few tenths of a micron are responsible for the scattering of optical radiation in starburst galaxies.

In §9.3 three grain models were chosen as feasible parameterizations of ISM-type Galactic dust. With the justifications that I made then, I adopt these same grains models for the optical extinction of starburst galaxies. For each model, I plot in figure 9.3 the normalized scattering cross-section against the size parameter X. In each case, $n(X)$ has been normalized over a different range in particle size. Therefore it is the *profiles* in figure 9.3 which are of immediate interest (rather than the absolute scattering cross-sections). The scattering cross-section of the Composite distribution has been multiplied by a factor of 10 for the sake of clarity.

The peak scattering in figure 9.3 tends to occur for $X \sim 1$. If the incident radiation has a wavelength of 0.55μm, the dominant scatterers will be dust grains of size $\sim 0.1\mu$m (equation 9.6). In general, smaller sizes are more numerous but they offer a smaller scattering cross-section. For large grains the converse is true with the result that most of the incident light is scattered by grains $\sim 0.1\mu$m in size. At first sight, the Composite particles in figure 9.3 may appear to be something of an exception to this statement. However, the usual limits on the model ($a_{min} = 0.03\mu$m and $a_{max} = 0.9\mu$m) actually forbid a contribution from micron-sized grains. Dust grains of size $\sim 0.1\mu$m are known as 'classical' particles. The identification of classical particles as the chief cause of optical interstellar extinction within the Galaxy has already been noted in §9.3.

In figure 9.3 the Greenberg distribution has been plotted as two separate populations of graphite and silicate grains (G:Gr and G:Si respectively). This uses equation 9.5 with $a_c = 0$, $a_i = 0.1\mu$m for graphite and $a_c = 0$, $a_i = 0.25\mu$m for silicate. Limits are generally not necessary for the Greenberg distribution because scattering falls off rapidly for particles much larger than or much smaller than a_i. By virtue of abundance constraints, silicate grains alone cannot provide the extinction observed in the ISM. If we wish to implement a Greenberg-type size distribution then a mixture of G:Gr and G:Si would be required in any plausible model. There are several reasons why I do not use the core-mantle form of equation 9.5. There is, as already pointed out, no observational evidence for mantles existing outside molecular clouds. More importantly, I am unaware of any published refractive indices for organic mantles. Greenberg and Chlewicki (1987) discuss the refractive index appropriate for ultraviolet light but do not provide any optical data. Although the Greenberg forms, as I use them, are not the commonly-adopted parameterizations they *do* reproduce the optical part of the Galactic extinction curve. At the same time, they provide an alternative size distribution to the MRN and Composite models. Hereafter, reference

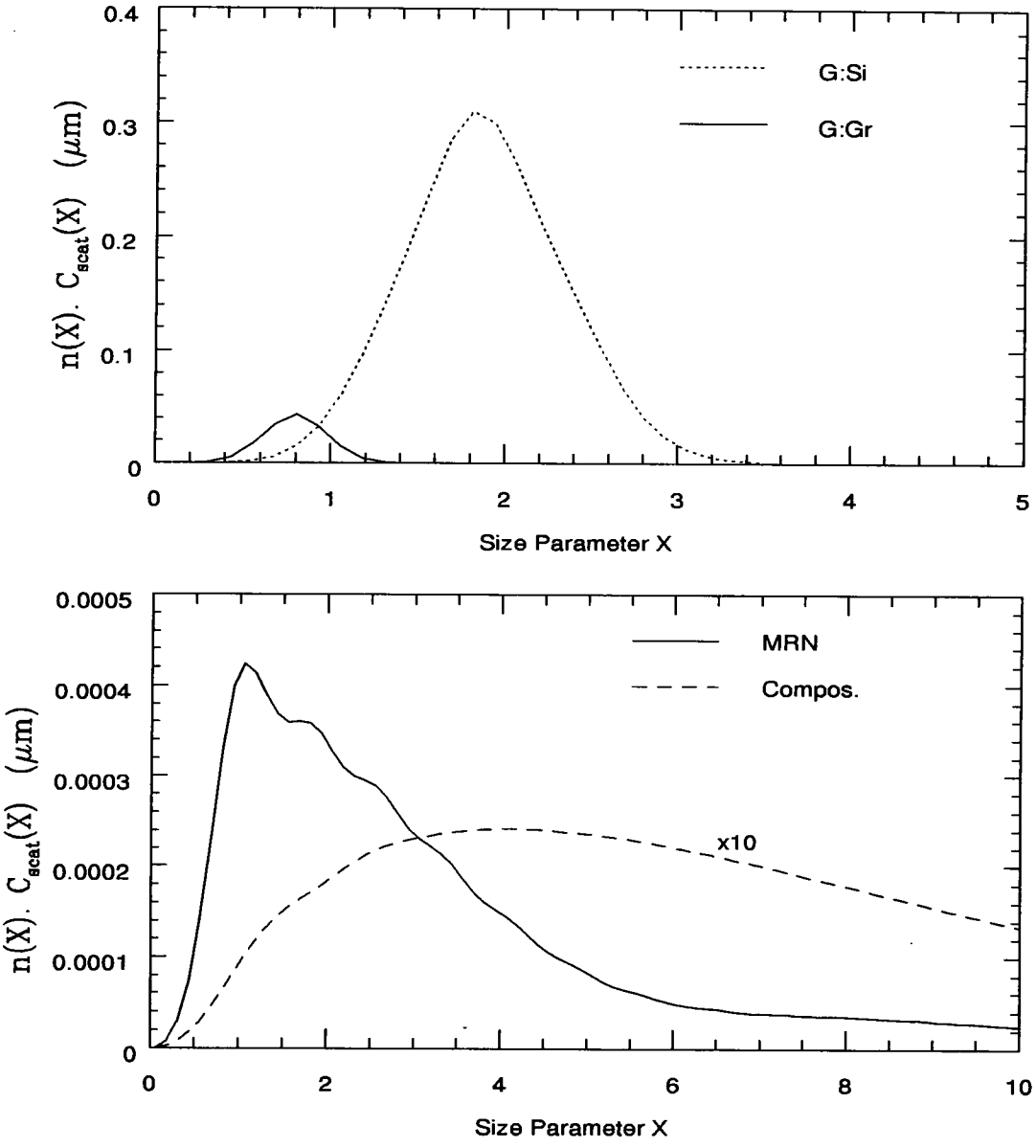

Figure 9.3: The normalized scattering cross-section for models approximating ISM-type grains. X is the size parameter (given by equation 9.6) and $n(X)$ is the number density at X. $n(X)$ is prescribed by the grain model in question. Thus, for MRN grains, it is given by equation 9.4. G:Si and G:Gr correspond, respectively, to silicate and graphite spheres distributed according to the Greenberg form (equation 9.5). 'Compos.' refers to composite grains postulated by Mathis and Whiffen (1989). In this case the scattering cross-section has been multiplied by a factor of 10 for clarity in the figure.

to a Greenberg distribution (either G:Gr or G:Si) implies the forms of equation 9.5 which are plotted in figure 9.3.

The refractive indices used to plot figures 9.2 and 9.3 have been taken from Mathis and Whiffen (1989) for the Composite grains and Draine and Lee (1984) for graphite and silicate material. Mathis and Whiffen begin with the refractive indices of the constituent components (mostly using data given in Draine and Lee) and apply a mixing rule to obtain the refractive index of the Composite particles. The refractive indices of graphite and silicate are somewhat uncertain because: (a) experimentally determined values show some variation amongst themselves (Draine and Lee 1984) and (b) the nature of *astronomical* graphite and silicate is probably somewhat different to their laboratory-produced counterparts. For the purposes of the scattering calculations that follow, this should not concern us unduly – uncertainties in the refractive index are small compared to uncertainties in, for example, the scattering geometry.

The other caveat worthy of note concerns the use of spheres as approximations to astronomical dust grains. As already pointed out (§9.3) there is evidence that dust grains are, in fact, elongated and perhaps even quite irregular. Some authors have carried out Mie calculations for shapes other than spheres, e.g. spheroids and cylinders (Mathis 1986; Bohren and Huffman 1983 and references therein) but on computational grounds spheres are preferred. The use of non-spherical particles also introduces several more unknowns into the problem; namely the efficiency with which grains align themselves in an external magnetic field and the degree to which the particles are elongated. It seems likely that spheres which contain the same volume as the actual interstellar particles themselves, provide a useful approximation (Mathis; private communication). Moreover, for the scattering simulated in this chapter the polarization data give no indication that scatterers are aligned in a galactic magnetic field. (A possible exception to this statement may be the very centre of NGC 3125 – §7.3). As a consequence, I would expect any asymmetry in grain shape to be randomised with respect to the incident radiation.

9.5 Scattering Models

In the preceding sections I have discussed the nature of interstellar grains and how they interact with optical radiation. This information provides the basis for scattering models which I now wish to construct for some of the objects studied in this thesis. First of all, however, let us clearly define what the known and unknown parameters of the problem are.

In principle, the problem is the same as that expressed by equation 9.2 which was used to describe electron scattering. In this case, however, the relevant scattering cross-section is that of dust grains and the polarization of the scattered light must be evaluated by Mie theory. (The observed polarizations cannot be used directly because the scattered light is diluted by an unknown amount of unpolarized stellar light). If the starburst is not greatly

obscured by foreground material its brightness relative to the observed polarized light can be measured. In addition, the distribution of scatterers in the plane of the sky is self-evident from the polarization map. Therefore, assuming a hypothetical dust distribution along the line-of-sight, one can calculate without much effort how much light is incident on the scatterers. Using Mie formulae, one can anticipate the polarized intensity produced by scattering from the dust distribution. By inverting the calculation, I estimate the amount of dust required to reproduce the observed polarized intensities.

9.5.1 Geometry of the Model

Of the 6 starburst galaxies investigated in this thesis, NGC 3125 and NGC 3077 appear to most suitable for modelling. Both show scattering over large (kiloparsec) regions of their ISM and the starburst which illuminates the dust grains is relatively unobscured.

NGC 3125

A salient feature of the polarization map produced for NGC 3125 (figure 7.2) is that the scattering region narrows towards the central starburst. Dust grains distributed within a solid bi-cone might therefore appear to provide an appropriate geometry in this case. It should be noted, however, that the **polarized intensity** detected across the scattering regions is not easily accommodated by a geometry of this type. In figure 9.4, I plot the polarized intensity for the vectors of figure 7.2. Scattering material distributed within a solid bi-cone should be characterized by maximum polarized intensities along the central axis and a decrease towards the limb where the dust vanishes. In figure 9.4, the limb has been denoted by two solid lines (AB and CD) and the projection of the apex angle onto the plane of the sky by the angle P. In the south-east quadrant, the highest level of polarized intensity does indeed appear to originate from the major axis but this effect may, in part, be attributable to the presence of aligned grains near the starburst (§7.2). In the north-west quadrant, where polarization arises purely from scattering, there is no real tendency for the polarized intensity to decrease further away from the major axis. With these considerations in mind, I decided **not** to use a bi-cone geometry. Instead, I opted for a dust geometry which maintains a greater degree of flexibility (although, like a bi-cone, it is still characterized by a narrower distribution of scatterers closer to the starburst). The basic geometry is illustrated in figure 9.5.

The dust grains in figure 9.5 are distributed within a **rectangular-based** bi-pyramid which is centred on the starburst. The stars at the origin O in figure 9.5 denote the starburst and the solid arrows trace a possible path for the light that is scattered towards the observer. Figure 9.6 shows the bi-pyramid model as it appears to the observer. The lines AB and CD delineate the distribution of the dust grains as projected onto the plane of the sky and therefore correspond to the same lines in figure 9.4 (the angle P also corresponds

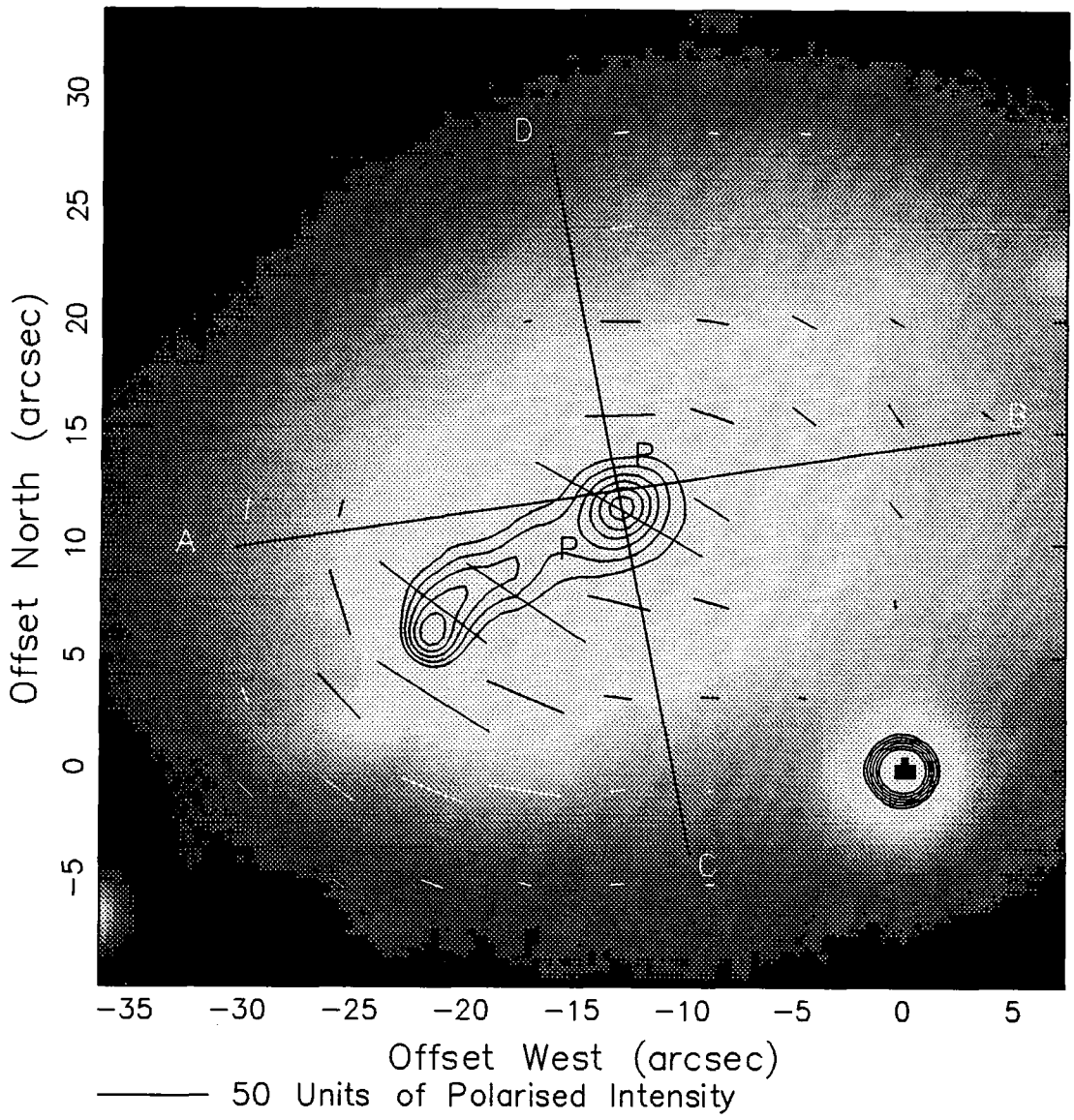

Figure 9.4: The polarized intensity detected from NGC 3125. How are the scatterers distributed along the line-of-sight ? See text for further details.

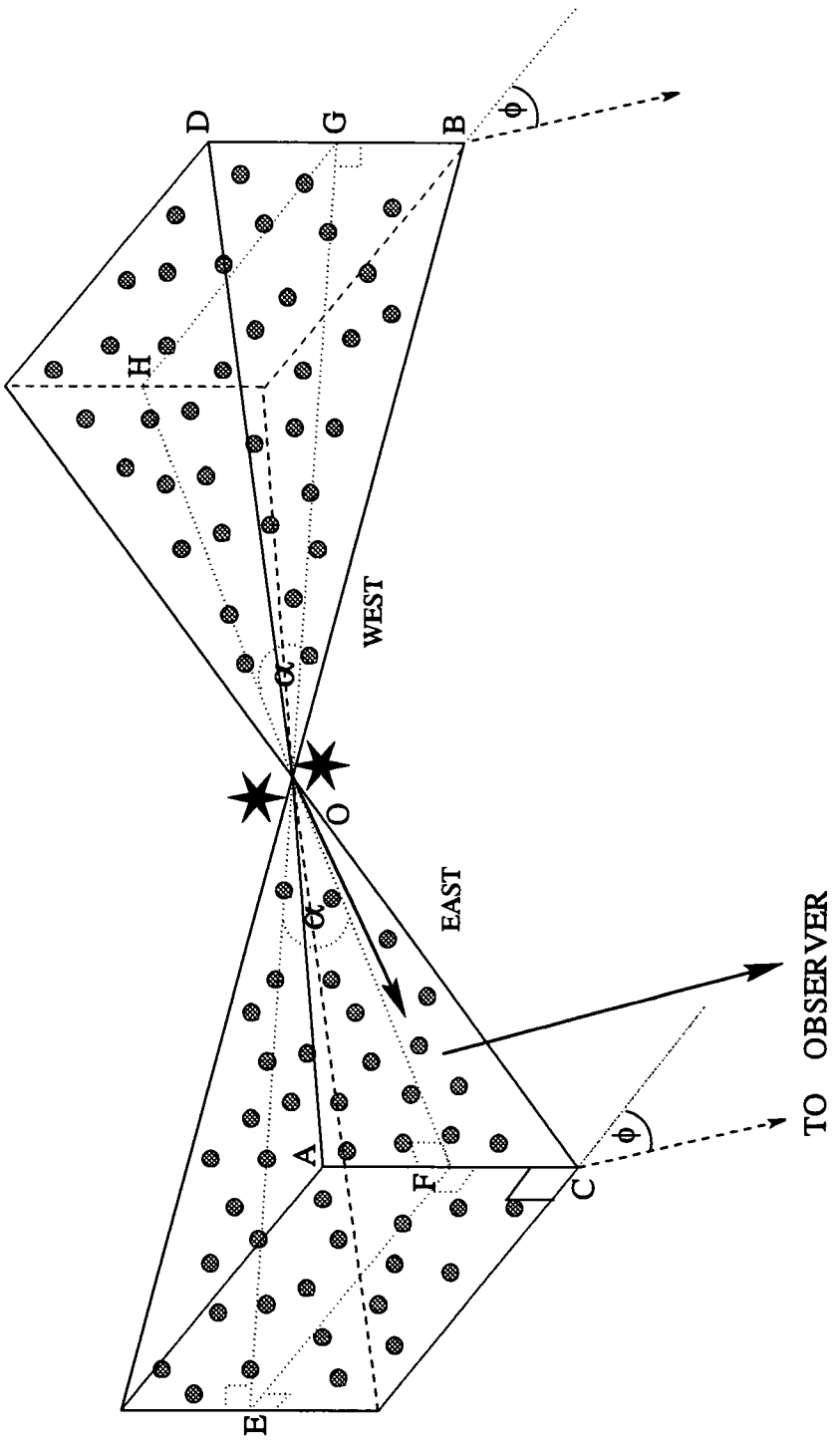

Figure 9.5: A schematic representation of the scattering models which are constructed in this chapter. The shaded spheres denote dust grains, the large stars represent the starburst. The free parameters describing the geometry are the angles α and ϕ and are defined in figure 9.7.

to the angle marked P in figure 9.4).

The free parameters describing the geometry are defined in figure 9.7 which is a plan view of the bi-pyramid. The opening angle along the line-of-sight is denoted by α and the tilt of the structure with respect to the line-of-sight is given by the angle ϕ. Both of these angles are also marked in figure 9.5. If ϕ is positive, dust to the east of the starburst is tilted towards the observer (and dust to the west is tilted by the same angle away). For negative ϕ the converse is true. The bi-pyramid is assumed to be face-on in a north-south direction. Therefore, the lines AC and DB in figure 9.5 are at all times perpendicular to the line-of-sight.

The density of dust at any point within the bi-pyramid is determined by the observed polarized intensity (as opposed to assuming a uniform dust density throughout the polarized regions of the galaxy and attempting a best fit to the data). This was carried out in the following way. First of all, the brightness of the starburst illuminating the dust was determined by placing an appropriately sized aperture at the centre of the galaxy and integrating. (This is discussed in the sections that follow for each individual case because sometimes corrections were necessary for extinction along the line-of-sight). For each measurement of polarized intensity in the observed data, dust was assumed to be uniformly distributed along the line-of-sight for the part of the sky subtended by the measurement (shaded region in figure 9.7). The dust column density of each measurement bin, however, was calculated by estimating the amount of light that leaves the starburst, scatters off the dust grains distributed along the line-of-sight and reaches the observer as polarized light. The column density within each bin was increased until the polarized intensity predicted by the model agreed with the observed value. This means that, for any given bin, dust is assumed to be uniformly distributed along the line-of-sight but the dust density will vary between contiguous bins. The total amount of scattering material within the galaxy is found by integrating the column density over all bins.

For reasons given below, the model is assumed at first to be optically thin. This means that optical photons travel unimpeded from the starburst to the dust grains, undergo a single scatter and then leave the reflection nebula. Dust scattering cross-sections and polarizations of the scattered beam were calculated using Mie theory (§9.4). FORTRAN code for the Mie formulae had already been written by a former member of the Durham Imaging Polarimetry Group – R. Warren-Smith (1979). This enabled the necessary cross-sections and scattering amplitudes to be computed. (These same subroutines were also used to produce figures 9.2 and 9.3). Simulations were carried out for several values of α and ϕ and independently for each of the grain parameterizations (MRN, Composites, G:Gr and G:Si). Material densities required for the derivation of dust mass were taken from Hildebrand (1983).

The model was assumed to be optically thin for the following reasons: (a) the scattering regions are not accompanied by any obvious signs of absorption (no evidence for

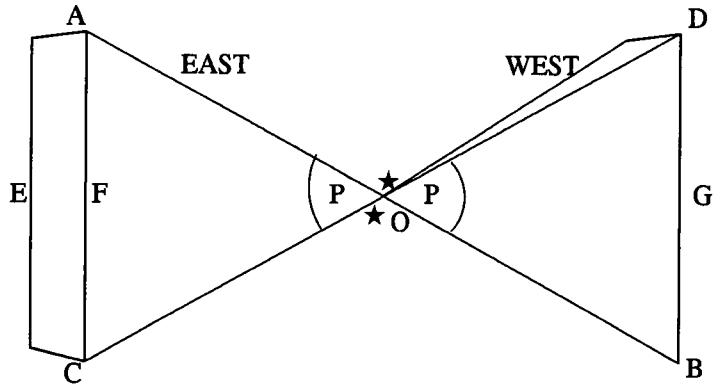

Figure 9.6: The bi-pyramid model of figure 9.5 as projected onto the plane of the sky. See text for details.

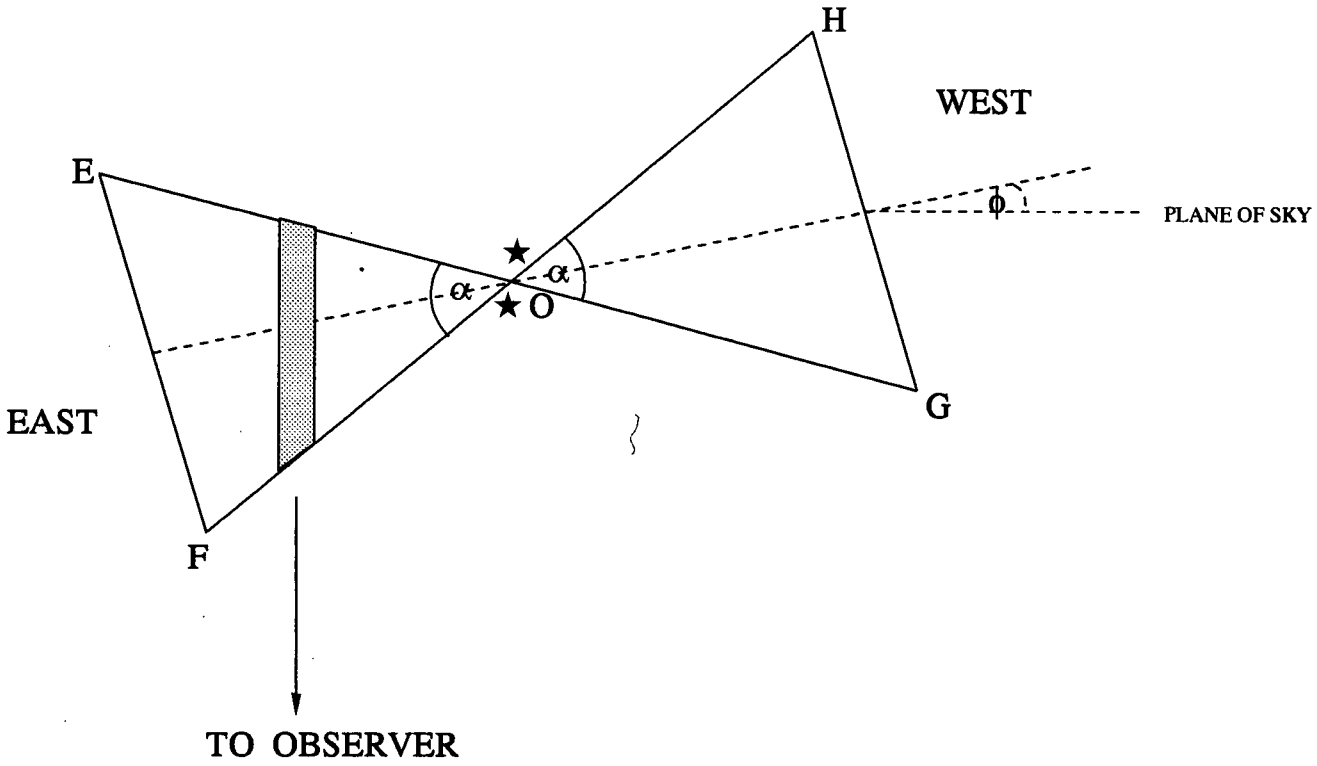

Figure 9.7: A plan view of the bi-pyramid model of figure 9.5. The free parameters of the model are the angles α and ϕ.

dust lanes or patches of obscuring material). Unfortunately, this is something of a weak argument. As I explain below, it is possible that large amounts of dust may be present in a galaxy without manifesting itself through absorption or obscuration. (b) an optically thick model would necessarily involve complicated Monte Carlo simulations. (c) An optically thin model can be checked without much difficulty for self-consistency. A natural 'by-product' of the scattering simulations is the determination of optical depth both along the line-of-sight and along the galactic radius. This allows one to calculate the attenuation of the pre- and post-scatter beams. If the optical depth is sufficiently low (say < 1) the attenuation is small and the original assumption of optical-thinness is justified.

The use of a bi-pyramid as model for the grain distribution is admittedly somewhat unusual. Therefore I wish to compare briefly with other geometries that could have been chosen:

1. For reasons already stated above, a dust-filled bi-cone seems to be a less favourable geometry - at least in the case of NGC 3125. If, nonetheless, we were to insist on this kind of geometry, the opening angle (or apex angle) of the bi-cone would effectively be determined by the distribution of dust projected onto the plane of the sky (in the case of NGC 3125, the projection of the apex angle onto the plane of the sky is about 90° - see figure 9.4). This leaves only one free parameter for a bi-cone geometry (the tilt angle ϕ) whereas the bi-pyramid of figure 9.5 is more flexible in that it is described by two free parameters (ϕ and α).

2. Another plausible dust distribution would be a **hollow** bi-cone or hollow bipolar bubble. Galactic-scale winds are known to 'snow-plough' interstellar gas in both low and high mass starburst galaxies (§6.7; §1.4) and this leads to the formation of shells of denser ambient gas surrounding a superwind bubble or cone. There are two main difficulties with a geometry of this kind: (i) the outflow in NGC 3125 is along the *minor* axis and **not** the major axis (where the dust is) (see §7.4); and (ii) as we shall see shortly, thin, dense shells or layers of dust tend to be optically thick to light travelling in a radial direction. The calculations in this chapter use an optically-thin approximation which is no longer valid under such circumstances.

3. The flexibility of the bi-pyramid geometry is such that it allows many general conclusions to be drawn about dust scattering in galaxies. These conclusions are more or less independent of the exact *shape* (bi-pyramid, bi-cone etc.) chosen for the dust distribution and one should not worry too much about this aspect of the model.

NGC 3077

Is it possible to apply the bi-pyramid model to NGC 3077 ? Admittedly this galaxy appears to be characterized by a far more irregular scattering distribution than NGC 3125

(figure 5.5). Due to incomplete polarimetry data, however, it is difficult to infer what overall dust geometry *is* most appropriate for this object. Where coverage is complete there is a tendency for the scattering distribution to narrow at closer proximity to the starburst. Indeed, in the east half of the galaxy scatterers appear to be arranged in filamentary-like structures which converge at the central starburst (§5.4). In lieu of more information, I decided to use the same free parameters as those in figure 9.5. The geometry along the line-of-sight is determined, once again, by the free parameters α and ϕ. In figure 9.5, the distribution of scatterers projected onto the plane of the sky is contained within two diametrically-opposed triangles which constitute the front faces of the bi-pyramid. The visible distribution of scattering material in NGC 3077 is clearly far more irregular than this but this is not important. The same basic framework can still be maintained - namely the distribution along the line-of-sight narrows towards the starburst (according to the parameter α). As before, positive ϕ means that scatterers east of the starburst are tilted towards the observer and those in the west are tilted by the same angle away from the observer.

9.5.2 Results: NGC 3125

The conclusion from §7.4 was that the galactic-scale reflection nebula detected in NGC 3125 was predominantly the result of light being scattering from the brightest star-forming region (the north-west knot). Accordingly, I took the polarimetry data presented in figure 9.4 and selected vectors with a signal-to-noise ratio > 2 which were also orientated at $90 \pm 20°$ to the north-west knot. It has already been noted (§7.3) that some of the vectors closest to the starburst may in fact be the result of dichroic extinction rather than scattering. If these vectors are removed from the scattering calculations the results which I present below must be modified by no more than 10%. We shall see shortly that errors of this order can be considered small relative to other uncertainties entering into the calculation.

The brightness of the north-west knot was measured using a circular aperture of diameter $\simeq 5''$. I note from §7.3 that some illumination may also originate from star forming regions extending to the east of the north-west knot. This introduces a sizeable uncertainty into the calculation (probably a factor of 2). In addition, Terlevich (1991) has calculated reddening for the hot-spots in NGC 3125. This information indicates an extinction of $A_V = 0.7 \pm 0.1$ mag for the north-west knot. I will assume this extinction arises from dust residing within the starburst itself (rather than foreground material). This assumption may be incorrect if the centre of NGC 3125 is subject to dichroic extinction because dichroism necessitates the presence of aligned grains along the line-of-sight. Correcting for 0.7 mag of extinction would reduce the masses and densities derived in the following scattering models by a factor of 2.

Table 9.1 summarizes the results for NGC 3125 using MRN dust grains. For each value

of ϕ and α, the dust mass required to reproduce the observed data is tabulated. Geometries requiring scattering material between the observer and the central starburst are precluded from the calculations (these geometries are not compatible with the 'narrowing' of the observed polarized intensity at smaller distances from the starburst). Masses and mean particle densities are given for both the north-west (NW) and south-east (SE) regions of the galaxy. The mean particle density is the total number of dust grains required per cubic metre if the grains follow the size distribution of equation 9.4 (this will vary according to the observed polarized intensity in different parts of the galaxy but an average value can be calculated). Table 9.1 also gives the total dust mass (denoted by M_s). The present discussion will concentrate on MRN grains at first. I shall then generalize the results to include other grain parameterizations.

The main trend in table 9.1 is best understood by consulting figure 9.2. For a given incident intensity, classical grains ($\sim 0.1\mu$m) produce maximum levels of polarized intensity at scattering angles close to about 70°. Therefore geometries constrained fairly close to the plane of the sky will tend to require less scattering material to reproduce the observations. If the majority of dust grains lie more than about 45° out of the plane of the sky there is a swift increase in the required dust mass and the scattering material rapidly becomes optically thick. The main reasons for this are that: (a) the mean scattering angle is less favourable for the production of polarized light and (b) the average distance separating the dust grains from the central light source is greater. If the opening angle α is $< 30 - 45°$ the scattering material tends to become optically thick along the galactic radius. In summary then, if the grains either occupy a fairly thin layer at the centre of the galaxy or if the dust is concentrated towards the front or back of the galaxy, the original assumption of optical-thinness is no longer valid and a more complicated analysis is required. For geometries which do not fall into this 'optically-thick category' the amount of 'MRN-dust' required to reproduce the observations is about $0.3 - 0.8 \times 10^6 M_\odot$.

It is also clear from table 9.1 that, if the dust distribution is significantly tilted with respect to the line-of-sight, then a considerable disparity begins to appear between the density of scatterers on either side of the starburst. In particular, for $\phi \leq -30°$ the number of scatterers required in the south-east quadrant exceeds that in the north-west quadrant by up to one order of magnitude. This finding is intuitively obvious because polarized intensity levels in the south-east part of the object are higher than elsewhere suggesting, if anything, that the eastern half of the galaxy is slightly closer to the observer (figure 9.4). For large asymmetries in the required dust densities it is necessary to identify a physical mechanism whereby dust is concentrated preferentially in one half of the galaxy.

Extinction considerations may also be relevant to the plausibility of any model. It was noted in §9.5.1 that the large-scale polarization of NGC 3125 is not accompanied by any visible signs of absorption. It may be possible to estimate the amount of dust that must be present before the scattering material becomes apparent in our images. To do this, an *apparent* extinction is calculated. Grains are assumed to contribute to the attenuation of

galactic light by absorption only. This is because an extended layer of dust will scatter as much background stellar light *into* the line-of-sight as it scatters light *out* of the line-of-sight. In addition, light from the starburst is also scattered into the line-of-sight and this reduces the observed extinction (hence the term 'apparent extinction'). In general, the reduction in observed extinction, due to scattered light from the starburst, is quite small. However, if one were to consider scattering from all stellar sources within the galaxy the reduction could become quite significant. Witt *et al.* (1992) used Monte Carlo methods to compute the transfer of radiation in various galaxian models. They found that scattering can significantly undermine the effects of reddening. Moreover, they show that in systems where dust and stars are well mixed (which may well apply to NGC 3125) naïve calculations of extinction can seriously underestimate the amount of dust present. (Similar conclusions are reached by Emsellem (1995) who models extinction in M101).

Unfortunately the light distribution in NGC 3125 is not known relative to the dust distribution and therefore the calculations of Witt *et al.* cannot be applied directly. My best estimate of apparent extinction is to assume that only half the stars along the line-of-sight are subject to extinction (through absorption only) and that light scattered from the starburst can partially compensate for this attenuation. Using this approach, I find that: (a) of the models in table 9.1, those with total dust masses $> 10^6 M_\odot$, tend to have apparent extinctions of $A_V > 0.5$ mag; and (b) lower mass models (few $\times 10^5 M_\odot$) have $A_V \leq 0.3$ mag. By comparing parts of the galaxy that manifest scattering against those that do not, I estimate $A_V < 0.3$ mag for the real data. This tends to make the lower mass models more appealing. I do not, however, attach *too* much significance to this result, because, as stated above, my calculation of apparent extinction is very naïve.

Much of the discussion thus far applies equally well to the the Greenberg and Composite grains models. Instead of tabulating more data, I summarize the main points as follows:

(i) All grains models exhibit a rapid increase in dust mass if most of the grains lie more than about 45° out of the plane of the sky.

(ii) α must be fairly large to maintain optical thinness along the galactic radius ($\alpha \geq 30 - 45°$). For Composite grains, $\tau_{radial} \geq 1.5$ for all α indicating that the optically thin approximation is no longer tenable. For geometries fairly close to the plane of the sky, Composite models require between 2 and 3 times as much dust mass as the equivalent MRN model. The minimum apparent extinction for these grains is $A_V \simeq 0.4$ mag.

(iii) For a given mass, G:Gr and G:Si grains scatter respectively $\simeq 2$ and 0.5 times as much polarized light as the MRN mixture. One of the main reasons for this is that graphite has a higher optical refractive index than silicate. This means that it is more effective at scattering light. Silicate models are more likely to be optically thin (both in the plane of the sky and along the line-of-sight) because the grains are less absorptive. (The opacity in the plane of the sky has been calculated assuming that light attenuation results from

absorption only. For classical grain sizes, scattering is forward-throwing - see figure 9.2 - which means that most of the scattered light is only deflected by small angles rather than being 'lost' from the nebula.)

(iv) More realistically, G:Gr and G:Si will be mixed in order to account for the presence of both carbon and silicate material in ISM-type dust (§9.3). For comparable masses of graphite and silicate, the Greenberg particle distribution requires about the same mass as MRN grains and produces roughly the same apparent extinction along the line-of-sight.

9.5.3 Checks on the Calculations

The scattering calculations were checked in a variety of ways: (a) computational output, such as extinction cross-sections and scattering amplitudes, were checked against data tabulated and plotted in Wickramasinghe (1973), van de Hulst (1953), Warren-Smith (1979) and Whittet (1992); (b) the flux scattered by a single sphere was integrated over all solid angles and compared with the incident flux. After allowing for absorption by the sphere, the scattered flux was consistent with the conservation of energy; (c) I derived the amount of extinction produced by unit mass of MRN grains obscuring a background light source. Using a Galactic gas-to-dust ratio, I use this value to calculate the extinction per hydrogen atom for the Galaxy. This agreed extremely well with the value given by Bohlin *et al.* (1978). Since the parameters of the MRN were obtained by fitting the Galactic extinction curve (§9.3), the comparison is a valid one; (d) Alton *et al.* (1995) published a simple isotropic scattering model for NGC 3125. The calculation made simple assumptions about grain sizes and albedos so that Mie analysis could be avoided (§7.4). I simulated this simple model with the present Mie calculations and found the two results consistent with each other.

9.5.4 Results: NGC 3077

The scattering observed in NGC 3077 was investigated in the same manner as NGC 3125. For reasons already stated (§9.5.1), I assumed geometries governed by the free parameters in figure 9.5. The illumination of the dust grains was determined in the following way. The polarized intensity vectors in figure 5.5 were rotated by 90° and used to minimize the following quantity:

$$\sum \frac{(\theta - \theta_o)^2}{d\theta^2} \tag{9.10}$$

where θ and $d\theta$ are, respectively, the position angles and corresponding errors of the rotated vectors. θ_o is the position angle of a line connecting the integration bin to the proposed center of the scattering pattern. The above quantity was minimized for a light source located $\simeq 2''$ north-west of the origin in figure 5.5 (the origin is also the location of the compact polarized source detected in NGC 3077 - see §5.3). The spatial extent of the illuminating source was determined by two methods. In the first procedure, regions of the starburst

having > 95% chance of **not** lying at the center of the scattering pattern, were discounted. The second method involved dividing the vector normals used in equation 9.10 into four quadrants (north-west, south-west, north-east and south-east). Minimization was then carried out for each quadrant. The relative separations of the four minimization points were taken as the spatial extent of the illuminating source. The first of the above methods gave a linear dimension of 4″ and the second method a size of 6″. I adopted the second value as more realistic but noted a factor of 2 uncertainty in the integrated brightness (the difference between integrating over a $(6'')^2$ bin as opposed to one of only $(4'')^2$).

Up to half of the region contributing to the illumination is partially obscured by a dust cloud residing on the nearside of the starburst. A correction for this was made for this cloud based on the optical depth estimated by Price and Gullixson (1989). Unfortunately neither emission-line ratios nor colour maps are available for NGC 3077. Consequently, it is difficult to estimate the overall obscuration of the star forming region along the line-of-sight. I assume therefore that any reddening, other than that due to the aforementioned dust cloud, arises from dust close to, or mixed in, with the star forming regions themselves (there is no evidence for foreground dust lanes in NGC 3077). If this is the case no other corrections should be necessary for the brightness of the illuminating source.

The results of scattering calculations carried out for NGC 3077 are summarized as follows:

(i) For all grain parameterizations, it is difficult to find solutions that remain optically thin. Even models with large α ($\alpha = 90° \rightarrow 120°$) have optical depths of ≥ 1. This problem might be circumvented if one assumes that light scatters off the surface of geometrically thin filaments which are radially oriented but curvi-linear in shape. In this case, the pre-scatter beam reaches the scattering location without undergoing attenuation by dust residing at smaller radii. This scenario is not unrealistic for at least part of the polarization pattern seen in NGC 3077 (scattering material to the east of the starburst, for example, appears to be arranged in filament-like structures - §5.4). It is also possible that I may have underestimated the brightness of the central source in NGC 3077. Increasing this quantity by a factor of 2 or 3 (effectively the estimated uncertainty in this parameter) allows some of the models with a lower dust mass to become fairly optically thin. Rather than modifying the brightness of the central source at this point, I maintain the original model parameters but note that an increase of factor 2 in this quantity will *decrease* the dust masses that follow by the same factor.

(ii) If most of the dust lies within 60° of the plane of the sky then the required mass of MRN grains is, within a factor of two, $1 \times 10^5 M_\odot$. Composite and Greenberg grain models require corresponding more or less dust mass according to the ratios given in (ii) - (iv) of §9.5.2. For larger $| \phi |$ the required dust mass increases rapidly.

For NGC 3077, a wavelength of $\lambda = 0.70 \mu$m was ascribed to the incident radiation.

This corresponds to the peak response of the CCD in the absence of a filter (no filter was used in making the observations). If λ changes by 50% of the FWHM of the unfiltered CCD (i.e. $\lambda = 0.53\mu$m or $\lambda = 0.87\mu$m) the required dust masses change by no more than 20%.

It may be possible to learn something about the spatial density of scattering material in NGC 3077 by examining the behaviour of polarized intensity with distance from the starburst. In figure 9.8, I have plotted the polarized intensities of figure 5.5 (which were also used for the above scattering models) against the distance in parsecs (denoted 'radius'). Using a χ^2 minimization, a power law can be made to fit the data in figure 9.8. The best fit (reduced $\chi^2 = 1.0$) has a gradient of -0.85 and is drawn into the figure.

The fit to figure 9.8 has some interesting ramifications. If the reflection nebula in NGC 3077 is optically thin (an assumption which may be marginally true for certain dust distributions along the line-of-sight), then the incident flux from the starburst should decrease as (radius)^2. Now, the observed polarized intensity (PI) should behave in proportion to both the incident flux and the dust column density (if the average scattering angle across the reflection nebula remains approximately the same). If the incident flux decreases as (radius)^2, the dust column density must increase in proportion to radius in order to reproduce the trend in figure 9.8 (PI approximately inversely proportional to radius). For the model of figure 9.5, this condition is fulfilled if there are a constant number of grains per cubic meter i.e. the starburst is surrounded by uniform density dust clouds. This is something of a surprise because, if the scattering material was originally expelled into the ISM by the central starburst (§5.4), we might expect the density of scattering material to decrease with radius. If the reflection nebula in NGC 3077 is marginally optically thick, the density of scattering material must then *increase* with radius in order to compensate for attenuation of the pre- and post-scatter beams. This too would imply far more dust at larger galactic radii compared with smaller galactic radii.

For NGC 3125, the dust column density was investigated in the same manner as above. Once again, the behaviour of polarized intensity against radius could be interpreted using optically-thin, uniform dust clouds. The case for NGC 3125, however, is less convincing because a trend of the form $PI \propto (1/\text{radius})$ is statistically weaker than that in figure 9.8.

For geometries where the optically-thin approximation is appropriate, the density of scattering material in both NGC 3077 and NGC 3125, is similar to the diffuse interstellar medium within our own galaxy. This conclusion is reached by taking the dust column densities from the scattering models and applying a Galactic dust-to-gas ratio. The resulting gas density, $\sim 0.1 - 10$ hydrogen atoms per cm^3, is comparable to the diffuse gas phase within our own Galaxy (Whittet 1992).

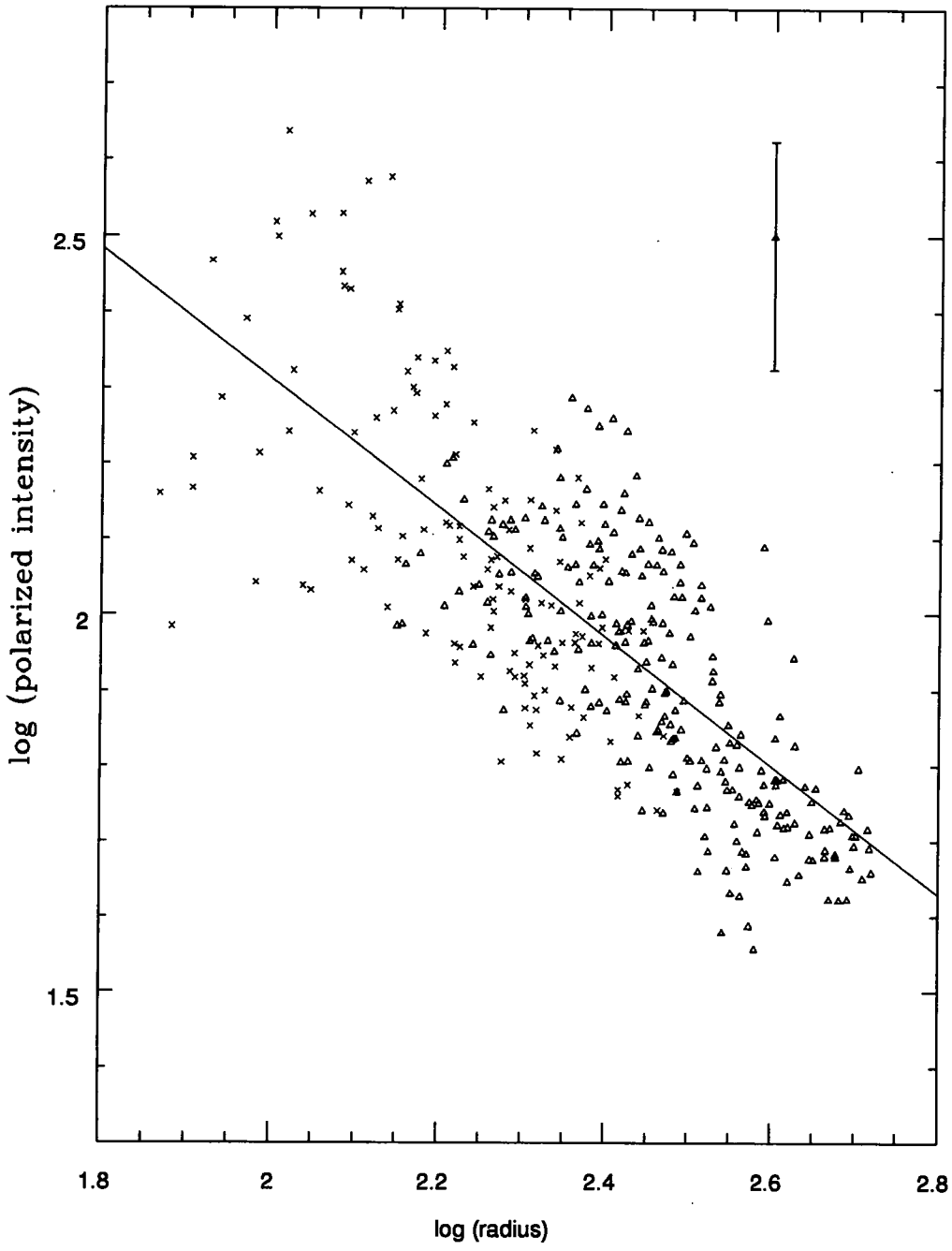

Figure 9.8: A plot of polarized intensity against radius for the galaxy NGC 3077. Triangles refer to points to the west of the starburst whereas diagonal crosses correspond to locations to the east. A typical error bar is shown at the top right of the plot. The solid line is a power-law best fit to the data.

9.5.5 Limitations of the Model

It is important to be aware of the limitations of the scattering calculations carried out above. An optically-thin approximation has been used which, for many of the scattering geometries investigated, appears to provide a self-consistent solution. Where optical thinness is no longer a valid assumption (and for many of the NGC 3077 simulations the situation is somewhat 'marginal'), a more complicated analysis is called for. This should allow for an attenuation of the pre- and post-scatter beams. A future development of the model might include an iterative technique which finds self-consistent solutions. One begins with the optically-thin approximation and calculates the amount of dust required to reproduce the observed polarized intensities. Using the calculated dust masses one determines the optical depth of the reflection nebula and allows for attenuation when carrying out subsequent calculations. This is carried out until a self-consistent solution is found.

Another assumption which is used to some extent in the scattering calculations of the previous sections, is that any obscuration of the illuminating source (i.e. the starburst) occurs close to the starburst itself. If this is not the case, I will have underestimated the intensity of light incident on the dust grains. As already mentioned in §9.5.2, reddening of the emission-line regions in NGC 3125 is quite small. If this, for example, were to arise from dust in the foreground of the galaxy, the amount of scattering material required for NGC 3125 is reduced by 50%. Unfortunately, for NGC 3077 the published data are not sufficient to determine the extinction of the starburst (although a correction *was* made for a prominent foreground dust cloud - §9.5.4). If further corrections for foreground obscuration are necessary, this will act to decrease the amount of scattering material required to reproduce the observations.

9.5.6 Summary of Results

For the two starburst galaxies NGC 3125 and NGC 3077, the quantity of dust detected in polarized light, depends on the distribution of scattering material and the brightness of the illuminating source. If the majority of dust grains lie within 60° of the plane of the sky, and are not concentrated within a fairly thin layer in the middle, then the optically-thin approximation used in this chapter is probably valid (the situation for NGC 3077 may, however, be somewhat 'marginal'). Under these conditions, the dust mass can be estimated satisfactorily but the range of values spans a factor of 2 in either direction. The integrated brightness of the young stars illuminating the dust is also only known to within a factor of 2 (at best). Therefore, for any given parametrization of the grains, the best estimate of dust mass is perhaps only good to within a factor of 4. Using the MRN parametrization, which has enjoyed some observational corroboration since its formulation, I estimate (for the optically-thin case) dust masses of $4.5 \times 10^5 M_\odot$ and $1.0 \times 10^5 M_\odot$ for NGC 3125 and NGC 3077 respectively. If the reflection nebulae are optically-thick, the mass of scattering material could be considerably more than these values.

9.6 Dust Detected by IRAS

It is of interest to compare the quantity of dust observed in polarized light with that detected in far-infrared emission. To do this I fitted the IRAS fluxes catalogued in Lonsdale *et al.* (1985) with a model of the form:

$$F_\nu \propto B(\nu,T)\, Q(\nu) \tag{9.11}$$

where F_ν is the flux in Janskys ($\equiv 10^{-26}\mathrm{Wm}^{-2}\mathrm{Hz}^{-1}$) at frequency ν. $B(\nu,T)$ is the intensity emitted at ν by a blackbody of temperature T. $Q(\nu)$ is the frequency dependent emissivity and is usually given the form $Q \propto \nu^\beta$ where $\beta = 0 \rightarrow 2$ (Hildebrand 1983; Draine and Lee 1984; Sanders *et al.* 1991). Only the 60μm and 100μm IRAS fluxes were used for the fit. The 12μm and 25μm fluxes may not be suitable because a significant part of the emission detected in these filters may arise from 'thermally spiked' small grains (Boulanger and Pérault 1988; Draine and Anderson 1985). The 60μm and 100μm fluxes were not 'colour corrected' - the corrections for cool dust (40-80K) are only of the order of 5% (Lonsdale *et al.* 1985). For a given value of β, I have two free parameters (temperature T and a normalization constant). These can be determined from the 60μm and 100μm fluxes.

Once a fit has been made to the IRAS fluxes, the FIR luminosity and mass of the FIR-emitting dust can be calculated. The former quantity is found by integrating under the blackbody curve calculated for (9.11). The relation given by Hildebrand (1983) provides an estimate of dust mass:

$$M_d = \frac{F_\nu}{B(\nu,T)\, Q(\nu)}\, D^2\, \frac{4a\rho}{3} \tag{9.12}$$

where: M_d is the dust mass; D is the distance to the galaxy; a is the classical grain size (§9.3) and ρ is the material density of the particles (Hildebrand 1983). Hildebrand gives the observed emissivity at 250μm; thus, for given β, Q_ν is known. F_ν and $B(\nu,T)$ have already been evaluated from 9.11. Therefore equation 9.12 can be solved for M_d.

Results for the galaxies NGC 3125, NGC 3077, NGC 660 (§3), NGC 1705 (§8) and M82 are shown in table 9.2. For $\beta = 1$, I give the blackbody temperature, FIR luminosity and dust mass of the FIR-emitting grains. The FIR luminosities in table 9.2 agree well with those given in the IRAS catalogue (Lonsdale *et al* 1985). For NGC 3125 and NGC 3077 I also give the amount of dust detected in polarized light for the optically-thin case (M_s). This mass is subject to the uncertainties given in §9.5.6. Scattering models were **not** constructed for the polarization detected in NGC 660 because the sources illuminating the dust are highly obscured along the line-of-sight. Very little scattering material was detected in NGC 1705 but IRAS data have been given in this case because the galaxy resembles NGC 3125 to a large extent (§8.3). Data for M82 are given in order to provide some sort of comparison.

For $\beta = 0$ and $\beta = 2$ the temperature of the grains generally deviates by about 10 K from the values given in table 9.2. The FIR luminosity, however, remains fairly constant. The reason for this lies in the fact that Q_ν is already determined at 250μm so that higher values of β lead to increased particle emissivity near the blackbody peak ($\sim 100\mu$m). Thus, whilst the temperature of the grains decreases for higher β, their emissivity undergoes a relative increase. For the same reasons, the mass of FIR-emitting dust changes by no more than 15% from the values cited in table 9.2.

One notes that, for the relevant galaxies, the quantity of dust discovered in polarized light exceeds the amount of IRAS-detected dust by at least an order of magnitude (if the reflection nebulae are optically thick this difference will be even greater). Now, the long wavelength IRAS filters are sensitive to dust with a peak emission in the $60 - 100\mu$m wavelength region. Therefore, the instrument has a tendency to 'overlook' dust much cooler than about $30 - 40$ K. In reality, most galaxies will contain several dust components some of which may be a lot cooler than $30 - 40$ K (Kwan and Xie 1992). Indeed, for galaxies observed at sub-mm and mm wavelengths there is some evidence that cooler components *do* exist (Chini *et al.* 1986). Unfortunately, the discrepancies between published measurements (Eales *et al.* 1989) are sufficiently large to make the existence of cold dust in galaxies something of a controversial matter. The main problem lies in the fact that cold dust radiates weakly at *any* wavelength and therefore uncertainties in the spectral distribution can lead to serious under- or over-estimations in the measured dust mass.

Whilst future instrumentation (e.g. SCUBA on the JCMT and ISO) may improve the estimation of cold dust in galaxies, I have shown that polarization measurements, at least in some cases, can offer a novel and opportunist method of calculating dust masses. The emission detected by IRAS arises mostly from dust-enshrouded star forming regions (although dust in the diffuse ISM also contributes - Calzetti *et al.* 1995). In contrast, the dust components investigated in this chapter lie well beyond the regions of active star formation. As such they are likely to be cold. Dust in the diffuse ISM of our own Galaxy is expected to have a temperature of only 10-20K (Mathis *et al.* 1983; Draine and Lee 1984). Whilst the general radiation field dominating starburst galaxies may be somewhat more intense than that characterizing our own galaxy, it would surprising if the scatterers in NGC 3125 and NGC 3077 are heated sufficiently well to ensure their detection by IRAS.

9.7 Summary

Scattering models were constructed for the starburst galaxies NGC 3125 and NGC 3077. With some justification, polarized light detected in these galaxies is assumed to arise from scattering by ISM-type Milky Way grains. If the majority of scatterers lie within 60° of the plane of the sky, and are not concentrated within a fairly thin layer in the middle, then an optically thin approximation can be used (although, even then, optical-thinness in NGC 3077 may be somewhat 'marginal'). Under these conditions, $4.5 \times 10^5 M_\odot$ and

Table 9.1: Scattering models for NGC 3125 using MRN grains

			$\alpha = 2°$	30°	60°	90°	120°
$\phi = -60°$	SE	Mass / $10^6 M_\odot$	16	16	100	–	–
		Density (10^{-3}m^{-3})	74	4.2	1.6	–	–
	NW	Mass / $10^6 M_\odot$	0.47	0.61	7.1	–	–
		Density (10^{-3}m^{-3})	6.0	0.40	0.22	–	–
		M_s / $10^6 M_\odot$	17	16	110	–	–
$\phi = -30°$	SE	Mass / $10^6 M_\odot$	0.59	0.62	0.70	1.0	11
		Density (10^{-3}m^{-3})	14	0.90	0.44	0.29	0.22
	NW	Mass / $10^6 M_\odot$	0.073	0.079	0.11	0.19	2.5
		Density (10^{-3}m^{-3})	2.7	0.18	0.10	0.080	0.073
		M_s / $10^6 M_\odot$	0.67	0.69	0.81	1.2	13
$\phi = 0°$	SE	Mass / $10^6 M_\odot$	0.21	0.21	0.24	0.29	0.42
		Density (10^{-3}m^{-3})	7.1	0.48	0.25	0.18	0.15
	NW	Mass / $10^6 M_\odot$	0.073	0.075	0.083	0.10	0.15
		Density (10^{-3}m^{-3})	3.3	0.22	0.11	0.080	0.068
		M_s / $10^6 M_\odot$	0.28	0.29	0.32	0.39	0.56
$\phi = +30°$	SE	Mass / $10^6 M_\odot$	0.21	0.23	0.30	0.54	7.2
		Density (10^{-3}m^{-3})	5.9	0.40	0.22	0.18	0.16
	NW	Mass / $10^6 M_\odot$	0.21	0.22	0.25	0.36	3.8
		Density (10^{-3}m^{-3})	6.2	0.41	0.20	0.13	1.0
		M_s / $10^6 M_\odot$	0.42	0.44	0.55	0.90	11
$\phi = +60°$	SE	Mass / $10^6 M_\odot$	1.3	1.7	20	–	–
		Density (10^{-3}m^{-3})	13	0.86	0.49	–	–
	NW	Mass / $10^6 M_\odot$	5.8	5.5	36	–	–
		Density (10^{-3}m^{-3})	34	1.9	0.74	–	–
		M_s / $10^6 M_\odot$	7.1	7.2	56	–	–

Table 9.2: The IRAS properties of starburst galaxies

	T (K)	FIR luminosity ($L_\odot$)	M_d ($M_\odot$)	M_s ($M_\odot$)
NGC 3125	43	9.8×10^8	3.5×10^4	4.5×10^5
NGC 1705	37	0.4×10^8	0.3×10^4	–
NGC 3077	38	2.4×10^8	1.7×10^4	1.0×10^5
NGC 660	39	1.9×10^{10}	1.2×10^6	–
M82	49	1.7×10^{10}	3.3×10^5	–

$1.0 \times 10^5 M_\odot$ of dust is required to reproduce the polarized intensities in NGC 3125 and NGC 3077 respectively. These masses are based on the grain parameterization of Mathis *et al.* (1977) which has enjoyed some observational corroboration. For other plausible grain parameterizations, estimates in the dust mass can vary significantly (e.g. a factor of 2). Apart from the grain parameterizations, the uncertainty in the estimated dust masses (for the optically-thin case) is believed to be about a factor of 4.

The quantity of dust detected in scattered light is at least an order of magnitude greater than that derived from IRAS fluxes. This is consistent with the hypothesis that some starburst galaxies may harbour sizeable quantities of cold dust.

Chapter 10

Discussion and Summary

The purpose of this closing chapter is to connect in some way the findings of this thesis with the unusual phenomena that characterize starburst galaxies. Probably the most stunning result from the present polarimetric study is the detection, in several starburst galaxies, of large amounts of dust residing outside the main star forming environment. In the following sections, I discuss the distribution of dust in quiescent (non-starburst/non-seyfert) spirals and then summarize the unusual situation for starburst galaxies. I then consider the origin of the dust detected in this work. This is done within the context of our current understanding of starburst galaxies and the superwind phenomenon (§1). Finally I suggest means by which my conclusions can be tested.

10.1 The Distribution of Dust in Quiescent Galaxies

At a 'local level', dust within our own Galaxy manifests a prominent association with dense molecular gas clouds and regions of star birth (e.g. Genzel and Stutzki 1989; Cernicharo *et al.* 1985). On a larger scale, Galactic dust appears to be contained within a layer which is approximately 200pc thick. Knowledge of this large-scale dust distribution is derived from: (a) observations of stellar reddening within the solar neighbourhood (Perry and Johnston 1982) and (b) the spatial correlation between cool dust (known as IRAS cirrus) and gas clouds located only 100pc from the Galactic plane (Weiland *et al.* 1986; Low *et al.* 1984; Burstein and Heiles 1982).

Within quiescent spiral galaxies, the situation seems to be similar to that just described for our own Galaxy. Most of the dust detectable by current instrumentation appears to be concentrated in the star forming disk. Optical studies of edge-on spirals confirm that the densest material is concentrated in dark dust lanes contained in the stellar disk. IRAS has been used to trace the distribution of FIR-emitting material in edge-on spiral galaxies (Wainscoat *et al.* 1987). Unfortunately even for nearby systems, the FWHM of the IRAS beam is only $\simeq$ 4 kpc which does not provide much of a constraint on the distribution of material perpendicular to the disk. I should also re-emphasize what has been said in

§9.6. IRAS is not sensitive to cold ($\sim$ 10-20 K) dust and therefore observations at longer wavelengths may be necessary if the true extent of dust in quiescent galaxies is to be known with any certainty. With regard to elliptical galaxies, the general consensus is (or was until quite recently) that these disk-less systems are dust poor. Some recent studies, however, which are discussed below in connection with galactic collisions, indicate that a significant fraction of ellipticals show evidence for absorption features and tenuous dust lanes.

From a theoretical point of view, we might expect diffuse dust in the ISM of quiescent spirals to eventually be driven out of the disk by radiation pressure (Ferrara *et al.* 1991). Evidence for dust in the bulge and halo environments of nearby galaxies is, however, sparse. A notable exception to this statement is found in the preliminary results of Zaritsky (1994). He analysed the B-I colour of numerous background galaxies visible through the halo of two nearby spirals. A systematic colour difference (0.067 ± 0.033 mag) was detected between galaxies visible at galactic radii of 60 kpc and those observed at galactic radii of 220 kpc. If this effect is genuinely attributable to reddening within the halo environment, significant quantities of dust may be present outside the disk of some galaxies.

Quiescent edge-on spirals imaged in polarized light (Ward-Thompson 1987; unpublished data within the Durham Polarimetry Group) indicate that their dust content is restricted to spiral dust lanes in the disk. The dust grains align themselves with the galactic magnetic field leading to dichroic extinction of disk light (§2.3.3). In general, there is little evidence in *these* systems to support the idea that large amounts of dust reside outside the disk and scatter light towards the observer. Within this context, the findings of the present study – extensive reflection nebulae displaced up to several kiloparsecs from the current star-forming environment – are quite remarkable. Bearing this in mind, let us now examine what is currently known about the distribution of dust in starburst galaxies.

10.2 Dust in Starburst Galaxies

The main indications, up until the present study, that starburst galaxies have unusual dust properties stems from observations of M82 and NGC 1808. I have already summarized, in §2.2.1 and §2.2.2 respectively, the relevant details for these two nearby FIRGs. Let us reiterate the main points so as to enable an easier comparison with the current study.

The spectacular dust filaments seen in colour maps of NGC 1808 (Phillips 1993) appear to emanate from the hot-spot (starburst) region at the centre of the galaxy. The reddening material appears to lie either *within* or *along* the edges of a 'cone' occupying the minor axis. Phillips calculates an opening angle of $\simeq 33°$ for the dust cone. Examined spectroscopically, the same region possesses a double-peaked emission-line profile attributable to outflow along the edges of a bi-cone (§1.4). Although the superwind is bipolar, dust escaping on the far side of the disk is not visible to the observer. On the near side, the filaments

extend for about 3 kpc along the minor axis and one of them appears to turn over and fall back towards the disk. Using a Galactic reddening law and a Galactic dust-to-gas ratio, Phillips estimates a gas mass of $6 \times 10^7 M_\odot$ associated with the dust-filament structure. This is based on his B-R colour image of the galaxy and assumes an equal amount of dust is present on the far-side of NGC 1808.

A quantity perhaps more relevant to the current study is the *dust mass* contained in the filaments of NGC 1808. Using the gas mass estimated by Phillips and a Galactic dust-to-gas ratio of 0.007 (Whittet 1992), this amounts to $\simeq 4 \times 10^5 M_\odot$. Intriguingly, similar masses have been estimated for the scattering material detected in two of the galaxies studied in this thesis (NGC 3125 and NGC 3077; §9.5.6). The connection is further substantiated by the conclusions drawn from polarimetric observations of NGC 1808 (Scarrott *et al.* 1993). Dust lying closest to the nucleus (i.e. within the inner kiloparsec of the 'dust cone' described above) scatters some of the intense starburst radiation towards the observer where it is detected in polarized light. A similar phenomenon is observed in some of the case studies in this work, namely NGC 660, NGC 3125 and NGC 3077. In contrast to NGC 1808, the reflection nebulae detected in the latter do not appear to be strongly associated with absorption regions or prominent dust filaments. Part of the reason for this (at least for NGC 3125 and NGC 3077) is that the scattering material might be interspersed amongst stars residing in the main body of the galaxy. Its presence might therefore be 'cloaked' by intrinsic emission and light scattered into the line-of-sight (§9.5.2).

NGC 1808 is not the only starburst galaxy known to have prominent dust filaments. Apart from M82, which I turn my attention to shortly, the morphologically-disturbed FIRG **NGC 2146** possesses both Hα filaments and dust streaks along its minor axis. The galaxy has also been the subject of a recent ROSAT study by Armus *et al.* (1995). The observational evidence indicates that NGC 2146 is also undergoing outflow along its minor axis.

The overall dust distribution **in M82** is best appreciated by inspecting the optical and near-IR colour maps of Ichikawa *et al.* (1994,1995). The inner disk, which also contains the starburst, is heavily reddened and appears to be part of an extremely warped dust lane that runs very approximately parallel to the major axis. This feature cannot be compared directly with the dust lanes in quiescent spirals because, at larger radii the deviation from the major axis is significant ($\pm$ 1 kpc). In addition to obscuration along the major axis, dust lanes are also apparent along the minor axis of the galaxy. These run parallel with the Hα filaments that trace the galactic superwind in M82 (§1.3). The startling new colour maps by Ichikawa *et al.*, show, however, that at $z \simeq 1.5$ kpc the dust departs from the minor axis and begins to run parallel with the major axis. The overall effect is very reminiscent of a galactic fountain (Corbelli and Salpeter 1988). Dust lying further out along the outflow axis is less optically thick than material closer to the starburst ($A_V \simeq 0.2$ mag against $A_V \sim 6$ mag). This suggests an overall 'thinning' in the amount of dust at larger galactic radii.

Polarization studies of M82 seem to highlight what I shall term the 'dual nature' of dust in starburst galaxies. Polarimetric imaging in the optical continuum suggests that scatterers exist over extensive regions above and below the galactic plane and that these grains reflect light from the stellar disk (§2.2.1). In contrast, polarimetric images taken in Hα indicate that radiation from the starburst is scattered primarily by dust grains close to the minor/superwind axis. Taken together, I am inclined to think that these observations are the result of **two** processes. One is the superwind and the other is the tidal event that probably initiated the starburst activity. To some extent these two scenarios have been explored in connection with the individual galaxies investigated in this thesis. Now, I wish to generalize these conclusions.

10.2.1 Dispersion via the Superwind

The dust filaments in NGC 1808 and M82 point strongly towards *galactic outflows* as the mechanism responsible for dust dispersion in starburst galaxies. Within my own data I note that: (a) the putative superwind region in NGC 660 is seen in polarized light and; (b) at least part of the scattering material in NGC 3077 appears to be physically connected to the starburst (§5.2.2). For both NGC 660 and NGC 3077 high resolution long-slit spectra are required in order to establish the prevalence and distribution of starburst-driven winds in these systems. It is only then that we can be sure that outflows form the starburst are responsible for the current dust distribution. The rôle of galactic winds in NGC 3125, which has also been discussed at length in §7.4, is somewhat ambiguous. Dust detected within this system appears to be excluded from the outflow region and one interpretation of this is that the superwind is currently removing dust from certain parts of the galaxy rather than transporting it outwards.

In an attempt to connect the dust detected in M82 with the presence of an outflow along the minor axis, I took the Hα polarization map of M82 (Scarrott *et al.* 1991a) and overlaid it onto the contoured $B - I_c$ colour map of Ichikawa *et al.* (1995). The result is shown in figure 10.1. Within this figure: (a) white contours trace the $B - I_c$ colour; (b) dark isophotes denote the highest and lowest levels of Hα emission; (c) vectors represent the polarization measured in the Hα line; and (d) the greyscale image represents a J-H image produced by Ichikawa *et al.* (darker shades represent redder colours). For both the Hα and $B - I_c$ contours, the highest values are recorded at the centre of the galaxy i. e. within the starburst. (The left hand side of the Hα overlay shows a more complete set of emission-line contours. This part of the figure has been retained in order to clarify some of the discussion which follows.) The registration between the Hα polarization map and the $B - I_c$ contours was carried out in a simple way by expanding the two images to the same scale and rotating one image with respect to the other. The former was then overlaid onto the latter so that the double-peaked Hα emission of the starburst was enclosed by the bi-lobal extinction at the centre of the galaxy. This is consistent with the findings of Waller *et al.* (1992) who found that the peak optical extinction in M82 surrounds the

maximum CO and Hα emission in what they term a 'circumnuclear pileup'. The method of alignment is somewhat crude but even if the registration is only good to 10″ this will suffice for the discussion that follows.

The $B - I_c$ contours in figure 10.1 trace an arched warp in the disk and two vertical dust filaments extending northwards into the halo. The lowest $B - I_c$ contours flank the Hα emission for about 0.75 kpc before turning back towards the disk. In contrast, the Hα morphology does **not** deviate in the same way from the minor axis. I reiterate once more the probable sources of Hα so that a better understanding of figure 10.1 might be gained. The generally accepted view is that the diffuse Hα nebulae detected along the minor axis of some starburst galaxies originates at the interface of plasma ejected by the starburst ('the superwind') and the ambient gas of the ISM. The temperatures and densities of the emission-line gas are consistent with this scenario (§1.4). For M82 the situation may be somewhat more complicated. Scarrott *et al.* (1991a) argue, on the basis of their polarization map, that some of the Hα detected along the minor axis is radiation from the starburst which has been scattered towards the observer. Indeed, in view of the large polarizations they measure (figure 10.1) scattered light must make a sizeable contribution. It seems likely, nevertheless, that the some of the diffuse emission-line radiation still arises from shocking of ambient gas as the superwind expands along the minor axis.

I shall argue, on the basis of figure 10.1, that dust and gas is being dragged up from the disk of M82 rather than being transported in the superwind fluid itself. The first indication that this might be true is demonstrated by the B-I contours to the north of the disk. At their lowest level they appear to turn back towards the disk rather than escape into the halo. The hot, low density plasma of the superwind, on the other hand, is travelling several 1000 kms^{-1} (Heckman *et al.* 1990) and can probably be expected to breach the halo and escape into the extragalactic environment. It seems much more likely that the dusty material traced by the B-I contours lies at the working surface of the superwind and is entrained by the viscous forces of the plasma flow. Within this context, the vertical filaments of the B-I contour map represent the limb brightening effect of a hollow cone of dust encompassing the superwind fluid. The diffuse Hα light which, in part, is due to intrinsic emission from shocked ambient gas, acts as a tracer of the superwind fluid. As already mentioned, the emission-line morphology does **not** deviate from the minor axis in the same way as the reddening material. This seems to confirm that the superwind plasma travels much further into the halo than the dusty material which it has dredged up from the disk.

The polarization vectors in figure 10.1 can be interpreted quite comfortably within the model proposed above. One notes a systematic increase in linear polarization towards the edges of the Hα morphology (the limb of the purported dust cone). Dust surrounding a hollow cavity can be expected to show maximum polarization levels at the limb because the scattering angle approaches 90° (recall the scattering behaviour of classical dust grains which is illustrated in figure 9.2). Indeed, in the past, several authors have exploited this

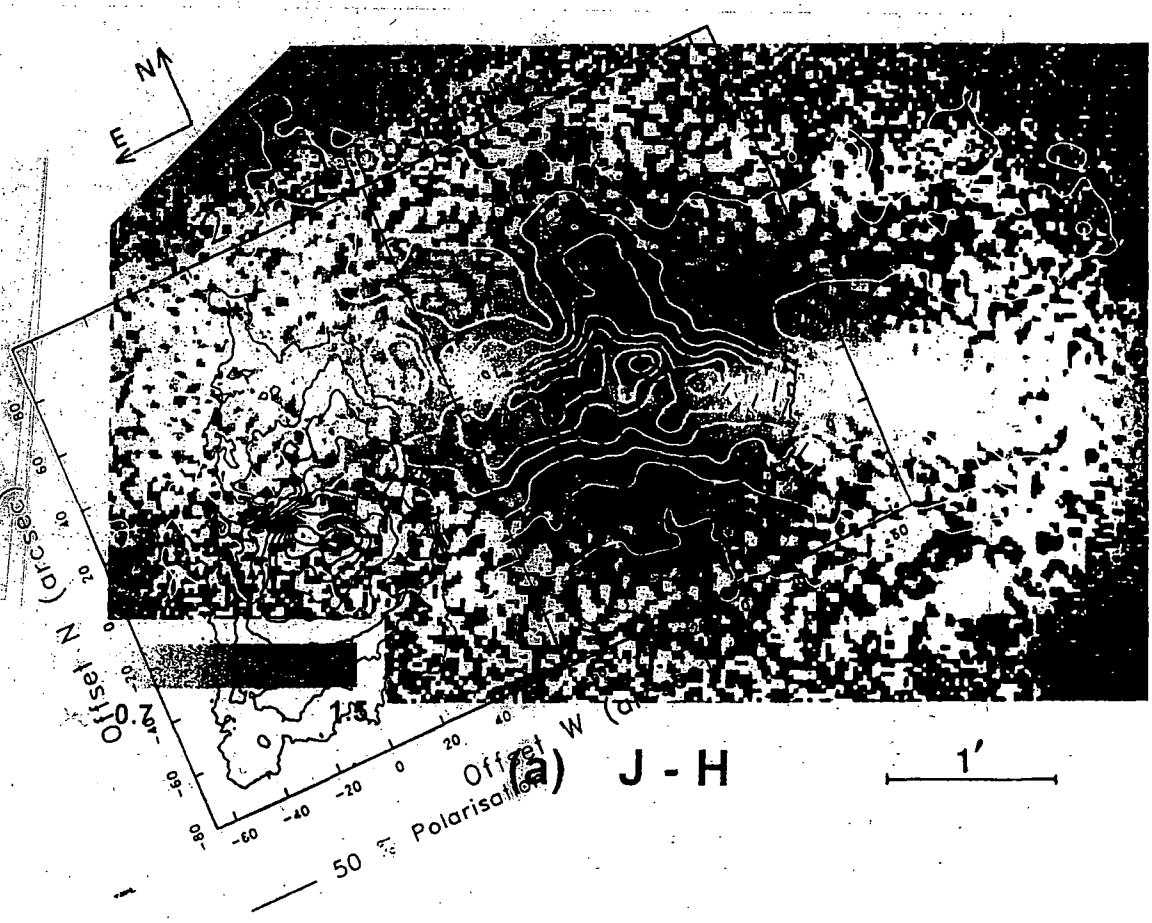
N
E
(a) J - H
1'
50 mas Polarisation
Offset W (arcsec)
Offset N (arcsec)
1.5
2.0
2.50

kind of information in order to infer the distribution of scattering material in some astronomical objects (e.g. Rolph 1990). I emphasize that other interpretations of the vectors in figure 10.1 are also possible. Intrinsic Hα emission, emitted *in situ* rather than scattered, is unpolarized and can therefore be expected to dilute any polarized component. Thus an alternative interpretation of figure 10.1 is that intrinsic emission increases closer to the minor/superwind axis.

Phillips (1993) attempted to address the issue of whether the emission-line gas detected in NGC 1808 can be expected to escape the galaxy's gravitational field. Interestingly, he found that the velocity of the emission-line gas (several 100 kms^{-1}) is comparable to the escape velocity. If this also describes the situation for M82 then the model derived from figure 10.1 becomes ever more plausible. In the scenario outlined above, the emission-line gas forms a 'buffer' or working surface between the superwind plasma and the dusty material that is entrained in the flow. If this is really the case, the velocity of the emission-line gas probably constitutes the maximum velocity with which neutral material is leaving the disk. If, as I suggest, the entrained material in M82 is falling back towards the disk (rather than escaping the galaxy) we can expect the velocity of the emission-line gas to be close to, but no more than, the escape velocity. Incidentally, M82 and NGC 1808 have similar emission-line velocities (Phillips 1993; Mckeith *et al.* 1995). The gravitational field in M82 might, however, be somewhat weaker than that in NGC 1808 suggesting that, of the two galaxies, the former is more susceptible to mass loss.

In an attempt to exclude the possibility that dust is contained **within** the superwind fluid, rather than being entrained by viscous forces, I calculate the depletion timescale for classical (0.1μm) dust grains residing in a hot plasma (recall from §9.4 that grains of this size are responsible for optical extinction. They also embody most of the mass contained in ISM-like dust). I assume, initially, that the grains move cospatially with the hot gas. This assumption may be incorrect because the grains are known to reside within a low density medium and are also subject to intense radiation fields. Under these conditions the transport of dust is expected to be dominated by radiation pressure rather than collisions with the gas (Spitzer 1978; Ferrara *et al.* 1991). Neglecting this for the time being, one notes that, for grains stationary in a hot gas of temperature $10^6 \rightarrow 10^9$ K, the lifetime against sputtering (τ) is given by the following approximation (Draine and Salpeter 1979):

$$\tau \approx 2 \times 10^4 \, yrs \, \frac{cm^{-3}}{n_H} \, \frac{a}{0.01 \mu m} \qquad (10.1)$$

where n_H is the gas density (in cm^{-3}) and a is the grain size (in microns). Using a gas density of 10^{-3}cm^{-3} for the superwind plasma (T.Heckman private communication) I calculate a depletion timescale of $\sim 10^8$ years for 0.1μm grains. The timescale for transit through the disk and near-halo environment, on the other hand, is $\sim 10^6$ years if a velocity of 3000 kms^{-1} and scale-length of 3 kpc are used (Heckman *et al.* 1990). The difference in time-scale seems to suggest that classical grains are unlikely to undergo significant erosion

by the superwind fluid if they are contained within the plasma (rather than entrained by it). If the grains are decoupled from the gas, and move more slowly, they have a greater chance of being eroded. This is because the average speed of the gas increases with respect to the grains and also the transit time is lengthened.

Dust grains are almost certainly subject to more hostile conditions within the starburst itself. Here, the gas density is considerably higher (Heckman *et al.* 1990) and frequent shocks from supernova ejecta can do considerable damage (Seab 1988). Presumably erosion and destruction will be severe if either the time-scale required to leave the starburst is long or if the grains are not concentrated in self-shielding molecular clouds (Carral *et al.* 1994; Wolfire *et al.* 1990). There is mounting evidence that small grains (size $\leq 0.01\mu$m) are depleted in active galaxies (§9.3).

Even if we cannot rule out the possibility that grains are contained within the superwind fluid itself, it is another question entirely whether the dust is actually synthesized by new stars in the starburst. This issue has already been explored, in a semi-quantitative way, for the low mass starburst galaxy NGC 3125 (§7.4). In that case, I concluded that star formation must continue over a considerable amount of time if new stars were to provide the dust detected in scattered light. The situation for larger starburst galaxies like M82, NGC 1808, NGC 660 etc. is less clear-cut. Firstly, the star formation rate in more massive systems is higher (typically 2 orders of magnitude greater than NGC 3125; Marlowe *et al.* 1995, Heckman *et al.* 1990) and secondly, the amount of gas available for star formation is much larger (again by about two orders of magnitude; §6.8). Within our own galaxy the primary sources of dust (currently known to us) are the cool, high density atmospheres of evolved stars (Gehrz 1989). Within starburst galaxies, red supergiants can be expected to appear 3-8 million years after the burst of star formation (Campbell and Terlevich 1984) but the progenitors of red giants will take significantly longer to complete their main-sequence evolution. If it is the latter that make the primary contribution to newly-synthesized dust, the current starburst is unlikely to have manufactured the material presently being transported by the superwind. An altogether more plausible scenario, I feel, is one in which the superwind sweeps up gas and dust that has collected at the centre of the galaxy and disperses it outside the star forming environment.

10.2.2 Dispersion via Galactic Collisions

Several findings in this thesis seem to indicate that, in conjunction with energetic outflows, *tidal encounters* may have a direct influence on the distribution of dust in some starburst galaxies. Observations that may be interpreted in this way are as follows:

1. The FIRG NGC 660, which has clearly undergone a violent galactic collision during its recent history, shows evidence for dust both above and below the disk. Material is detected along the minor axis but also in regions that are unlikely to be affected

by any superwind in the galaxy. For example, there are large amounts of scattering material surrounding the south-west part of the disk and significant amounts of dust are also detected in the polar ring. The presence of gas and dust at significant distances from the minor axis (particular within the polar ring) suggests that mass has been obtained from an external source.

2. I inferred, from scattering simulations carried out in chapter 9 that the column density of dust in both NGC 3077 and NGC 3125 probably increases at larger galactic radii. This is somewhat surprising if the scattering material was originally expelled from a central source such as the starburst (assuming of course the rate of outflow is roughly constant with time). One solution to this problem is to assume that dust clouds, of uniform density, occupy selective regions of the starburst galaxy. What is the likely source of these dust clouds if the central starburst is **not** the origin ? It has already been noted for NGC 3125 (§7.4.2), that mass transfer is unlikely to be the source of scattering material in that galaxy. It is a fairly isolated system and probably could not have undergone a tidal collision within the last two gigayears. For NGC 3077, the accretion of gas from external sources seems much more likely. The 'bridges' of atomic gas, which connect both NGC 3077 and M82 with the nearby spiral galaxy M81, suggest that at least *neutral gas* has been transfered between these neighbouring systems (van der Hulst 1979). It has already been noted, however (§5.2.2), that at least part of the scattering material in NGC 3077 appears to exist within filament-like structures which are physically attached to the central starburst. It seems highly improbable that external material could be ingested in such a way so as to produce these converging dust filaments. Clearly more kinematic information is required in order to resolve the issue of dust infall/outflow in NGC 3077. Long-slit spectroscopy of the central kiloparsec would establish the prevalence and distribution of any starburst winds whilst radio maps in the 21cm emission-line may determine the movement of neutral gas within the system.

By constructing a simple scattering model, Solinger *et al.* (1977) argue, that M82 is drifting through a near-uniform dust cloud pervading the intracluster medium. On the basis of polarization data, the authors propose that scattering material outside the disk is illuminated by both disk stars and, to a lesser extent, the nucleus. Given these sources of illumination, they predict in a simple fashion the surface brightness of the halo and compare it with photometric data. A reasonable fit to the observed values is obtained if the dust density is uniform for $z > 1.8$ kpc but increases exponentially at closer proximity to the starburst. Unfortunately the model of Solinger *et al.* assumes *a priori* that the surface brightness above the galactic disk results exclusively from scattered light and that none of the emission is intrinsic. We cannot be sure that stars do not exist well outside the disk of M82 particularly in view of its disturbed appearance. If the distribution of scattering material is to be known with greater certainty I advocate the approach adopted in §9. This uses the polarized intensity observed in the scattering region (rather than the total intensity). One indication that stars may be present outside the disk of M82 is the

observed decrease in the polarization at longer optical wavelengths (§2.2.1). This is quite conceivably the result of older halo stars diluting the scattered radiation with unpolarized red light.

Whilst the model of Solinger *et al.* may not be all that convincing, the concept of static dust clouds in the halo of M82 resolves another problem which confounds our understanding of this complex galaxy. As noted in §2.2.1, spectra obtained by Bland and Tully (1988), and more recently by McKeith *et al.* (1995), indicate that scatterers along the minor axis are either stationary or have a significant velocity towards the observer. Clearly there is a dilemma here for I have argued in §10.2.1 that dust is entrained in the galactic flow and is therefore moving radially outwards ! The situation must be clarified with spectropolarimetry which will hopefully: (a) establish what proportion of the Hα along the minor axis arises from scattering (as opposed to intrinsic emission) and; (b) ascertain the velocity of the dust.

Finally, I note that the idea of galaxies accreting dust from external sources is not new. Elliptical galaxies are generally thought to have a tenuous, relatively dust-free ISM with little signs of recent star formation. On closer inspection, however, some ellipticals *do* indeed show optical evidence for dust lanes and absorption features (Sparks 1992). Hawarden *et al.* (1981) carried out an indepth optical survey of disk-less galaxies and found that a large number of their sample harboured dust lanes. They concluded, from the varied orientation of the dust lanes, that material is accrued externally through the cannibalization of gas-rich companions. Goudfrooij *et al.* (1992) reached the same conclusion after producing CCD colour images of nearby giant elliptical galaxies. The amount of dust detected in some ellipticals must be provided by an external source because the depletion of dust grains proceeds at a faster rate than replenishment by stellar mass loss.

10.2.3 Conclusions and Proposed Observations

The preceding sections have shown us that starburst galaxies are not easy systems to understand and that their dust properties may be governed by several unusual phenomena. Evidence that starburst galaxies expel dust and gas from their normal star forming environment seems fairly convincing. There are, however, several difficulties with this scenario. For example, two of the galaxies observed in this thesis, manifest polarization phenomena which are best explained by an increasing amount of scattering material at greater distances from the starburst. If the starburst is the original source of the scattering material we might expect an overall 'thinning' of dust at larger radii. The other anomaly arises from spectroscopic studies of M82. Optical spectra taken along the minor axis seem to indicate that the scattering material in this region might be stationary.

The other likely source of dust in starburst galaxies is tidal encounters. It is possible that gas transfer might have taken place within the M81 group (of which M82 and NGC 3077 are both members). In addition, the FIRG NGC 660, which was also observed in

this thesis, appears to have received dust and gas in a tidal event. I conclude that dust in starburst galaxies may reach its present environment either through galactic-scale outflows or through close tidal encounters (and probably through both). Both mechanisms possess the dynamic energy to disperse material over large volumes of the host galaxy. A consensus has been forming over the last few years that tidal interactions often initiate starburst activity in the local Universe (Lonsdale 1993). Therefore, it seems likely that galactic collisions and superwinds occur in the same system either simultaneously or in close succession.

I propose a series of observations that examine the dust and gas properties of starburst galaxies in various phases of isolation and pairing. This will tend to confirm or eliminate some of the suggestions made above. Kinematic studies are essential to understanding the flow of gas (and therefore dust) around the starburst system. These should include the acquisition of long-slit spectra, the use of spectro-polarimetry and the velocity measurement of both atomic and molecular gas. The colour maps of Ichikawa *et al.* (1995;1994) seem to offer a promising way forward in tracing the spatial distribution of dust in starburst galaxies. This approach, however, is naturally biassed towards more optically thick material. Optical polarimetry may be more sensitive to a more tenuous distribution of scattering material. This dust component may be too cold for detection by FIR/sub-mm instrumentation.

10.3 Summary

1. I have carried out optical polarimetric imaging of several starburst galaxies. The objects of study have been of various morphological type: NGC 660, NGC 1667, NGC 1614 are FIR-bright galaxies (FIRGs); NGC 3125 and NGC 1705 are blue compact dwarf galaxies (BCDGs); and NGC 3077 is a low mass irregular in the M81-M82 group.

2. 3 out of 6 galaxies show evidence for giant (kpc-scale) reflection nebulae (NGC 3125, NGC 660, NGC 3077). In general, the scattering material is displaced up to several kpc from the current star-forming environment and in one case (NGC 660), dust is distributed like M82; namely above and below the galactic disk. The dust grains tend to be illuminated by intense radiation from the starburst.

3. It is now well established that galactic-scale outflows (superwinds) are prevalent in starburst galaxies (Heckman *et al.* 1990) and it is tempting to attribute the anomalous dust distributions detected in this thesis with these powerful processes. In two better-studied superwind galaxies, NGC 1808 and M82, there appears to be strong indications, from polarimetry and extinction measurements, that dust is expelled along the outflow axis. Spectro-polarimetry is required, however, to clarify whether (or how) the dust is moving relative to the systemic velocity.

4. Some of the galaxies in the present study are known to be experiencing galactic-scale

outflows and, in some cases, a connection can be drawn between the outflow region and the scattering material. For the disk galaxy NGC 660, for example, scattering is prominent along the outflow (minor) axis. NGC 3125 is an example of a low mass galaxy experiencing large-scale winds. In this case, however, the outflow appears to have *cleared* scattering material from the minor axis. There are several possibilities that might explain these contrasting observations: (a) weaker gravitational fields in NGC 3125 may allow dust and gas to escape more easily from this galaxy; (b) winds may disperse dust at one particular stage of their development and remove material during some other (perhaps SN-dominated) phase. The dwarf disk-less galaxy NGC 3077 shows evidence for scattering within the inner kiloparsec. A long-slit spectroscopic study is required to establish the presence of energetic winds in this system. At least part of the scattering material appears to be physically connected to the starburst suggesting that it has been expelled in the recent past.

5. Galactic collisions, which in many cases probably initiate starburst activity, are also potential sources of dust and gas. There are signs that NGC 660 has accrued material in this manner. 'Bridges' of neutral gas are also known to exist between NGC 3077 and M81 and similarly between M82 and M81.

6. I carried out simulations of dust scattering using Mie theory. For many plausible dust distributions along the line-of-sight, an optically-thin approximation can be used and, in this case, dust masses of $4.5 \times 10^5 M_\odot$ and $1.0 \times 10^5 M_\odot$ are required to account for the polarized light detected in NGC 3125 and NGC 3077 respectively. These estimates assume ISM-like MRN grains (Mathis *et al.* 1977) and are also subject to an uncertainty of about a factor of 4.

7. For both NGC 3125 and NGC 3077, dust masses based on scattering calculations exceed those derived from IRAS fluxes by an order of magnitude. This seems to indicate that, at least in some cases, IRAS fluxes do not give a good indication of the dust content of a galaxy.

8. The quantity of dust detected in NGC 3125 is somewhat surprising. This galaxy belongs to a metal-poor, gas-rich class of objects called blue compact dwarf galaxies (BCDGs). Many galaxies under the same classification are perhaps making stars for the first time in their history (although for NGC 3125 this is probably *not* the case). In contrast to NGC 3125, a second BCDG observed with the polarimeter (NGC 1705) showed little evidence for galactic-scale scattering. Without more data it is difficult to understand why two galaxies, with otherwise such similar global properties, exhibit different dust properties.

9. The 2 remaining galaxies not covered by (4)-(8) above, are the face-on FIRGs NGC 1667 and NGC 1614. The polarization pattern in these two galaxies is characterized by a spiral structure which is the signature of dust grains aligned in a spiral magnetic field. Neither showed evidence for large-scale scattering but this may be attributable

to orientation effects more than anything else. In future, programmes to observe starbursting disk galaxies (which includes most FIRGs) should preferably restrict themselves to highly-inclined systems. This ensures that the superwind axis is visible and allows any dust outside the disk to be detected in scattered light.

Appendix A

Removal of Extraneous Light from NGC 3077

We recall from §2.3.1 that the percentage polarization, P, is given by:

$$P = \frac{100}{I} \times \sqrt{(Q^2) + (U^2)} \tag{A.1}$$

where I is the total intensity and Q and U are the Stokes parameters. Consider Q which is normally given by $I_0 - I_{90}$ (equation 2.2). If s_0 and s_{90} are the corresponding components of extraneous light which are also present in the image frames, then the desired value of Q becomes:

$$Q = (I_0 - I_{90}) - (s_0 - s_{90}) \tag{A.2}$$

Since the object fills most of the CCD, subtracting s_0 and s_{90} also removes a small amount of object signal. Thus, in reality, the value derived for Q becomes:

$$Q' = (I_0 - I_{90}) - (s_0 - s_{90}) - (dI_0 - dI_{90}) \tag{A.3}$$

where dI_0 and dI_{90} are the components of the subtracted object signal.

If the subtracted object signal is unpolarized then $dI_0 = dI_{90}$ and $Q' \longrightarrow Q$.

The same reasoning which was used for Q can also be applied to the Stokes parameter U. Since the polarized intensity depends only on the values of Q and U (equations 2.4 and 2.2), we obtain the value of polarized intensity that we require. For the same reason, the direction of polarization, $\arctan 0.5(U/Q)$, is also unaffected by the removal of unpolarized object signal. The total light intensity, on the other hand, has been reduced from its true value by an amount $(dI_0 + dI_{90})$. The result of this is that the percentage polarization (equation A.1) is increased by a factor:

$$\frac{I_0 + I_{90}}{(I_0 + I_{90}) - (dI_0 + dI_{90})} \tag{A.4}$$

from its true value. If $(dI_0 + dI_{90})$ is small compared to I, which is true for most of the galaxy, the systematic increase in polarization is only slight.

Acknowledgements

This work has been possible through the award of a research studentship by the Science and Engineering Research Council. Dr. S. M. Scarrott is thanked for overseeing the research carried out in this thesis and arranging observing trips etc. . I also acknowledge Professor A. D. Martin and Professor D. Bloor for all the facilities provided by the Physics Department at Durham.

My sincere thanks go to my fellow polarimetrists in Room 117 for their help, friendship and occasional laughter – Steve Bowlzer, Steve Fullerton and David Stockdale. I am also grateful to Alan ("sigh") Lotts for his maintenance of STARLINK facilities under extreme pressure.

Large parts of this work have benefitted from invaluable discussions with the following people: Lee Armus, Peter Conti, Peter Draper, David Flower, Tim Heckman, John Mathis, Bob Thomson, Martin Ward and Ray Wolstencroft.

References

Aalto, S., Booth, R.S., Black, J.H. & Johansson, L.E.B., 1995 *A.&A.* **300**, 369

Achtermann, J.M. & Lacy, J.H., 1995 *Ap.J.* **439**, 163

Aitken, D.K., Roche, P.F., Allen, M.C. & Phillips, M.M., 1982 *M.N.R.A.S.* **199**, 31P

Alton, P.B., Draper, P.W., Gledhill, T.M., Stockdale, D.P., Scarrott, S.M. & Wolstencroft, R.D., 1994 *M.N.R.A.S.* **270**, 238

Appleton, P.N., Davies, R.D. & Stephenson, R.J., 1981 *M.N.R.A.S.* **195**, 327

Armus, L., Heckman, T.M. & Miley, G.K., 1989 *Ap.J.* **347**, 727

Armus, L., Heckman, T.M. & Miley, G.K., 1990 *Ap.J.* **364**, 471

Armus, L., Heckman, T.M., Weaver, K.A. & Lehnert, M.D., 1995 *Ap.J.* **445**, 666

Arnaboldi, M. & Galletta, G., 1993 *A.&A.* **268**, 411

Arnault, P., Casoli, F., Combes, F. & Kunth, D., 1988 *A.&A.* **205**, 41

Arp, H.A., 1966 *Atlas of Peculiar Galaxies*, Caltech, Pasadena

Arp, H.C. & Madore, B.F., 1989 *Catalog of Southern Peculiar Galaxies & Associations* (Cambridge University Press)

Axon, D.J. & Ellis, R.S., 1976 *M.N.R.A.S.* **177**, 499

Axon, D.J. & Taylor, K., 1978 *Nature* **274**, 37

Baan, W.A., Rhoads, J. & Haschick, A.D., 1992 *Ap.J.* **401**, 508

Barbieri, C., Bertola, F. & di Tullio, G., 1974 *A.&A.* **35**, 463

Barnes, J.E. & Hernquist, L., 1991 *Ap.J.* **370**, L75

Baum, S.A., O'Dea, C.P., Dallacassa, D., de Bruyn, A.G. & Pedlar, A., 1993 *Ap.J.* **419**, 553

Beck, R., Wielebinski, R. & Kronberg, P.P., 1990 *IAU Sympos.* **140**, 568

Becker, R., Schilke, P. & Henkel, C., 1989 *A.&A.* **211**, L19

Benacchio, L. & Galletta, G., 1981 *Ap.J.* **243**, L65

Benvenuti, P., Capaccioli, M. & D'Odorico, S., 1976 *A.&A.* **53**, 141

Bi, H.G., Arp, H. & Zimmermann, H.U., 1994 *A.&A.* **282**, 386

Bingham, R.G., McMullam, D., Pallister, W.S., White, C., Axon, D.J. & Scarrott, S.M., 1976 *Nature* **259**, 463

Bland, J. & Tully, R.B., 1988 *Nature* **334**, 43

Bohlin, R.C., Savage, B.D. & Drake, J.F., 1978 *Ap.J.* **224**, 132

Bohren, C.F. & Huffman, D.R., 1983 in *Absorption & Scattering of Light by Small Particles* (John Wiley & Sons, New York)

Bouchet, P., Lequeux, J., Maurice, E., Prévot, L. & Prévot-Burnichon M.L., 1985 *A.&A.* **149**, 330

Boulanger, F. & Pérault, M., 1988 *Ap.J.* **330**, 964

Bregman, J.N., Schulman, E. & Tomisaka, K., 1995 *Ap.J.* **439**, 155

Brownlee, D.E., 1987 in *Interstellar Processes*, edt. Hollenbach, D.J. & Thronson Jr, H.A., p513

Burbidge, E.M., Burbidge, G.R. & Rubin, V.C., 1964 *Ap.J.* **140**, 942

Burstein, D. & Heiles, C., 1982 *A.J.* **87**, 1165

Calzetti, D., Kinney, A.L. & Storchi-Bergmann, T., 1994 *Ap.J.* **429**, 582

Calzetti, D., Bohlin, R.C., Kinney, A.L., Storchi-Bergmann, T. & Heckman, T.M., 1995 *Ap.J.* **443**, 136

Campbell, A.W. & Terlevich, R., 1984 *M.N.R.A.S.* **211**, 15

Campbell, A., Terlevich, R. & Melnick, J., 1986 *M.N.R.A.S.* **223**, 811

Carilli, C.L., Holdaway M.A., Ho, P.T.P. & de Pree C.G., 1995 *Ap.J.* **399**, L59

Carral, P., Hollenbach, D.J., Lord, S.D., Colgan, S.W.J, Haas, M.R., Rubin, R.H. & Erickson, E.F., 1994 *Ap.J.* **423**, 223

Casoli, F., Dupraz, C., Combes, F. & Kazes, I., 1991 *A.&A.* **251**, 1

Cernicharo, J., Bachiller, R. & Duvert, G., 1985 *A.&A.* **149**, 273

Chesterman, J.F. & Pallister, W.S., 1980 *M.N.R.A.S.*, **191**, 349
Chevalier, R.A. & Clegg, A.W., 1985 *Nature* **317**, 44

Chini, R., Kreysa, E, Kruegel, E. & Mezger, P.G., 1986 *A.&A.* **166**, L8

Collison, P.M., Saikia, D.J., Pedlar, A., Axon, D.J. & Unger, S.W., 1994 *M.N.R.A.S.* **268**, 203

Combes, F., Braines, J., Casoli, F., Gerin, M. & van Driel, W., 1992 *A&A* **259**, L65

Condon, J.J., Condon, M.A., Gisler, G. & Puschell, J.J., 1982 *Ap.J.* **252**, 102

Condon, J.J., Anderson, M.L. & Helou, G.H., 1991 *Ap.J.* **376**, 95

Conti, P.S., 1991 *Ap.J.* **377**, 115

Conti, P.S. & Vacca, W.D., 1994 *Ap.J.* **423**, 97

Corbelli, E. & Salpeter, E.E., 1988 *Ap.J.* **326**, 551

Cottrell, G.A., 1977 *M.N.R.A.S.* **178**, 577

Cox, P., Kruegel, E. & Mezger, P.G., 1986 *A.&A.* **155**, 380

Davies, R.D., Staveley-Smith, L. & Murray J.D., 1989 *M.N.R.A.S.* **236**, 171

Davis, L. & Greenstein, J.L., 1951 *Ap.J.* **114**, 206

Debye, P., 1909 *Ann. Phys.*, NY **30**, 59

Deckel, A. & Silk, J., 1986 *Ap.J.* **303**, 39

de Jong, R.S. & van der Kruit, P.C., 1994 *A.&A.S.* **106**, 451

de Jong, T., Clegg, P.E., Rowan-Robinson, M., Soifer, B.T., Habing, H.J., Houck, J.R., Aumann, H.H. & Raimond, E., 1984 *Ap.J.* **278**, L67

Demoulin, M.H., 1969 *Ap.J.* **157**, 81

Désert, F.X., Boulanger, F. & Puget, J.L., 1990 *A.&A.* **237**, 215

de Vaucouleurs, G., de Vaucouleurs, A. & Pence, W., 1974 *Ap.J.* **194**, L119

de Vaucouleurs, G., de Vaucouleurs, A., Corwin Jr, H.G., Buta, R.J., Paturel, G. & Fouque, D., 1991 *Third Reference Catalog of Bright Galaxies* (Springer-Verlag)

de Young, D. & Heckman, T.M., 1994 *Ap.J.* **431**, 598

Donner, K.J. & Brandenburg, A., 1990 *A.&A.* **240**, 289

Draine, B.T. & Salpeter, E., 1979 *Ap.J.* **231**, 77

Draine, B.T. & Lee, H.M., 1984 *Ap.J.* **285**, 89

Draine, B.T. & Anderson, N., 1985 *Ap.J.* **292**, 494

Draper, P.W., 1987 *PhD thesis*, Univ. of Durham

Duffy, A.G., Erickson, E.F., Haas, M.R. & Houck, K.R., 1987 *Ap.J.* **315**, 68

Duley, W.W. & Williams, D.A., 1988 *M.N.R.A.S.* **231**, 969

Dwek, E., 1989 in *IAU Sympos.* **135**, 479

Eales, S.A., Wynn-Williams, C.G. & Duncan, W.D., 1989 *Ap.J.* **339**, 859

Eiroa, C. & Hodapp, K.W., 1989 *A.&A.* **210**, 345

Emsellem, E., 1995 *A.&A.* **303**, 673

Fabbiano, G., Heckman, T.M. & Keel, W.C., 1990 *Ap.J.* **355**, 422

Ferrara, A., Ferrini, F., Franco, J. & Barsella, B., 1991 *Ap.J.* **381**, 137

Fitzpatrick, E.L., 1986 *A.J.* **92**, 1068

Fitzpatrick, E.L., 1989 *IAU Sympos.* **135**, 37

Gallagher, J.S. & Hunter D.A., 1987 *A.J.* **94**, 43

Gehrz, R.D., 1989 in *IAU Sympos.* **135**, 445

Genzel, R. & Stutzki, J., 1989 *A.R.A.&A.* **27**, 41

Gerola, H., Seiden, P.,E. & Schulman, L.S., 1980 *Ap.J.* **242**, 517

Gledhill, T.M., 1987 *PhD thesis*, Univ. of Durham

Gondhalekar, P.M., Morgan, D.H., Dopita, M. & Ellis, R.S., 1986 *M.N.R.A.S.* **219** ,505

Goodrich, R.W. & Miller, J.S., 1994 *Ap.J.* **434**, 82

Goudfrooij, P., de Jong, T., Norgaard-Nielson, H.U., Hansen, L. & Jorgensen, H.E., 1992

in *Structure, Dynamics & Chemical Evolution of Elliptical Galaxies*, edt. Danziger, I.J., Zelinger, W.W. & Kjaer, K. (ESO/EIPC workshop), p579

Graham, J., 1981 *P.A.S.P.* **93**, 552

Greenberg, J.M., 1978 in *Cosmic Dust*, edt. McDonnell, J.A.M. (John-Wiley & Sons)

Greenberg, J.M. & Chlewicki, G., 1987 *Q.J.R.A.S.* **28**, 312

Hawarden, T.G., Elson, R.A., Longmore, A.J., Tritton, S.B. & Corwin, H.G., 1981 *M.N.R.A.S.* **196**, 747

Hecht, E. & Zajac, A., 1974 *Optics* (Addison-Wesley, New York)

Hecht, E., 1987 *Optics* 2nd Edition

Heckman, T.M., 1986 *P.A.S.P.* **98**, 159

Heckman, T.M., 1987 IAU Sympos. **121**, 421

Heckman, T.M., Armus, L. & Miley, G.K., 1990 *Ap.J.S.* **74**, 833

Heiles, C., 1990 *Ap.J.* **354**, 483

Hernquist, L., 1989 *Nature* **340**, 687

Hildebrand, R.H., 1983 *Q.J.R.A.S.* **29**, 267

Hines, D.C., Schmidt, G.D., Smith, P.S., Cutri, R.M. & Low, F.J., 1995 *Ap.J.* **450**, L1

Ho, L.C., Filippenko A.V. & Sargent, W.L.W., 1993 *Ap.J.* **417**, 63

Hodge, P., 1966 *Ap.J.* **146**, 593

Hodge, P., 1974 *Ap.J.* **191**, L21

Hough,J.H., Bailey,J.A., Rouse,M.F. & Whittet,D.C.B., 1987 *M.N.R.A.S.* **227**, P1

Huchtmeier, W.K. & Richter, O.G., 1989 *A General Catalog of HI Observations of Galaxies* (Springer, Berlin)

Hummel, E., van der Hulst, J.M., Keel, W.C. & Kennicutt Jr, R.C., 1987 *A.&A.S* **70**, 517

Hummel, E. & Dettmar, R.J., 1990 *A.&A.* **236**, 33

Ichikawa, T., van Driel, W., Aoki, T., Soyano, T., Tarusawa, K. & Yoshida, S., 1994 *Ap.J.* **433**, 645

Ichikawa, T., Yanagisawa, K., Itoh, N., Tarusawa, K., van Driel, W. & Ueno, M., 1995 *A.J.* **109**, 2038

Israel, F.P., Tacconi, L.J. & Baas, F., 1995 *A.&A.* **295**, 599

Issa, M.R., Maclaren, I. & Wolfendale, A.W., 1990 *A.&A.* **236**, 237

Jenkins, E.B., 1989 *IAU Symp.* **135**, 23

Johnson, P.E., 1982 *Nature* **295**, 371

Jura, M., 1986 *Ap.J.* **303**, 327

Keel, W.C., 1988 *A.&A.* **202**, 41

Kinney, A.L., Bohlin, R.C., Calzetti, D., Panagia, N. & Wyse, R.F.G., 1993 *Ap.J.S.* **86**, 5

Klein, U., Wielebinski, R. & Thuan, T.X., 1984 *A.&A.* **141**, 241

Knapp, G.R., 1990 in *Interstellar medium in Galaxies*, edt. Thronson & Shull, p24

Kunth, D. & Sargent, W.L.W., 1981 *A.&A.* **101**, L5

Kunth, D. & Sevre, F., 1985 in *Star-forming Dwarf Galaxies & Related Objects*, edt. Kunth, D., Thuan, T.X. & Tran Thanh van, J. (Editions Frontieres), p331

Kunth, D., Maurogordato, S. & Vigroux, L., 1988 *A.&A.* **204**, 10

Kwan, J. & Xie, S., 1992 *Ap.J.* **398**, 105

Lamb, S.A., Gallagher, J.S., Hjellming, M.S. & Hunter, D.A., 1985 *Ap.J.* **291**, 63

Lang, K.R., 1980 *Astrophysical Formulae* (Springer-Verlag)

Leech, K.J., Rowan-Robinson M., Lawrence, A. & Hughes, J.D., 1994 *M.N.R.A.S.* **267**, 253

Leitherer, C., 1993 *Reviews in Modern Astronomy* Vol.7

Leitherer, C., Robert, C. & Drissen, L., 1993 *Ap.J.* **401**, 596

Leitherer, C & Heckman, T.M., 1995 *Ap.J.S.* **96**, 9

Lester, D.F., Joy, M., Harvey, P.M., Ellis Jr, H.B. & Parmar, P.S., 1987 *Ap.J.* **321**, 755

Lo, K.Y., Cheung, K.W., Masson, C.R., Phillips, T.G., Scott, S.L. & Woody, D.P., 1987 *Ap.J.* **312**, 574

Loiseau, N., Reuter, H.P., Wielebinski, R. & Klein, U., 1990 *A.&A.* **200**, L1

Lonsdale, C.J., Helou, G., Good, J.C. & Rice, W., 1985 *Cataloged Galaxies & Quasars Observed in the IRAS Survey* (Jet Propulsion Laboratory, Pasadena, U.S.A.)

Lonsdale, C., 1993 in *Panachromatic Views of Galaxies*, edt. Hensler, G., Theis, J. & Gallagher, J. p83

Lonsdale, C.J., Smith, H.E. & Lonsdale, C.J., 1993 *Ap.J.* **405**, L9

Low, F.J., Beintema, D.A., Gautier, T.N., Gillett, F.C., Beichman, C.A., Neugebauer, G., Young, E., Aumann, H.H., Boggess, N., Emerson, J.P., Habing, H.J., Hauser, M.G., Houch, J.R., Rowan-Robinson, M., Soifer, B.T., Walker, R.G. & Wesselius, P.R., 1984 *Ap.J.* **278**, L19

Lynds, C.R. & Sandage, A.R., 1963 *Ap.J.* **137**, 1005

Marconi, G., Matteucci, F. & Tosi, M., 1994 *M.N.R.A.S.* **270**, 35

Marlowe, A.T., Heckman, T.M., Wyse, R. & Schommer, R., 1995 *Ap.J.* **438**, 563

Marston, A.P. & Appleton, P.N., 1995 *A.J.* **109**, 1002

Mathis, J.S., Rumpl, W. & Nordsieck, K.H., 1977 *Ap.J.* **217**, 425

Mathis, J.A., Mezger, P.G. & Panagia, N., 1983 *A.&A.* **128**, 212

Mathis, J.S., 1986 *Ap.J.*, **308**, 281

Mathis, J.S., 1988 *IAU Sympos.* **135**, 357

Mathis, J.S. & Whiffen, G., 1989 *Ap.J.* **341**, 808

Mathis, J.S., 1990 *A.R.A.&A.* **28**, 37

Matthewson, D.S. & Ford, V.L., 1970 *Mem. R.A.S.* **74**, 139

Mazzarella, J.M. & Balzano, V.A., 1986 *Ap.J.S.* **62**, 751

Mazzarella, J.M., Bothun, G.D. & Boronson, T.A., 1991 *A.J.* **101**, 2034

Mazzarella, J.M. & Boroson, T.A., 1993 *Ap.J.S.* **85**, 27

McCarthy, P., Heckman, T.M. & van Breugel, W., 1987 *A.J.* **93**, 264

McKeith, C.D., Greve, A., Downes, P. & Prada, F., 1995 *A.&A.* **293**, 703

Melnick, J., Moles, M. & Terlevich, R., 1985 *A.&A.* **149**, L24

Meurer, G.R., Freeman, K.C., Dopita, M.A. & Cacciari, C., 1992 *A.J.* **103**, 60

Mie, G., 1908 *Ann. Phy.*, NY **25**, 377

Mihos, J.C. & Hernquist, L., 1994 *Ap.J.* **431**, L9

Mirabel, I.F. & Sanders, D.B., 1988 *Ap.J.* **335**, 104

Mirabel, I.F., Booth, R.S., Garay, G., Johansson, L.E.B. & Sanders, D.B., 1990 *A.&A.* **236**, 327

Morgan, D.H. & Nandy, K., 1982 *M.N.R.A.S.* **199**, 979

Noguchi, M., 1991 *M.N.R.A.S.* **251**, 360

O'Connell, R.W. & Mangano, J.J., 1978 *Ap.J.* **221**, 62

O'Connell, R.W., Gallagher, J.S. & Hunter, D.A., 1994 *Ap.J.* **433**, 65

O'Connell, R.W., Gallagher, J.S., Hunter, D.A. & Colley, W.N., 1995 *Ap.J.* **446**, L1

Perry, C.L. & Johnston, L., 1982 *Ap.J.S.* **50**, 451

Phillips, A.C., 1993 *A.J.* **105**, 486

Pietsch, W., 1993 in *Panachromatic Views of Galaxies*, edt. Hensler, G., Theis, J. & Gallagher, J., p137

Pildis, R.A., Bregman, J.N. & Schombert, J.M., 1994 *Ap.J.* **423**,190

Prévot, M.L., Lequeux, J., Maurice, E., Prévot, L. & Rocca-Volmerange, B., 1984 *A.&A.* **132**, 389

Price, J.S. & Gullixson, C.A., 1989 *Ap.J.* **337**, 658

Purcell, E.M., 1979 *Ap.J.* **231**, 404

Reif, K., Mebold, U., Goss, W.M., van Woerden, H. & Siegman, B., 1982 *A.&A.S.* **50**, 451

Reuter, H.P., Klein, U., Lesch, H., Wielebinski, R. & Kronberg, P.P., 1995 *A.&A.* **293**, 287

Rieke, G.H., Cutri, R.M., Black, J.H., Kailey, W.F., Mcalary, C.W., Lebofsky, M.J. & Elston, R., 1985 *Ap.J.* **290**, 116

Roberts Jr, W.W. & Hausman, M.A., 1984 *Ap.J.* **277**, 744

Roche, P.F., Aitken, D.K., Smith, C.H. & Ward, M.J., 1991 *M.N.R.A.S.* **248**, 606

Rolph, C.D., 1990 *PhD thesis* Univ. of Durham

Ruzmaikin, A., Sokolov, D., Shururov, A. & Beck, R., 1990 *A.&A.* **230**, 284

Ryder, S.D., Staveley-Smith, L., Malin, D. & Walsh, W., 1995 *A.J.* **109**, 1592

Saikia, D.J., Pedlar, A., Unger, S.W. & Axon, D.J., 1994 *M.N.R.A.S.* **270**, 46

Sandage, A.R., 1961 *The Hubble Atlas of Galaxies* (Washington D.C., Carnegie Institute of Washington)

Sandage, A. & Tammann, G.A., 1975 *Ap.J.* **196**, 313

Sanders, D.B., Solomon, P.M. & Scoville, N.Z., 1984 *Ap.J.* **276**, 182

Sanders, D.B., Scoville, N.Z. & Soifer, B.T., 1991 *Ap.J.* **370**, 158

Sanders, W.L. & Balamore, 1971 *Ap.J.* **166**, 7

Scarrott, S.M., Warren-Smith, R.F., Pallister, W.S., Axon, D.J. & Bingham, R.G., 1983 *M.N.R.A.S.* **204**, 1163

Scarrott, S.M., Ward-Thompson, D. & Warren-Smith, R.F., 1987 *M.N.R.A.S.* **224**, 299

Scarrott, S.M., 1988 *M.N.R.A.S.* **231**, 1055

Scarrott, S.M. & Rolph, C.D., 1989 *M.N.R.A.S.* **238**, 349

Scarrott, S.M., Rolph, C.D. & Semple, D.P., 1990a *IAU Sympos.* **140**, 245

Scarrott, S.M., Rolph, C.D., Wolstencroft, R.D. & Sechiguchi, K., 1990b *M.N.R.A.S.* **245**, 484

Scarrott, S.M., 1991 *Vistas Astron.* **34**, 163

Scarrott, S.M., Eaton, N. & Axon, D.J., 1991a *M.N.R.A.S.* **252**, 12P

Scarrott, S.M., Rolph, C.D., Wolstencroft, R.D. & Tadhunter, C.N., 1991b *M.N.R.A.S.* **249**, 16P

Scarrott, S.M., Draper, P.W., Stockdale, D.P. & Wolstencroft, R.D., 1993 *M.N.R.A.S.* **264**, L7

Schmidt, G.D., Angel, J.R.P. & Cromwell, R.H., 1976 *Ap.J.* **206**, 888

Schweizer, F., Whitmore, B.C. & Rubin, V.C., 1983 *A.J.* **88**, 909

Scoville, N.Z., Sargent, A.I., Sanders, D.B. & Soifer, B.T., 1991 *Ap.J.* **366**, L5

Seab, C.G., 1988 in *Dust in the Universe*, edt. Bailey, M.E. & Williams, D.A. (Cambridge University Press)

Seaquist, E.R., Bell, M.B. & Bignell, R.C., 1985 *Ap.J.* **294**, 546

Searle, L. & Sargent, W.L.W., 1972 *Ap.J.* **173**, 25

Serkowski, K., Matthewson, D.S. & Ford, V.L., 1975 *Ap.J.* **196**, 261

Shlosman, I., Begelman, M.C. & Frank, J., 1990 *Nature* **345**, 679
Smith, M.G., Aguirre, C. & Zemelmann, M., 1976 *Ap.J.S.* **32**, 217

Soifer, B.T., Sanders, D.B., Madore B.F., Neugebauer, G., Danielson, G.E., Elias, J.H., Lonsdale, C.J. & Rice, W.L., 1987 *Ap.J.* **320**, 238

Soifer, B.T., Boehmer, L., Neugebauer, G & Sander, D.B., 1989 *A.J.* **98**, 766

Solinger, A.B., 1969 *Ap.J.* **158**, L25

Solinger, A.B. & Markert, T., 1975 *Ap.J.* **197**, 309

Solinger, A.B., Morrison, P. & Markert, T., 1977 *Ap.J.* **211**, 707

Solomon, P.M., Downes, D. & Radford, S.J.E., 1992 *Ap.J.* **387**, L55

Sparks, W.B., 1992 in *Structure, Dynamics & Chemical Evolution of Elliptical Galaxies*, edt. Danziger, I.J., Zelinger, W.W. & Kjaer, K. (ESO/EIPC workshop), p567

Spitzer Jr, L., 1978 in *Physical Processes in the Interstellar Medium* (John Wiley & Sons, New York)

Storchi-Bergmann, T., Kinney, A.L. & Challis, P., 1995 *Ap.J.S.* **98**, 103

Struck-Marcell, C. & Tinsley, B.M., 1978 *Ap.J.* **221**, 562

Suchov, A.A., Balsara, D.S., Heckman, T.M. & Leitherer, C., 1994 *Ap.J.* **430**, 511

Telesco, C.M., Becklin, E.E., Wynn-Williams, C.G. & Harper, D.A., 1984 *Ap.J.* **282**, 427

Telesco, C.M., 1988 *A.R.A.&A.* **26**, 343

Telesco, C.M., Decher, R. & Joy, M., 1989 *Ap.J* **343**, L13

Telesco, C.M., Campins, H., Joy, M., Dietz, K. & Decher, R., 1991 *Ap.J.* **369**, 135

Telesco, C.M., Dressel, L.L. & Wolstencroft, R.D., 1993 *Ap.J.* **414**, 120

Terlevich, R., Melnick, J., Masegosa, J., Moles, M. & Copetti, M.V.F., 1991 *A.&A.S.* **91**, 285

Thronson Jr, H.A., Wilton, C. & Ksir, A., 1991 *M.N.R.A.S.*, **252**, 543

Thuan, T.X. & Martin, G.E., 1981 *Ap.J.* **247**, 823

Thuan, T.X., 1983 *Ap.J.* **268**, 667

Thuan, T.X., 1984 *Ap.J.* **281**, 126

Tinsley, B.M., 1978 *Ap.J.* **222**, 14

Vacca, W.D. & Conti, P.S., 1992 *Ap.J.* **401**, 543

van den Broeck, A.C., van Driel, W., de Jong, T., Lub, J., de Grijp, M.H.K. & Goudfrooij, P., 1991 *A.&A.S.* **91**, 61

van der Hulst, H.C., 1957 in *Light Scattering by Small Particles* (John Wiley & Sons, New York)

van de Hulst, J.M., 1979 *A.&A.* **75**, 97

van der Kruit, P.C., 1971 *A.&A.* **15**, 110

van Driel, W., Combes, F., Casoli, F., Gerin, M., Nakai, N., Miyaji, T., Hamabe, M., Sofue, Y., Ichikawa, T., Yoshida, S., Kobayashi, Y., Geng, F., Minezaki, T., Arimota, N., Koduma, T., Goudfrooij, P., Mulder, P.S., Wakamatsu, K. & Yanagisawa, K., 1995 *A.J.* **109**, 942

van Driel, W., van den Broeck, A.C. & de Jong, T., 1991 *A.&A.S.* **90**, 55

Viallefond, F. & Thuan, T.X., 1983 *Ap.J.* **269**, 444

Wainscoat, R.J., de Jong, T. & Wesselius, P.R., 1987 *A.&A.* **181**, 225

Waller, W.H., Gurwell, M. & Tamura, M., 1992 *A.J.* **104**, 63

Ward-Thompson, D.W., 1987 *PhD thesis*, Univ. of Durham

Warren-Smith, R.F., 1979 *PhD thesis*, Univ. of Durham

Watson, M., Stanger, V. & Griffiths, R., 1984 *Ap.J.* **286**, 144

Weiland, J.L., Blitz, L., Dwek, E., Hauser, M.G., Magnani, L. & Rickard, L.J., 1986 *Ap.J.* **306**, L101

White, S. & Frenk, C., 1991 *Ap.J.* **379**, 52

Whittet, D.C.B., 1992 *Dust in the Galactic Environment* (IOP Publishing)

Wickramasinghe, N.C., 1973 in *Light Scattering Functions for Small Particles* (Hilger, London)

Wilking, B.A., Lebofsky, M.J. & Rieke, G.H., 1982 *A.J.* **87**, 695

Willick, J.A., Bowyer, S. & Brodie, J.P., 1990 *Ap.J.* **355**, 393

Witt, A.N., Thronson, H.A.J. & Capuano, J.M.J., 1992 *Ap.J.* **393**, 611

Wolfire, M.G., Tielens, A.G.G.M. & Hollenbach, D., 1990 *Ap.J.* **359**, 116

Wright, G.S., Joseph, R.D., Robertson, N.A., James, P.A. & Meikle, W.P.S., 1988 *M.N.R.A.S.* **233**, 1

Young, Y.S., Kleinmann, S.G. & Allen, L.E., 1988 *Ap.J.* **334**, 63

Yun, M.S., Ho, P.T.P. & Lo, K.Y., 1994 *Nature* **372**, 530

Zaritsky, D., 1994 *A.J.* **108**, 1619

Zwicky,F, 1964 *Ap.J.* **139**, 514